2 March 2020

Cruise Science Report: TN376 R/V Thompson
25 January – 3 March, 2020

William Balch, Bigelow Laboratory for Ocean Sciences, East Boothbay, ME 04544 USA
Colin Brownlee, Marine Biological Assn. of the UK, Plymouth, Devon, U.K.
Dennis McGillicuddy, Woods Hole Oceanographic Inst., Woods Hole, MA USA
Peter Morton, National High Magnetic Field Laboratory/Florida State University Tallahassee, Florida 32310 USA

Cruise narrative

Cruise track overview

This cruise was loaded in Cape Town, South Africa, beginning 22 January, 2020 and departed Cape Town on 25 January. The cruise track took us southeast from Cape Town for our first shakedown station at 38o35'S x 024oE, a station which was ultimately cancelled due to heavy weather conditions. Two days out of Cape Town, the coupler between the ship's number 3 main engine and generator broke. This meant that the ship only had one main engine, with associated generator, plus two smaller engine/generators for all power needs. With the loss in redundancy, this meant that we had to cut our cruise plans short, in order to stay within several hundred miles of Durban, SA, such that the ship could go in for repair once a replacement coupler could be found. This also meant that we had to abandon the planned meridional transect that was to be done on this trip, since the travel to the ship yard, the repair, and return to the next station took over a week of sampling out of the cruise, and our proximity to Durban (and long distance from the Crozet Islands) meant that we couldn't possibly accomplish the meridional transect and make it to Mauritius within the UNOLS ship schedule. We are now trying to get this leg added onto the ship schedule for next year's cruise.

Given the above engine issues, we therefore decided to stay within the Agulhas meander system, an area that is part of the Great Calcite Belt (Balch *et al.*, 2016), known for massive coccolithophore-rich, (and PIC-rich) frontal boundaries and eddies. This evidence goes back to the NASA SeaWiFS ocean color sensor in the late 1990's and the NASA MODIS mission from 1998 to the present (Fig. 1 shows the average austral summer PIC concentration for the region of the Southern Indian Ocean, as detected by the NASA MODIS Aqua sensor). These averages are for all austral summer seasons between 2002-2018.

Given the constraints described above, we focused on sampling (and re-sampling) two features, a filament of the Aghulas and south subtropical fronts and a cyclonic eddy spun off from these frontal boundaries in the preceding December. The actual cruise track (plus the planned original cruise track with meridional transect are overlaid in Fig. 1. For the first leg of the cruise (white overlay in Fig. 1), we focused on a region within one

of the meanders which had shown persistent elevated PIC over a mesoscale meander, a feature that was over 80,000 km^2 (400km long and 200 kilometers wide). We surveyed the feature zonally and meridionally with the video plankton recorder (VPR), then repeated the same transects with CTD sections (doing 12-depth water sample profiles for chlorophyll, nutrients, dissolved oxygen, particulate inorganic carbon (PIC), particulate organic carbon (POC), biogenic silica (BSi), quantitative coccolithophore counts and quantitative FlowCAM samples (for enumeration of algal classes, cell volumes, and slope of the particle-size distribution function). We also performed carboy experiments in each feature. In this, and all subsequent feature surveys, the Morton lab drew trace-metal clean surface water using a surface water sampler for carboy experiments to be incubated on board the ship under simulated *in situ* conditions. All carboy experiments involved incubation of trace-metal-clean surface water, collected by a novel surface sampler that was, for the first time, deployed laterally away from the ship while steaming at a few knots speed ("Big Jon Scientific Surface Sampler"). It maintains a distance of 10-15m from the ship as it steams, insuring no trace metal contamination from the ship's hull. The carboy experiments involved triplicate incubations of untreated control water plus

five treatments with a)10% dilution with deep SAMW water, b) 12µM trace metal-clean nitrate, (c) 5µM trace metal-silicate, (d) 4nM of iron and (e) 4nM of iron+5µm of silicate. The carboys were then sampled daily for 4-5 days while being incubated under surface light conditions in an on-deck incubator, with temperature maintained at *in-situ* surface conditions. The carboys were sampled daily by the Balch group for chlorophyll, nutrients, PIC, POC, biogenic silica, quantitative coccolithophore counts and quantitative flow cam samples (for enumeration of algal classes, cell volumes, and slope of the particle-size distribution). Photosynthetic parameters were also measured in the carboy experiments by the Brownlee group using a PAM fluorometer (Water PAM, Walz, Germany). Ph.D. student, Julia Middleton (Ph.D. student of Dr. Tristan Horner, WHOI) performed experiments on barite formation in all the features studied in this expedition.

We started the second leg of the cruise (yellow cruise track overlay, Fig. 1), heading for an eddy that we had observed since December using PIC and altimetric satellite remote sensing (from the point that the eddy had pinched off from the Agulhas/Southern Subtropical frontal regions). This eddy formerly had contained more PIC (based on higher remote sensing reflectance) and now the coccolithophore

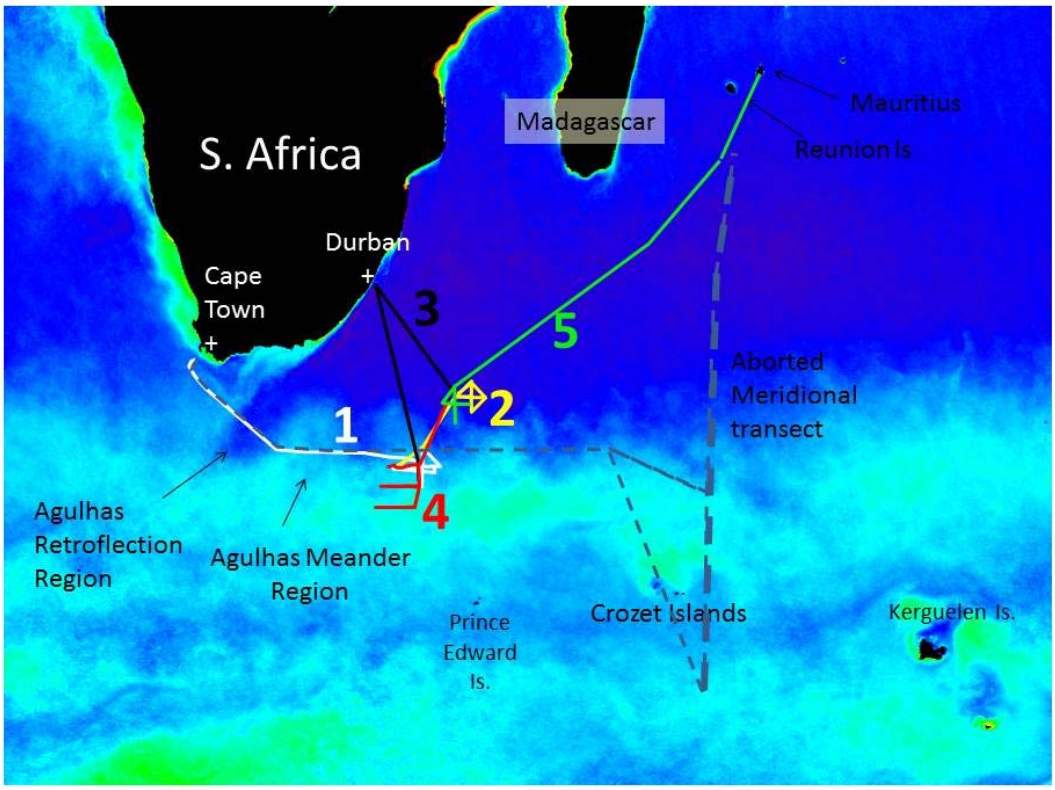

Fig. 1-Average PIC concentration in the SW Indian Ocean/Southern Ocean as detected by MODIS Aqua. Note how the elevated PIC reflects the Agulhas Retroflection and Agulhas meander system. This is the austral summer season average for the Aqua sensor for years 2002-2018. The cruise track of TN376 is shown with numbered, colored lines corresponding to the five cruise legs. The original planned cruise track is shown with a grey dashed line and the aborted meridional transect is shown with a thick grey dashed line.

concentrations appeared to be waning. For both the filament and eddy, the altimetric and PIC products showed good coherence with the oceanographic structures, suggested that these would be good study sites to examine the conditioning of SubAntarctic Mode Water by coccolithophores and other resident phytoplankton species. We sampled for another carboy experiment in this eddy, deployed a 10m sock drifter in the eddy center on 8 February, 2020, in order to follow the eddy feature in our absence, then stopped all science and headed for Durban for the ship repair (leg 3; grey thick cruise track in Fig. 1). The repair was complete by the evening of 13 February, 2020 and the ship subsequently set sail from Durban, to head back to the filament that we had studied in Leg 1 (which was now showing increased PIC levels; Leg 4; red cruise track, Fig. 1). We performed another deck carboy experiment in the filament, conducted VPR and CTD surveys, and we performed a deep CTD cast for nutrient and carbonate chemistry, then re-occupied the eddy that we had studied prior to Durban (Leg 5; orange cruise track, Fig. 1), surveyed with both VPR and CTD casts, performed yet another carboy experiment, recovered the drifter. We performed two more deep casts (072.01 and 073.01) in transit to Mauritius.

Detailed Leg Summary

Leg 1; Transit from Cape Town, S.A., zonal transect through Agulhas meander system, and sampling of a coccolith-rich filament; CTD stations 1-17, VPR tows 1-7; trace metal casts 1, 3, 5, 6, 7, 8, 12 and 17; 0800h, 25 January- 0222h, 4 February, 2020. (Fig. 1 white line)

For this leg, we transited across the Agulhas Meander system, beginning with a station in the Agulhas Retroflection eddy (station 2), criss-crossing the Agulhas, Southern Subtropical Fronts with VPR and underway bio-optical systems running, and performed full CTD water casts (stations 2-4). This line of stations crossed into the end of our filament of interest, which showed (with the Acoustic Doppler Current Profiler (ADCP), cyclonic circulation around a zero-velocity core of this frontally-embedded eddy. Station 5 was situated in the western interior side of this eddy. This was where we collected water for our first carboy experiment and also performed a trace metal cast consisting of nine Niskin X samplers deployed on a Kevlar line. After collecting seawater for the carboy experiment, the VPR was deployed and towed for the entire west-to-east section, then north-to-south section through the center of the eddy. The same sections were then visited (in reverse) for CTD casts. Daily productivity casts to measure photosynthesis and calcification, plus trace metal casts were run at stations 1, 3, 4, 5, 6, 7, 8, 12, and 17. The carboy experiment for this feature was run from surface water taken at station five. Measurements of photosynthetic variables were made underway and at stations 1-17. These included photosynthetic efficiency and rapid light curve data. An imaging PAM system (PSI, Cz) was also used to obtain cell type-specific photosynthetic efficiency data (see Brownlee group report for more details of imaging PAM and measurements made). Filter/freeze/transfer (FFT) preparations were made for qualitative viewing of surface and fluorescence maxima phytoplankton assemblages (400x magnification bright-field, polarized microscopy and epi-fluorescence using 480nm and 530nm excitation) viewing at stations 5,6,7,8, 12, and 17. Barite precipitation measurements were performed at station & in this feature.

Leg 2; Transit to eddy feature and its survey; CTD stations 18-25; VPR tows 8-9; trace metal casts 18, 20, and 23; 0222h,4 Feb.-1400h, 8 Feb., 2020 (Fig. 1; yellow line)

This leg of the cruise involved sampling a cyclonic eddy roughly centered at 35^{o} 53'S and 37^{o}38'E. We first did a full 195 kilometer east-to-west VPR survey, towed it from the east end of the eddy to the northern end of the eddy followed by a complete VPR section (163 kilometers) from north to south. The area of this PIC-enhanced, elliptical eddy was about 25,000 km^{2}. Productivity and trace metal casts were performed at stations 18, 20, 23 and the water for a second carboy experiment was collected from station 18 (eddy interior). Measurements of photosynthetic variables were made underway and at stations 18-25. FFT preparations were made for semi-quantitative viewing of surface and fluorescence maxima phytoplankton assemblages (400x magnification bright-field, polarized microscopy and epi-fluorescence using 480nm and 530nm excitation) viewing at stations 18, 23, and 25. Barite precipitation measurements were performed at station && in this feature. A 10m-sock drogue equipped with a satellite Argos transmitter was deployed in the eddy center prior to our departure for Durban as a means to track the feature in our absence.

Leg 3; science stopped and ship diverted for engine repair; 1400h, Feb. 8, with science sampling resumed at 1726h, 16 February. (Fig. 1; thick, black line)

All overboard sampling at Leg 2 stopped on 8 February for the steam back to the port of Durban for engine repairs. Only the carboy experiments were sampled during the two-day transit to the port but given that we had a temperature-controlled seawater incubator, the carboy experiments could be maintained at their *in situ* temperatures for the duration of the multi-day experiment. The engine repair work in Durban was completed by the evening of 13 February, after which the ship sailed for station 26 to resample the first filament that we had sampled in Leg 1.

Leg 4; Re-sampling the meander filament and transit to first deep CTD; CTD Stations 26-53; VPR tows 10-12; trace metal casts 28 and 39; 0347h,16 Feb. - 0418h, Feb. 20, 2020 (Fig. 1; red line)

The ship proceeded to re-sample the meander filament by performing three east-to-west, VPR sections across the feature, followed by three CTD sections made immediately afterwards across the same lines, from west-to-east. Those sections were made zonally at 41o30', 40o30'S and 39o30'S and had lengths of 222km, 222km and 167km, respectively, such that they adequately sampled the cross-section of the feature. Beginning with station 27, we alternated each CTD full-water cast with a "trip on the Fly" water cast. These later casts were used only to sample DIC and nutrients and served to provide grfeater resolution sections across the features. This pattern of Ctd sampling was continued for the remaining feature surveys. Following the completion of each VPR and CTD zonal leg, the VPR was towed to the next zonal leg. Productivity/TM casts were made at stations 28, 39 and 50, near the mid-points of the filament. The carboy experiment in this feature was run using water from station 28. Measurements of photosynthetic variables were made underway and at stations

26,28,30,32,34,35,37,39,41,43,44,46,48,50,52. FFT preparations were made for semi-quantitative microscopy viewing at stations 28, 29, 30, 39, 42, and 50. Barite precipitation measurements were performed at station && in this feature.

Leg 5; Re-sampling Eddy 3, Deep water casts, transit to Mauritius; CTD Stations 54-73; VPR tows 13-14; trace metal casts 50, 56, and 70; 0418h, Feb. 20 – 0800h, March 3, 2020. (Fig. 1; green line)

From leg 4, we proceeded to re-sample the cyclonic eddy, originally sampled in leg 2. On the way, we made the first deep CTD cast to sample for nutrients, oxygen and carbonate chemistry down to the sea floor (4500m). The eddy re-sampling consisted of a 163km west-to-east VPR tow followed by a 203km east to west CTD section. Heavy seas forced us to cancel the west-most CTD station. The ship then proceeded to the north eddy station with all weather decks secured. Again, heavy sea-states made deployment of the VPR impossible, so we performed the north-to-south CTD section but had to call off some of the middle CTDs from that section due to heavy seas. The drogue had spiraled about 100km from eddy center by this point, so the ship broke from the N-S line to recover it, after which the interior eddy stations (that had been skipped due to weather) were re-sampled under safer sea states, finally arriving at the southern eddy station, #71 at 1853h on 2/24/20. At this point, the VPR could finally be re-deployed to tow the entire south-to-north eddy survey transect. Two productivity/trace-metal stations were run in the eddy at stations 56 and 70. (The carboy experiment was sampled at station 56. Measurements of photosynthetic variables were made underway and at stations 54,56,58,60,62,64,66,68,70,71. FFT preparations were made for semi-quantitative microscopy viewing at stations 56 (east eddy interior) and 70 (eddy center). Barite precipitation measurements were performed at station && in this feature. We performed a deep, 24-bottle, cast for nutrients, oxygen and dissolved inorganic carbon chemistry 183km NE of the eddy (34.42^{o}S x 38.04^{o}E; depth 5217m), sampled to 5200m. The last station of the cruise was a 24-bottle deep cast at 27^{o} 24.5' S 049^{o} 49.33' E for freons, nutrients, temperature, salinity, PIC, POC, biogenic silica, coccolithophore and coccolith abundance, dissolved oxygen and dissolved inorganic carbon chemistry. The purpose of this cast was to examine water ages of SAMW, examine the stoichiometry of the changes in the chemistry from assumed preformed levels, and to provide comparative values for the meridional transect to be performed next year.

Overview of preliminary findings

The VPR sections, done concurrently with the surface underway optical and hydrographic measurements, demonstrated that peak backscattering [b_b] (and acid-labile backscattering [b_b'], a good proxy of PIC concentration) and chlorophyll fluorescence were found in cold, low salinity, oxygenated water. Seawater with the density characteristics of SAMW (σ_θ between 26.5 and 27.1) shoaled within the features at depths ranging from 100 -550m depth. The potential vorticity (PV) of these waters had low to moderate values (50-100 x10^{-12} m^{-1} s^{-1}); depending on the PV criteria used to describe the SAMW pycnostad, this water is technically not SAMW but appears to be capped off by a surface-warmed layer. It is, however, close to fulfilling the definition with a number of the observed PV values between 50- 100 x10^{-12} m^{-1} s^{-1}. Subsequent

mixing of this cooled water during austral winter would inject this water into the SAMW layer (see McGillicuddy report for more detail of this).

The acid-labile backscattering (directly correlated to PIC concentrations) was elevated in the centers of each feature, contributing up to 50% of the total backscattering. The on-board microscopy using the filter-freeze-transfer technique (see Balch lab section later in this report) which confirmed that the elevated acid-labile backscattering was originating from plated coccolithophores and their detached coccoliths, not some other carbonate biomineralizer (e.g. foraminifera). The phytoplankton assemblage in both the surface and fluorescence maximum depths of the features was dominated by a surprisingly diverse assortment of coccolithophore species (as well as detached coccoliths), not just *Emiliania huxleyi*. For example, the species observed in the shipboard light microscopy were: *E. huxleyi*, *Acanthoica quattrospina*, several species of the genus *Syracosphaera (*both holo- and heterococcolith forms such as *S. ossa* and *S. pulcra)*, *Discosphaera tubifera*, *Rhabdosphaera clavigera*, *Michaelsarsia elegans*, *Saturnulus helianthaformis*, *Papposphaera* sp., *Pappomonas* sp., *Calciosolenia* murrayi and *Helicosphaera* sp.. More exact identifications of these will be determined following scanning electron microscopy ashore, as well as quantitative abundance estimates using polarized microscopy coccolithophore counts, post-cruise. This diversity is consistent with previous Great Calcite Belt observations in the Indian sector of the Southern Ocean (Smith *et al.*, 2017). Secondarily, the assemblage also contained surprising numbers of several species of dinoflagellates, both armored and unarmored. In some stations from the feature interior, cyanobacteria (*Synechococcus*) appeared to roughly co-vary with the coccolithophore abundance, and were relatively abundant (based on epifluorescence microscopy using 530nm excitation). Diatoms were almost non-existent in most samples. The only samples where there was any abundance of diatoms was in the middle of the frontal filament during its second sampling (stn 39) in the fluorescence maximum at 47m depth. For an example of the phytoplankton assemblage from the center of the filament, showing bright-field (all cells), polarized birefringence (highlighting calcium carbonate); blue epifluorescence (showing eukaryotic cells containing chlorophyll; green epifluorescence (showing fluorescent cyanobacteria) (see Fig. 2).

Nutrient concentrations in these features typically showed low nitrate, phosphate and silicate concentrations in the surface layers except in the zonal section of the filament (the furthest south sampling of the cruise in leg 4). There, the surface nitrate and silicate concentrations were elevated above background. A this moment, we don't yet know if nitrate was limiting in the Redfieldian sense. However, in the carboy experiments, the only enhanced growth of phytoplankton (as indicated by increasing chlorophyll concentrations over the multi-day experiments) were observed in the nitrate and SAMW augmented treatments and nitrate concentrations were depleted to background within a few days. Thus, the phytoplankton populations (as quantified by chlorophyll a) showed distinct signs of nitrogen limitation whereas there was no effect of iron, silicate or iron plus silicate augmentations in any of the experiments. Future evaluation of the photophysiology data (PAM fluorometry and single cell PAM fluorescence imaging) will reveal the control of algal photophysiology and photosynthetic efficiency by nutrients and trace metals (Fig. 3).

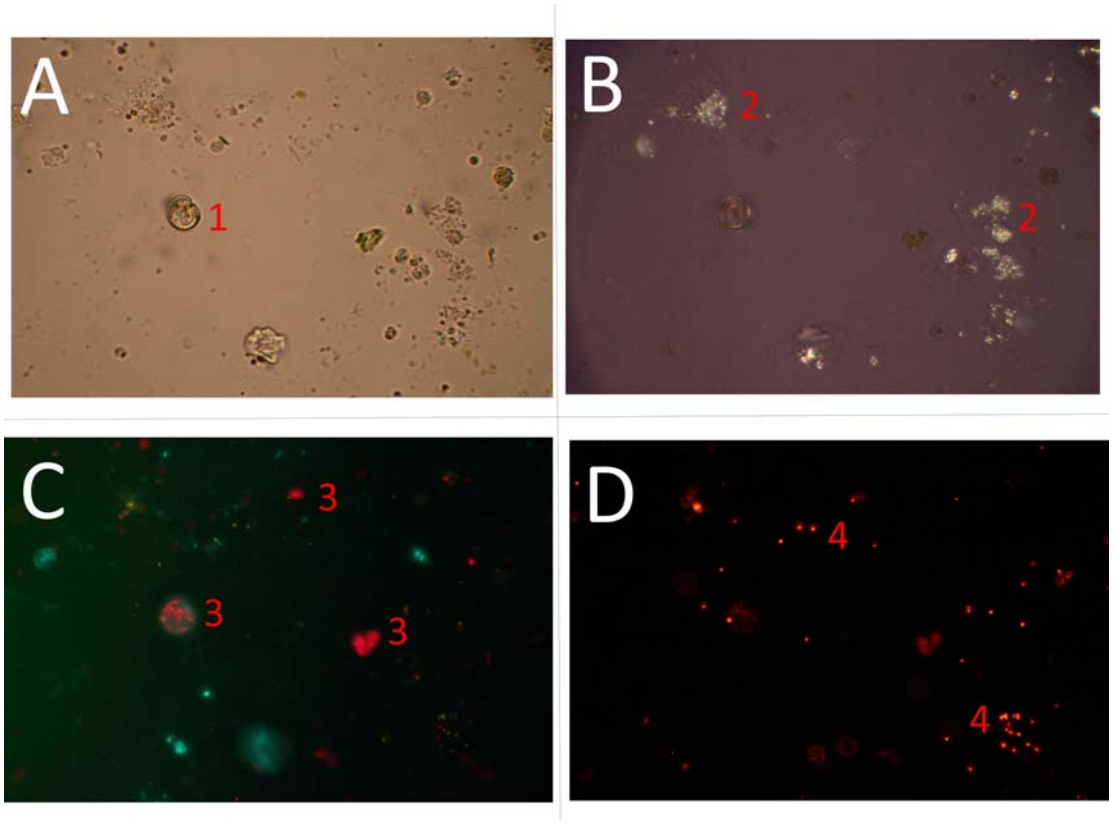

Fig. 2- Example of four micrographs of the same microscope field at 400X magnification. These images were made from a 250mL seawater sample filtered on a 0.4um-poresize, 25mm diameter, polycarbonate filter. The slide was prepared using the Filter-Freeze-Transfer technique (Hewes and Holm-Hanson, 1983). These photos were photographed using (a) brightfield illumination, (b) polarized light illumination showing irefringent calcium carbonate particles as white particles against the darker background, (c) chlorophyll fluorescence by photosynthetic eukaryotes (epi-fluorescence microscopy with 490nm excitation) and d) epifluorescence microscopy by photosynthetic prokaryotic algae (Synechococcus) under 530nm excitation. Numbered particles designate 1)-dinoflagellate, 2)-coccolithophores, 3)-photosynthetic eukaryotes containing chlorophyll and 4) *Synechoccus* cyanobacteria. This field did not contain diatoms but they were present in other fields of the same sample. The dimensions of the field are 281mm x 187.5mm. This method is semi-quantitative and allows approximate particle concentrations to be estimated.

In this cruise, we had the remarkable opportunity to observe the continuous formation of rich coccolithophore populations within the energetic Agulhas meander system, the formation of a PIC-enhanced cyclonic ring, and the subsequent demise of the resident algal population within the semi-enclosed cyclonic ring over time. Regarding the conditioning of SAMW water by the resident phytoplankton, there is little doubt that the water south of the Southern Subtropical and SubAntarctic Fronts (in the filament) was the site of active coccolithophore growth and dinoflagellate growth. We hypothesize that his growth was sustained over the course of our observations in the same manner that phytoplankton experience continuous growth in a chemostat. The filament feature actually became brighter with coccolithophore reflectance during the period of the cruise.

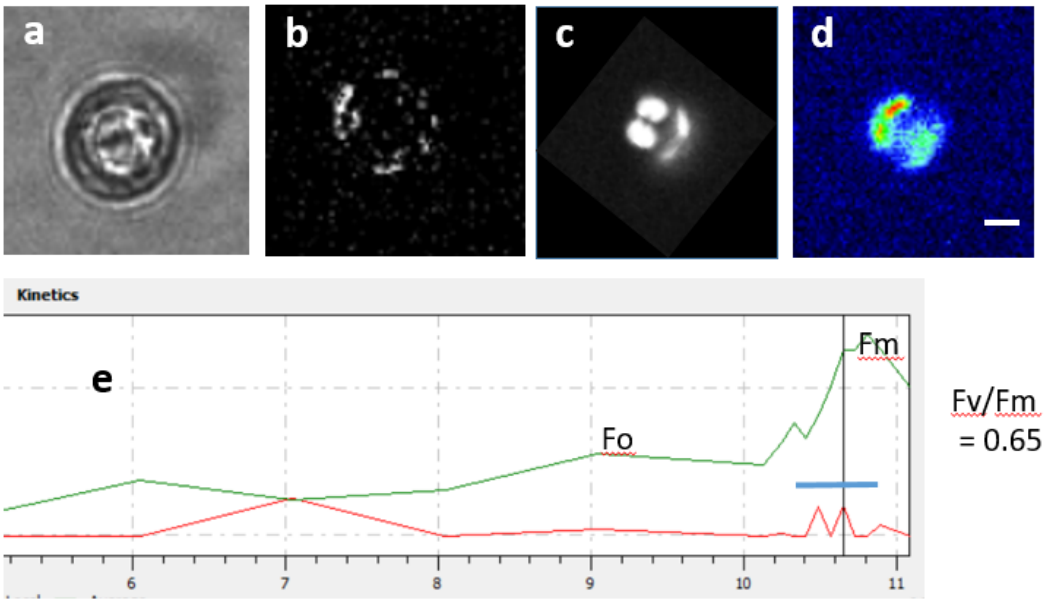

Fig. 3 Single cell PAM fluorescence imaging of a calcifying coccolithophore. a) Bright filed image, b) polarized light image of external coccoliths , c) chlorophyll fluorescence, d) Maximum chlorophyll fluorescence image following a saturating light pulse, e) fluorescence plots of dark-adapted state, Fo and following a saturating light pulse, Fm (blue bar in e). The cell was from a surface underway sample taken at 16:00 h on 01.31.2020. Bar in d) = 10 µm

The water that appeared to be supporting this growth was cold, low salinity water, probably upwelled or advected into the region from further south of the filament.

From the survey and re-survey of the semi-enclosed eddy, we hypothesize that the cyclonic eddy phytoplankton populations were behaving more like a batch culture approaching stationary phase, with a phytoplankton population in significant decline. Satellite imagery demonstrated that the reflectance of the feature was decreasing over time, even though the eddy was still observable using satellite altimetry. The fluorescence maximum at eddy center descended from 54m to 82m depth between first and second samplings, separated by a 2.5 week period. The levels of backscattering (both total and acid-labile) also decreased as this phytoplankton assemblage was "crashing". Post-cruise, as we work up all the biogeochemical samples, we will determine the full extent that these mixed coccolithophore and dinoflagellate populations conditioned the DIC and nutrient chemistry prior to its subduction during the ensuing winter. At this juncture, however, this "proto-SAMW" water appears to have been significantly conditioned by coccolithophores and dinoflagellates. Any conditioning of SAMW by diatoms (in the Sarmiento et al. sense (Sarmiento *et al.*, 2004)) appears to have already happened further south, with the consumption of all the silicate. What we have observed in this cruise is the next level of conditioning by the coccolithophores and dinoflagellates before the long transit of SAMW north from the Southern Ocean towards the equator.

Ship's Data

The R/V Thompson's underway surface sampling system collects a huge amount of data, beyond the scope of this report. However, some of the data sets gathered routinely during the cruise were: ADCP current velocity profiles, bathymetric measurements using

the ship's multibeam system, meteorogical data and underway surface water properties (e.g. temperature, salinity, fluorescence) and pCO_2.

Acknowledgements- We would like to thank Captain Russ DeVaney, officers and crew of the *R/V Thomas G. Thompson*. The engine coupler issue was a major challenge for the ship's crew and scientists alike, and the fact that we were still able to accomplish the surveys of the two eddies in this trip (which was two thirds of the proposed work) is a real testimonial to the seamanship and "can-do" attitude of the ship's crew in this emergency situation. The University of Washington marine technicians that accompanied us (Elizabeth Ricci and Jennifer Nomura) provided excellent oversight of all deck operations and utmost safety at all times, Scripps chemists John Ballard and Zac Anderson were indispensable for the accurate measurement of oxygen, nutrients and salts. Norman Kuring (NASA Goddard Space Flight Center, Greenbelt, MD) provided us with regular basin scale (as well as high resolution) MODIS imagery before, during and after Thompson 376 to help us locate features. All the members of the ship operations office at the University of Washington are to be thanked for the immense organizational and logistical tasks associated with the planning a cruise of this size as well as working through the mechanical challenges that we faced (Robert Kamphaus, Meegan Corchoran, Loren Tuttle, Croy Carlin and others too numerous to mention here). Without their help, we could have never have completed this important work. Primary support of the National Science Foundation for this project is gratefully appreciated.

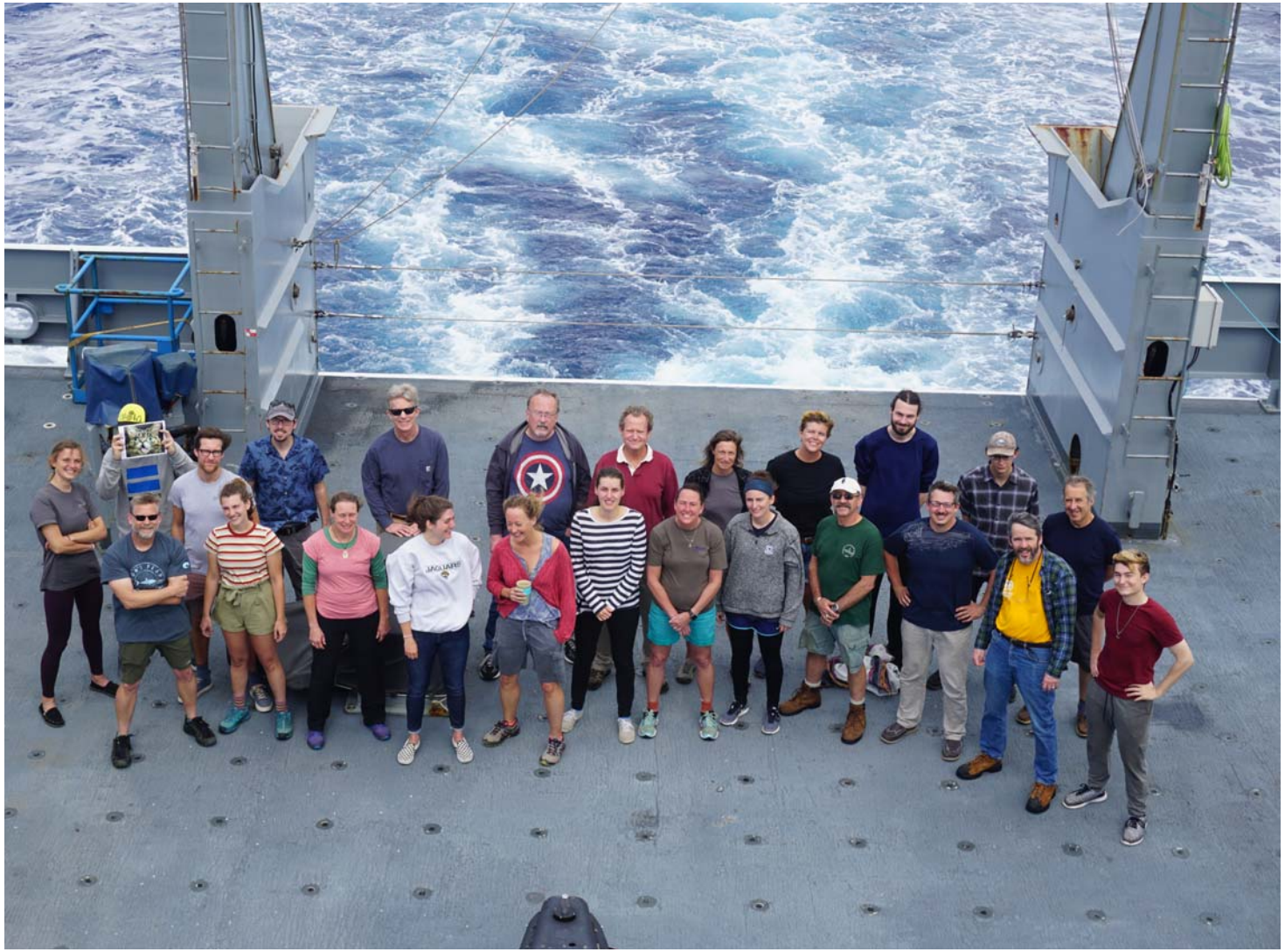

Fig 3- Science party of TN376 (front left to right) Loren Hearn, David Drapeau, Sydney Greenlee, Judith Murdoch, Kristy Dick, Rebecca Garley, Daniella Sturm, Marcy Train, Shannon Burns, Phil Altalo, Pete Morton, Barney Balch, Colin Fischer. (Back row, left to right) Matthew Enright, Zachary Anderson, John Ballard, Dennis McGillicuddy, Bruce Bowler, Fred Thwaites, Sara Rauschenberger, Julia Middleton, Joose DeVries, Andrew Hirzel, Colin Brownlee

Table 1- Science party participants of *R/V Thompson* and their affiliations/roles.

First Name	Last Name	Institution	Position
Phil	Alatalo	Woods Hole Oceanographic Inst. Woods Hole, MA, USA	Research Associate
Zachary	Anderson	Bermuda Inst. Of Ocean Sciences, Prince George, Bermuda	Marine Tech /ODF
William	Balch	Bigelow Laboratory for Ocean Sciences, East Boothbay, ME, USA	Chief Scientist/ Principal Investigator
John	Ballard	Scripps Inst. Of Oceangraphy, La Jolla, CA US	Marine Tech/Chemist
Bruce	Bowler	Bigelow Laboratory for Ocean Sciences, East Boothbay, ME, USA	Senior Res. Assoc.
Colin	Brownlee	Marine Biological Assn of the UK, Plymouth, UK	Principal Investigator
Shannon	Burns	Univ. South Florida, Saint Petersburg, FL, USA	Research Technician
Joost	de Vries	Marine Biological Assn of the UK, Plymouth, UK	Ph.D. Student
Kristie	Dick	Florida State University, Tallahassee	Undergrad Student
David	Drapeau	Bigelow Laboratory for Ocean Sciences, East Boothbay, ME, USA	Senior Res. Assoc.
Matthew	Enright	Bermuda Inst. Of Ocean Sciences, Prince George, Bermuda	Research Specialist
Colin	Fischer	Bigelow Laboratory for Ocean Sciences, East Boothbay, ME, USA	Research Technician
Rebecca	Garley	Bermuda Inst. Of Ocean Sciences, Prince George, Bermuda	Senior Res. Assoc.
Sydney	Greenlee	Colby College, Waterville, ME, USA	Undergrad Student
Lauren	Hearn	Florida State University, Tallahassee	Undergrad Student
Andrew	Hirzel	Woods Hole Oceanographic Inst. Woods Hole, MA, USA	Graduate Student
Dennis	McGillicuddy	Woods Hole Oceanographic Inst. Woods Hole, MA, USA	Principal Investigator
Julia	Middleton	Woods Hole Oceanographic Inst. Woods Hole, MA, USA	Graduate Student
Peter	Morton	Florida State University, Tallahassee	Principal Investigator
Judith	Murdoch	University of Otago, New Zealand	Research Technician
Jennifer	Nomura	Univ. Washington	Marine Tech
Sara	Rauschenberg	Bigelow Laboratory for Ocean Sciences, East Boothbay, ME, USA	Res. Assoc.
Elizabeth	Ricci	Univ. Washington	Marine Tech
Daniela	Sturm	Marine Biological Assn of the UK, Plymouth, UK	Ph.D. Student
Fred	Thwaites	Woods Hole Oceanographic Inst. Woods Hole, MA, USA	Senior Res. Assoc.
Marcia	Train	Long Island School, Maine	Teacher at Sea

Table 2- Summary of scientific deck operations performed during *R/V Thompson* #376.

Deck Operation	Number or duration of operations
1. CTD with 24x10L Niskin bottle samples; Full water casts (all biogeochemical variables,Nutrients, bottle oxygens, bottle salts)	53
2. CTD "trip on fly" casts for nutrients, salts	20
3. Trace metal casts using 5L TM clean Niskin bottles; Kevlar line	17
4. Trace metal-clean samples of surface water for carboy experiments	4
5. Underway DIC samples	
6. Underway surface samples for Chl, POC, PIC, BSi, FlowCAM, coccolith microscopy	95
7. Underway samples for photosynthetic parameters	
8. Number days for drogue deployment	18
9. VPR tows	14
10. Number of CTD casts with DAVPR	68
11. Samples processed for PAM photosynthesis properties from CTD casts	
12. Calcification/Productivity casts	16
13. Days continuous underway inherent optical property measurements	27.4
14. Days continuous bow mounted apparent optical measurements (daytime hours only when solar azimuth >20o)	27.4
15. Four-five-day Deck carboy experiments	4
16. Aerosol Samples for airborne particulate matter	27

References

Balch, W.M., Bates, N.R., Lam, P.J., Twining, B.S., Rosengard, S.Z., Bowler, B.C., Drapeau, D.T., Garley, R., Lubelczyk, L., Mitchell, C.E., Rauschenberg, S., 2016. Factors regulating the Great Calcite Belt in the Southern Ocean and its biogeochemical significance. Global Biogeochemical Cycles, doi: 10.1002/2016GB005414.

Sarmiento, J.L., Gruber, N., Brzezinski, M.A., Dunne, J.P., 2004. High-latitude controls of thermocline nutrients and low latitude biological productivity. Nature 427, 56-60.

Smith, H.E.K., Poulton, A.J., Garley, R., Hopkins, J., Lubelczyk, L.C., Drapeau, D., Rauschenberg, C., Twining, B., Bates, N.R., Balch, W.M., 2017. The contribution of mineralising phytoplankton to carbon export in the Great Calcite Belt. Biogeosciences 14, 4905–4925, https://doi.org/4910.5194/bg-2017-4110

TN376 VPR Team Cruise Report
Draft February 29, 2020

Dennis McGillicuddy
Phil Alatalo
Andrew Hirzel
Fred Thwaites

Contents

1. Summary of findings

Sampling on TN376 focused on two mesoscale features: a PIC-rich meander south of the Agulhas Front, and a cyclonic eddy to the north of it. Both features were sampled twice.

Meander survey 1	30 January – 4 February
Eddy 3 survey 1	5-8 February
Meander survey 2	16-21 February
Eddy 3 survey 2	22-26 February

In both cases, there were significant temporal changes in satellite-derived PIC: an increase in the meander, and a decrease in the eddy (note different color scales in the satellite images). These changes are accompanied by similar trends in total backscatter measured with the VPR.

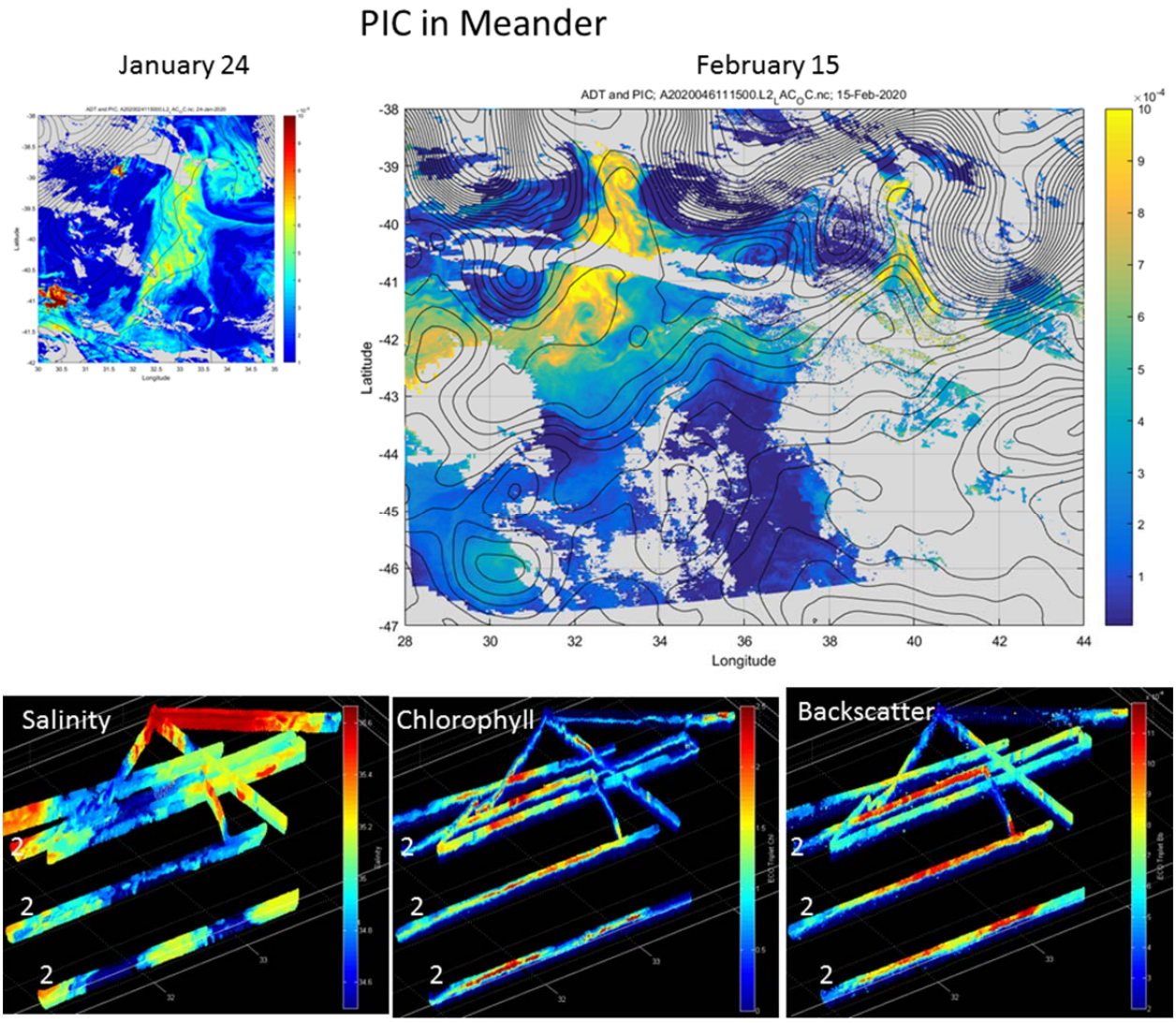

The three transect lines of Survey 2 are indicated by the numeral “2”; all other lines from Survey 1.

PIC in Eddy 3

February 4

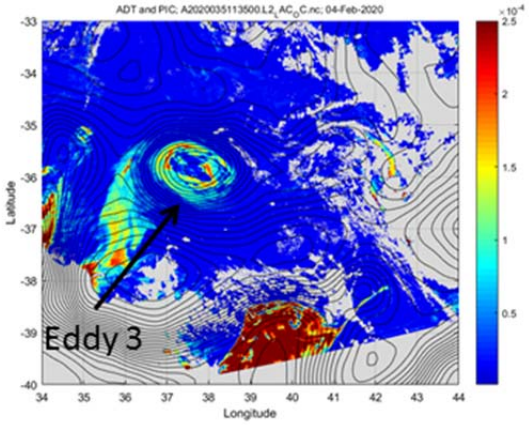

February 21

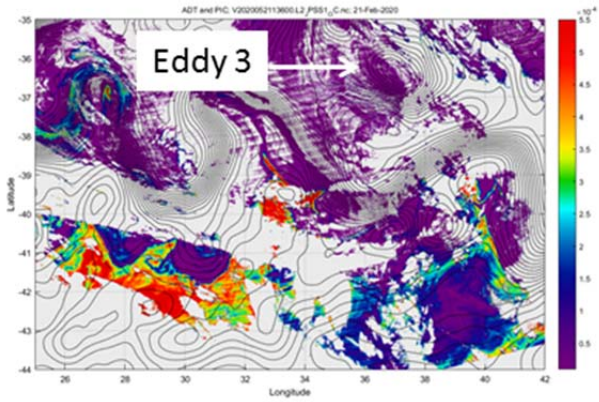

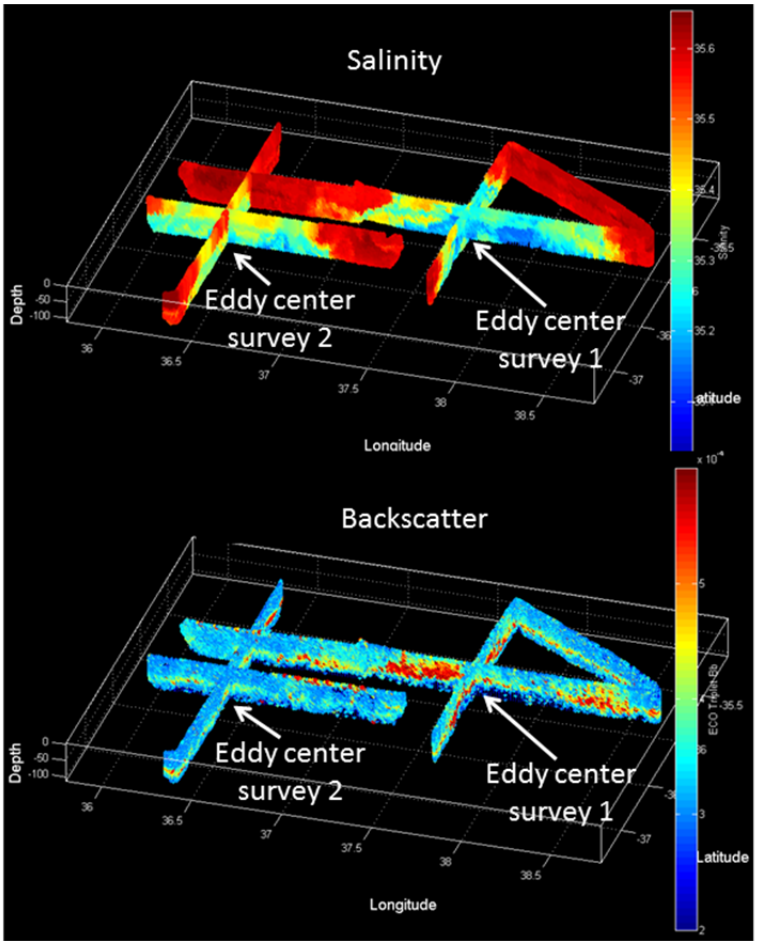

1.1 Meander Survey 1

This stanza of the cruise was inspired by satellite imagery from January 24 depicting an area of high chlorophyll and high particulate inorganic carbon (PIC) in a northward meander of the Southern Subtropical Front (SSTF) embedded within a meander of the Agulhas Front (AF) (Figure 1.1.1).

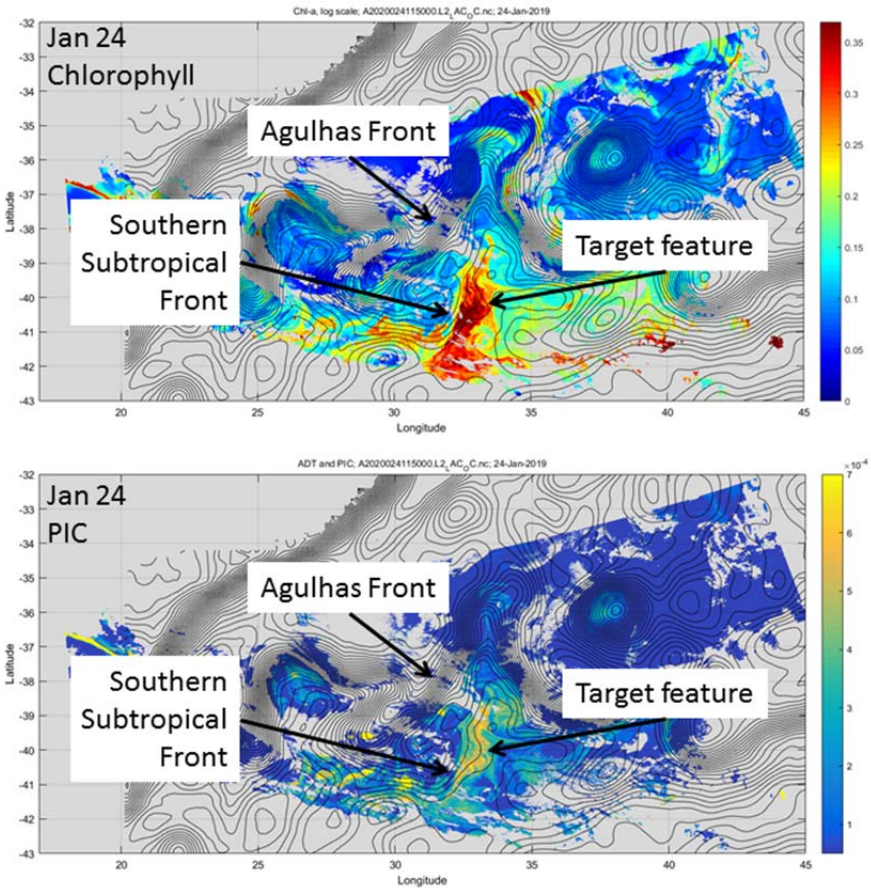

Figure 1.1.1 MODIS chlorophyll and PIC for 24 January 2020. Contours of absolute dynamic topography are overlayed.

Our initial survey focused on two main features of interest in the northern portion of the meander feature: an area of high chlorophyll and high PIC, referred to as “Eddy 1” which refers to the mesoscale character of this feature (Figure 1.1.2). Eddy 2 is a vortex like structure containing lower chlorophyll as well as appreciable backscatter. From January 24 to January 30 these features interact, with the northern limb of “Eddy 1” wrapping around the periphery of Eddy 2. Note that the apparent decrease/increase of chlorophyll/PIC is a result of changing colorbars between the upper and lower panels.

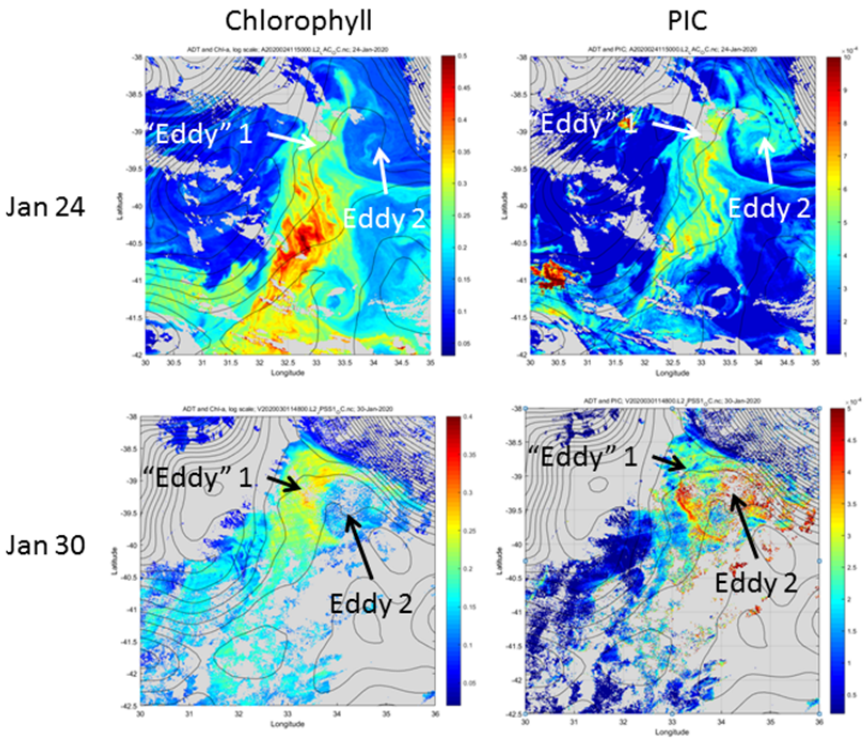

Figure 1.1.2: Chlorophyll (left) and PIC (right) images for January 24 and 30. Clouds obscured this region during the time period of *in situ* observations.

The altimetric history of this area (Figure 1.1.3) provides some context for the two eddies that we observed. In mid-October a meander system developed between 30 E and 34 E, leading to formation of a cyclone inside the northward meander pocket (presumable SAW) and an anticyclone to the south-southeast (October 25). By November 10, the cyclone had deepened and the vortex pair was oriented north-south. Their orientation then retrograded back northwest-southeast, with the cyclone splitting into two features and the anticyclone merging back into the Agulhas Front. On December 5, cyclone 2 and the remnant of the anticyclone were oriented north-northeast – south-southwest, and cyclone 1 had retreated farther northwest into the northward meander pocket. By December 24, cyclone 1 had pinched off into a new eddy north of the Agulhas Front, and the cyclone 2 / anticyclone pair was oriented almost east-west. On 8 January, the anticyclone began to merge with the Agulhas Front to the west, subsequently interacting with the Agulhas front to the east on 20 January. At the same time, cyclone C1 rejoins the Agulhas Front, drawing it northward, inducing flow northward up the eastern periphery of the deep meander stretching from 40S 30E to 36S 33E. That basic configuration of the meander system persisted through the time period of our observations from 30 January – 4 February (VPR) and 3-4 February (CTD). Although the general flow of in the vicinity of Eddy 1 and Eddy 2 is depicted by the altimetric fields, the detailed mesoscale and submesoscale characteristics are not resolved.

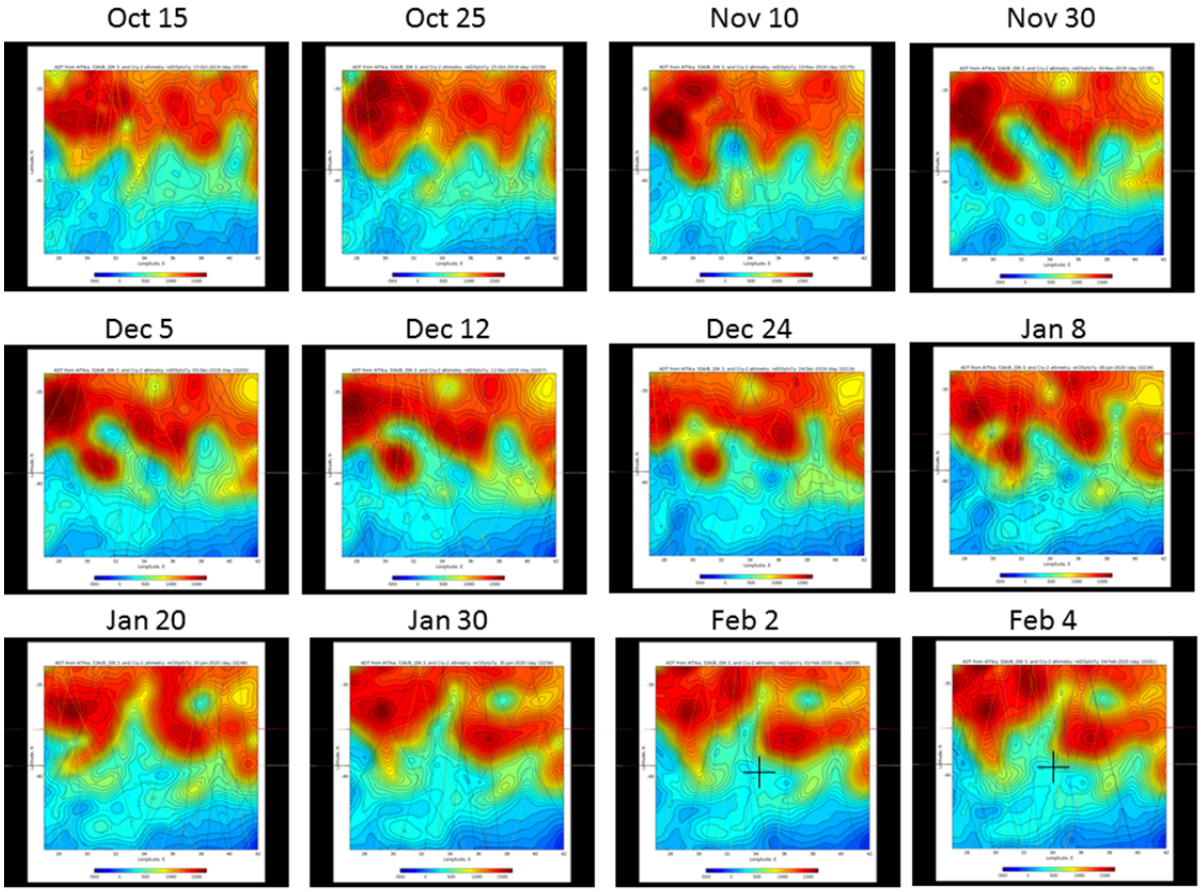

Figure 1.1.3. Time-series of absolute dynamic topography for the area of interest. The black cross in the last two panels provides the approximate position of the two CTD sections occupied on February 3-4.

Eddies 1 and 2 depicted in Figure 1.1.2 were sampled intensively from 30 January – 4 February (VPR) and 3-4 February (CTD). Joining the final portion of VPR2 with VPR3-7 provides a map of the survey region (Figure 1.1.4). Warm and salty waters of the Agulhas front are present in the northern and northeastern quadrant of the survey; they contain low fluorescence and low oxygen. High Chl / high Bb / high Bb' water is found in the cooler fresher waters in the western portion; this is also where the highest oxygen is found. To the east of that feature lies the saltier low Chl / high Bb / high Bb' eddy. Interestingly, the highest Bb' was found at the southernmost terminus of the north-south line. We also encountered lower salinity water with high Chl / high Bb / high Bb' on the eastern end of the survey, as the track passed out of the southward meander of the Agulhas front.

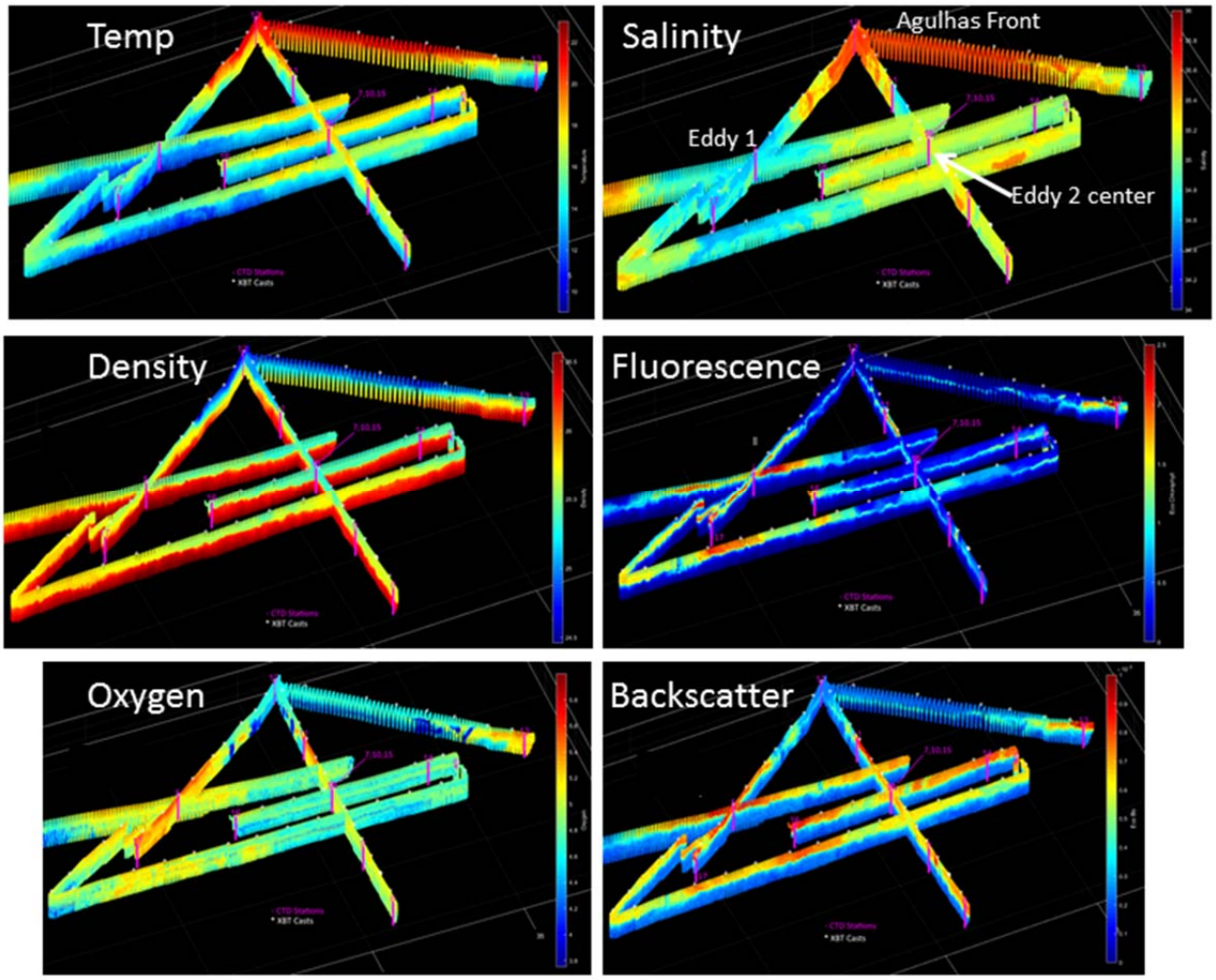

Figure 1.1.4 VPR surveys 2-7 combined. CTD stations and XBT locations indicated by magenta lines and asterisks, respectively.

The VPR surveys were used to orient CTD transects in the north-south (transect 2) and east-west (transect 3) directions (Figure 1.1.5,6; Table 1.1.1). The northern end of transect 2 (station 12) shows the depression of the thermocline in association with the Agulhas Front. Station 11 contains high-chlorophyll water apparently associated with the limb of Eddy 1 wrapping around the northern periphery of Eddy 2. The center of eddy 2 is clearly depicted at station 10 with uplift of the seasonal thermocline, which is confined mostly to the upper 400 m. Isotherms below that are comparatively flat, especially to the south.

Transect 3 shows Eddy 2 center located at station 15 where surface fluorescence is at a minimum, flanked by higher values to both the east and west. The low salinity water of Eddy 1 (station 17) contains the highest surface chlorophyll and highest oxygen. Interleaving of these two water masses is evident at the boundary between these two water masses (station 16). Eddy 2 center is located at station 15, flanked at station 14 which contains low salinity high chlorophyll water which may be the southward extent of the Eddy 1 limb wrapping around the northern portion of Eddy 2.

Transect	Station	Feature / comments
2	12	AF, depressed thermocline, low fluorescence, low oxygen
	11	High chlorophyll limb of Eddy 1 wrapping around Eddy 2
	10	Eddy 2 center
	9	Eddy 2 periphery
	8	
3	17	Eddy 1
	16	Eddy 1, Eddy 2 boundary – interleaving
	15	Eddy 2 center
	14	Eddy 2 periphery; interleaving; Eddy 1 wrap-around?
	13	Outside Eddy 2

Table 1.1.1. Station list for CTD transects 2 and 3.

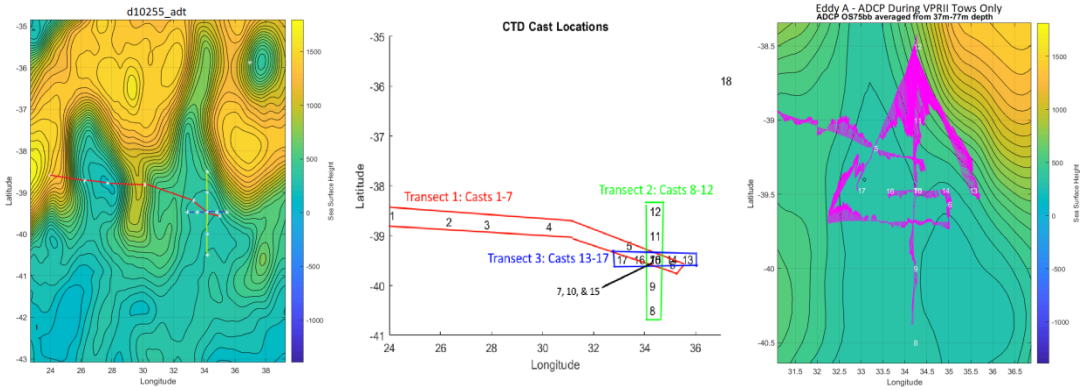

Figure 1.1.5 CTD transect and station locations (middle) overlayed on absolute dynamic topography (left) and 37-77m ADCP currents (right).

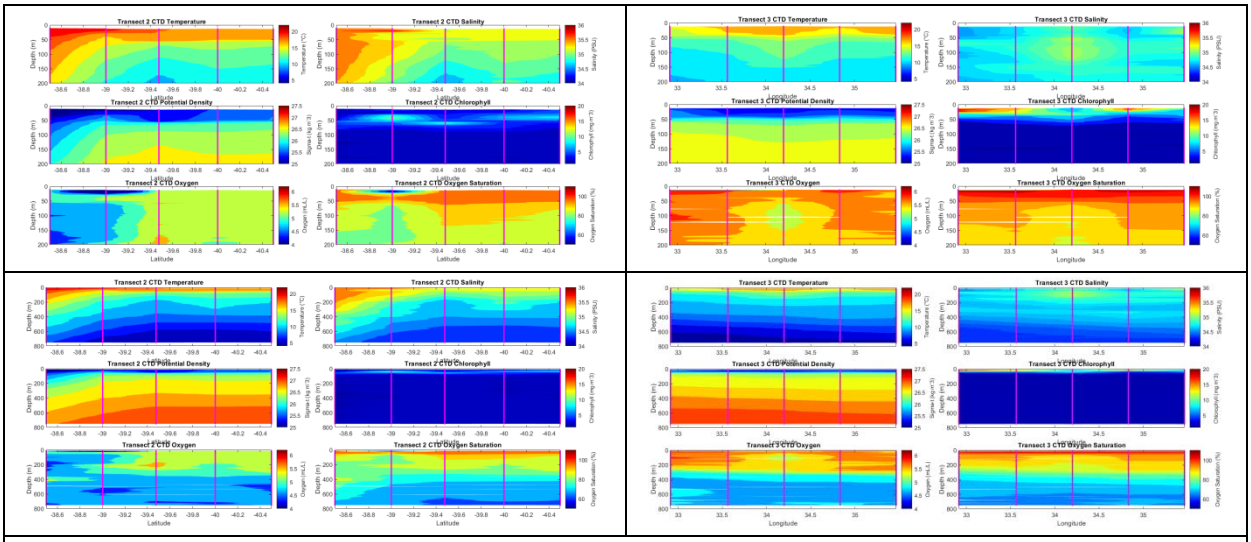

Figure 1.1.6. CTD transects 2 (left) and 3 (right). Upper panels 0-200m, lower panels 0-800m.

CTD data reveal water mass characteristics (Figure 1.1.7) consistent with those described by Gordon et al. (1987): end members consisting of Antarctic Intermediate Water (AAIW), Subtropical Surface Water (STSW), with mixing in between them to create South Indian Central Water (SICW). SAMW falls within the SICW envelope, although from the profile data it does not appear the survey captures much if any of that water mass—at least in terms of a thermostad / pycnostad.

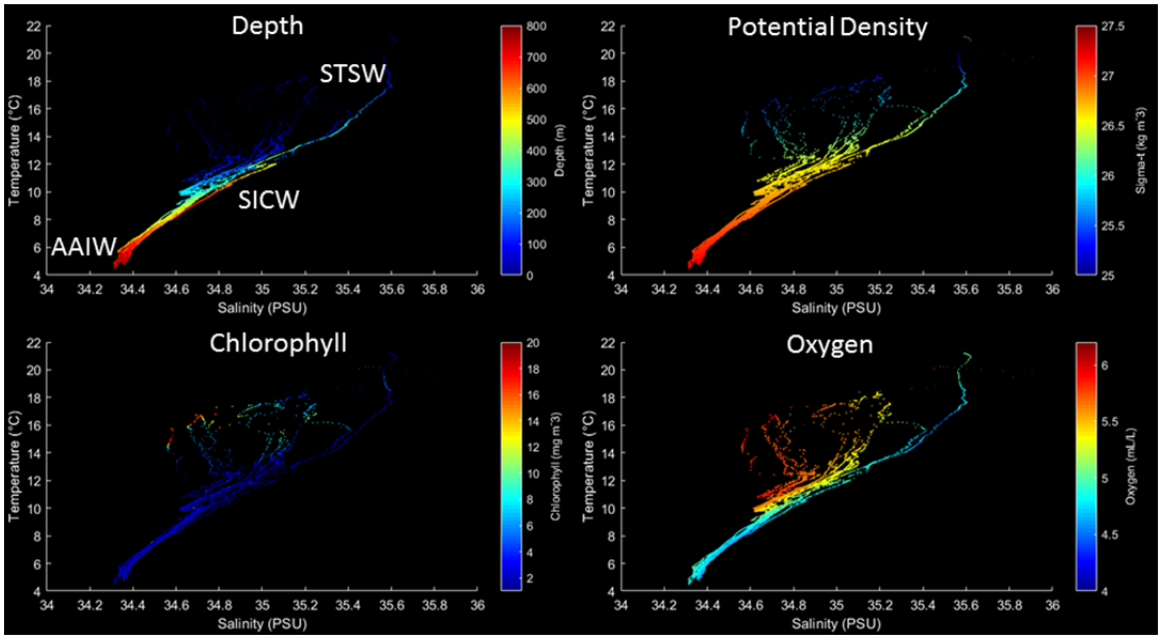

Figure 1.1.7. Depth, potential density, chlorophyll (fluorescence), and oxygen from CTDs 5-18 plotted in temperature-salinity space.

Merging of the CTD and VPR data in T-S space provides more extensive coverage of the upper water column (Figure 1.1.8).

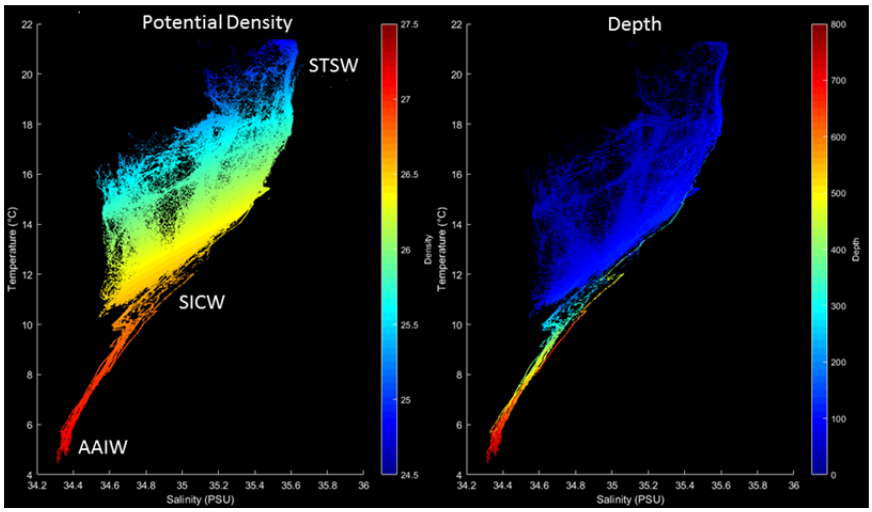

Figure 1.1.8. Potential density and depth from CTDs 5-18 and VPR tows 2-7 plotted in temperature-salinity space.

Zooming in on the VPR portion (Figure 1.1.9) facilitates delineation of the water masses associated with Eddies 1 (high chlorophyll / high Bb) and 2 (low chlorophyll / high Bb).

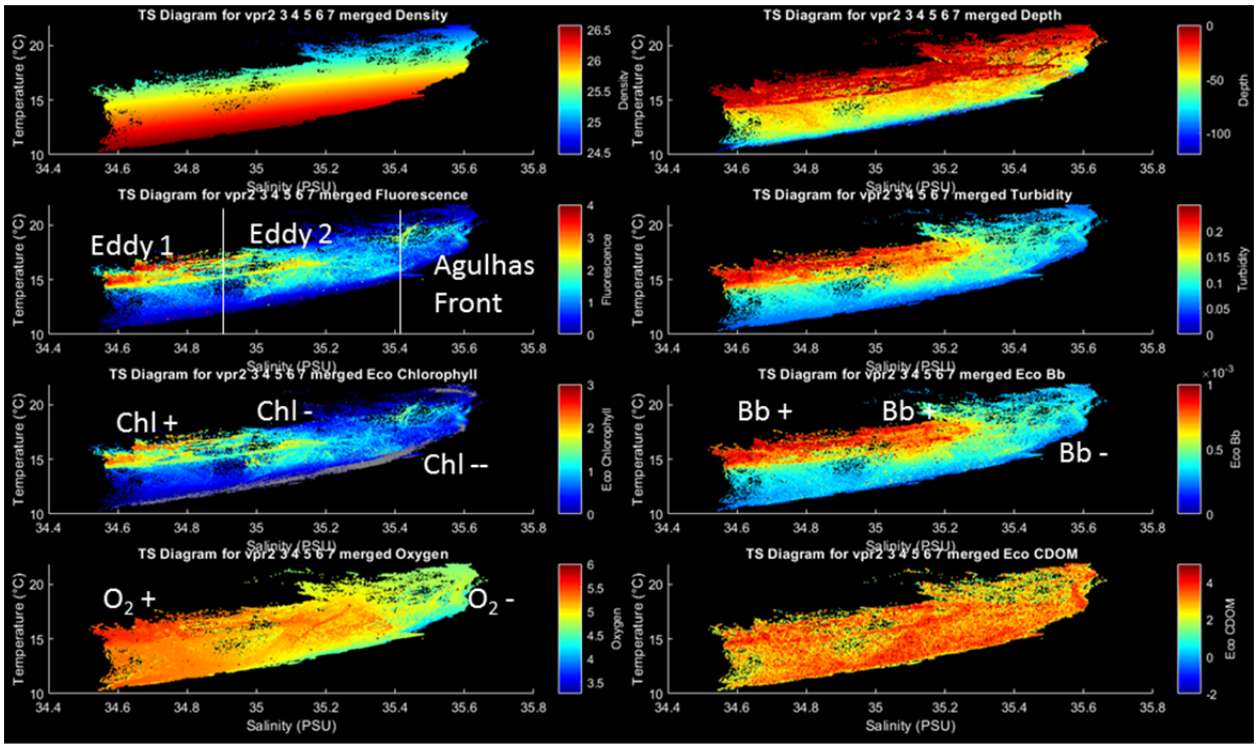

Figure 1.1.9. Potential density, depth, chlorophyll (fluorescence), turbidity, chlorophyll (fluorescence from Eco triplet), backscatter (from Eco triplet), oxygen, and CDOM (from Eco triplet) from VPR tows 2-7 plotted in temperature-salinity space.

Belkin and Gordon (1996) provide some guidance for categorization of the upper ocean water masses sampled in the VPR surveys (Figure 1.1.9). Their Tables 3, 6, and 10 report ranges for surface salinity in the SAF, SSTF, and AF respectively. One can infer that the surface waters in between the fronts are comprised of salinities falling in between the specified ranges (Table 1.1.2). In that context, Eddies 1 and 2 can be characterized as SAW and SSTW, respectively; they are bounded by AF water.

SAF		SSTF		AF	
33.88	34.6	34.30	35.18	35.39	35.54
	SAW		SSTW		

Table 1.1.2. Surface salinity ranges for the Subantarctic Front (SAF), South Subtropical Front (SSTF), and Agulhas Front (AF) from Belkin and Gordon (1996). Surface salinities for Subantarctic Water (SAW) and South Subtropical Water (SSTW) are inferred as bracketed by the frontal ranges.

1.2 Meander Survey 2

Our second visit to the SSTF meander targeted 3 zonal sections across the high chl / high PIC feature, which appears to have intensified since our prior occupation (Figure 1.2.1).

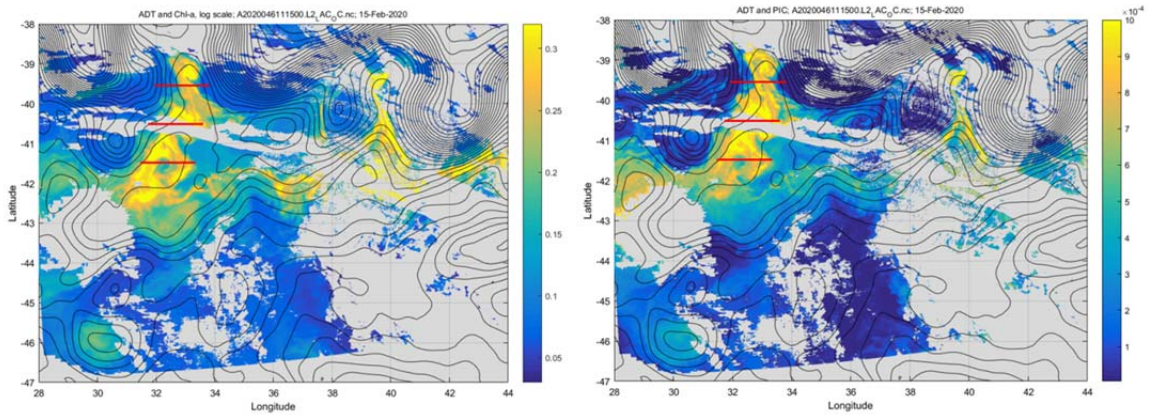

Figure 1.2.1: Chlorophyll (left) and PIC (right) images for January 24 and 30. Clouds obscured this region during the time period of *in situ* observations.

ADCP observations depict the northward flow on the western flank of the meander and southward flow on the eastern flank (Figure 1.2.2).

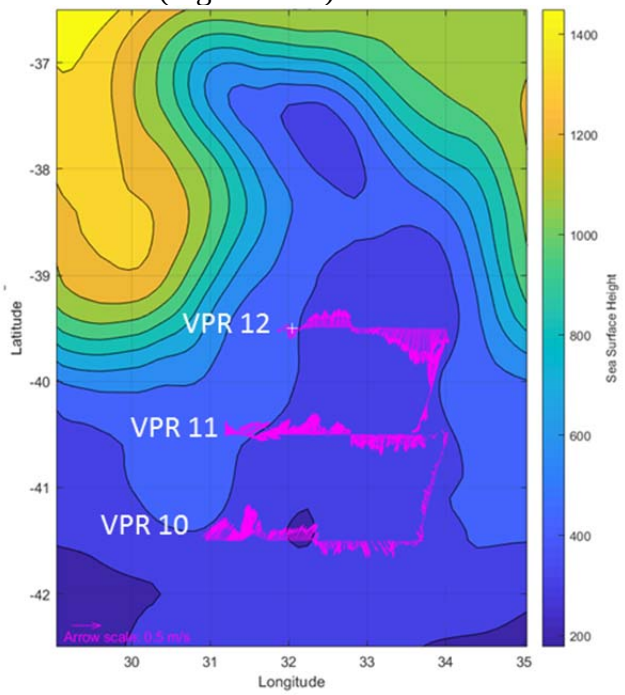

Figure 1.2.2. ADCP currents (37-77m) from VPR tows 10, 11, and 12 overlayed on absolute dynamic topography.

Combining VPR tows 10, 11, and 12 provides a view into the hydrographic and bio-optical structure of the meander (Figures 1.2.3 and 4). In general, the cooler and fresher waters in the

core of the meander contain higher chlorophyll and backscatter (HPCLS); this core is flanked by warmer waters of intermediate (moderate) salinity, lower chlorophyll, and high PIC (HPLCMS). The periphery of the meander is delineated by warmer and saltier waters that are low in both chlorophyll and PIC (LPCHS). These labels are added to a duplicate view of salinity field (Figure 1.2.4, top panel) for clarity.

LPCHS waters of the western periphery of the meander are captured in all three tows, whereas these waters were only encountered once on the eastern side, in between VPR11 and VPR12. Note that the HPCLS waters in the interior of VPR10 are interrupted by the HPLCMS waters of Eddy 4, clearly visible in the satellite images of chlorophyll and PIC (Figure 1.2.1).

The three biogeographic regions described above (HPCLS, HPLCMS, LPCHS) are clearly discernible in temperature salinity space (Figure 1.2.5).

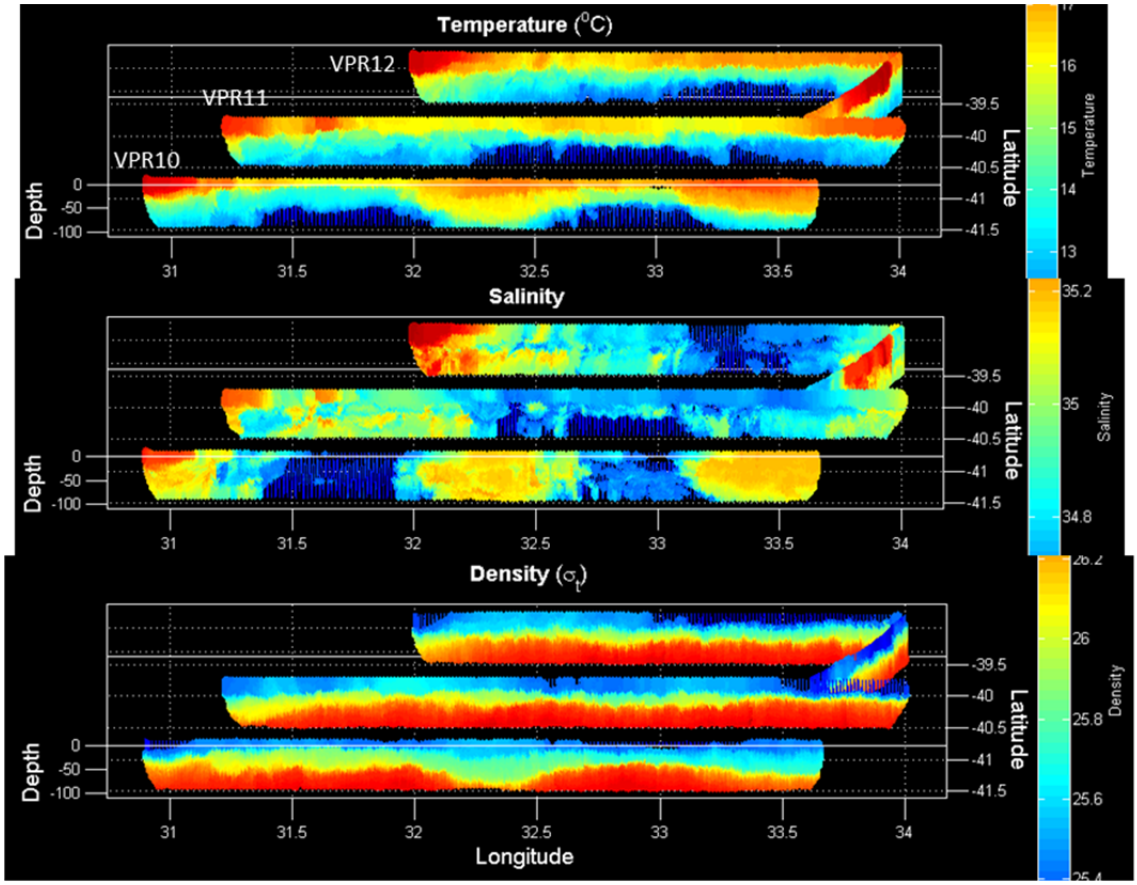

Figure 1.2.3 VPR surveys 10, 11, and 12 combined. CTD stations and XBT locations indicated by magenta lines and asterisks, respectively.

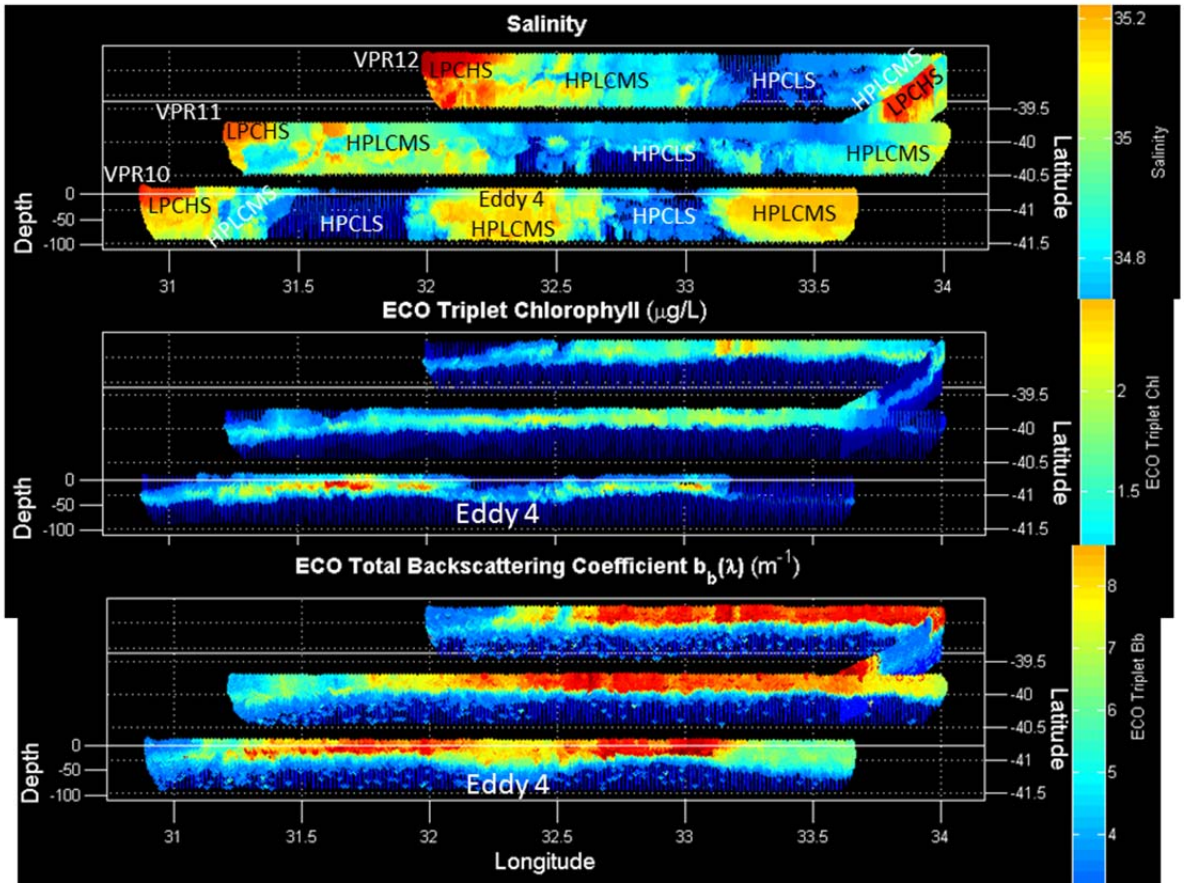

Figure 1.2.4 VPR surveys 10, 11, and 12 combined. Note the salinity field from Figure 1.2.3 is repeated here with water mass labeling (see text). CTD stations and XBT locations indicated by magenta lines and asterisks, respectively.

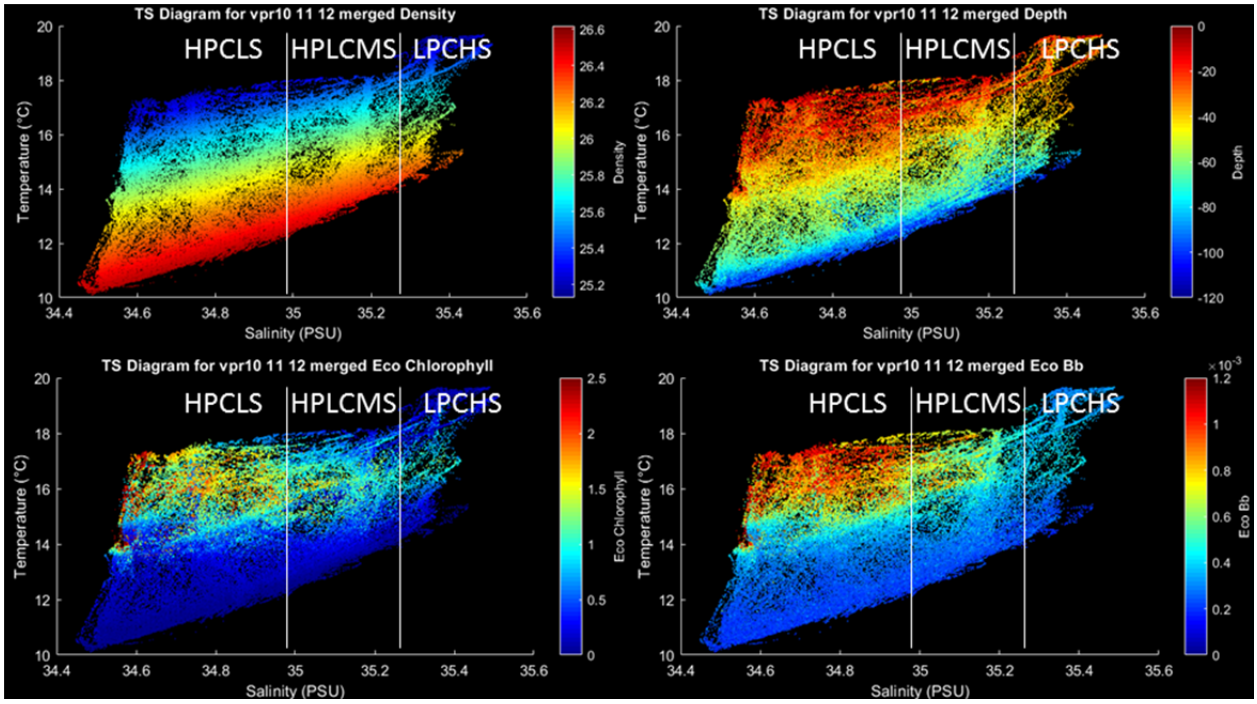

Figure 1.2.5. Potential density, depth, chlorophyll (fluorescence from Eco triplet), and backscatter (from Eco triplet), from VPR tows 10-12 plotted in temperature-salinity space. Salinity ranges for the three biogeographic regimes indicated by white vertical bars: high PIC / high Chl / low salinity (HPCLS), high PIC / low Chl / moderate salinity (HPLCMS), and low PIC / low Chl / high salinity (LPCHS).

Three CTD transects across the meander feature were collocated with the VPR lines (Figure 1.2.6), with station positions informed by the VPR observations (Table 1.2.1). The meander structure is manifested in the CTD data as upward domain of the thermocline, halocline, and pycnoline, centered at 33.4 E (station 49) in the northern transect and 32.8 E (station 40) in the middle transect. In the southern transect, the core of the meander structure is interrupted by Eddy 4, characterized by upward doming of the main pycnocline and depression of the seasonal pycnocline. This “mode-2” or “cyclonic thinny” structure creates anomalies of opposing signs in near-surface and deep ocean temperature, salinity, and oxygen saturation. As expected from the satellite image (Figure 1.2.1), chlorophyll in the eddy core is quite low.

Transect	Station	Feature / comments
6	26	Western periphery outside feature
	27	Frontal boundary - nutrients only
	28	Frontal boundary – PP cast, TM cast, incubation water collection
	29	HPCLS – nutrients only
	30	Eddy 4: Low PIC, low chlorophyll, high salinity (LPCHS)
	31	Frontal boundary
	32	HPCLS
	33	East of frontal boundary with HPCLS
	34	Eastern periphery outside feature (no DAVPR)
7	35	Western periphery outside feature

	36	Frontal boundary – WS over CF submesoscale feature
	37	HPLCMS
	38	Frontal boundary – nutrients only
	39	HPCLS - PP cast, TM cast, incubation water collection
	40	Center of HPCLS – nutrients only
	41	HPCLS
	42	HPLCMS
	43	HPLCMS
8	44	Western periphery outside feature
	45	Frontal boundary – WS over CF submesoscale feature
	46	HPLCMS
	47	HPLCMS
	48	HPCLS - PP cast, TM cast [peak chl, Bb]
	49	Center of HPCLS – nutrients only
	50	HPCLS
	51	HPLCMS
	52	HPLCMS

Table 1.2.1. Station list for CTD transects 6-8 across the high PIC / high chlorophyll feature.

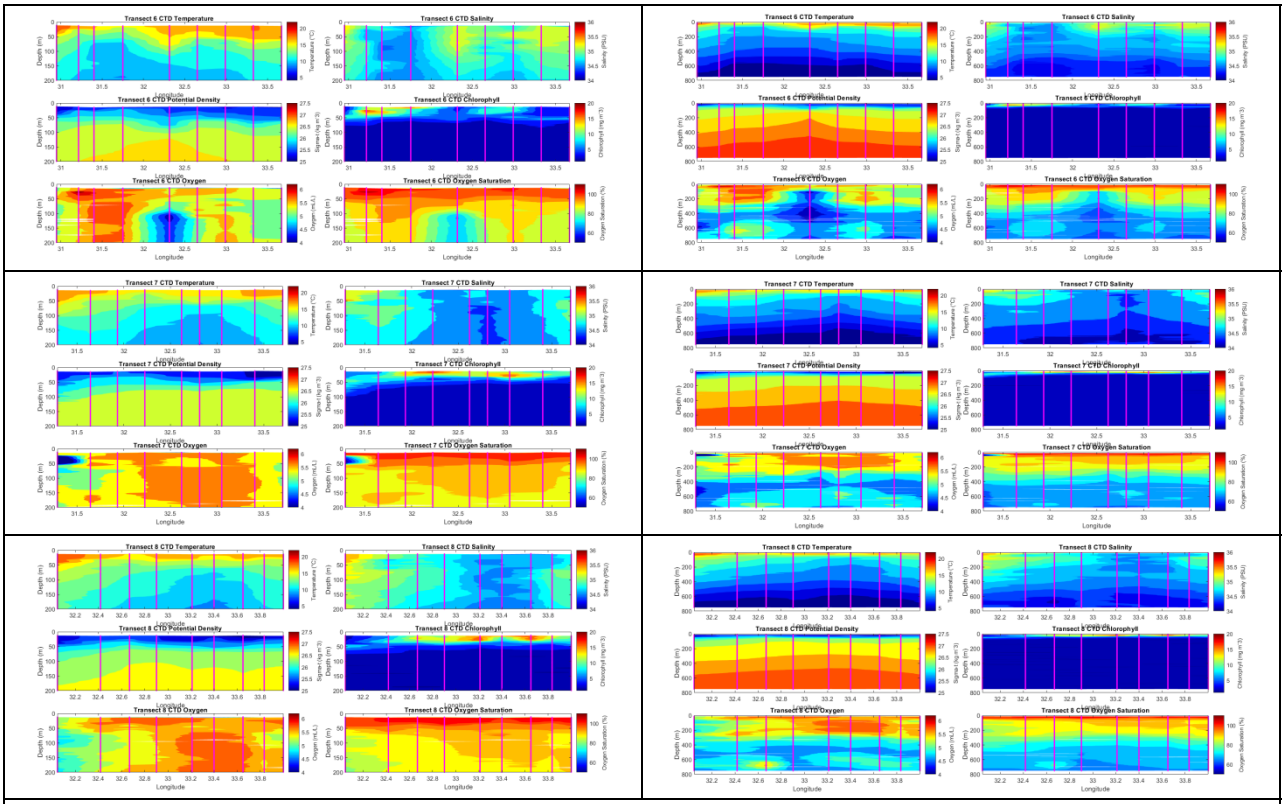

Figure 1.2.6. CTD transects 6 (top), 7 (middle), and 8(bottom). Left column 0-200m, right column 0-800m.

Overall, water mass characteristics of the second survey were similar to that of the first, although a slightly broader region of T-S space was observed (Figure 1.2.7).

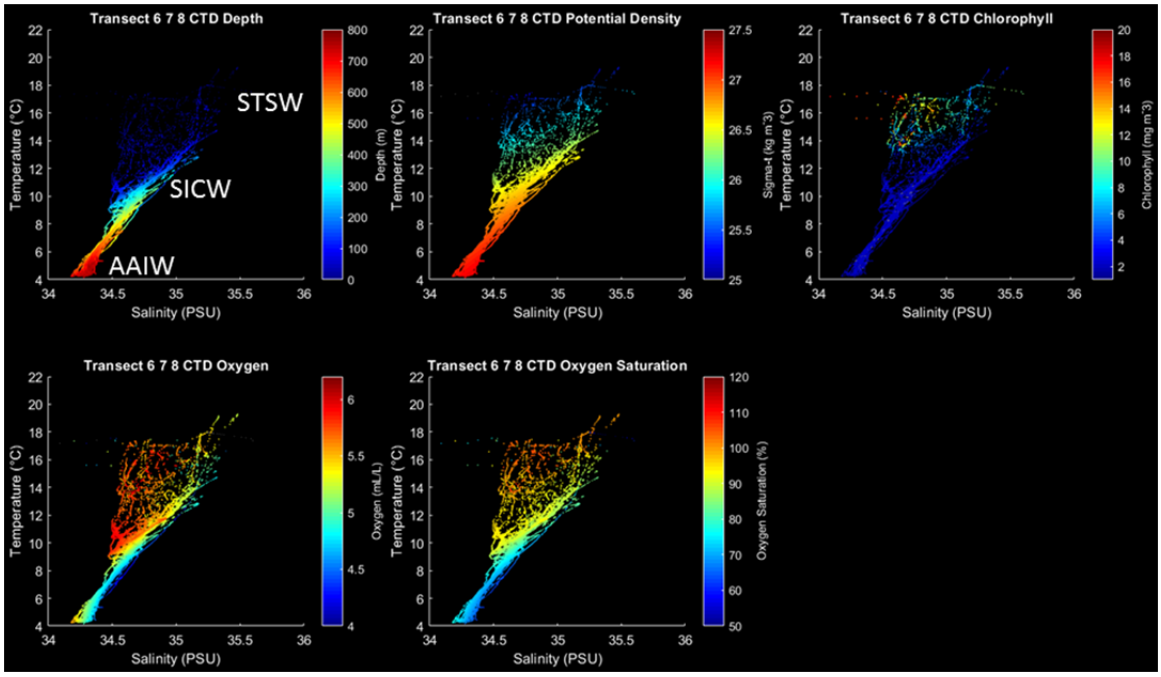

Figure 1.2.7. Depth, potential density, chlorophyll (fluorescence), oxygen, and oxygen saturation from transects 6-8 (stations 26-52) plotted in temperature-salinity space.

Merging of the CTD and VPR data in T-S space provides more extensive coverage of the upper water column (Figure 1.2.8).

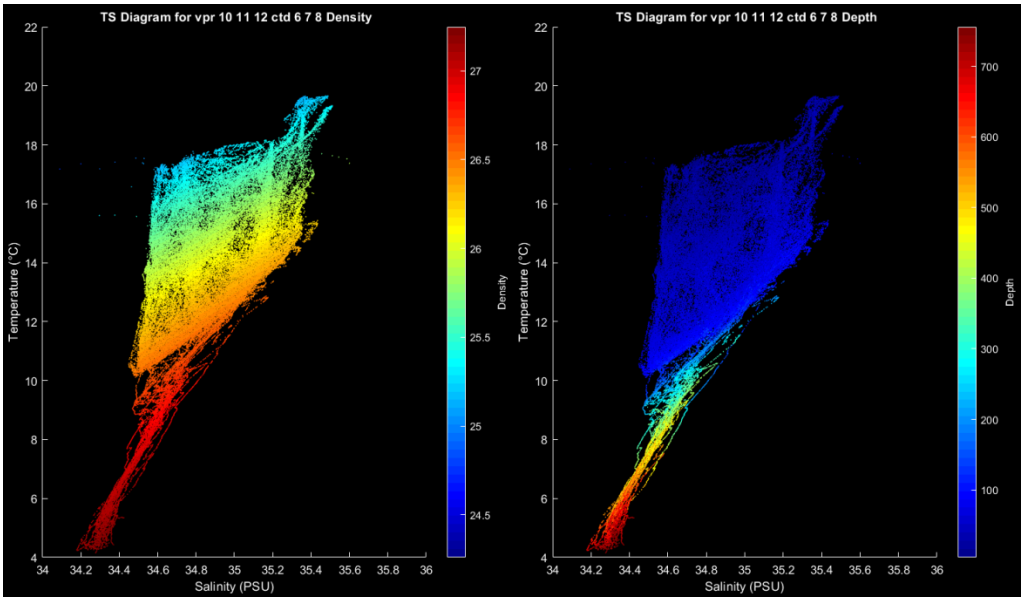

Figure 1.2.8. Potential density and depth from transects 6-8 (stations 26-52) and VPR tows 10-12 plotted in temperature-salinity space.

MODIS and VIIRS images from 16 February (Figure 1.2.9) indicate that the southern terminus of the high chlorophyll / high PIC feature meander appears to be connected to the SSTF, with high chlorophyll and high PIC extended well east of our present position. Thus what we have observed here may be generalizable over a much larger area.

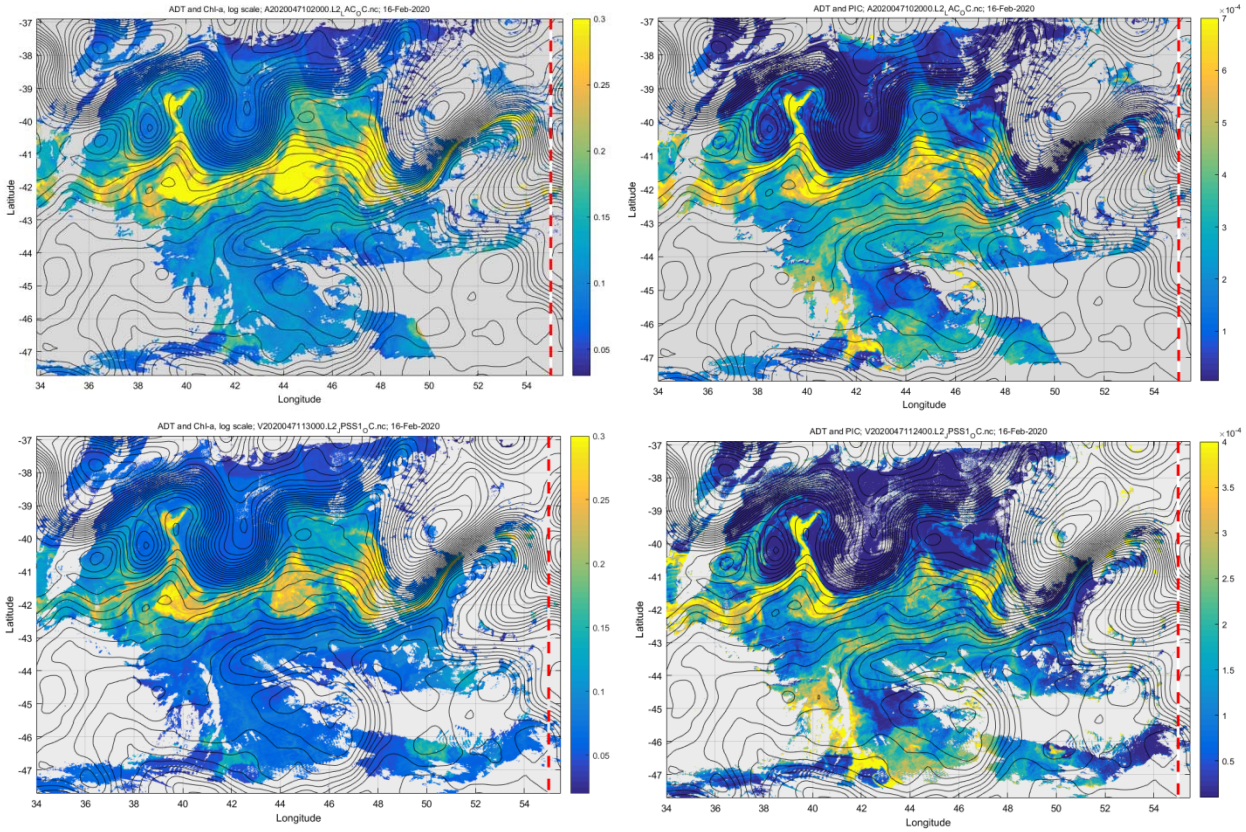

Figure 1.2.9. MODIS (top) and VIIRS (bottom) chlorophyll (left) and PIC (right) for 16 February 2020. Contours of ADT overlayed.

1.3 Eddy 3 Survey 1

This stanza of the cruise was motivated by an image from February 4 (Figure 1.3.1) depicting a ring of enhanced PIC in a ring around the center of a cyclonic eddy pinched off from a meander of the Agulhas Front (Figure 1.3.2). From February 4 to February 5, the amplitude of the PIC ring decreased, although these two images come from two different sensors (MODIS on February 4 and VIIRS on February 5).

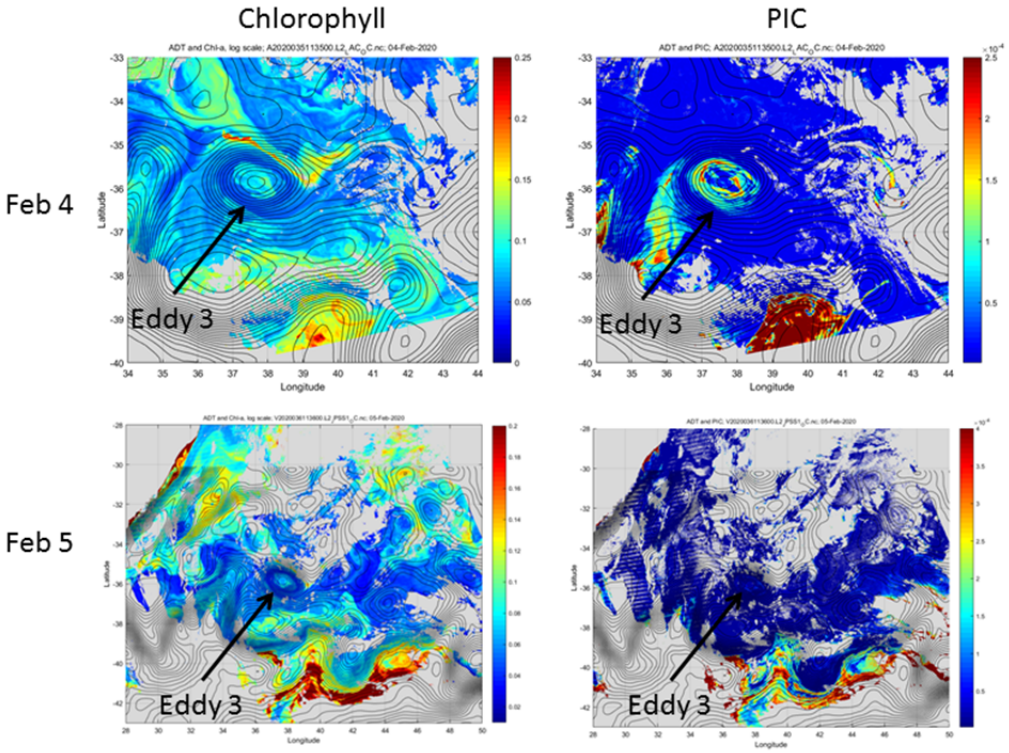

Figure 1.3.1: Chlorophyll (left) and PIC (right) images for February 4 and 5.

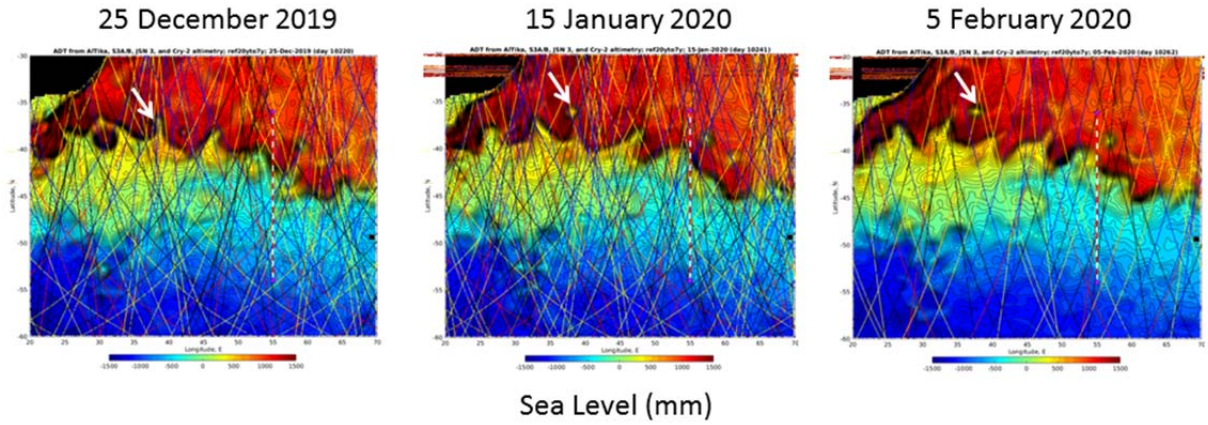

Figure 1.3.2. Time-series of absolute dynamic topography illustrating the formation of Eddy 3.

VPR surveys 8 and 9 (Figure 1.3.3) were used to orient CTD transects (Figure 1.3.4) in the north-south (transect 4) and east-west (transect 5) directions (Table 1.3.1).

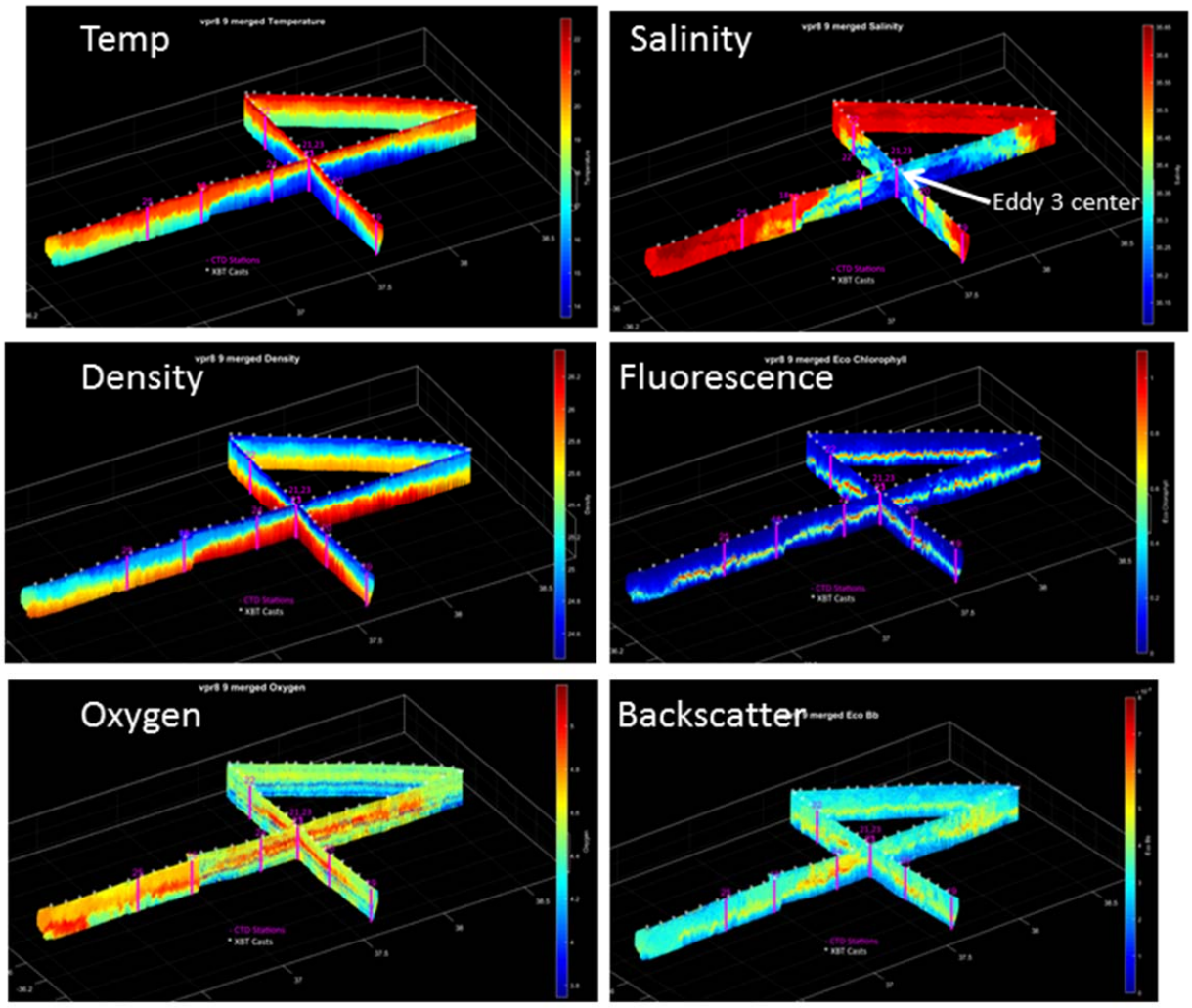

Figure 1.3.3 VPR surveys 8 and 9 combined. CTD stations and XBT locations indicated by magenta lines and asterisks, respectively.

Weather conditions precluded occupying the northernmost station planned for transect 4, as well as the two stations east of Eddy 3 center planned for transect 5. We distinguished between "inner periphery" and "outer periphery" stations in an attempt to resolve the band of high PIC present in the former; we expected to see low PIC at eddy center as well as in the outer periphery.

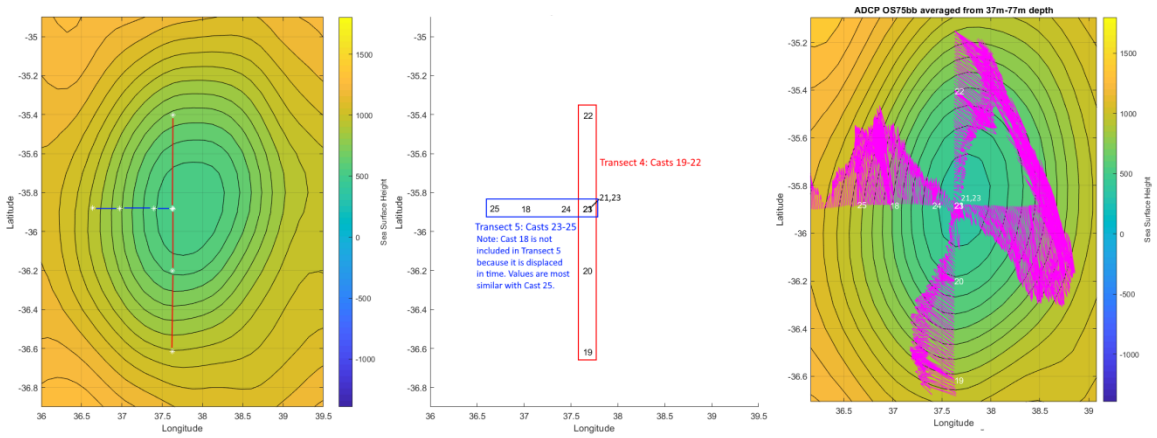

Figure 1.3.4 CTD transect and station locations (middle) overlayed on absolute dynamic topography (left) and 37-77m ADCP currents (right).

Upward doming of the pycnocline is evident at Eddy 3 center (stations 21, 23), with steeper sloping isopycnals to the north than to the south (Figure 1.3.5). Waters of the inner core are clearly fresher than the surroundings, consistent with Eddy 3 being a ring pinched off of the Agulhas Front comprised of SSTW. In contrast to Eddies 1 and 2, Eddy 3 extends well into the main thermocline.

The inner periphery station to the west of eddy center (station 24) was much closer to eddy center than those in the north-south section (stations 20 and 22), reflecting asymmetry of the band of high backscatter (Figure 1.3.1) and PIC surrounding eddy center. Interleaving of water masses between the inner periphery and eddy center is evident in the 0-200m salinity distribution at station 24 (Figure 1.3.5).

Transect	Station	Feature / comments
[5]	18	Eddy 3 periphery; water drawn for incubation experiments
4	19	Eddy 3 outer periphery
	20	Eddy 3 inner periphery
	21	Eddy 3 center
	22	Eddy 3 periphery
5	23	Eddy 3 center
	24	Eddy 3 inner periphery; interleaving
	18	Eddy 3 inner/outer periphery; water drawn for incubation experiments
	25	Eddy 3 outer periphery

Table 1.3.1. Station list for CTD transects 4 and 5.

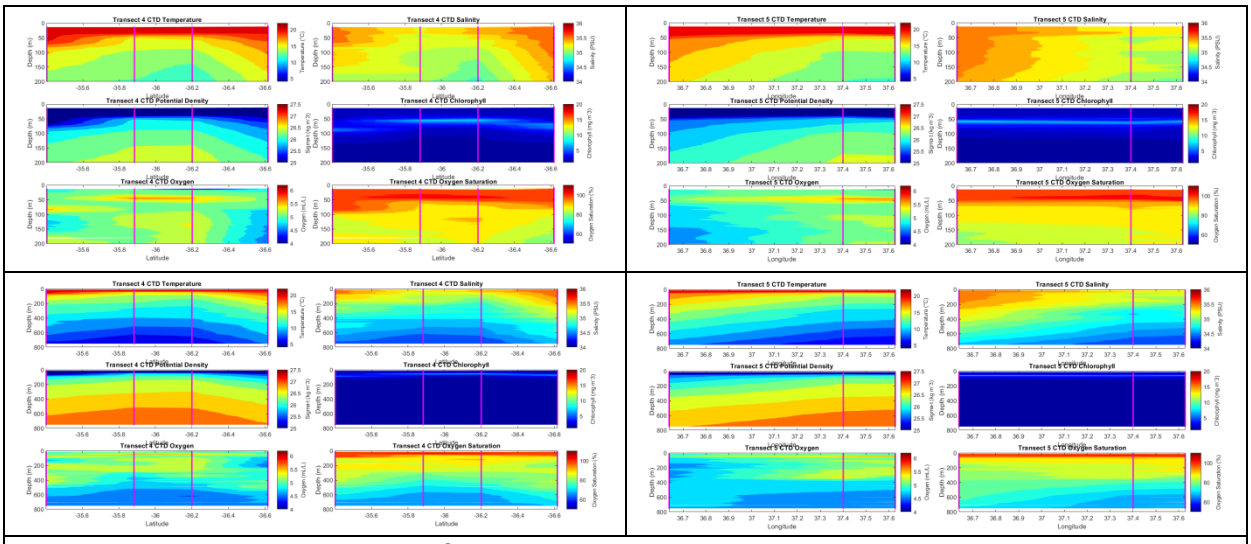

Figure 1.3.5. CTD transects 4 (left) and 5 (right). Upper panels 0-200m, lower panels 0-800m.

Water mass characteristics of the Eddy 3 CTD survey (Figure 1.3.6) are generally similar to that of the Eddy 1 and 2 survey, as described by Gordon et al. (1987): AAIW, STSW, and SICW.

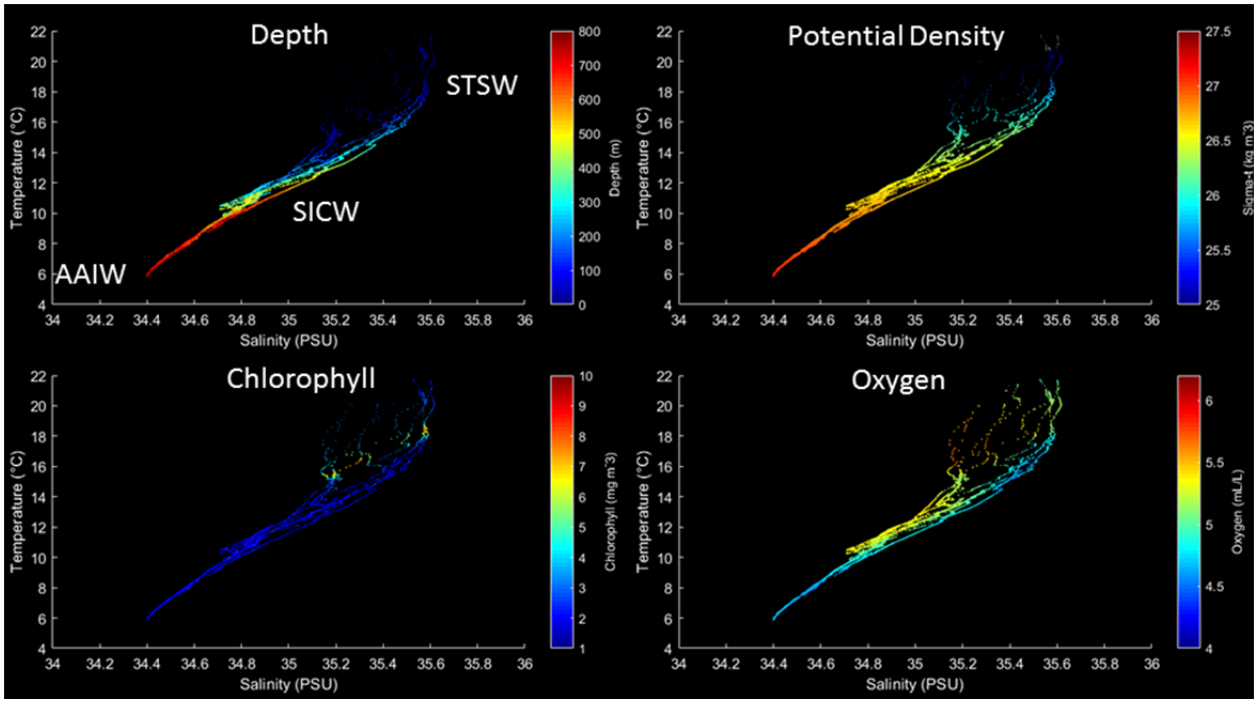

Figure 1.3.6. Depth, potential density, chlorophyll (fluorescence), and oxygen from CTDs 19-25 plotted in temperature-salinity space.

Merging of the CTD and VPR data in T-S space provides more extensive coverage of the upper water column (Figure 1.3.7).

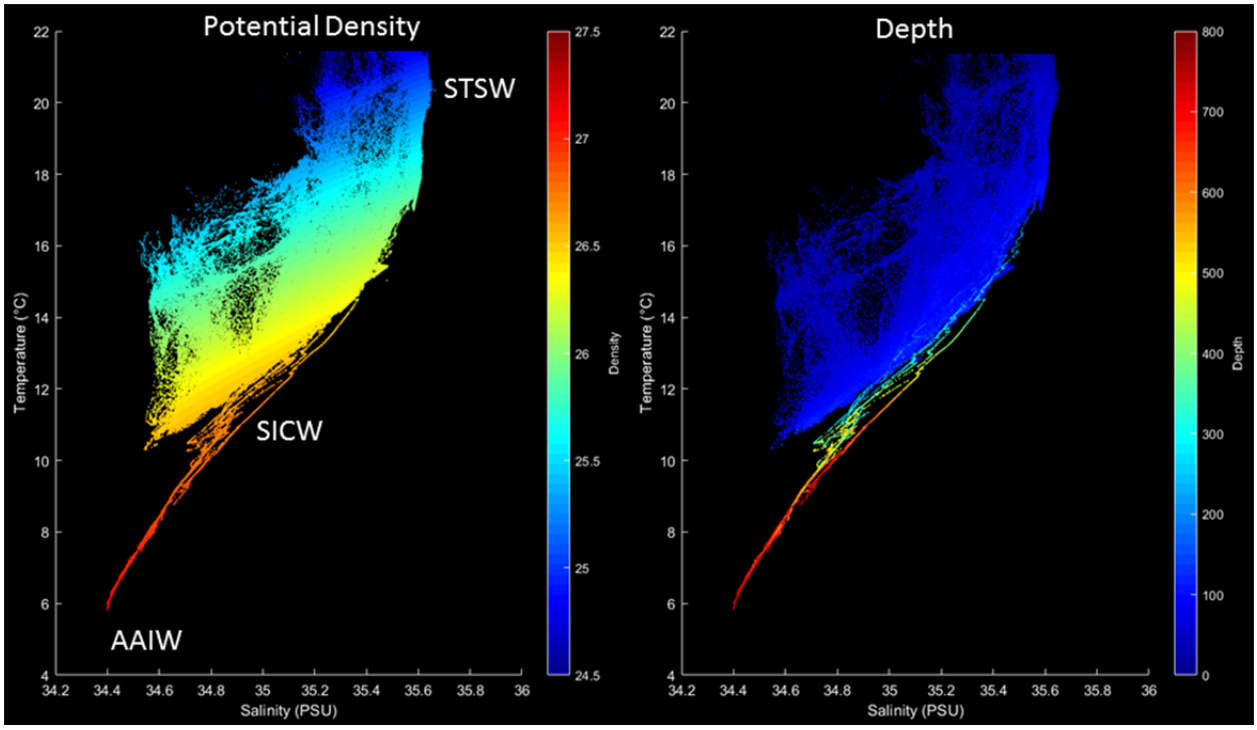

Figure 1.3.7. Potential density and depth from CTDs 19-25 and VPR tows 8-9 plotted in temperature-salinity space.

Zooming in on the VPR portion (Figure 1.3.8) illustrates the details of the eddy structure.

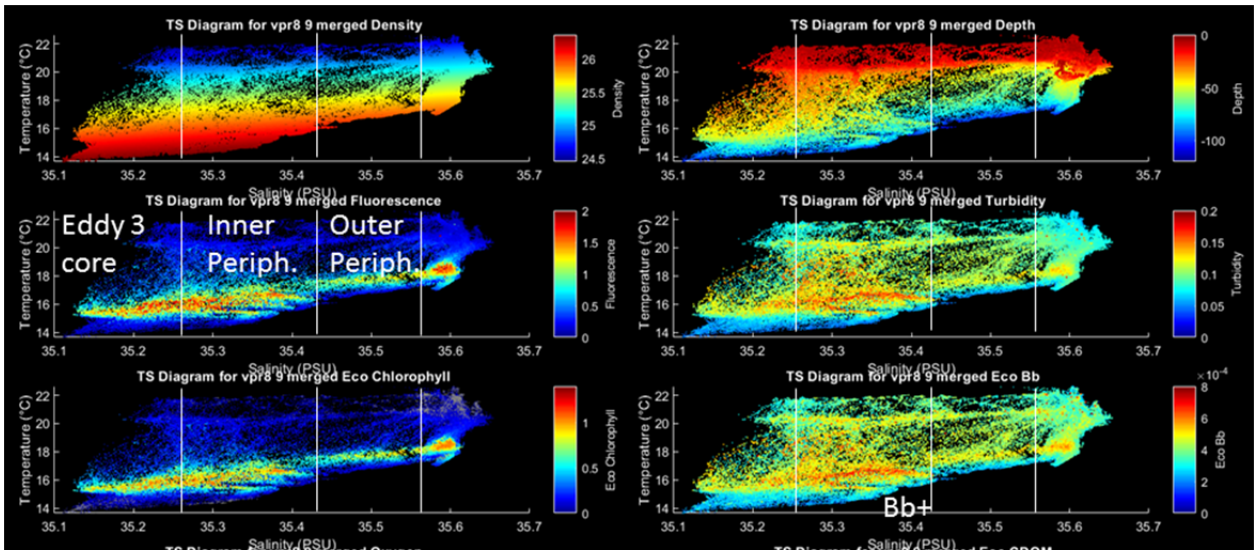

Figure 1.3.8. Potential density, depth, chlorophyll (fluorescence), turbidity, chlorophyll (fluorescence from Eco triplet), backscatter (from Eco triplet), oxygen, and CDOM (from Eco triplet) from VPR tows 8-9 plotted in temperature-salinity space.

Comparing the T-S distributions from the Eddy 1 & 2 survey with that of Eddy 3, it is clear that the core of eddy 3 water is comprised of SSTW rather than SAW (Figure 1.3.9,10).

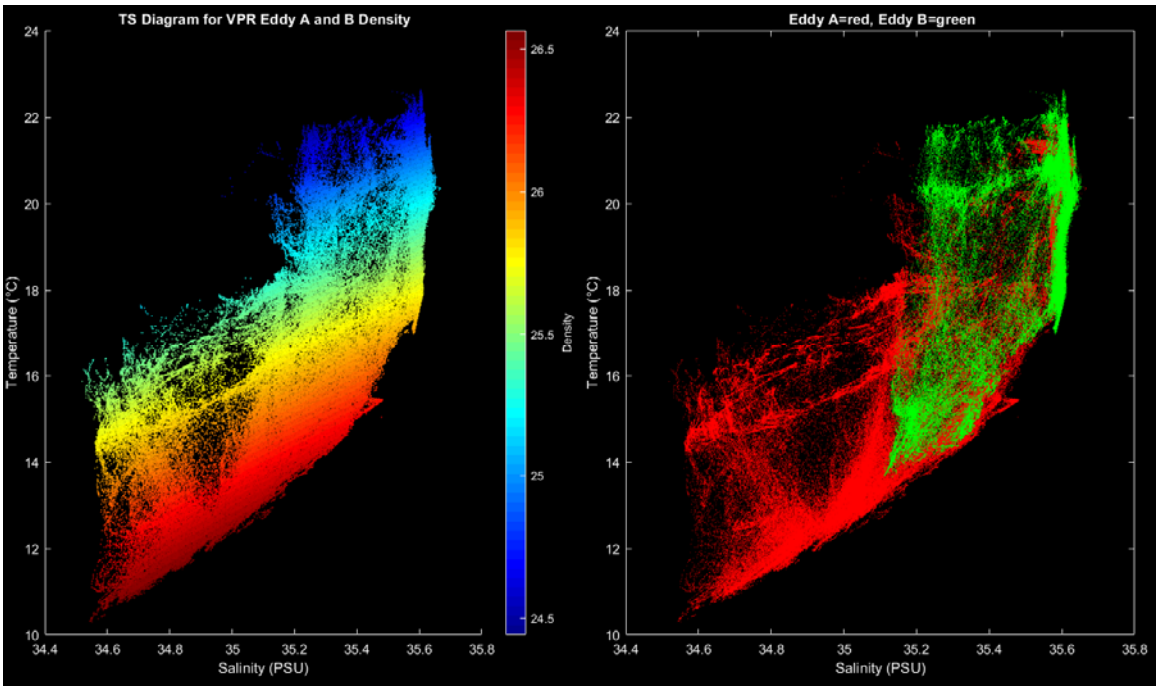

Figure 1.3.9. Left: potential density for VPR tows 2-9 (Eddy 1&2, Eddy 3 surveys) plotted in temperature-salinity space. Right: VPR tows 2-7 in red (Eddy 1 & 2 survey), VPR 8-9 in green (Eddy 3 survey).

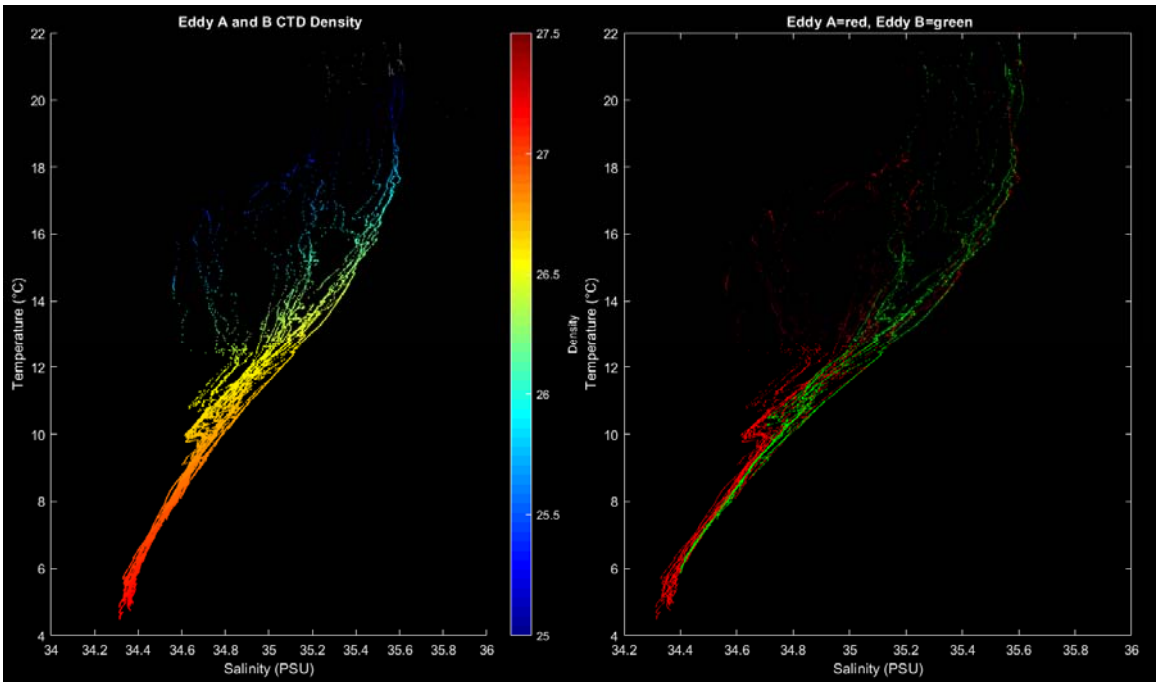

Figure 1.3.10. Left: potential density for CTDs in Eddy 1&2 and Eddy 3 surveys plotted in temperature-salinity space. Right: Eddy 1 & 2 CTD survey in red, Eddy 3 CTD survey in green.

1.4 Eddy 3 Survey 2

Two weeks later, it appears that the surface signatures of chlorophyll and PIC have diminished in Eddy 3, excepting for an area in the southwest quadrant of the eddy in the MODIS PIC image, although this may be a cloud artefact (Figure 1.4.1).

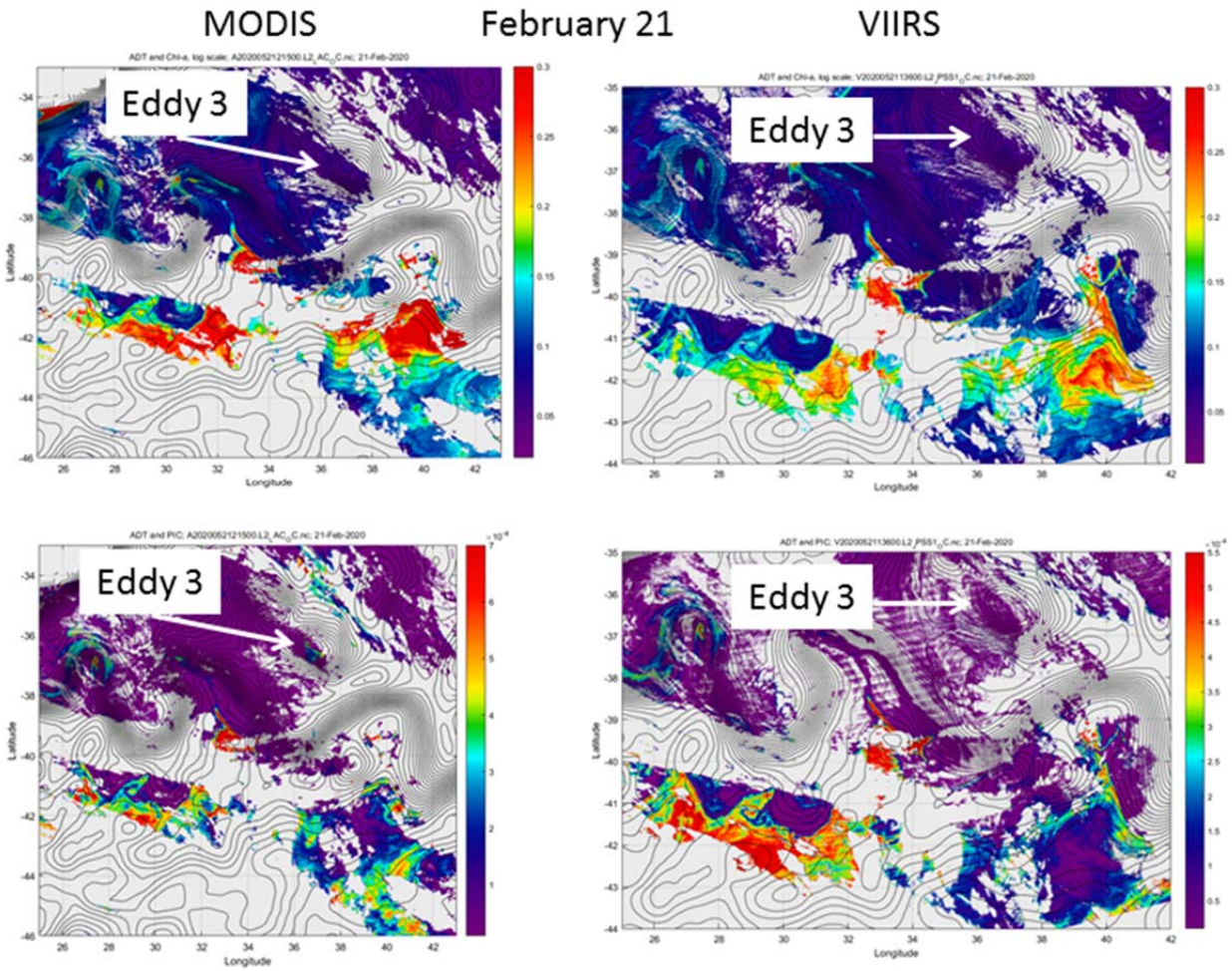

Figure 1.4.1: Chlorophyll (top row) and PIC (bottom row) images for MODIS (left column) and VIIRS (right column) on February 21.

VPR surveys (Figure 1.4.2) are consistent with a decrease in the Bb signal, especially near the surface. Very modest enhancements are present in a band surrounding eddy center at stations 56, 60, 64-65, and 67.

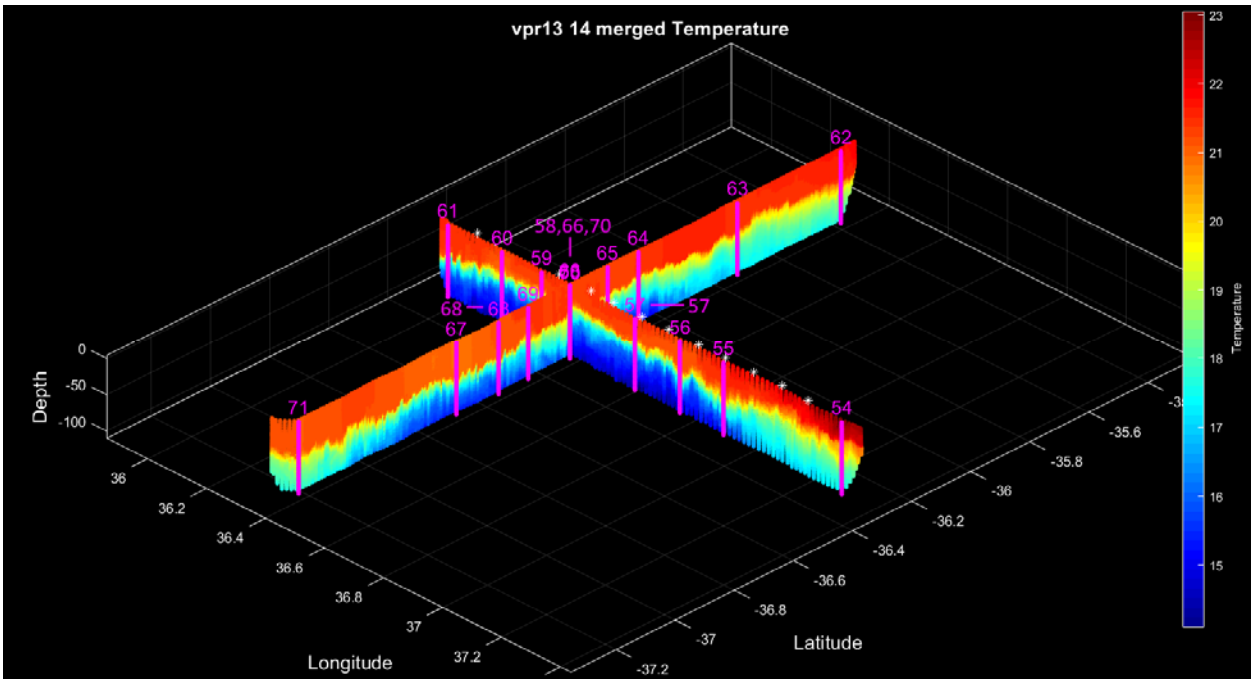
vpr13 14 merged Temperature
Depth
0
-50
-100
Longitude
36
36.2
36.4
36.6
36.8
37
37.2
Latitude
-36
-36.2
-36.4
-36.6
-36.8
-37
-37.2
-35.6
-35.8
Temperature
23
22
21
20
19
18
17
16
15
61
60
58,66,70
59
65
64
63
62
68
67
57
56
55
54
71

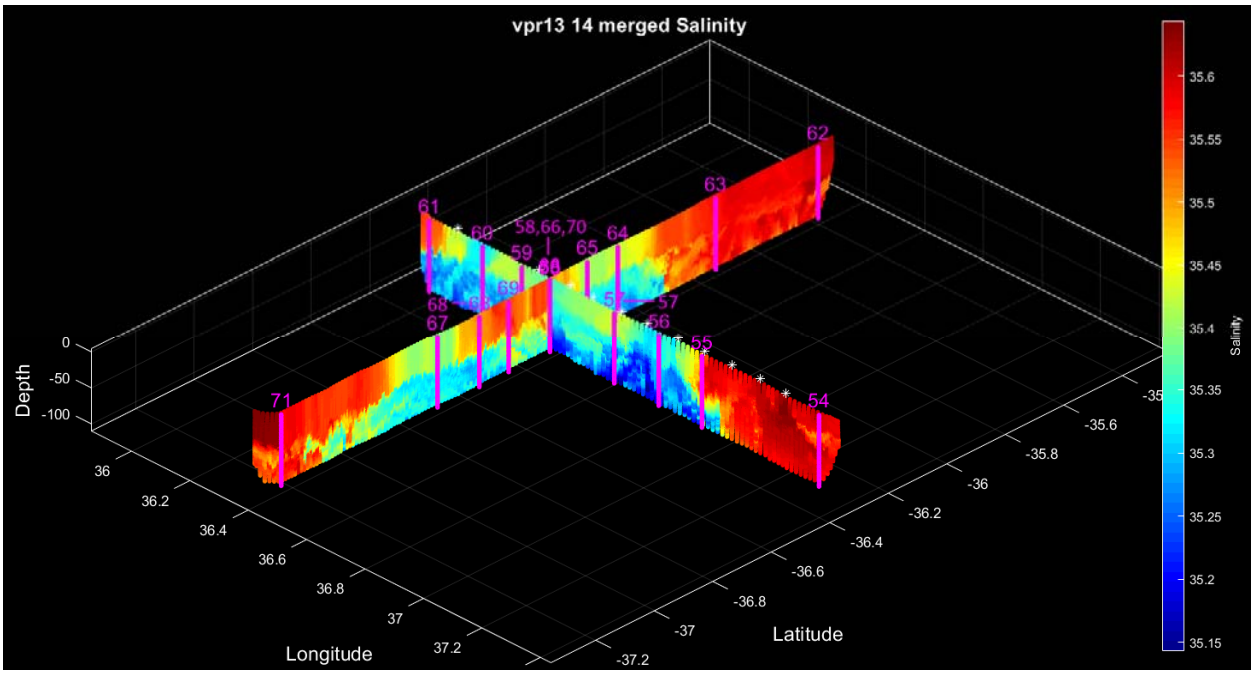
vpr13 14 merged Salinity
Depth
0
-50
-100
Longitude
36
36.2
36.4
36.6
36.8
37
37.2
Latitude
-36
-36.2
-36.4
-36.6
-36.8
-37
-37.2
-35.6
-35.8
Salinity
35.6
35.55
35.5
35.45
35.4
35.35
35.3
35.25
35.2
35.15
61
60
58,66,70
59
65
64
63
62
68
67
57
56
55
54
71

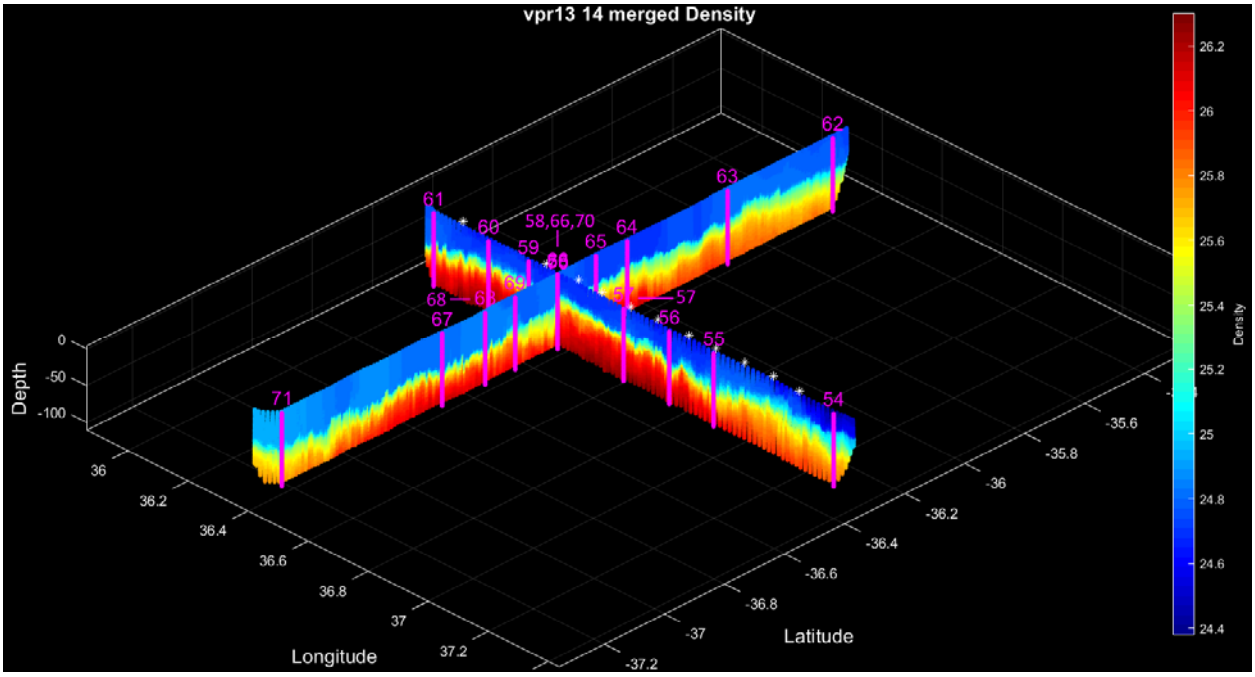
vpr13 14 merged Density
Depth
0
-50
-100
Longitude
36
36.2
36.4
36.6
36.8
37
37.2
Latitude
-36
-36.2
-36.4
-36.6
-36.8
-37
-37.2
-35.6
-35.8
Density
26.2
26
25.8
25.6
25.4
25.2
25
24.8
24.6
24.4
61
60
58,66,70
59
65
64
63
62
68
67
57
56
55
54
71

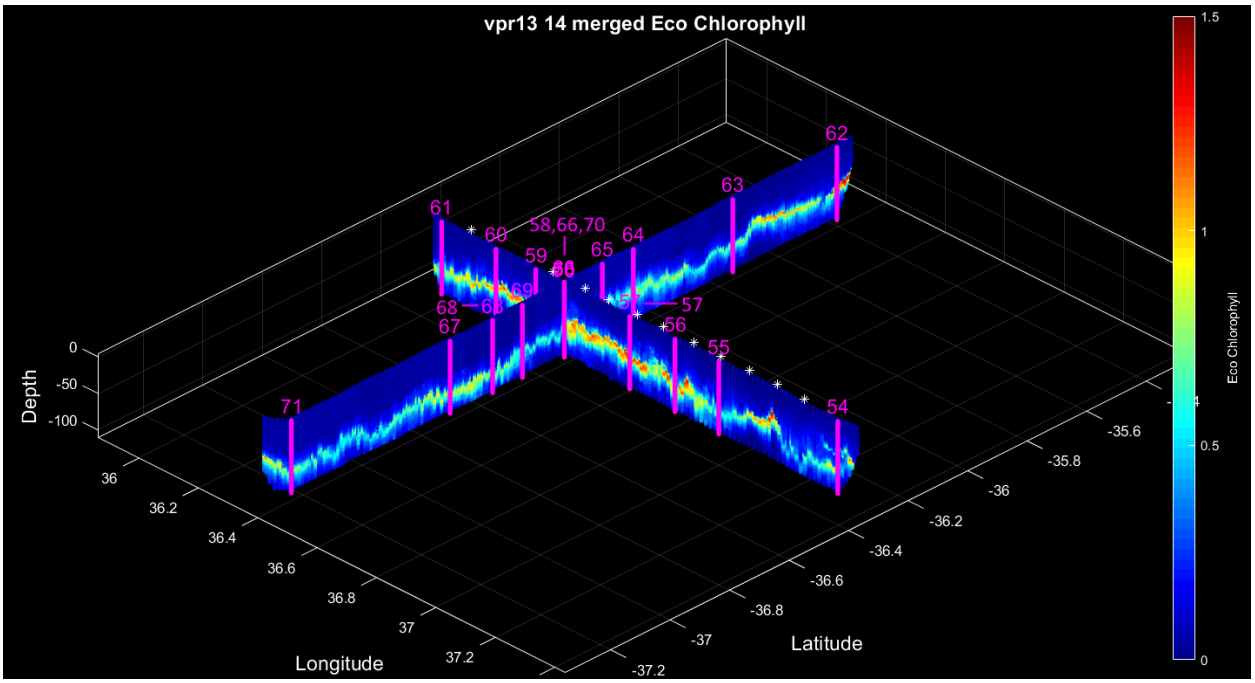
vpr13 14 merged Eco Chlorophyll
Depth
0
-50
-100
Longitude
36
36.2
36.4
36.6
36.8
37
37.2
Latitude
-36
-36.2
-36.4
-36.6
-36.8
-37
-37.2
-35.6
-35.8
Eco Chlorophyll
1.5
1
0.5
0
61
60
58,66,70
59
65
64
63
62
68
67
57
56
55
54
71

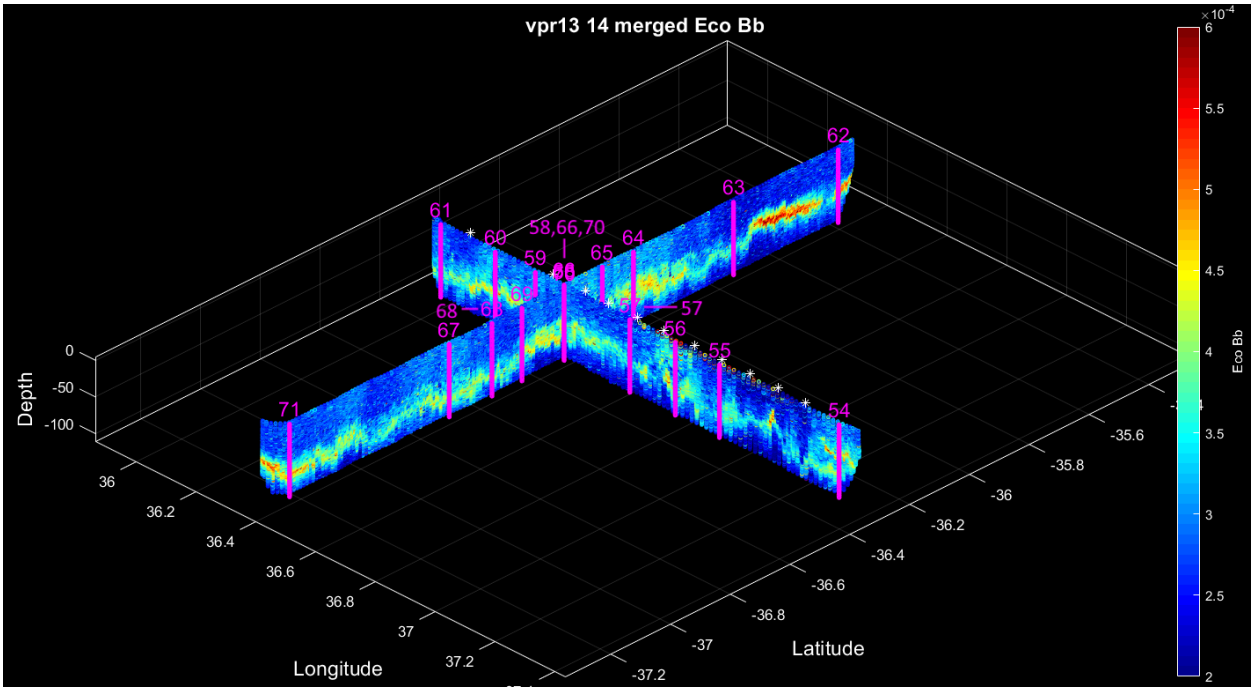

Figure 1.4.2 VPR surveys 13 and 14 combined. CTD stations and XBT locations indicated by magenta lines and asterisks, respectively.

During the two weeks in between surveys, the eddy propagated to the southwest (Figure 1.4.3). It also interacted with a newly formed cyclone to the northwest, apparently beginning to merge with it toward the end of the second survey. Eddy 3 appears to have weakened during this process, with a noticeable decrease in sea level anomaly associated with the feature.

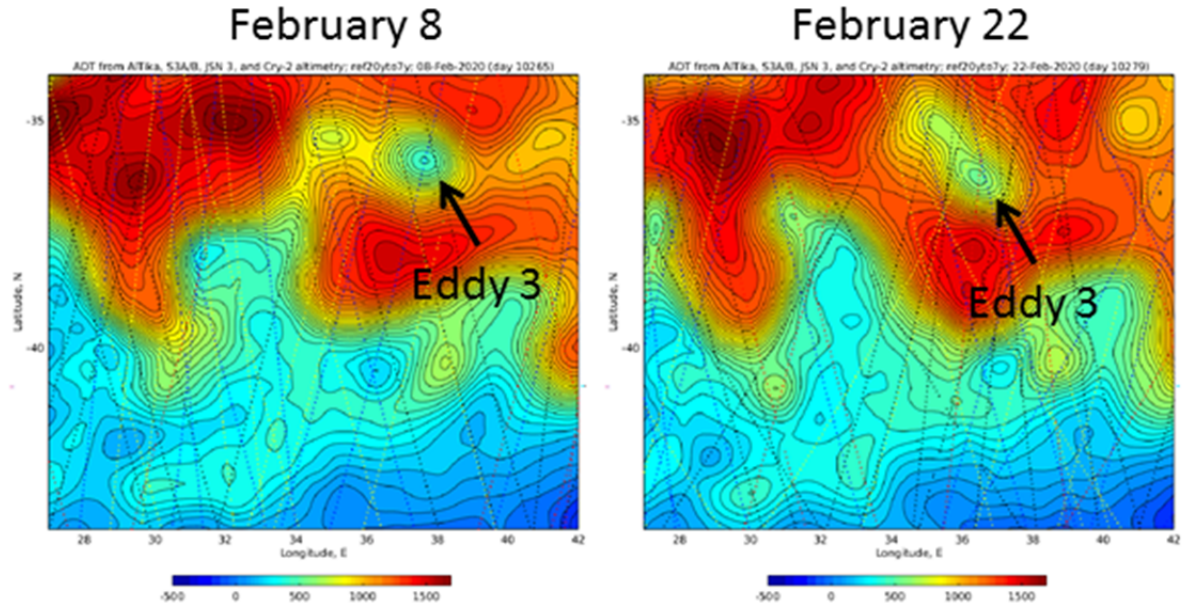

Figure 1.4.3. Altimetric changes in Eddy 3 from February 8 (left) to February 22 (right).

CTD surveys (Figure 1.4.4; Table 1.4.1) are consistent with the altimetric analysis, with modest subsidence of the main pycnoline. However, at least a portion of this apparent temporal trend could be due to the fact that the north-south section passed east of eddy center, according to the ADCP (Figure 1.4.5).

Transect	Station	Feature / comments
9	54	Eastern periphery – high salinity
	55	Local Smax
	56	High Bb, low S: PP cast, TM cast
	57	Smed
	58	Eddy center
	59	Smed
	60	Bb slight enhancement
	61	Local Smax
10	62	Northern station
	63	
	64	
	65	
	66	Eddy center
	67	3 south of EC; diverted to get drifter
	68	2 south of EC
	69	1 south of EC
	70	Eddy center repeat / TM cast
	71	Southern station

Table 1.4.1. Station list for CTD transects 9 (east to west) and 10 (north to south) across Eddy 3.

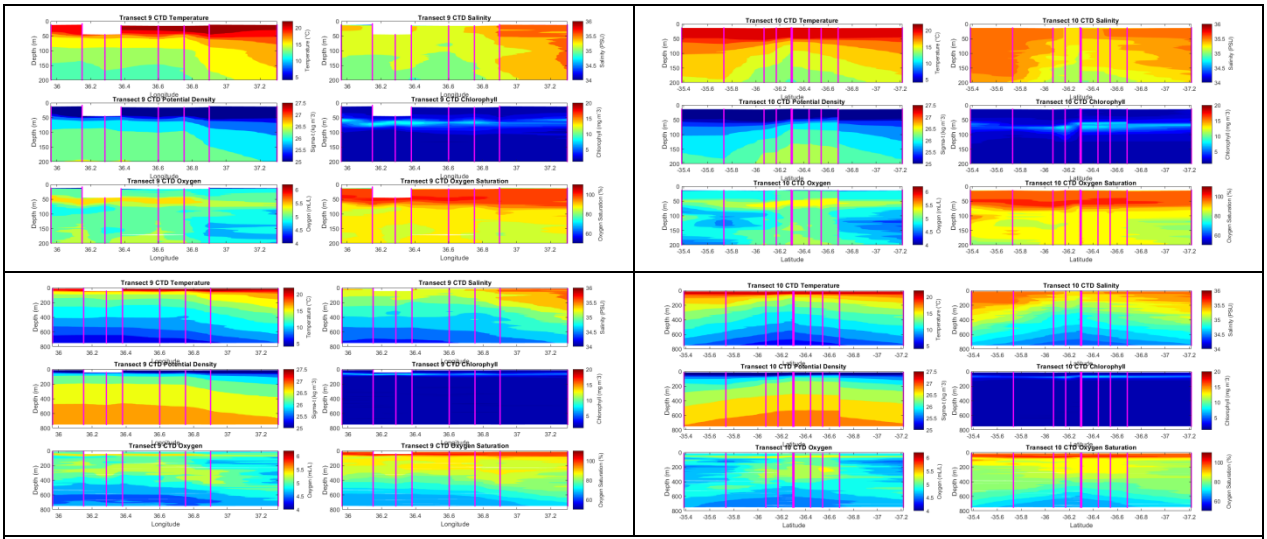

Figure 1.4.4. CTD transects 9 (left) and 10 (right). Upper panels 0-200m, lower panels 0-800m.

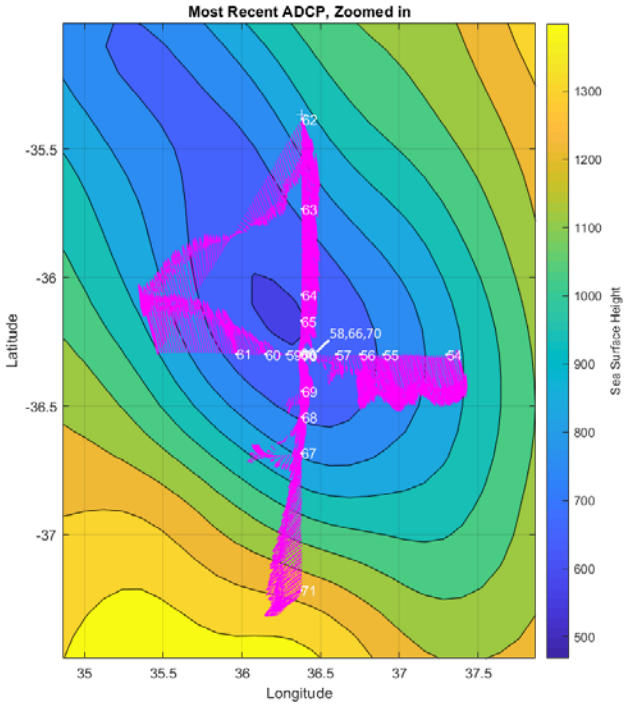

Figure 1.4.5. ADCP surveys associated with VPR 13 and VPR 14. Note that eddy center had propagated west (northwest according to the altimetry) during the time in between surveys, thus the north south line (VPR14) passed east of eddy center.

Weakening of Eddy 3 indicated by the altimetric measurements is also evident in the CTD data. North-south (Figure 1.4.6) and east-west (Figure 1.4.7) sections show subsidence of the upward deflections of the thermocline, halocline, and pycnocline. XBT data show a similar trend, with subsidence of the thermocline in the east-west section (Figure 1.4.8); note that a north-south section was not available in the second survey.

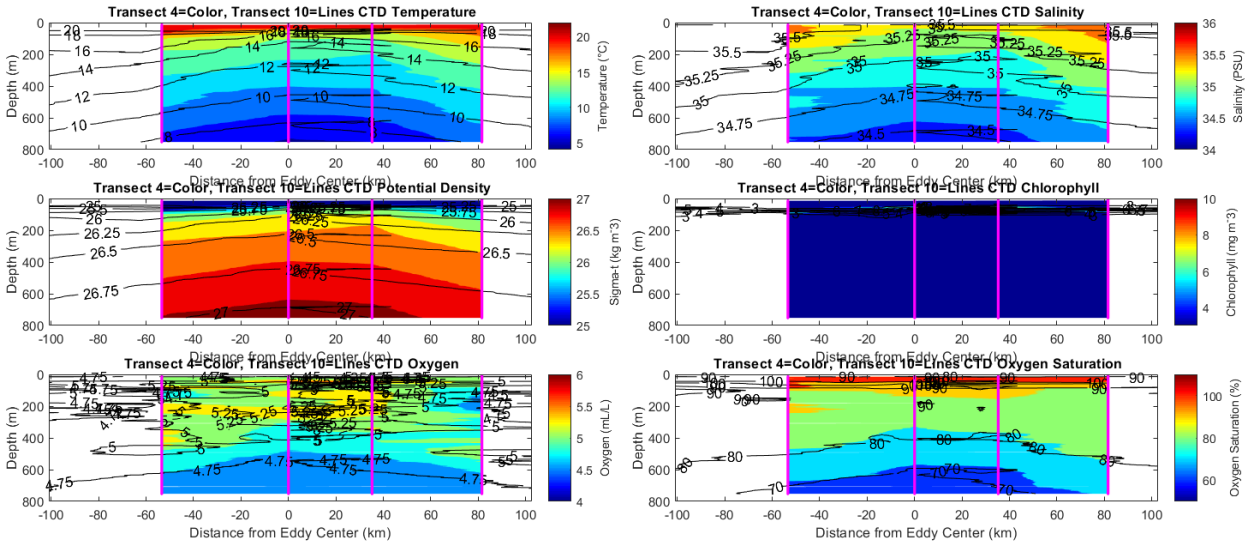

Figure 1.4.6. North-south CTD transects 4 (color) and 10 (contours).

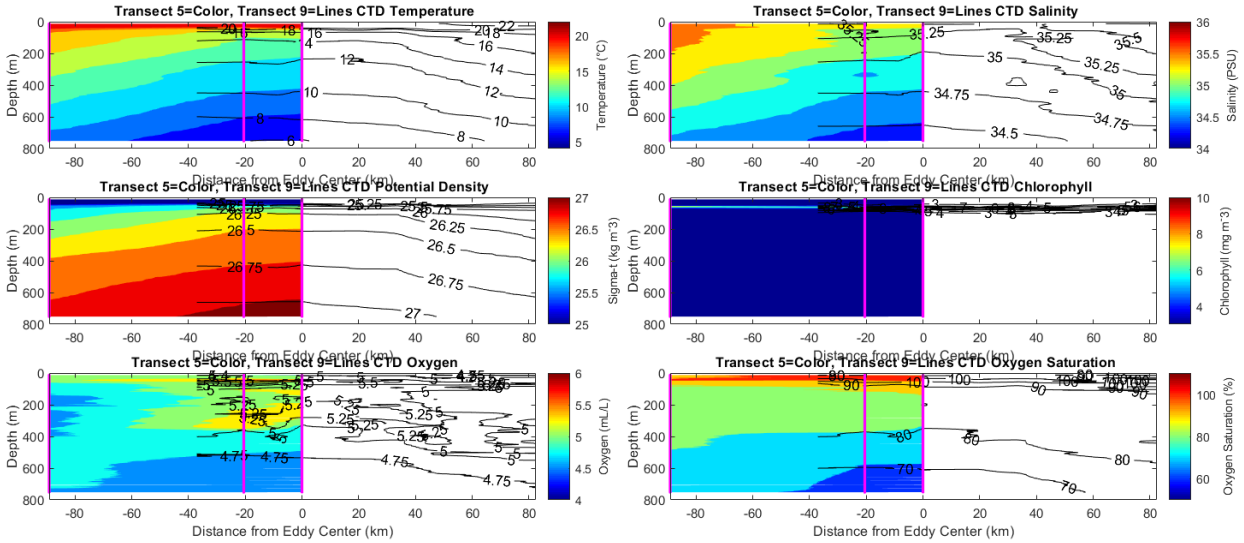

Figure 1.4.7. East-west CTD transects 5 (color) and 9 (contours).

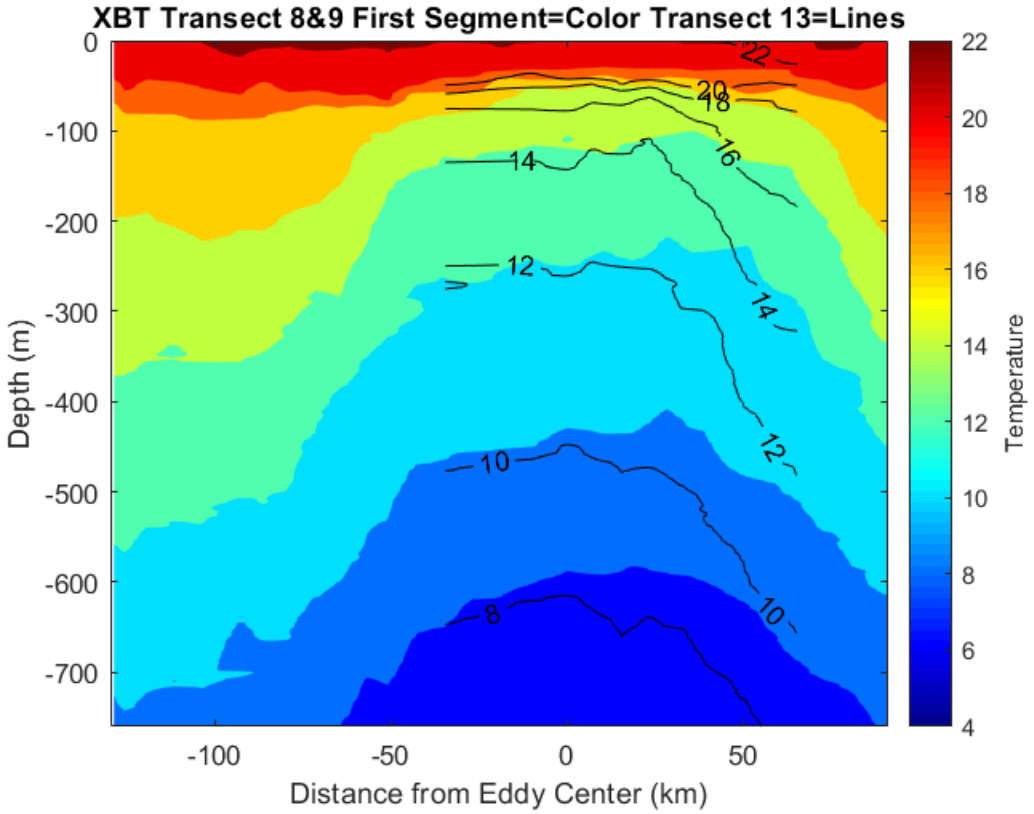

Figure 1.4.8. East-west XBT transects associated with the first segment of VPR 8&9 (color) and 13 (contours).

2. Some comments on Subantarctic Mode Water and its presence in our observations

SAMW is characterized by a thick layer of relatively uniform properties, formed by deep mixed layers in the wintertime, capped off by spring/summer stratification, and subsequently subducted into the main thermocline. McCartney (1977) provides an example from a hydrographic section:

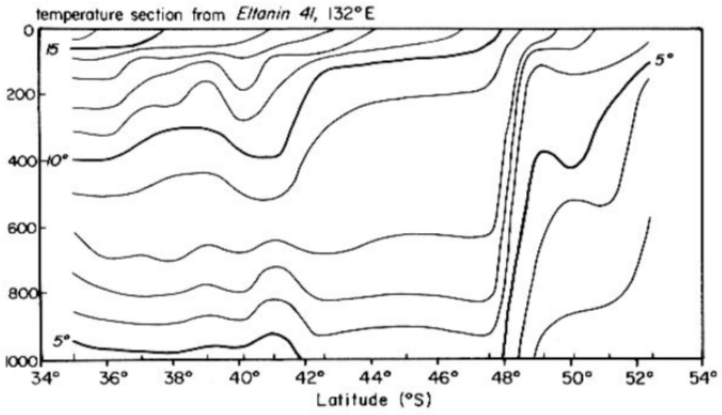

Fig. 6. A summertime temperature section south of Australia along 132°E from *Eltanin* 41. The subantarctic front is at 48° to 49°S. The SAMW north of the front is overlayed by a seasonal thermocline above 200 m, but persists as a pronounced thermostad between 200 and 600 m. North of 42°S the SAMW thermostad is still easily detectable, although not as pronounced as within the formation site between 43° and 48°S. The Australian continental shelf lies north of 35°S.

Simple conceptual models convey a zonally averaged view, e.g. Sarmiento et al. (2004):

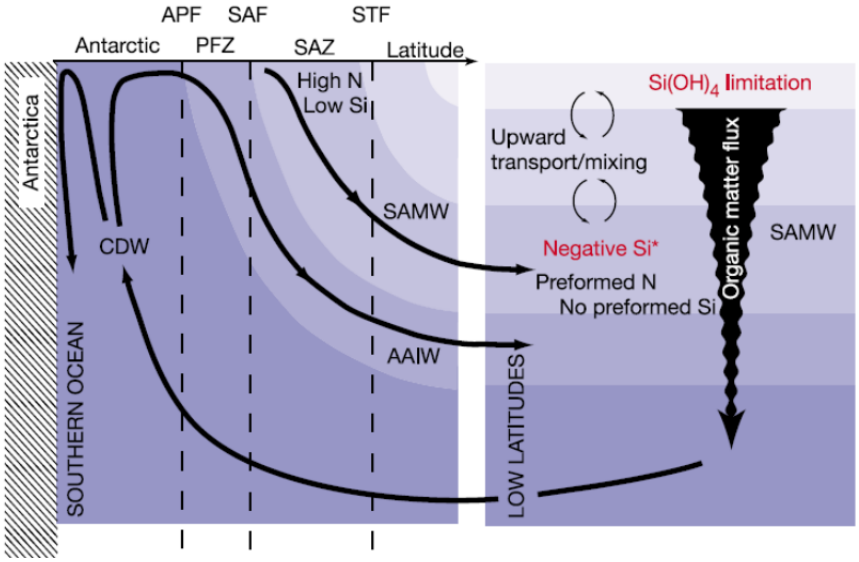

However, the production and distribution of SAMW are far from zonally uniform, as depicted in schematics by Belkin and Gordon (1996) and Koch-Larrouy et al. (2010):

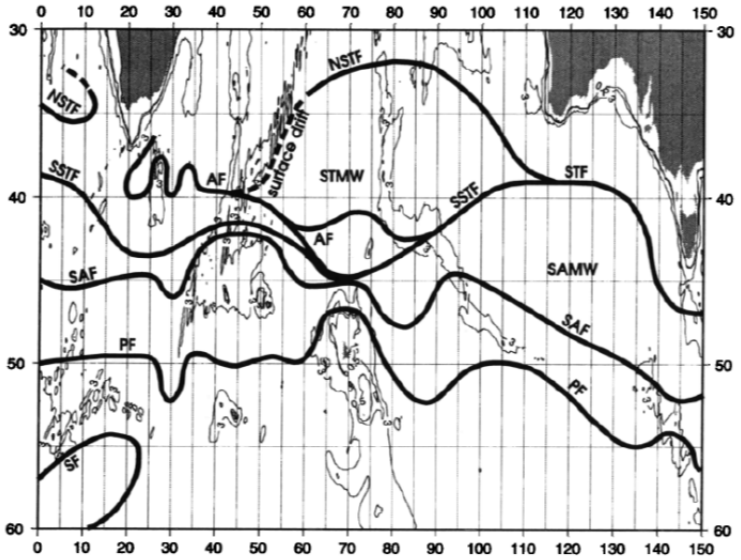

Figure 4. Frontal pattern from 0° to 150°E. Shown are the North and South Subtropical fronts (NSTF and SSTF, respectively), the Agulhas Front (AF), the Subantarctic Front (SAF), the Polar Front (PF), and the Scotia Front (SF). In the Crozet Basin (60°-85°E), two alternative paths of the AF are shown (discussed in section 4.5). In the Australian sector the SSTF is termed the STF downstream of its confluence with the NSTF (110°-115°E). The Subtropical and Subantarctic Mode Water areas are roughly indicated by STMW and SAMW, respectively.

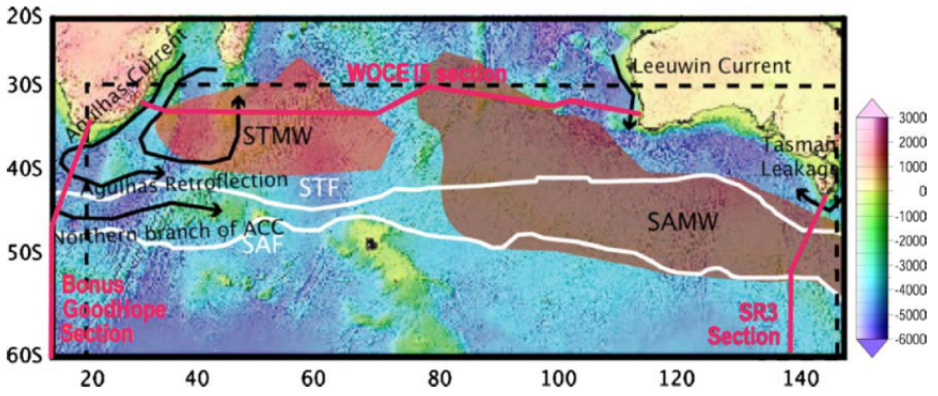

Fig. 1 Bathymetry in the southern Indian Ocean. *White contours* show the Subtropical Front (STF) and Sub-Antarctic Front (SAF) from Orsi et al. (1995). *Shaded zones* show the distribution of Subtropical Mode Waters (*red*) and Subantarctic Mode Waters north of the Subantarctic Front (*brown*) after Talley (1999). The hydrographic sections of WOCE SR3 and I5 and the Bonus GoodHope section are marked in *magenta*, the *dashed black line* indicates the domain considered in this study

A commonly used indicator of SAMW is a thick layer of low potential vorticity, which reflects low stratification: $PV \sim \frac{f}{\rho}\frac{d\rho}{dz}$. Herraiz-Borreguero and Rintoul (2010) diagnose SAMW from climatology, showing a volumetric hotspot in the eastern Indian Ocean:

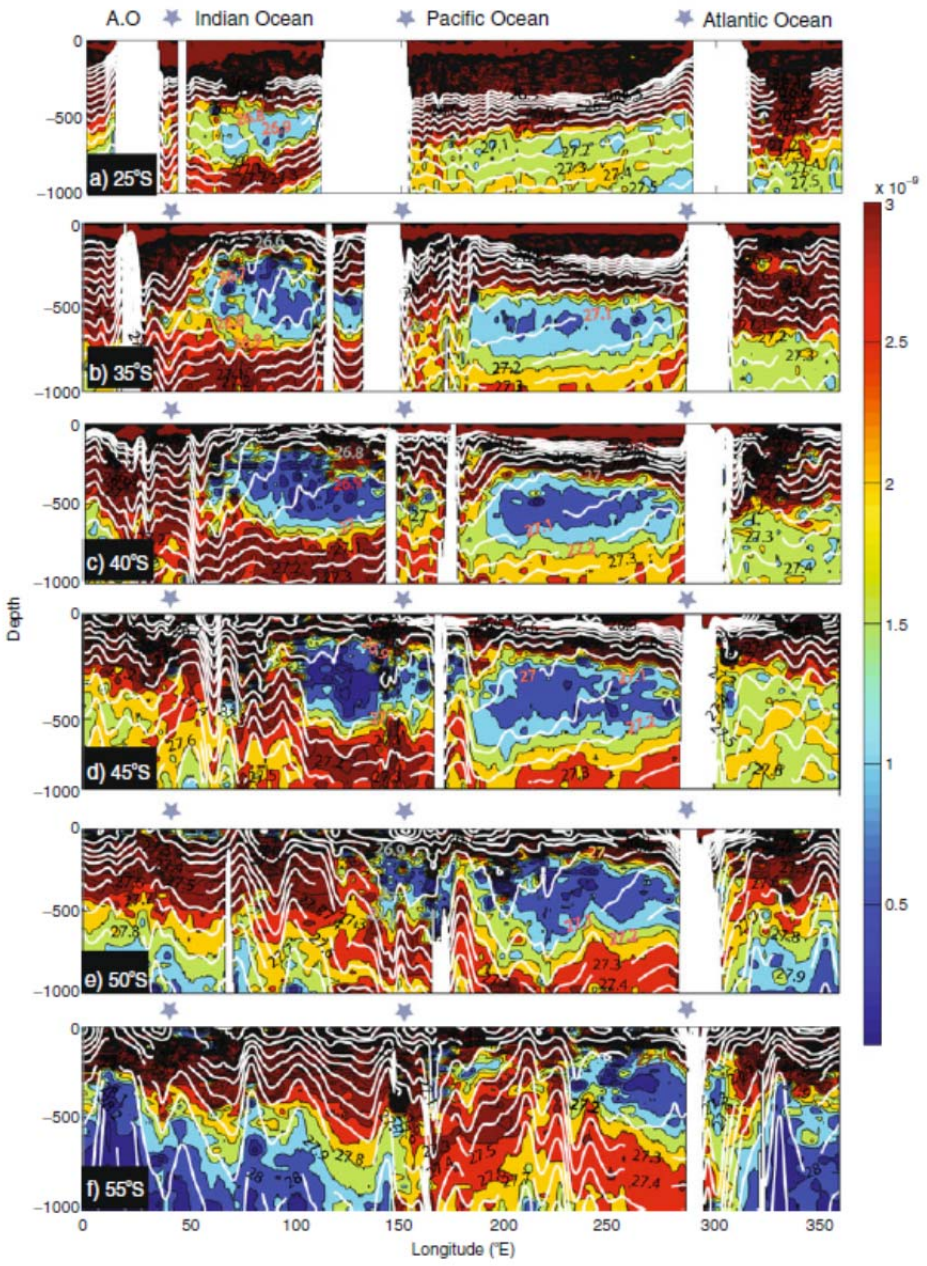

Fig. 2 Annual mean potential vorticity (PV) as a function of depth and longitude (°E) at 55° S (**f**), 50° S (**e**), 45° S (**d**), 40°S (**c**), 35° S (**b**) and 25° S (**a**). Data taken from CARS Climatological Atlas for Regional Seas (CARS2006a). *White lines* depict neutral density isopycnals. *Grey stars* in the *x*-axes show the extent of the Atlantic, Indian and Pacific Oceans

This general view is corroborated by their analysis of ARGO float data. Lower two panels show temperature and salinity characteristics of the SAMW identified in the upper panel as PV < 1.5 10^{-9} m^{-1} s^{-1}.

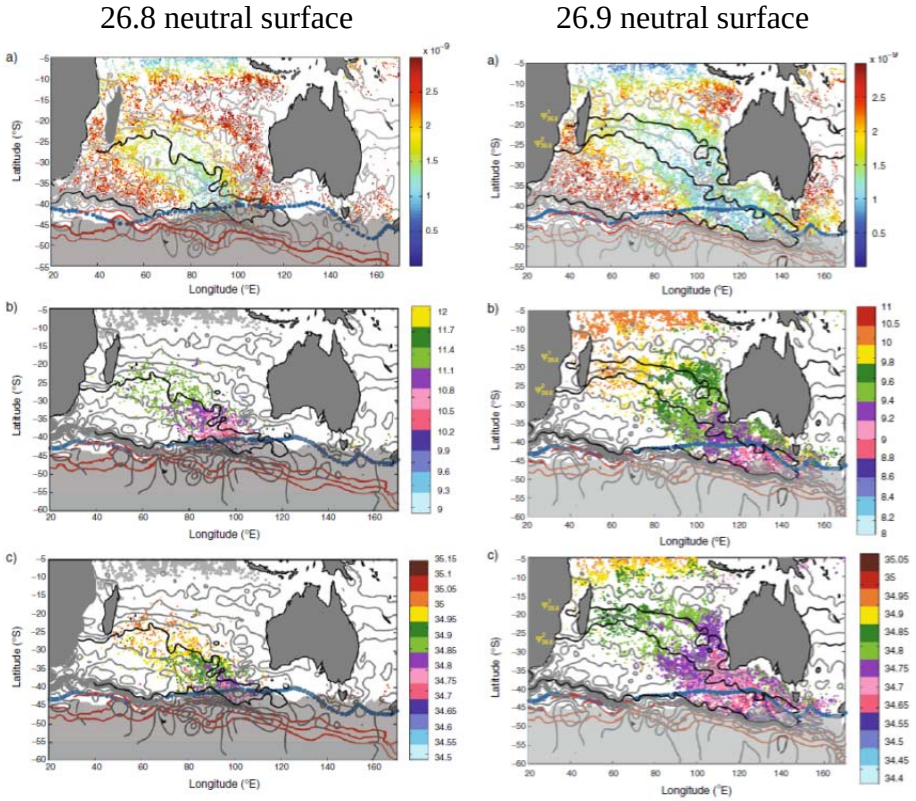

Fig. 4 Distribution of SAMW on the 26.8–γ^n surface. a Potential vorticity, b temperature and c salinity of the SAMW, where SAMW is identified as PV≤1.5×10^{-9} m^{-1} s^{-1}. Modified montgomery streamlines are depicted by *grey lines*. The area south of this neutral density surface outcrop has been masked by a *grey* surface to mark regions where the streamlines loose accuracy. $\Psi_{26.8}$, the streamline that best represents the SAMW flow, is highlighted a *thick black line*. *Blue dotted* and *red lines* depict the subtropical front and the subantarctic front, respectively. Note that the front positions were calculated using different techniques, and they overlap at some locations. Each *dot* represents an Argo profile

Cerovecki et al. (2013) use the SOSE model to diagnose the low-potential vorticity layer associated with SAMW:

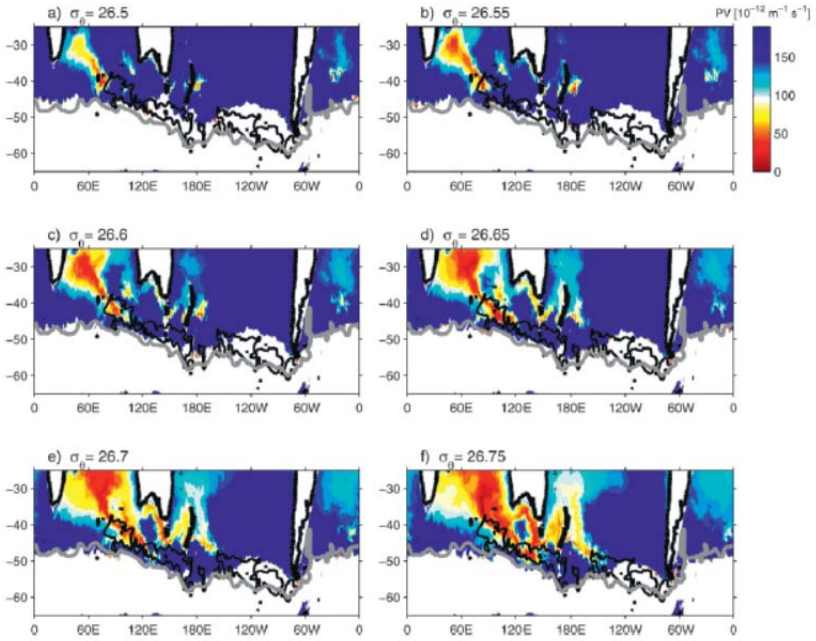

FIG. 3. Potential vorticity given by Eq. (9) [10^{-12} $(m\ s)^{-1}$], on constant σ_θ surfaces ranging from (a)–(f) 26.50 to 26.75 with the contour increment of 0.05, averaged over years 2005 and 2006 from SOSE. Black line is the 300-m contour of September mixed layer depth from Dong et al. (2008). Thick gray line is the climatological position of the SAF given by Orsi et al. (1995).

Gordon et al. (1987) document SAMW hydrographic properties in the western Indian Ocean and how they relate to other water masses present in the region:

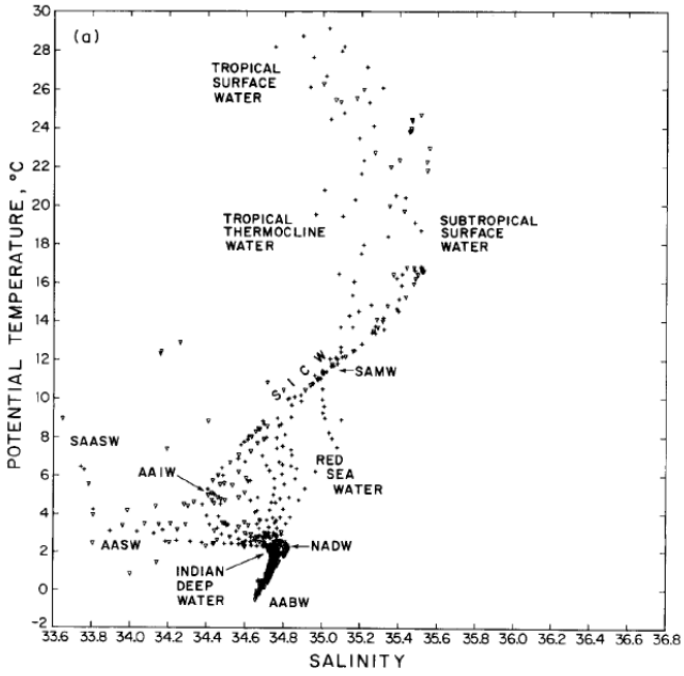

Fig. 8a.

Where is the SAMW in TN376 observations?

The first step in answering this question is what do we mean by SAMW? Various criteria have been used, usually based on a PV threshold, density interval (typically 26.5 to 27.0), and minimum depth (typically deeper than 200m in order to avoid seasonal stratification and mixing effects). Herraiz-Borreguero and Rintoul (2010) use a PV threshold of PV < 1.5 10^{-9} m^{-1} s^{-1}, whereas Wong (2005) uses PV < 0.5 10^{-10} m^{-1} s^{-1}. These differ by a factor of 30, which likely reflects different choices of the density used for the denominator in the first component of the PV computation: $PV = \frac{f}{\rho}\frac{d\rho}{dz}$. Apparently Herraiz-Borreguero and Rintoul (2010) use σ_θ, whereas Wong (2005) uses the in situ density ρ. For σ_θ=26.5, the effective multiplier is $\frac{1026.5}{26.5} = 38.7$, whereas for σ_θ=27.0, it is $\frac{1027.0}{27.0} = 38.0$. Choice of density does not affect the second component of the PV computation, as it is a first derivative of that quantity. Units of 10^{-12} m^{-1} s^{-1} are now commonly used for PV (Schlitzer, 2020), reflecting use of *in situ* density in the computation. In those units, the Herraiz-Borreguero and Rintoul's threshold is ca. 40 $\cdot 10^{-12}$ m^{-1} s^{-1} and Wong's is 50 $\cdot 10^{-12}$ m^{-1} s^{-1}.

In our data (Figure 2.1), the σ_θ = 26.5 isopycnal is mostly shallower than 200m and embedded within the seasonal pycnocline, excepting for stations in subtropical gyre water (e.g. outside of Eddy 3) where it is deeper than 300m. There does appear to be a relatively thick layer of water in the σ_θ = 26.6 to 26.7 interval, which appears to be a remnant of a wintertime mixed layer of ca.

300m: note the high oxygen content in the 0-300m stratum, indicating recent ventilation (presumably this past austral winter). In a sense, mode water appears to have been formed in this location, only to be capped off locally by seasonal stratification. However, applying even the more generous criteria of Wong ($50 \cdot 10^{-12}$ m^{-1} s^{-1}), none of the profiles included in this analysis meet that definition of SAMW. However, if we relax the threshold to $100 \cdot 10^{-12}$ m^{-1} s^{-1}, several points appear in the σ_θ = 26.5 to 27.0 depth interval. There are also mode waters in the deeper layers (600-800m) with σ_θ of ca. 27.1 – 27.2, which is presumably AAIW.

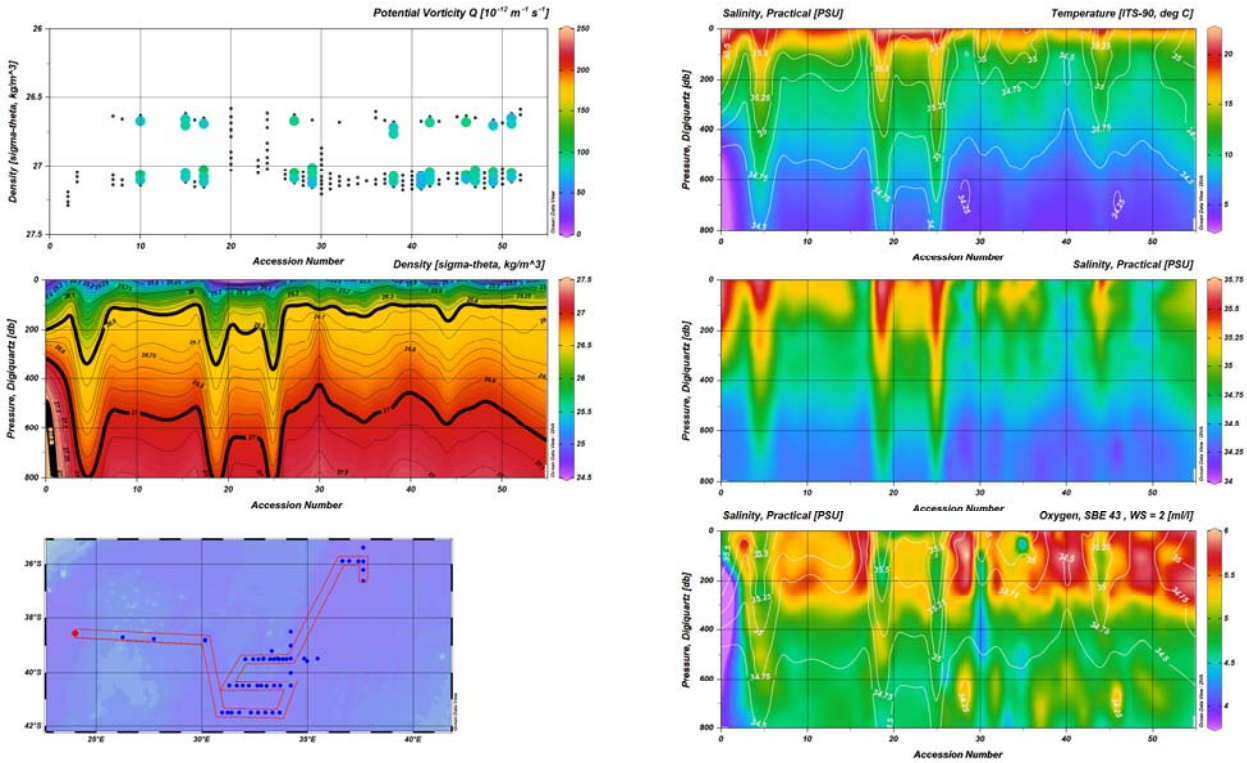

Figure 2.1. Potential vorticity, density, temperature, salinity, and oxygen for stations 1-52 on TN376. Salinity contours overlayed on temperature and oxygen panels.

3. Daily narrative

27 January 2020

VPR1 transited across the eastern flank of the Agulhas eddy (Figure 3.1). Beginning in the warm and salty waters of the eddy, the fluorescence maximum was located at ca. 60-80m. Microscopic analysis of a Niskin sample from station 1 by Colin Brownlee suggested the phytoplankton community was dominated by dinoflagellates. VPR imagery showed copepods, diatom rods, fecal pellets, and gelatinous zooplankton.

A sharp salinity front was observed at 24.15E, and the fluorescence distribution was concentrated near the surface.

As we proceeded east, a relatively warm and fresh water mass was encountered at 24.6E, with much higher fluorescence values. This area was also associated with high backscatter. VPR imagery showed a large amount of particulate matter in the upper 20m, with fewer gelatinous zooplankton present. Proceeding further east, fluorescence dropped but high backscatter persisted. As we exited the warm and fresh water mass at 25.1E, backscatter decreased back to background levels.

At around 25.2E, the pycnocline began to rise, with relatively cold and fresh waters doming upward toward the surface. It was at this front that we observed highest fluorescence values, although this could be due to a reduction in quenching as light levels dropped toward the end of the day.

Oxygen values (uncorrected) show some oceanographic trends, with lowest values in relatively fresh waters underneath the area of high backscatter.

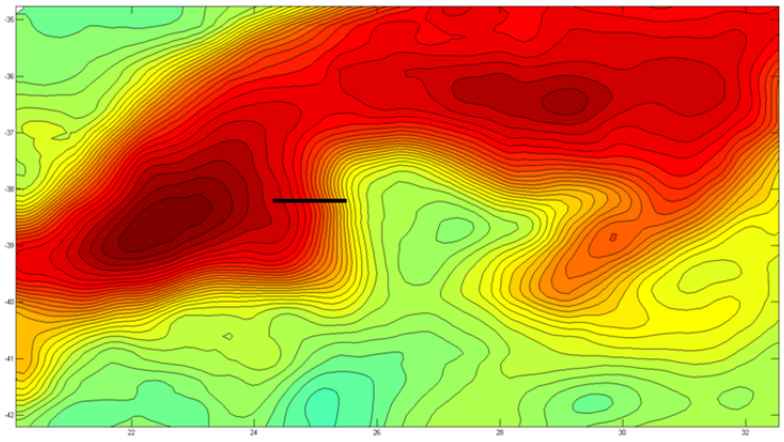

Figure 3.1. VPR1 track overlayed on absolute dynamic topography for 27 January, 2020. VPR data panels follow below.

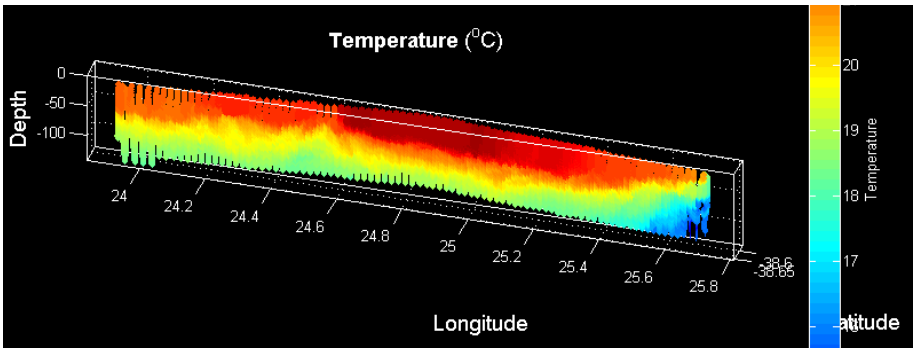
Temperature (°C)
Depth
0
-50
-100
24
24.2
24.4
24.6
24.8
25
25.2
25.4
25.6
25.8
Longitude
20
19
18
17
Temperature

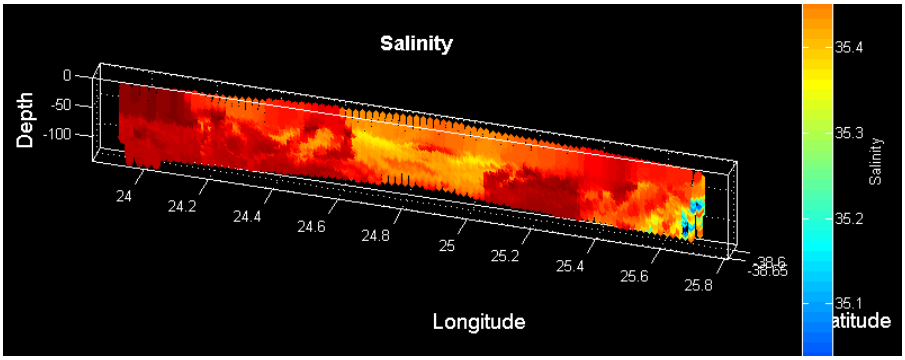
Salinity
Depth
0
-50
-100
24
24.2
24.4
24.6
24.8
25
25.2
25.4
25.6
25.8
Longitude
35.4
35.3
35.2
35.1
Salinity

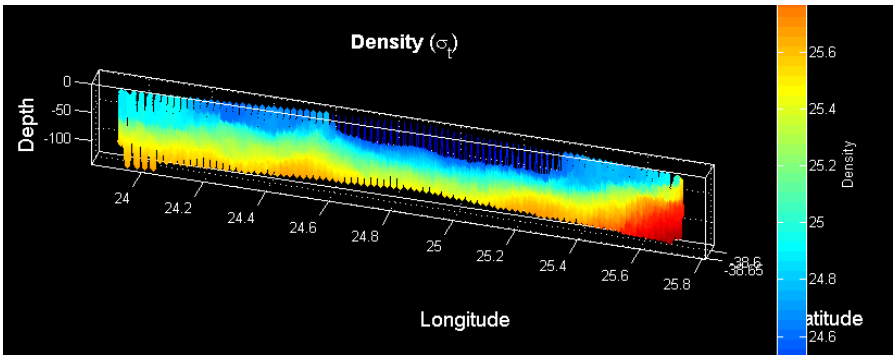
Density (σt)
Depth
0
-50
-100
24
24.2
24.4
24.6
24.8
25
25.2
25.4
25.6
25.8
Longitude
25.6
25.4
25.2
25
24.8
24.6
Density

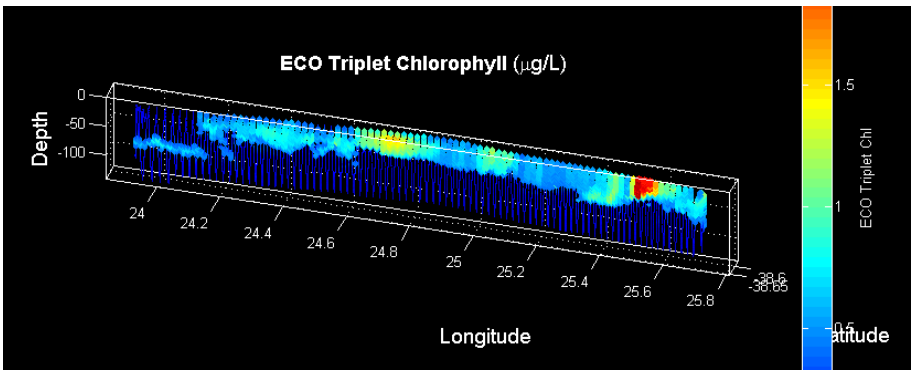
ECO Triplet Chlorophyll (µg/L)
Depth
0
-50
-100
24
24.2
24.4
24.6
24.8
25
25.2
25.4
25.6
25.8
Longitude
1.5
1
ECO Triplet Chl

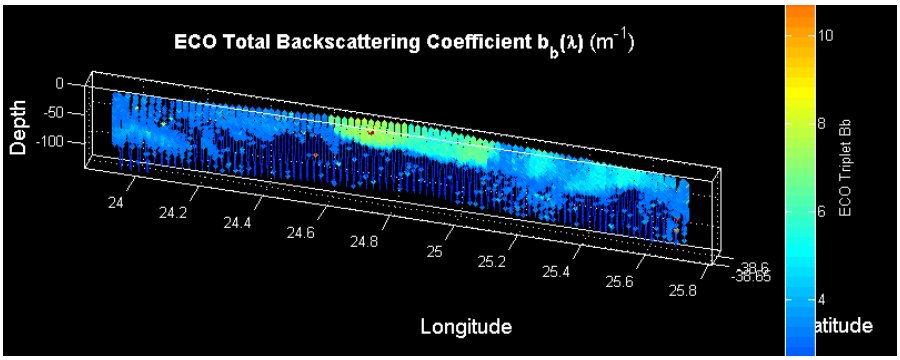

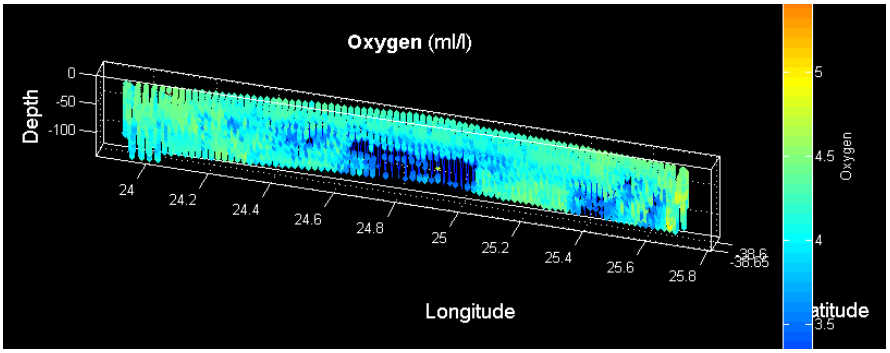

29 January 2020

Satellite imagery from 24 January indicates an area of high Chl / high PIC water in the pocket of a northward meader of the Agulhas Front (Figure 3.2). VPR2 began on the western flank of the meander, with characteristic warm and salty water. Stratification was relatively low in the upper ocean, and the fluorescence maximum was at the surface.

High Chl / high backscatter (hereafter Bb) was encountered along the track at ca. 32.7 E, indicating some eastward movement of the feature since the satellite image on 24 January. Within the broad area of high Chl / high Bb, there were two local maxima which are reminiscient of the roughly north-south banding structure in the satellite image. Underway measurements of Bb' confirm this area to be high in PIC.

As we proceeded eastward, both Chl and Bb decreased sharply at ca. 33.6 E. After a short segment of low values, Bb rose back to levels nearly as high as was observed in the high Chl / high Bb area. Underway Bb' measurements indicate PIC was similarly elevated. This low Chl / high Bb / high Bb' water mass is clearly distinct from the high Chl / high Bb / high Bb' water: the latter is moderately warmer and saltier, but clearly not as warm and salty as the Agulhas Front waters encountered earlier in the transect. Might this be a result of mixing of waters south of the front with the Agulhas Front to generate this water which is conducive to low Chl / high Bb / high Bb'?

Note the oxygen (uncorrected) is highest in the high Chl water mass.

Figure 3.2. VPR2 track overlayed on Chl (left) and PIC (right). Contours are ADT. VPR data panels follow below.

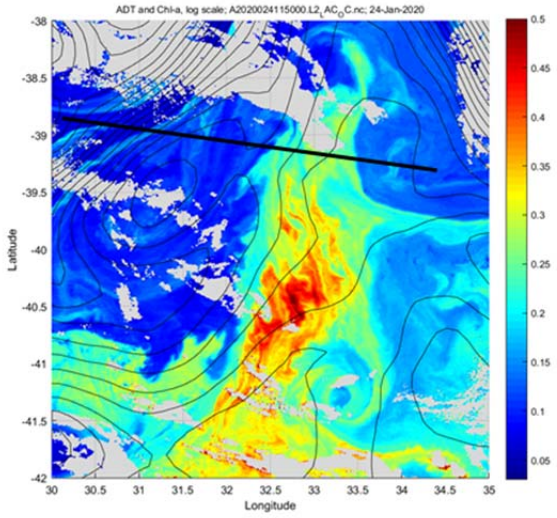
ADT and Chl-a, log scale; A2020024115000.L2_AC_O.C.nc; 24-Jan-2020
Latitude
Longitude

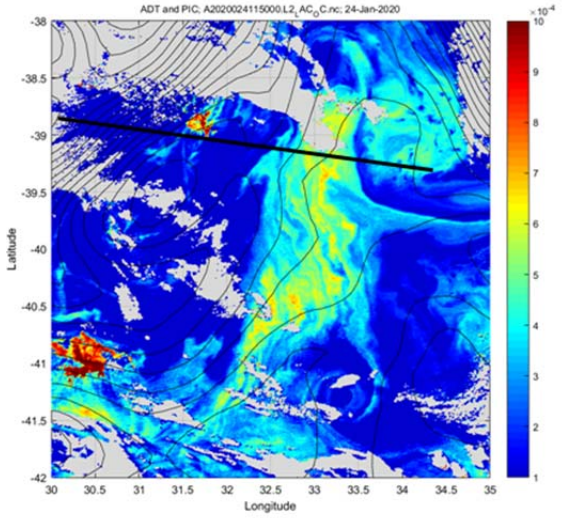
ADT and PIC; A2020024115000.L2_AC_O.C.nc; 24-Jan-2020
Latitude
Longitude

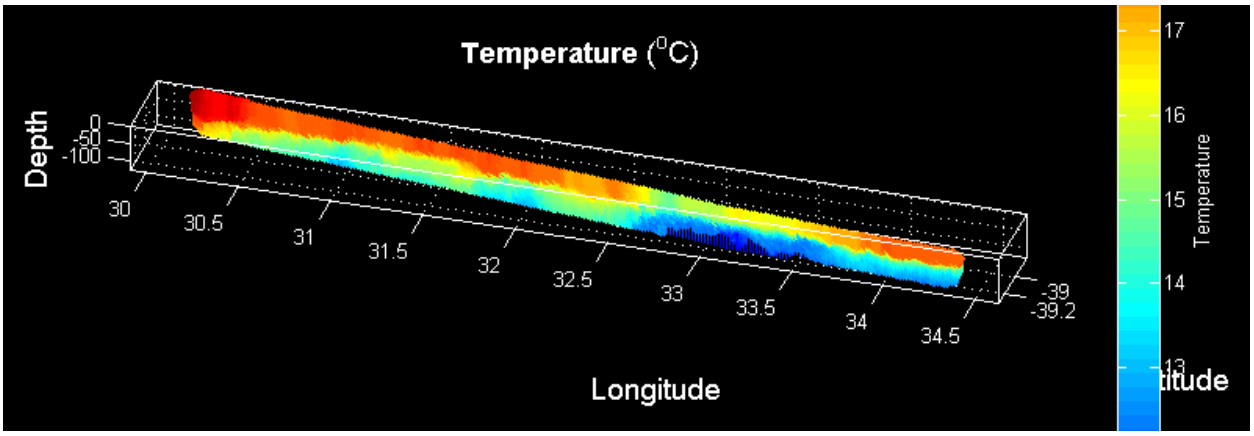
Temperature (⁰C)
Depth
Longitude
Temperature

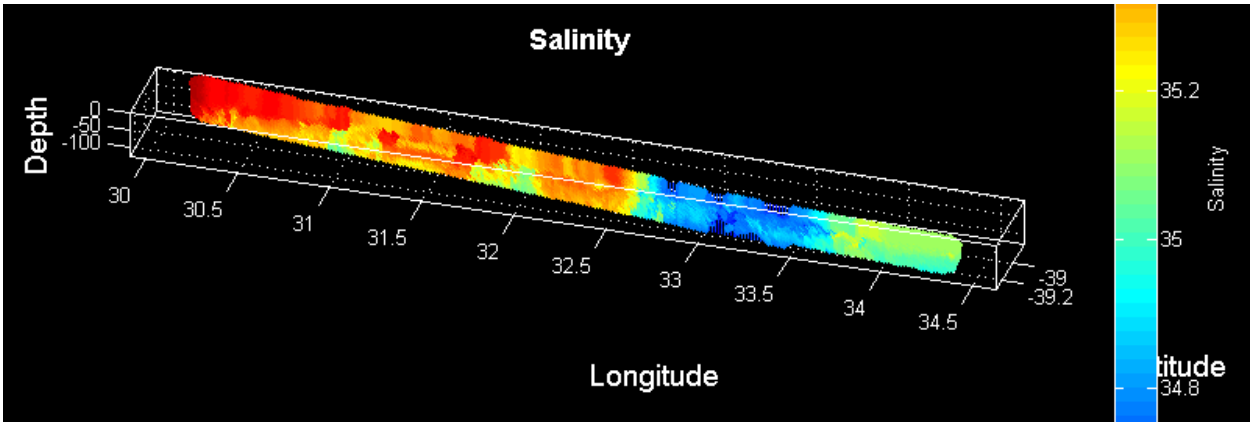
Salinity
Depth
Longitude
Salinity

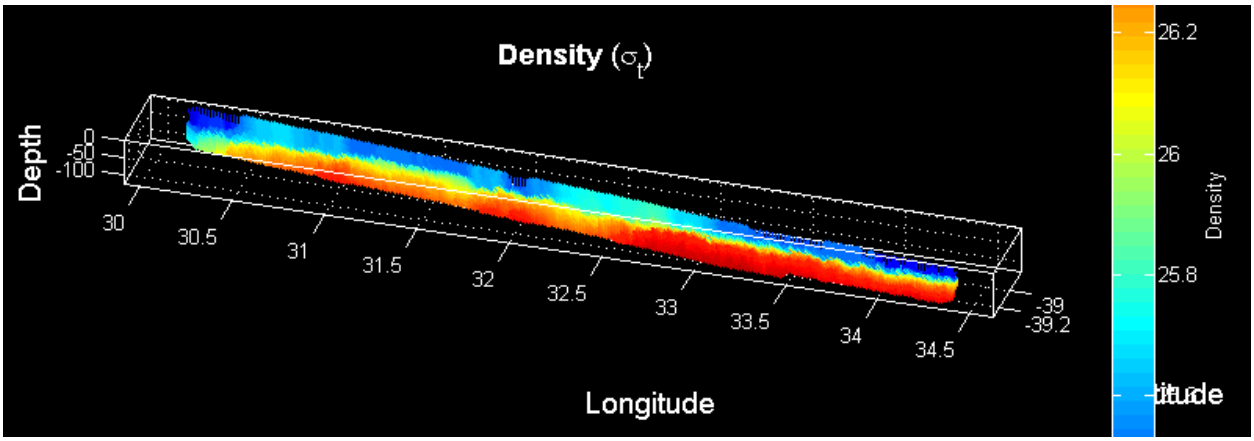
Density (σ_t)
Depth
-50
-100
30
30.5
31
31.5
32
32.5
33
33.5
34
34.5
-39
-39.2
Longitude
26.2
26
25.8
Density

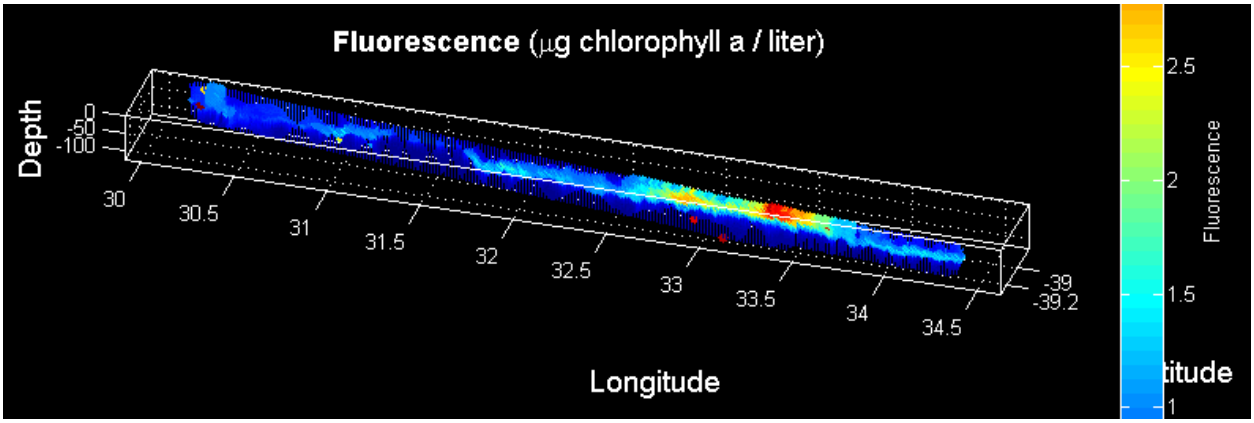
Fluorescence (μg chlorophyll a / liter)
Depth
-50
-100
30
30.5
31
31.5
32
32.5
33
33.5
34
34.5
-39
-39.2
Longitude
2.5
2
1.5
1
Fluorescence

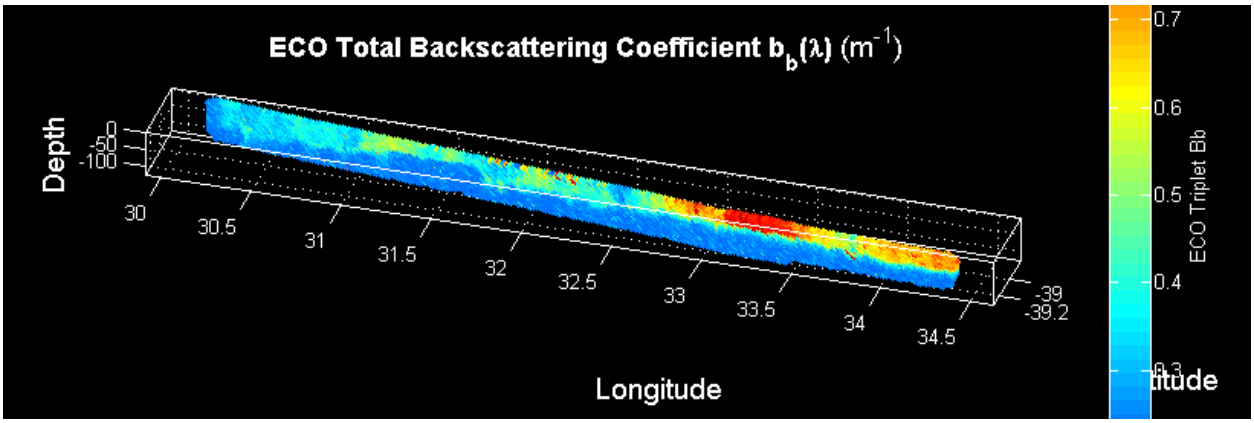
ECO Total Backscattering Coefficient $b_b(\lambda)$ (m^{-1})
Depth
-50
-100
30
30.5
31
31.5
32
32.5
33
33.5
34
34.5
-39
-39.2
Longitude
0.7
0.6
0.5
0.4
ECO Triplet Bb

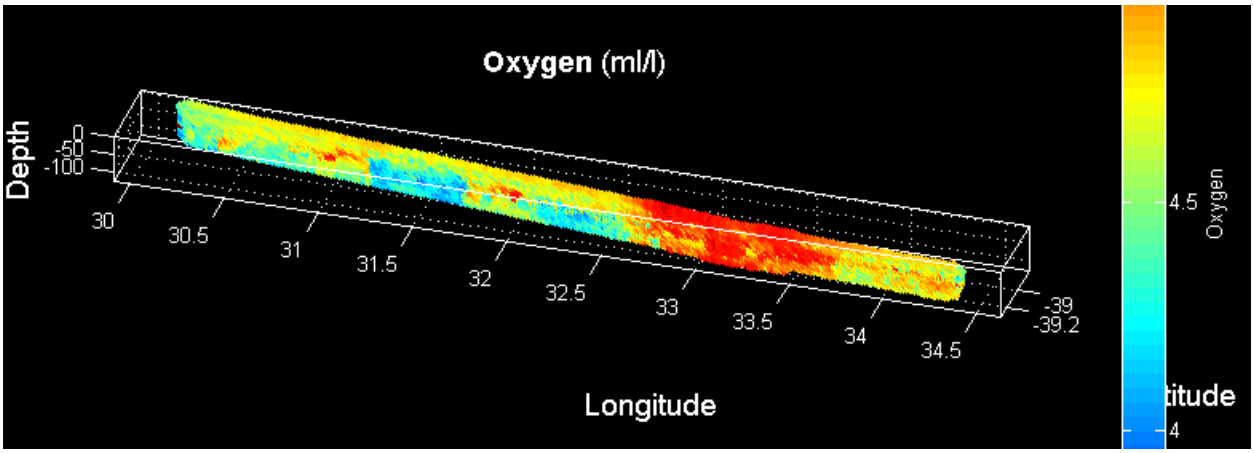

30-31 January

VPR3 deployed to start a spatial survey to the south. The initial plan was based on the imagery from 24 January, and new imagery suggests an alternative strategy. The high Chl / high Bb tendril to the south appears to have moved north; the tendril to the north appears to have wrapped eastward around the low Chl / high Bb water (Figure 3.3). ADCP data indicate an eddy-like feature associated with the low Chl / high Bb water, so the decision was made to survey in between the two quasi-zonal tracks to determine eddy center. On the transit northward on the eastern side of the survey grid, we lost communications with the flight control computer. VPR was recovered safely, and troubleshooting began. Reseating the connector on the engineering can restored communications.

It turns out that our stopping point corresponded with a high value of Bb', perhaps the largest of the trip thus far. This may be associated with southeastward transport of the high PIC water southeast along the meander. CTD and trace metal casts were carried out at the station while VPR maintenance was taking place.

VPR4 deployed to continue areal survey. Flight control communitcations were restored for several hours, then dropouts started. Brief periods of communications were restored during the bottom of the tow, suggesting a loose connector. ROI detection has short dropouts as well, indicating a problem with comms over the science fiber as well. Toward the end of the tow, flight control comms resumed continuous operation.

VPR4 appears to have delineated eddy center at ca. 34 00 E, as confirmed by the ADCP (not shown). A local salinity maximum in surface waters at eddy center coincides with a local minimum in Bb' based on the Balch group's underway measurements. This appears to be consistent with the satellite Bb image. Location for the primary productivity station was chosen to be just east of eddy center (34 12'E) to be in a higher Bb' regime within the eddy.

Underway XBT measurements along the E-W portion of VPR2 characterize thermocline variability associated with this meander / eddy system.

Figure 3.3. Tracks of VPR2, 3, and 4 overlayed on Chl (left) and PIC (right). Contours are ADT. VPR data panels follow below.

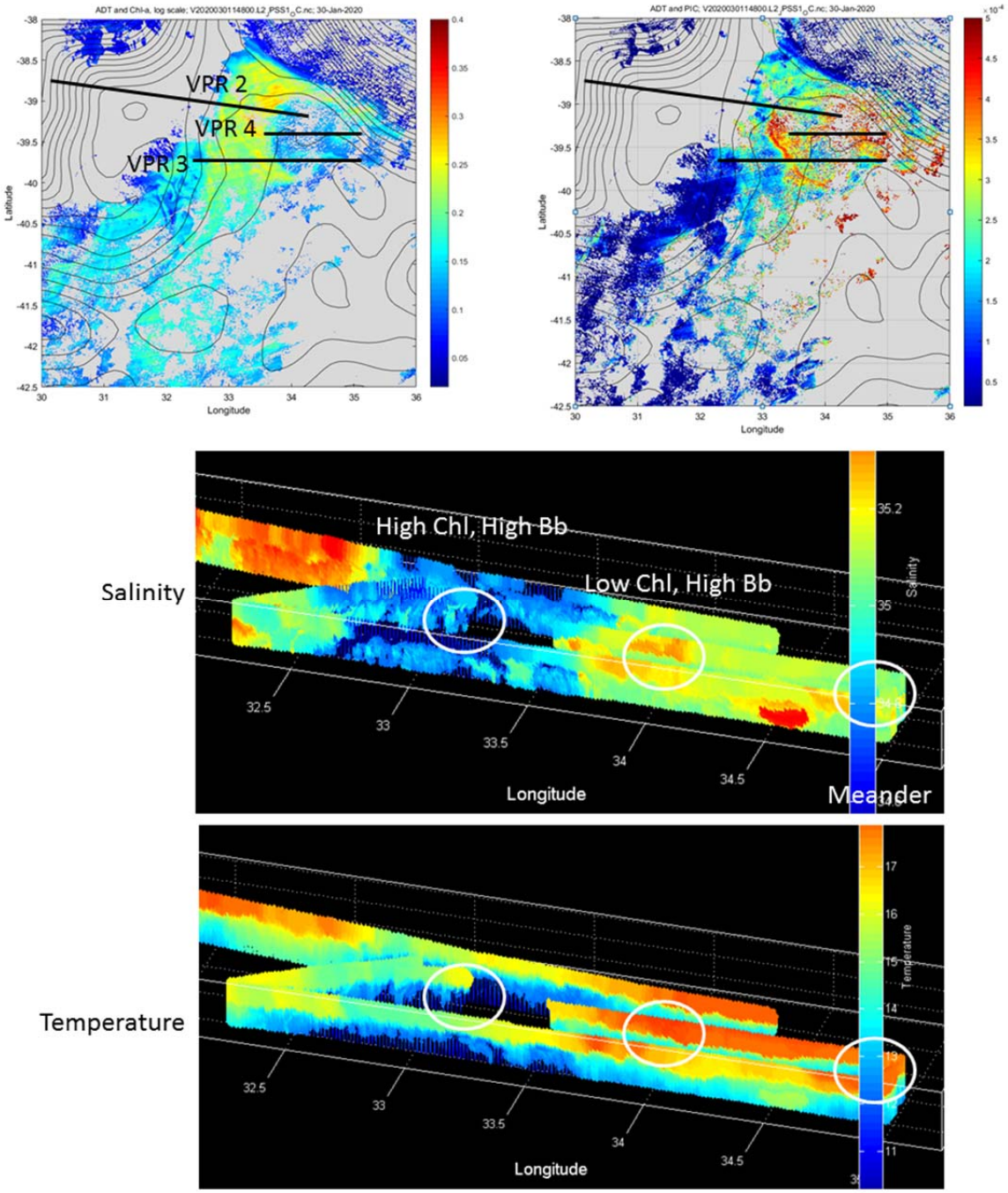

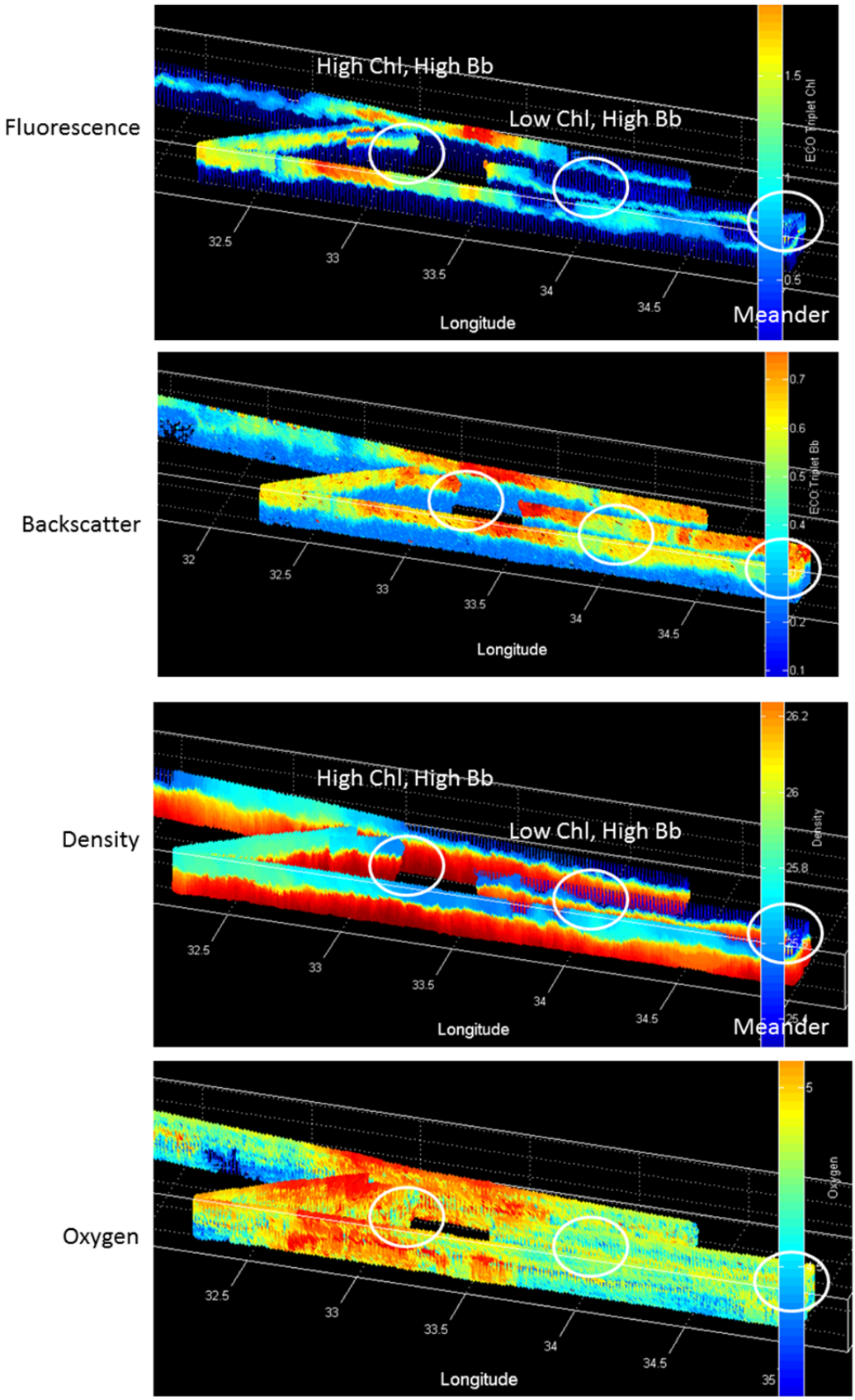
Fluorescence
High Chl, High Bb
Low Chl, High Bb
Meander
Longitude
ECO Triplet Chl
Backscatter
Longitude
ECO Triplet Bb
Density
High Chl, High Bb
Low Chl, High Bb
Meander
Longitude
Density
Oxygen
Longitude
Oxygen

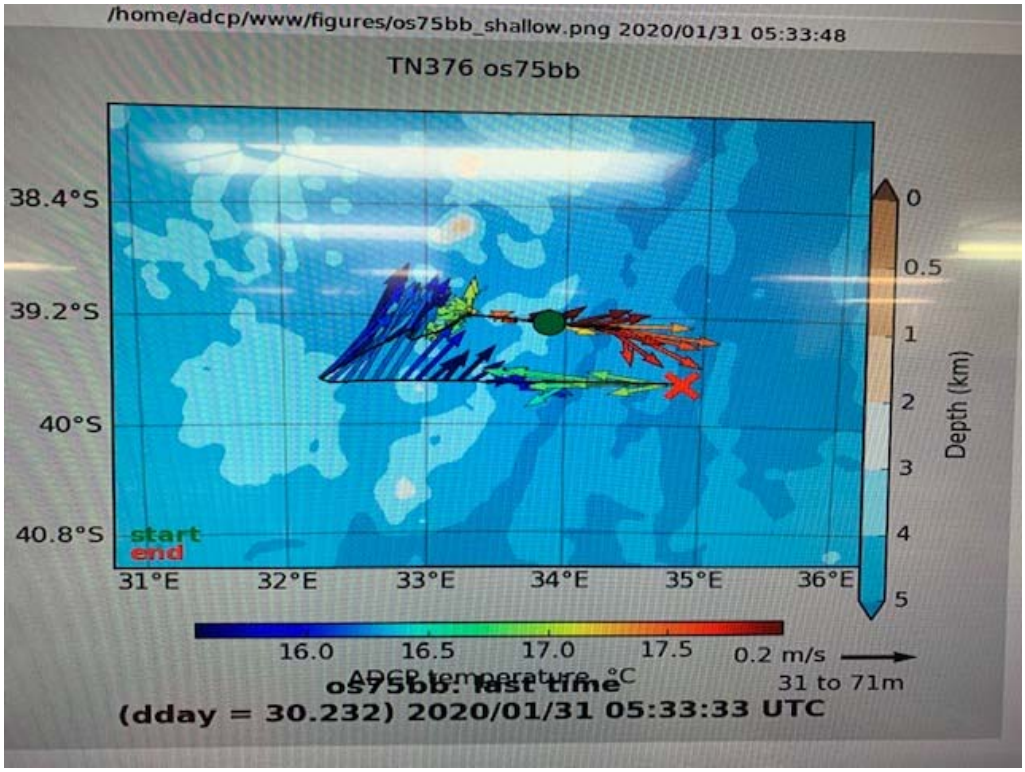
/home/adcp/www/figures/os75bb_shallow.png 2020/01/31 05:33:48
TN376 os75bb
38.4°S
39.2°S
40°S
40.8°S
start
end
31°E
32°E
33°E
34°E
35°E
36°E
0
0.5
1
2
3
4
5
Depth (km)
16.0
16.5
17.0
17.5
ADCP temperature, °C
0.2 m/s
31 to 71m
os75bb: fast time
(dday = 30.232) 2020/01/31 05:33:33 UTC

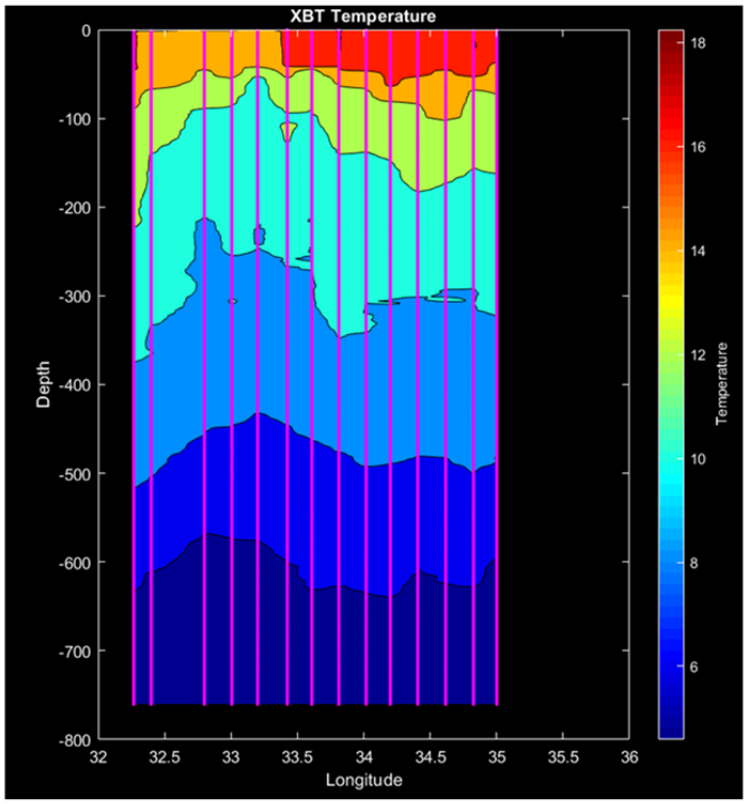
XBT Temperature
Depth
0
-100
-200
-300
-400
-500
-600
-700
-800
32
32.5
33
33.5
34
34.5
35
35.5
36
Longitude
18
16
14
12
10
8
6
Temperature

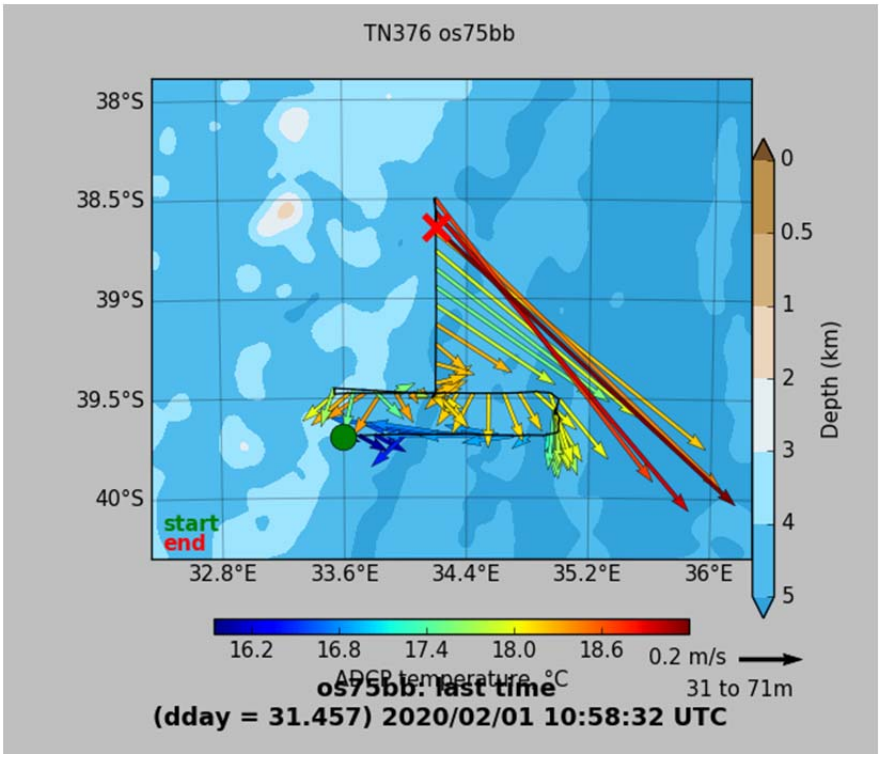

1-2 February

From the primary productivity station just east of eddy center (34 12'E, in a high Bb' regime within the eddy), we steamed north to 38.5S. Underway measurements indicate decreasing Bb' as we entered the Aguhlas Front. This set the stage for a southward VPR tow through the features (Figure 3.4). The warm, salty, low density water of the Aguhlas Front is associated with low Chl, Bb, and oxygen. Proceeding southward, we crossed through the limb of cool and fresh high Chl / high Bb / high oxygen waters wrapping eastward around the eddy. Farther south we entered the warmer and saltier waters of the low Chl / high Bb eddy, whose southern boundary was in the vicinity of 39.8 S. South of the eddy there was a regime of low Chl / high Bb, although the low Chl extended from the surface down to 50-60m, in contrast to the subsurface Chl max inside the eddy.

Underway XBT measurements along VPR5 characterize thermocline variability associated with the features described above.

Figure 3.4. VPR5 track overlayed on Chl (left) and PIC (right). Contours are ADT. VPR data panels follow below.

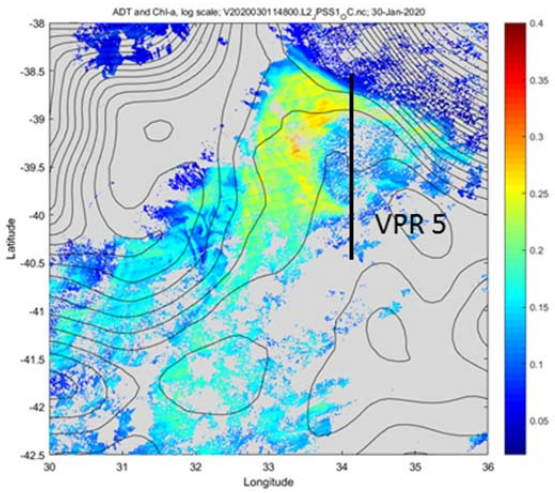
ADT and Chl-a, log scale; V2020030114800.L2_PSS1_0C.nc; 30-Jan-2020
VPR 5
Latitude
Longitude

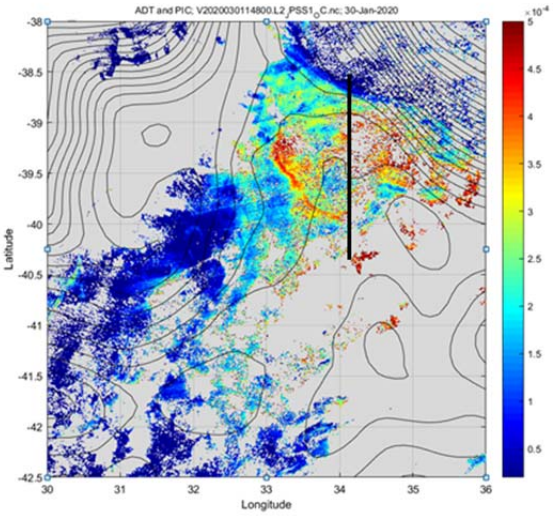
ADT and PIC; V2020030114800.L2_PSS1_0C.nc; 30-Jan-2020
Latitude
Longitude

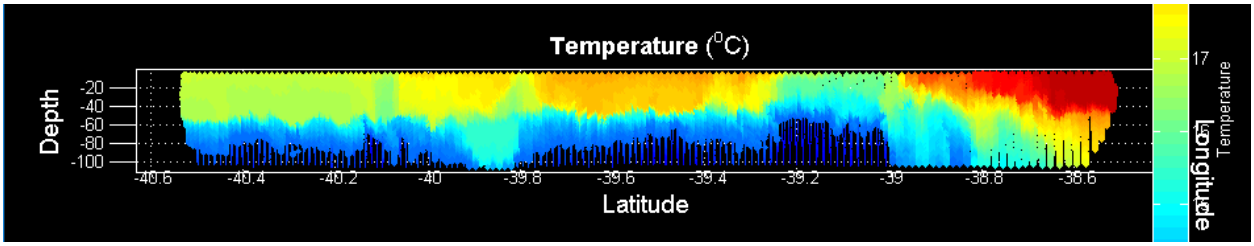
Temperature (°C)
Depth
Latitude
Temperature
Longitude

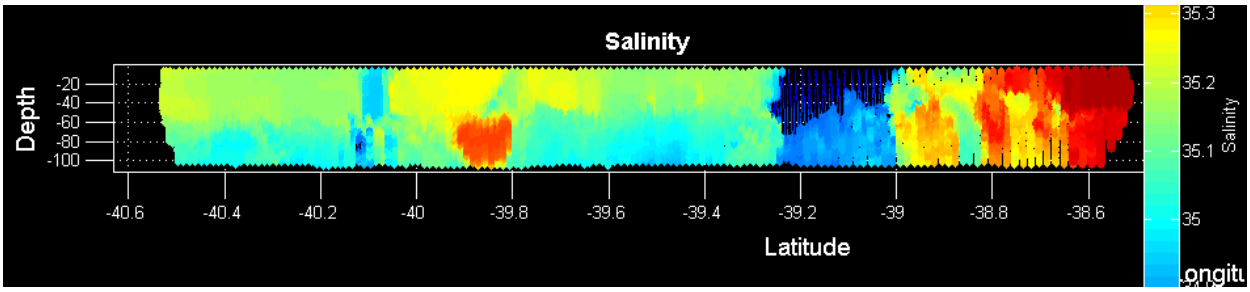
Salinity
Depth
Latitude
Salinity

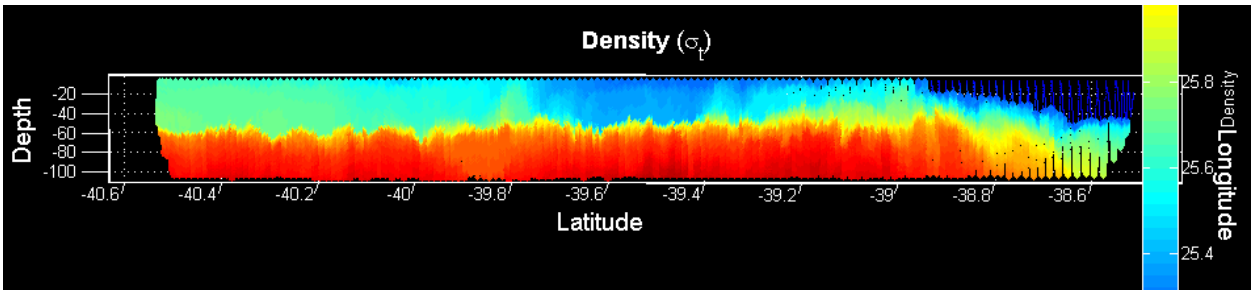
Density (σt)
Depth
Latitude
Density
Longitude

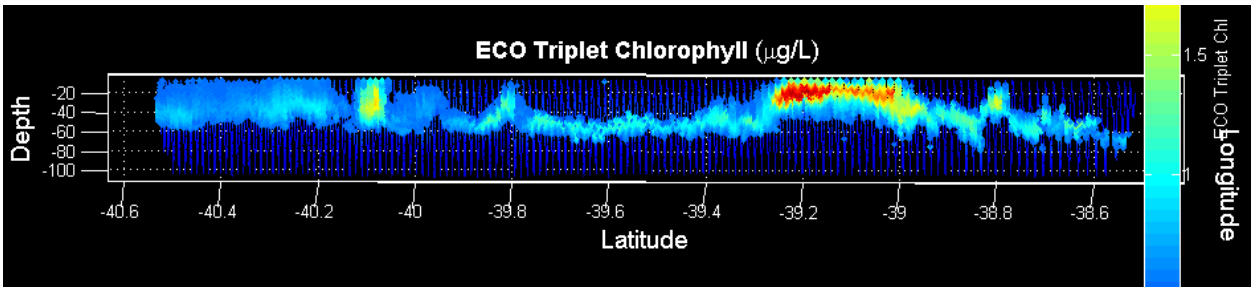
ECO Triplet Chlorophyll (µg/L)
Depth
-20
-40
-60
-80
-100
-40.6
-40.4
-40.2
-40
-39.8
-39.6
-39.4
-39.2
-39
-38.8
-38.6
Latitude
1.5
1
ECO Triplet Chl
Longitude

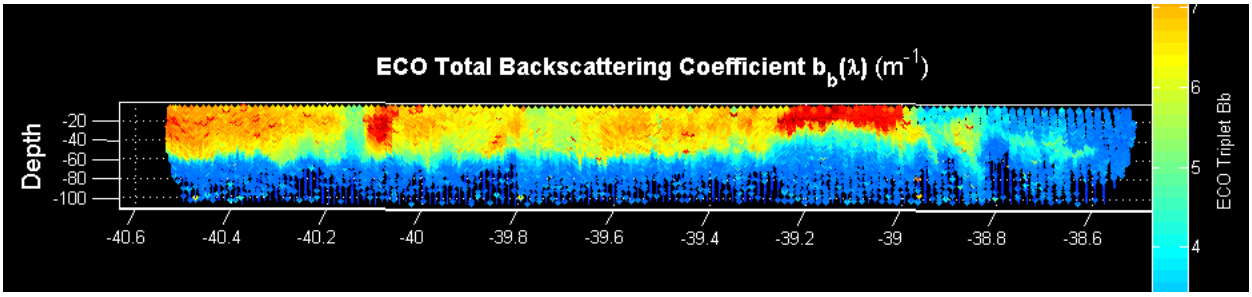
ECO Total Backscattering Coefficient $b_b(\lambda)$ (m^{-1})
Depth
-20
-40
-60
-80
-100
-40.6
-40.4
-40.2
-40
-39.8
-39.6
-39.4
-39.2
-39
-38.8
-38.6
7
6
5
4
ECO Triplet Bb

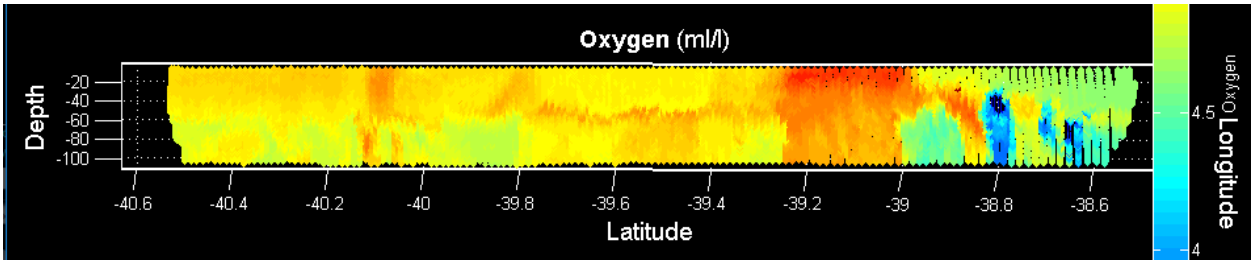
Oxygen (ml/l)
Depth
-20
-40
-60
-80
-100
-40.6
-40.4
-40.2
-40
-39.8
-39.6
-39.4
-39.2
-39
-38.8
-38.6
Latitude
4.5
4
Oxygen
Longitude

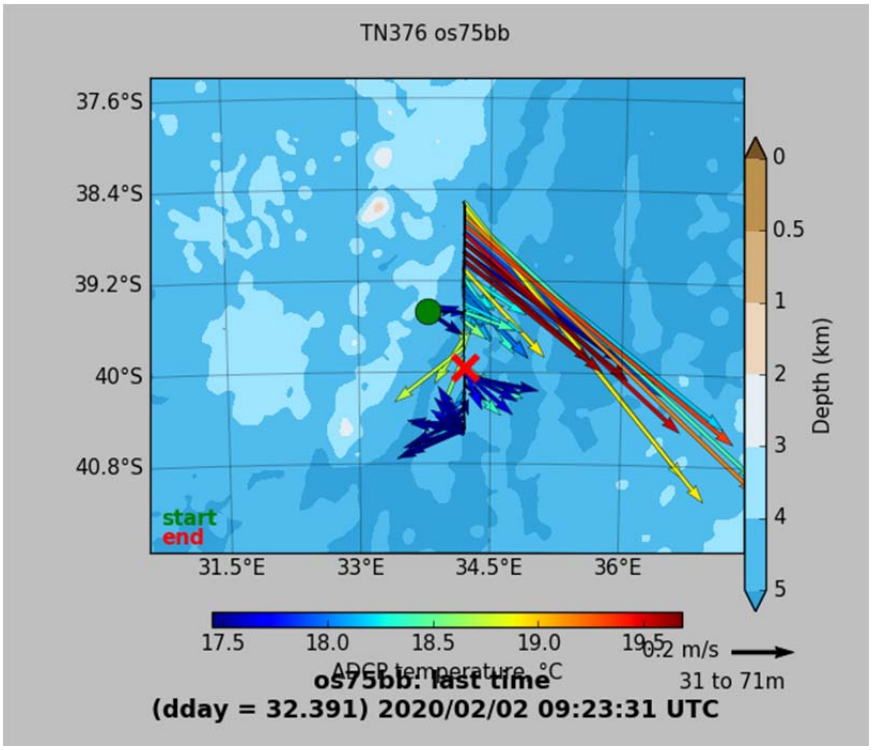
TN376 os75bb
37.6°S
38.4°S
39.2°S
40°S
40.8°S
start
end
31.5°E
33°E
34.5°E
36°E
0
0.5
1
2
3
4
5
Depth (km)
17.5
18.0
18.5
19.0
19.5
ADCP temperature °C
0.2 m/s
31 to 71m
os75bb: last time
(dday = 32.391) 2020/02/02 09:23:31 UTC

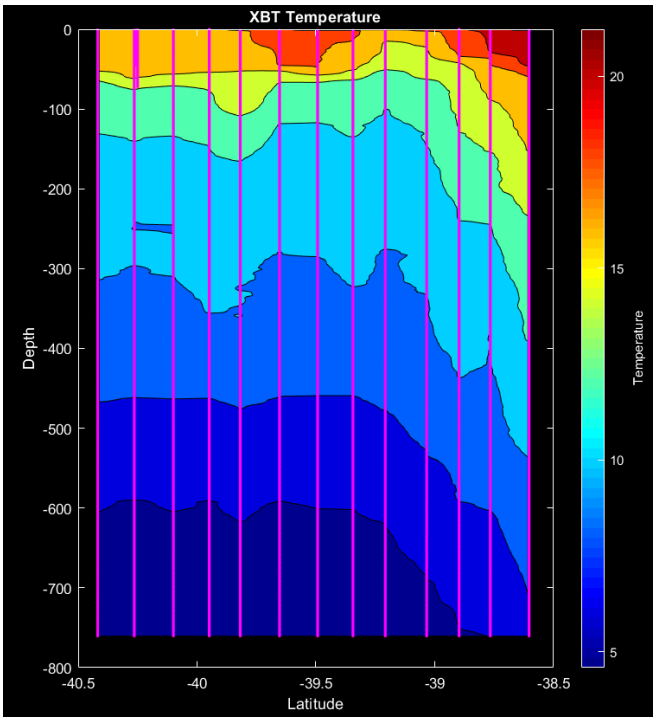

3 February

A line of CTDs was completed running back northward along the VPR5 transect. Upon completion of that, we made a towVPR 6 from the northernmost CTD station to the easternmost on the E-W line. This tow had us proceeding southeastward along the meander of the Agulhas Front, breaking out into the adjacent water mass toward the very end. Evidence of small scale frontal subduction / upwelling is present in both the hydrographic and bio-optical properties. The tow ended with a transition from high Chl / high backscatter to low Chl / low backscatter.

Figure 3.5. VPR6 track overlayed on Chl (left) and PIC (right). Contours are ADT. VPR data panels follow below.

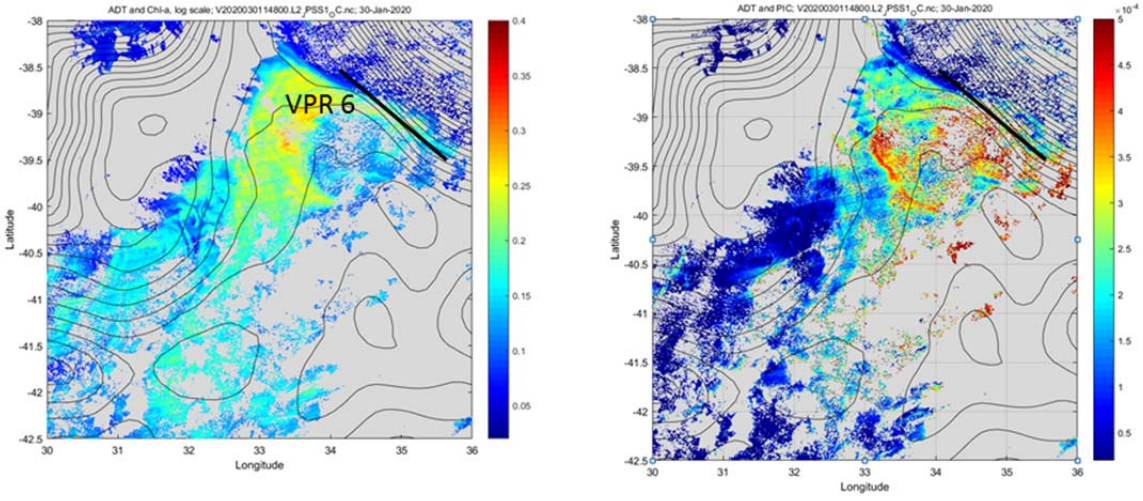

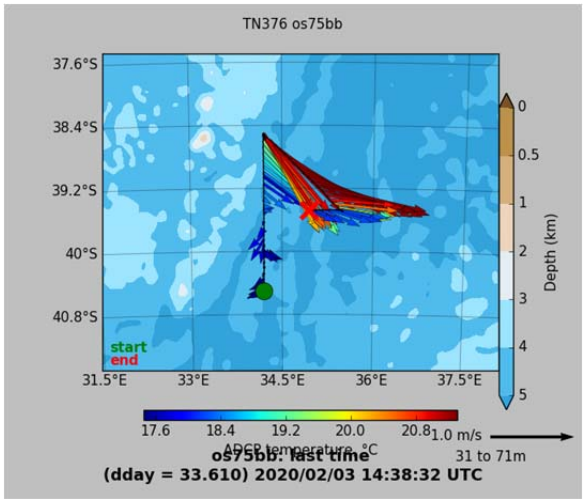
TN376 os75bb
37.6°S
38.4°S
39.2°S
40°S
40.8°S
start
end
31.5°E
33°E
34.5°E
36°E
37.5°E
0
0.5
1
2
3
4
5
Depth (km)
17.6
18.4
19.2
20.0
20.8
ADCP temperature, °C
1.0 m/s
31 to 71m
os75bb: last time
(dday = 33.610) 2020/02/03 14:38:32 UTC

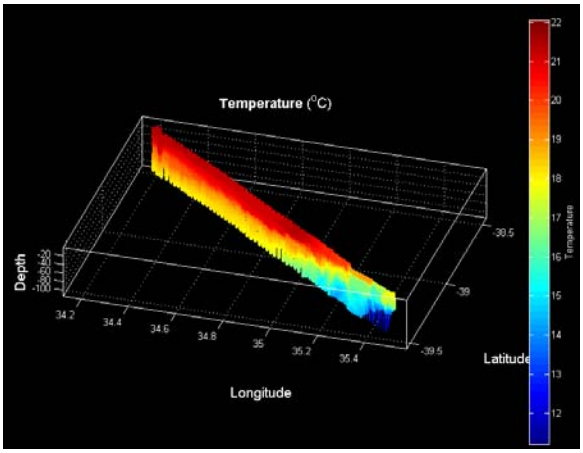
Temperature (°C)
Depth
Latitude
Longitude

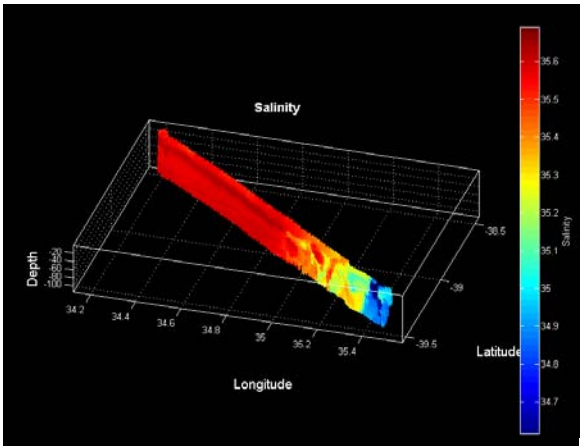
Salinity
Depth
Latitude
Longitude

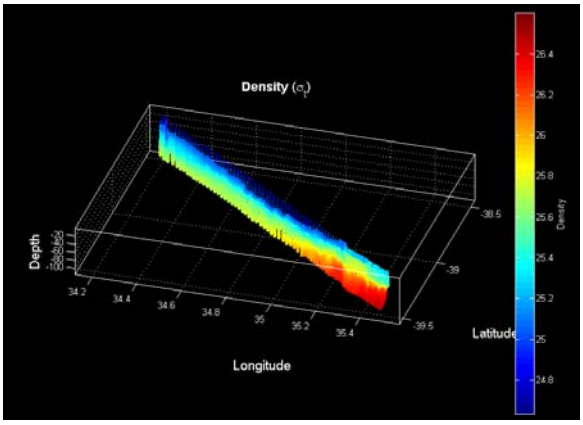
Density (σt)
Depth
Latitude
Longitude

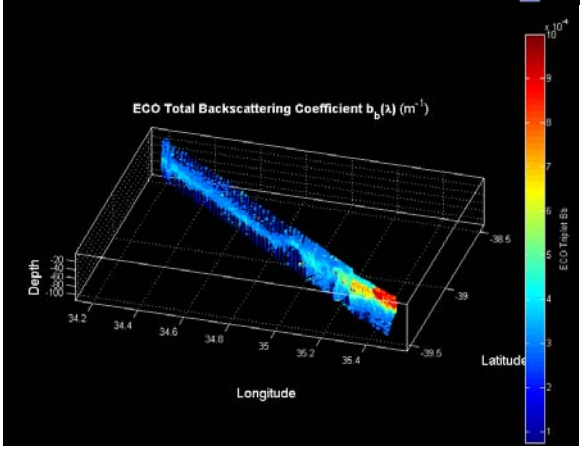
ECO Total Backscattering Coefficient bb(λ) (m-1)
Depth
Latitude
Longitude

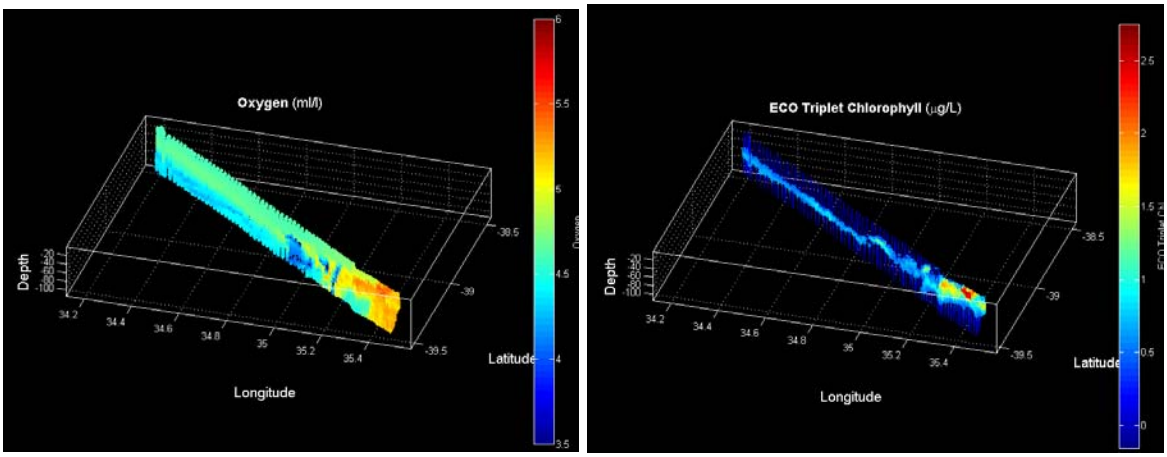

4 February

A line of CTDs was completed from east to west across the low Chl / high Bb and high Chl / High Bb feature. Upon completion of that line of CTDs, we made a towVPR 7 (Figure 3.6) from the westernmost CTD station to the northernmost on the N-S line, as this tow is almost on course with our route to the next eddy. This section shows high contrast between the cool, fresh, high chl, and high oxygen waters south of the Agulhas front, with the warm, salty, low chl, low oxygen in the front.

Figure 3.6. VPR7 track overlayed on Chl (left) and PIC (right). Contours are ADT. VPR data panels follow below.

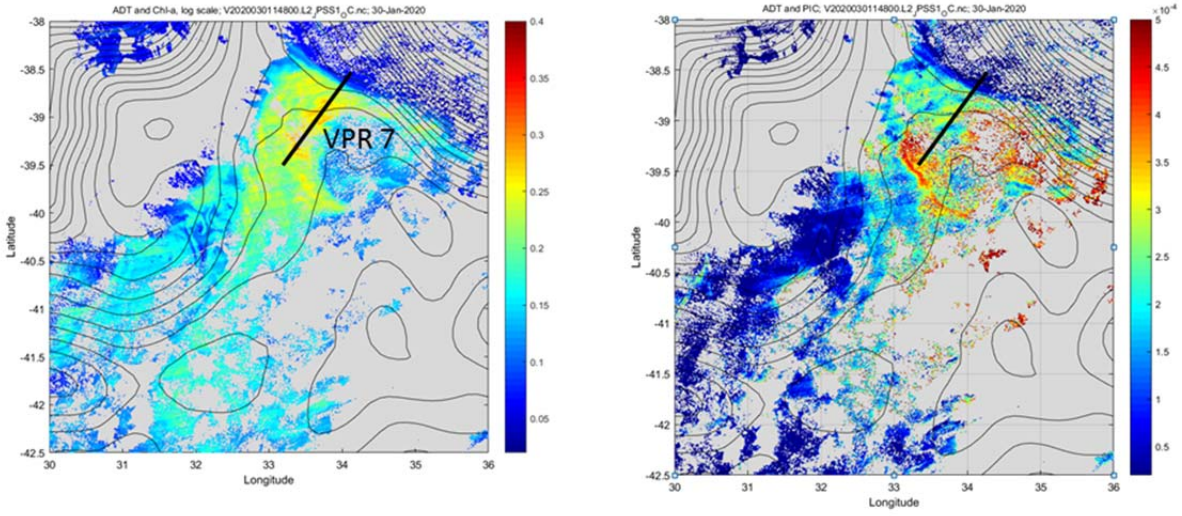

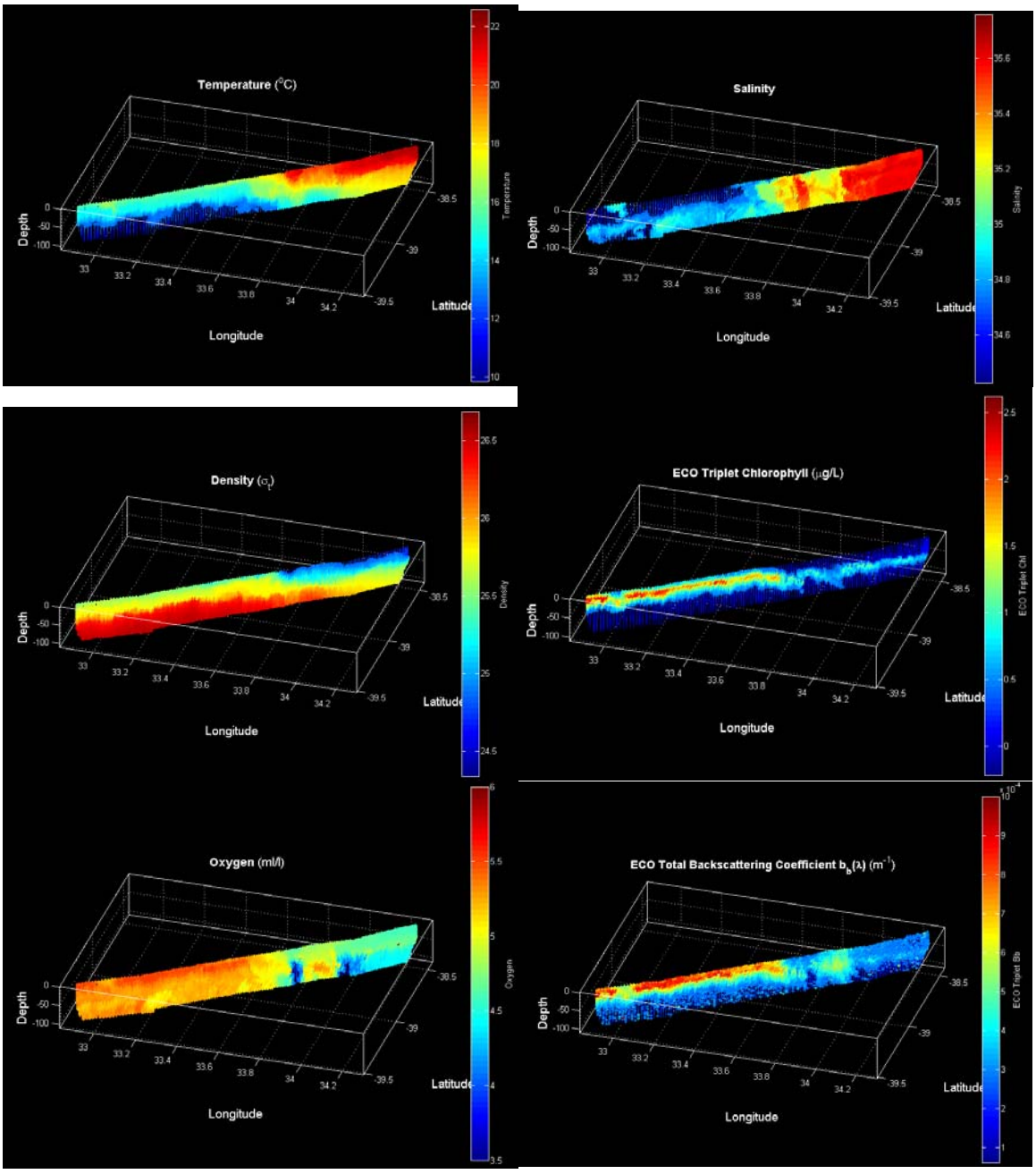

5-6 February

Steamed northeast to begin the eddy 2 survey. VPR8 entry began west of the feature, transiting east with the objective of locating the band of high Bb water encircling the eddy (Figure 3.7). Upon arriving in that area, the VPR was recovered so a station could be occupied and water collected for incubation experiments. VPR9 picked up where VPR8 left off, completing the east-west transect then proceeding northwest to occupy a north-south transect. ADCP data confirm the clockwise circulation of the cyclonic eddy, and that crossing between the two transects was very close to eddy center, just slightly to the northeast. XBT transects in the E-W direction (T-7s

down to 700m) and N-S direction (T-5s down to 1300m) depict the upward doming of the main thermocline.

VPR data delineate the spatial extent of the low salinity water comprising the core of the eddy. Highest backscatter coincides with these frontal boundaries, where interleaving of water masses is apparent. Unfortunately the oxygen sensor appears to have been airlocked in VPR9, rendering those data useless.

Interior points of the CTD transects were chosen to coincide with peaks in Bb' residing at the salinity front surrounding the eddy core.

South
36 37.0 S
37 37.7 E
Interior south
36 12.0 S
37 37.7 E
Eddy center
35 53.0 S
37 37.7 E
Interior north
35 24.0 S
37 37.7 E
North
35 09.0 S
37 37.7 E

East
35 53.0 S
38 39.0 E
Interior east
35 53.0 S
38 24.0 E
Eddy center
35 53.0 S
37 37.7 E
Interior west
35 53.0 S
37 24.0 E
West
35 53.0 S
36 30.0 E

Figure 3.7. ADT contours overlayed on Chl (left) and PIC (right). ADCP and VPR data panels follow below.

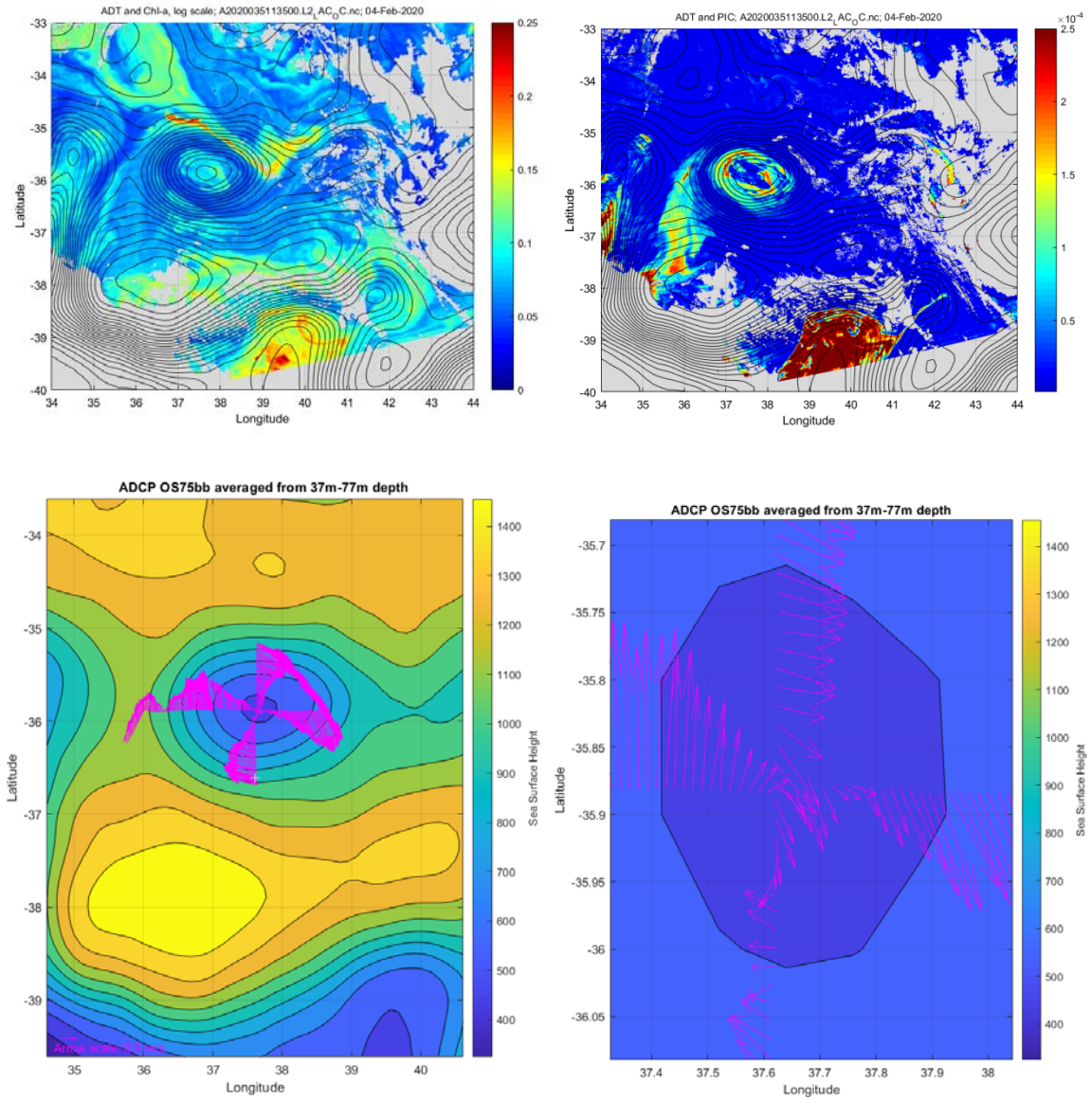

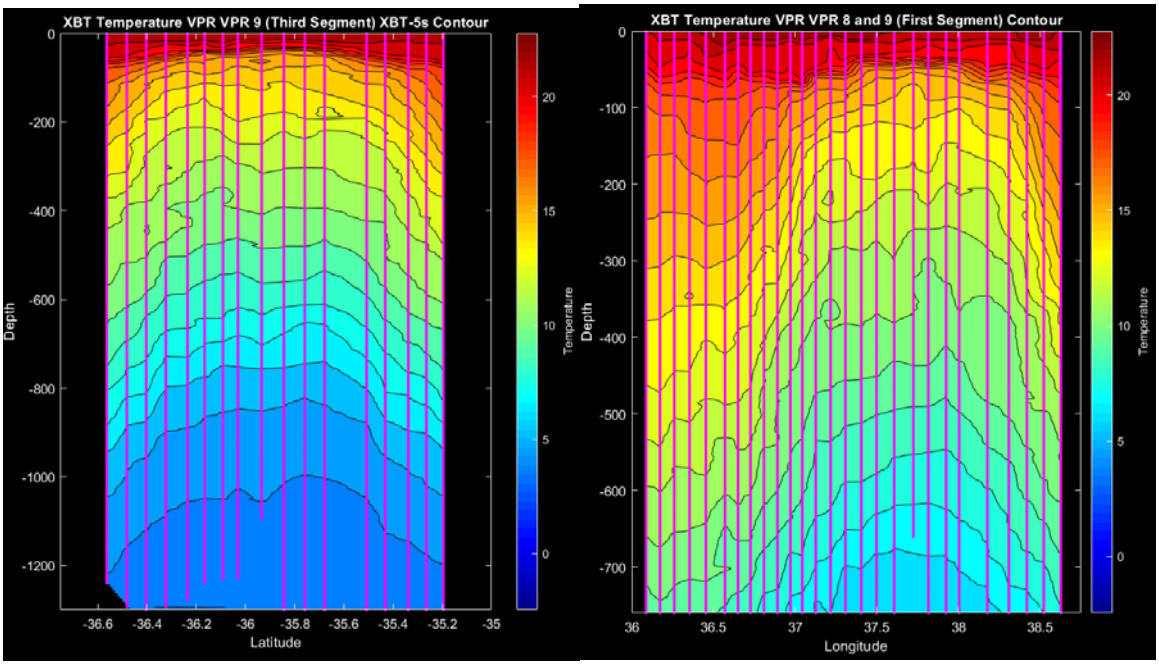
XBT Temperature VPR VPR 9 (Third Segment) XBT-5s Contour
Depth
Latitude
Temperature
XBT Temperature VPR VPR 8 and 9 (First Segment) Contour
Depth
Longitude
Temperature

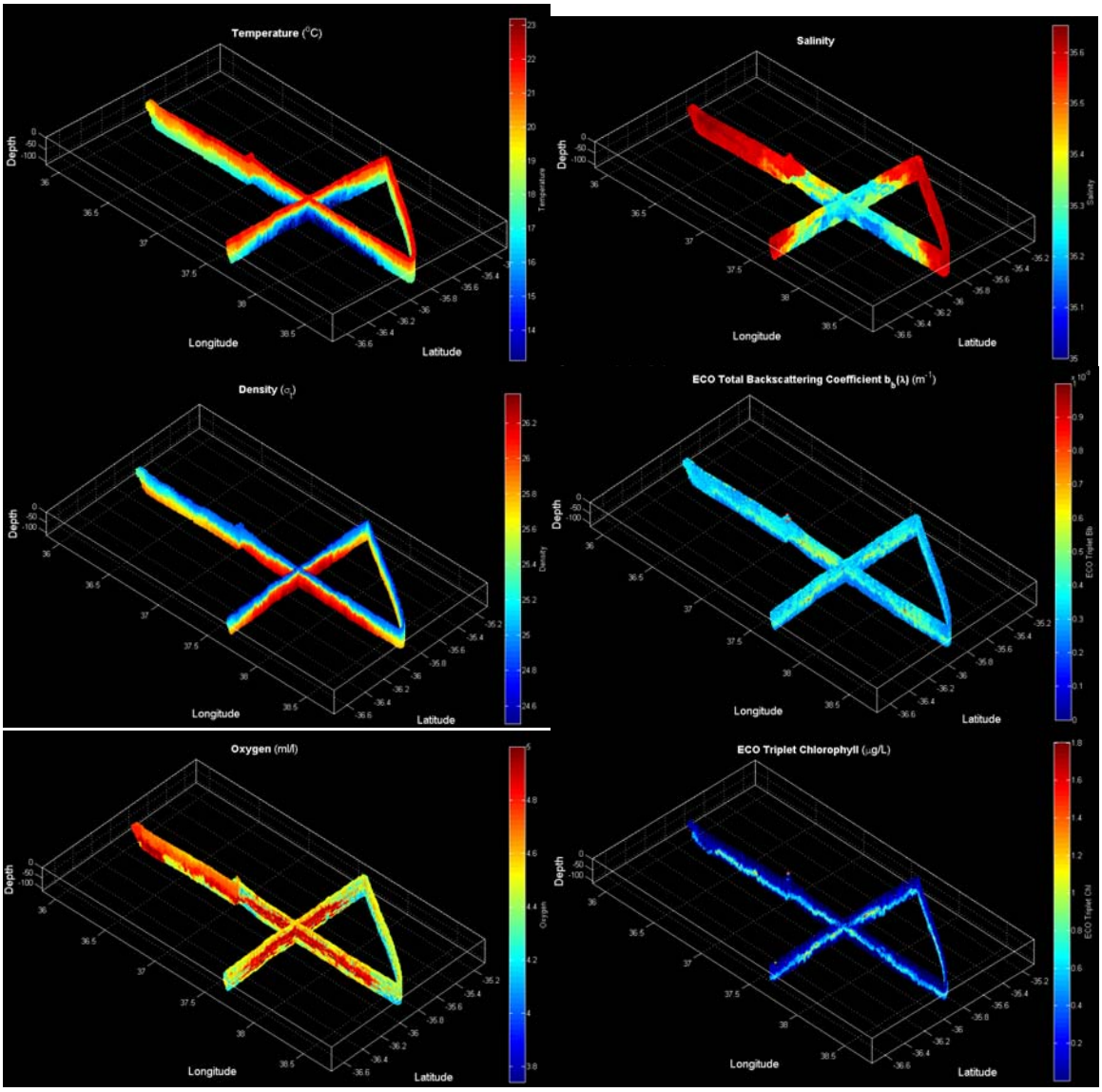

7-8 February

CTD sampling of eddy feature.

8-10 February

Transit to Durban.

10-13 February

Engine repairs in Durban

13 February

As we prepared for departure from Durban, we deliberated on which 2 features to focus on with our remaining science time, roughly two 3.5 day stanzas. There are four candidates:

Resample Eddy 3: dimishing PIC
Satellite PIC:
Feb 2 – 0.2
Feb 3 – 0.2 VIIRS
Feb 4 – 0.2 MODIS
Feb 4 – 0.1 VIIRS In situ 0.6
Feb 12 – background MODIS

Resample Eddy 1: rising PIC
Satellite PIC:
Jan 24 – 0.4 MODIS
Feb 8 – 0.4 VIIRS
Feb 11 – 0.8 VIIRS
Feb 12 – 1.2 MODIS

40/50 Eddy: quasi-stable PIC in a different regime (AC to the north of AF)
Satellite PIC:
Feb 1 – 0.6 MODIS
Feb 1 – 0.5 VIIRS
Feb 12 – 0.3 (interior) 0.5(spur) VIIRS
Feb 12 – 0.5 (interior) 1.0 (spur) MODIS

New eddy to the west of Eddy 3:
Satellite PIC:
Feb 12 – background MODIS
Feb 12 – background VIIRS

Weighing all of the scientific and logistical constraints, the choice was clear: (1) resample eddy 1, then (2) resample eddy 3.

Departed Durban at ca. 1930 Thurs 13 Feb.

14-15 February

Steamed to the high PIC region.

16 February

Carried out VPR survey of the southernmost transect of three in the high-PIC feature formerly known as Eddy 1 & 2 (Figure 3.8). The area is generally northward flowing to the west, and southward flowing to the east, with an eddy of low chlorophyll and PIC in the middle. T-S characteristics are similar to that observed in Eddy 1 and 2, with high PIC / high chl assocated with low salinity SAW (HPCLS) and low chlorophyll / high backscatter assocaited with more

saline waters (SSTW) in Eddy 4. Ironically, satellite-based PIC in Eddy 4 in a local minimum rather than a local maximum as indicated by underway measurements of Bb'.

Began CTD survey back from west to east.

Figure 3.8. ADT contours overlayed on Chl (left) and PIC (right). ADCP, XBT, and VPR data panels follow below.

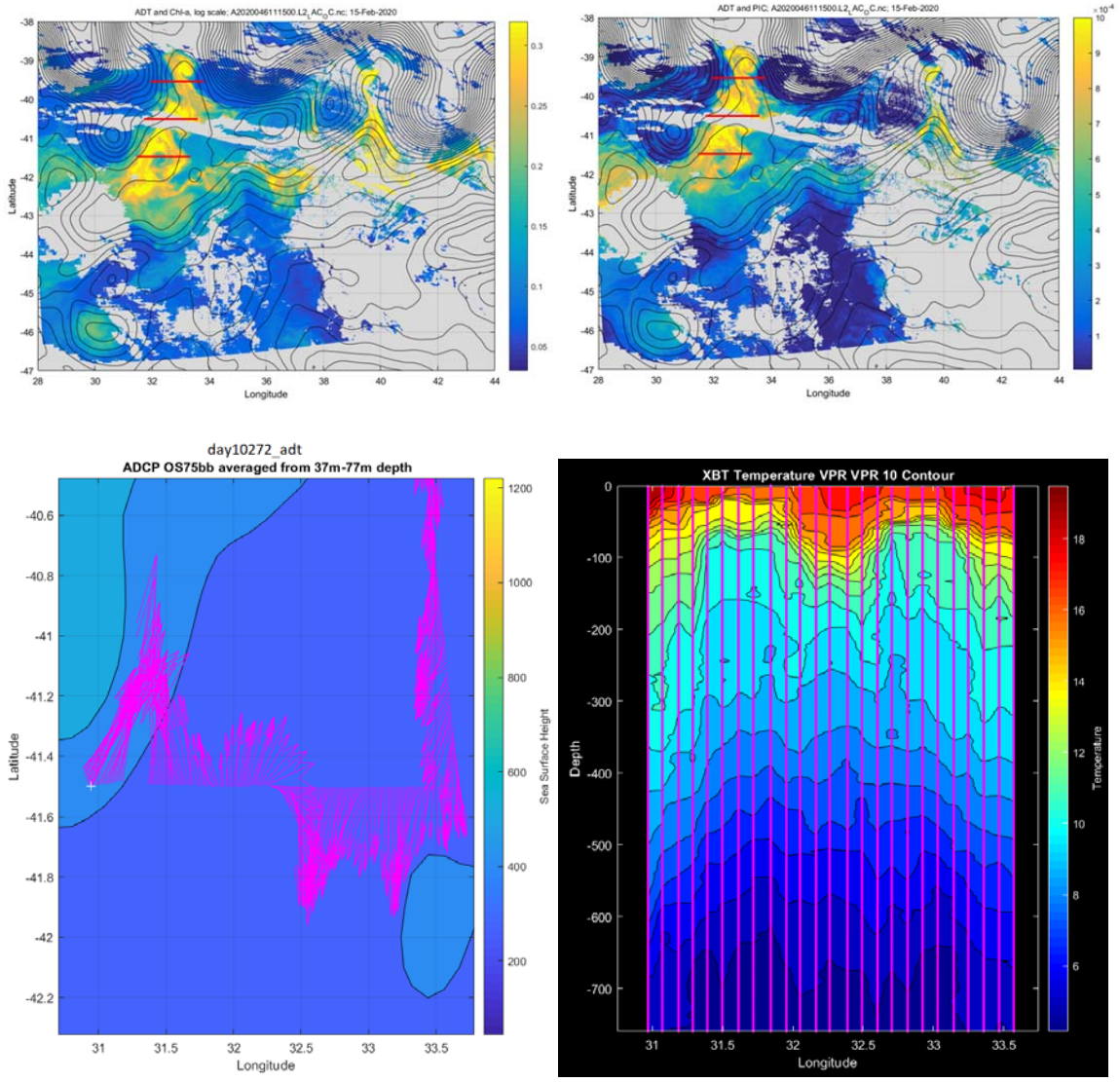

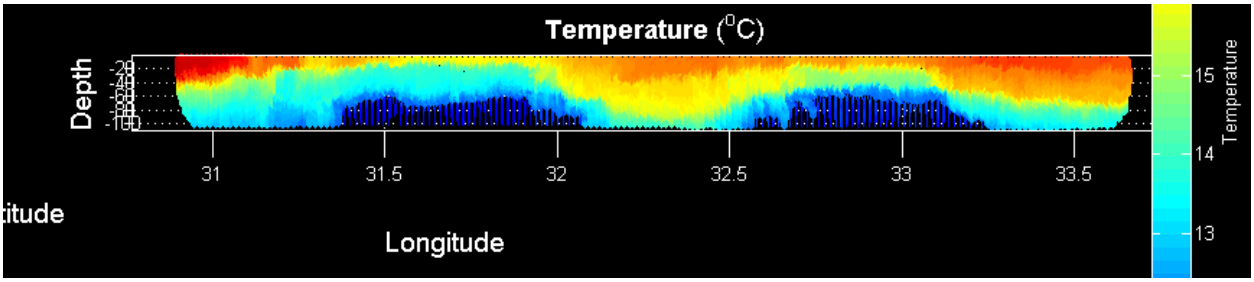
Temperature (°C)
Depth
-20
-40
-60
-80
-100
31
31.5
32
32.5
33
33.5
Longitude
15
14
13
Temperature

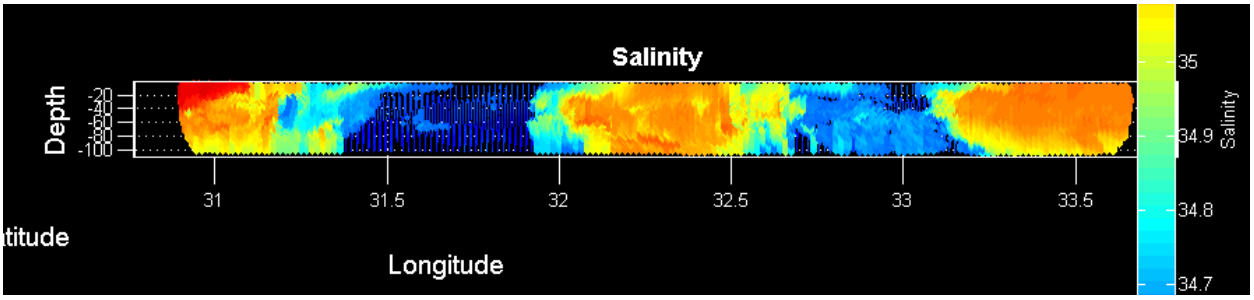
Salinity
Depth
-20
-40
-60
-80
-100
31
31.5
32
32.5
33
33.5
Longitude
35
34.9
34.8
34.7
Salinity

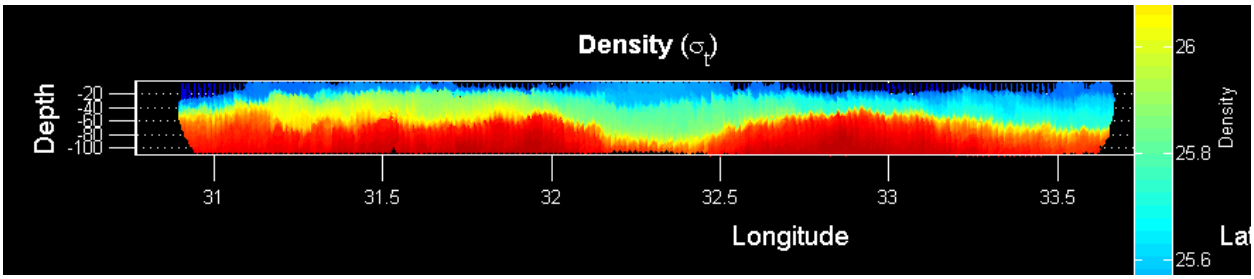
Density (σt)
Depth
-20
-40
-60
-80
-100
31
31.5
32
32.5
33
33.5
Longitude
26
25.8
25.6
Density

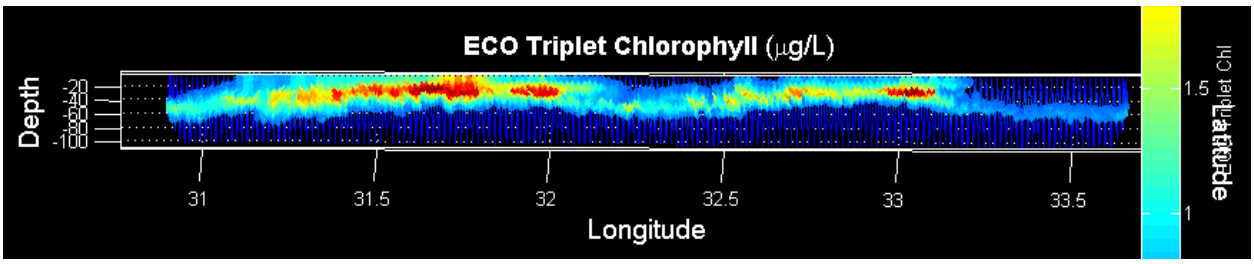
ECO Triplet Chlorophyll (µg/L)
Depth
-20
-40
-60
-80
-100
31
31.5
32
32.5
33
33.5
Longitude
1.5
1

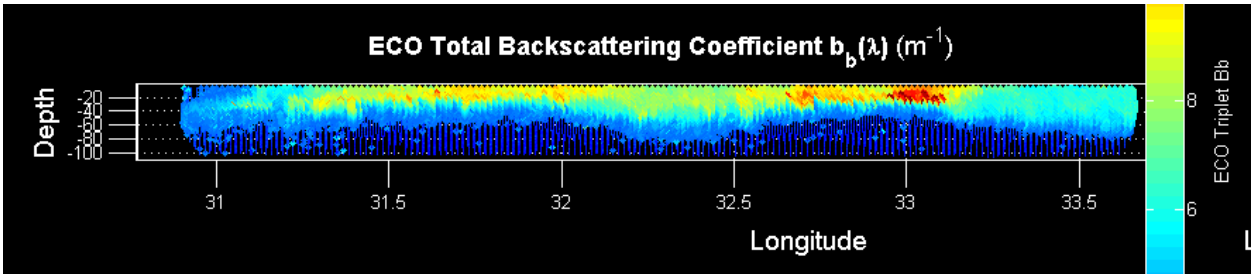
ECO Total Backscattering Coefficient bb(λ) (m-1)
Depth
-20
-40
-60
-80
-100
31
31.5
32
32.5
33
33.5
Longitude
8
6
ECO Triplet Bb

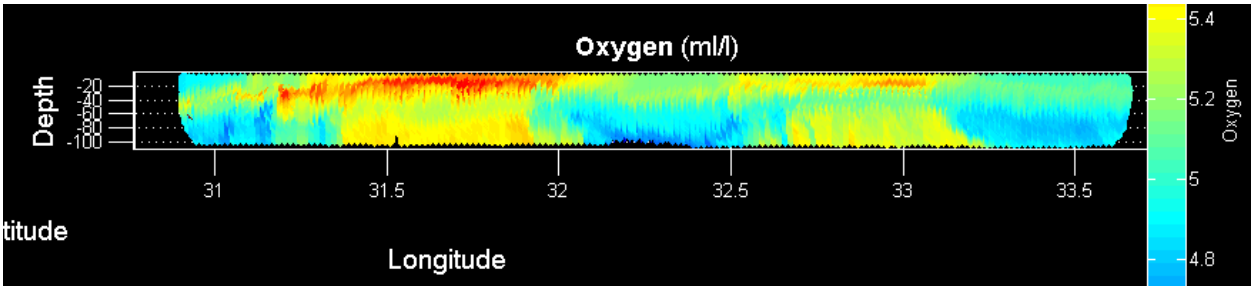

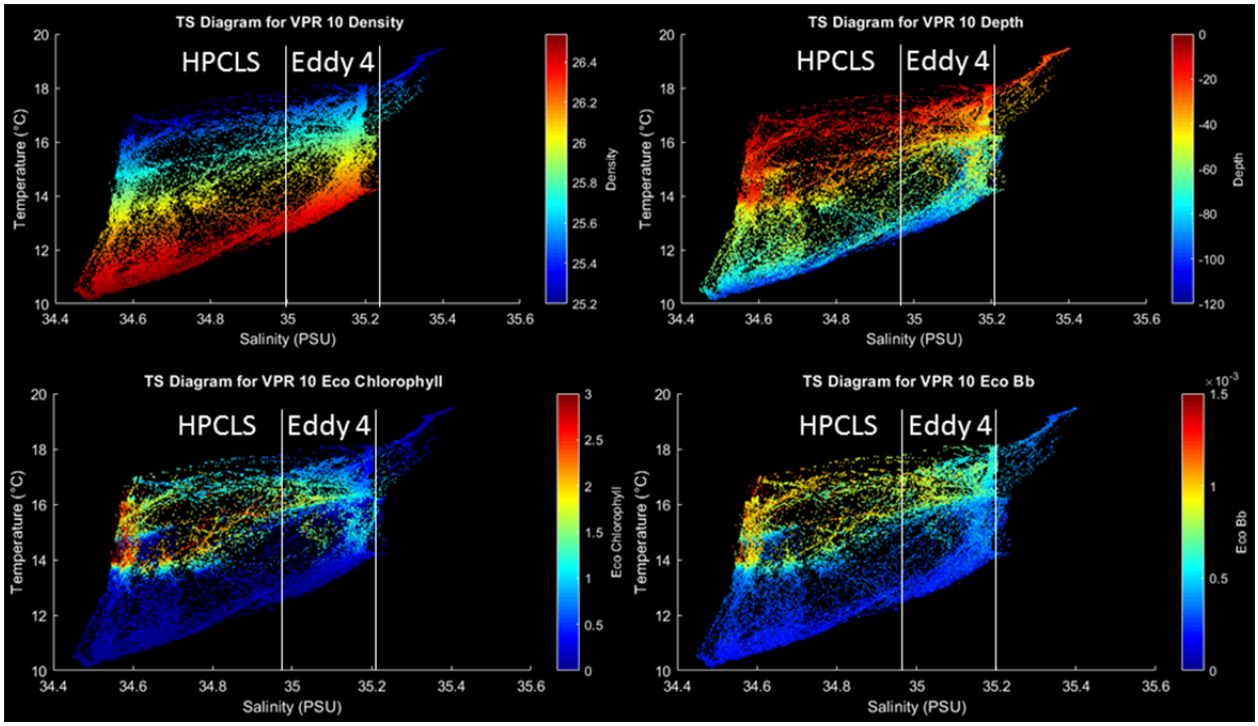

17 February

Continued CTD line (Table 3.1). Reached the end of the line in rough conditions; DAVPR removed for station 34. Too rough to deploy VPR, so transited to middle section.

Transect	Station	Feature / comments
6	26	Western periphery outside feature
	27	Frontal boundary – nutrients only
	28	Frontal boundary – PP cast, TM cast, incubation water collection
	29	HPCLS – nutrients only
	30	Low PIC, low chlorophyll, high salinity (LPCHS) eddy
	31	Frontal boundary
	32	HPCLS
	33	East of frontal boundary with HPCLS

	34	Eastern periphery outside feature (no DAVPR)

Table 3.1. Station list for CTD transect 6 across southern section of the high PIC / high chlorophyll feature.

18 February

Deployed VPR in rough but subsiding conditions at the eastern end of the middle line of the high PIC region (Figure 3.9). Extended line a bit farther west to get to the edge. CTD transect begun, with station positions revised to (1) measure ambient conditions to the west (station 35), (2) avoid the 40-50m salinity anomaly at the planned station 39, in favor of a higher Bb (and Bb' according to underway) area, and (3) target meander center as defined by the VPR salinity, the north-south swing in ADCP velocity, and peak of the seasonal thermocline in the XBT data (station 41).

Analysis of bio-optical characteristics in T-S space reveals consistent water mass characteristics: highest chl and Bb in HPCLS waters less than 35 psu (SAW), with lower chl and consistent Bb in HPLCMS associated with the moderate salinities of SSTW.

Transect	Station	Feature / comments
7	35	Western periphery outside feature
	36	Frontal boundary – WS over CF submesoscale feature
	37	HPLCMS
	38	Frontal boundary – nutrients only
	39	HPCLS – PP cast, TM cast, incubation water collection
	40	Center of HPCLS – nutrients only
	41	HPCLS
	42	HPLCMS
	43	HPLCMS

Table 3.2. Station list for CTD transect 7 across the middle section of the high PIC / high chlorophyll feature.

Figure 3.9. VPR survey 11, the middle section of the high PIC meander (Figure 3.8 above).

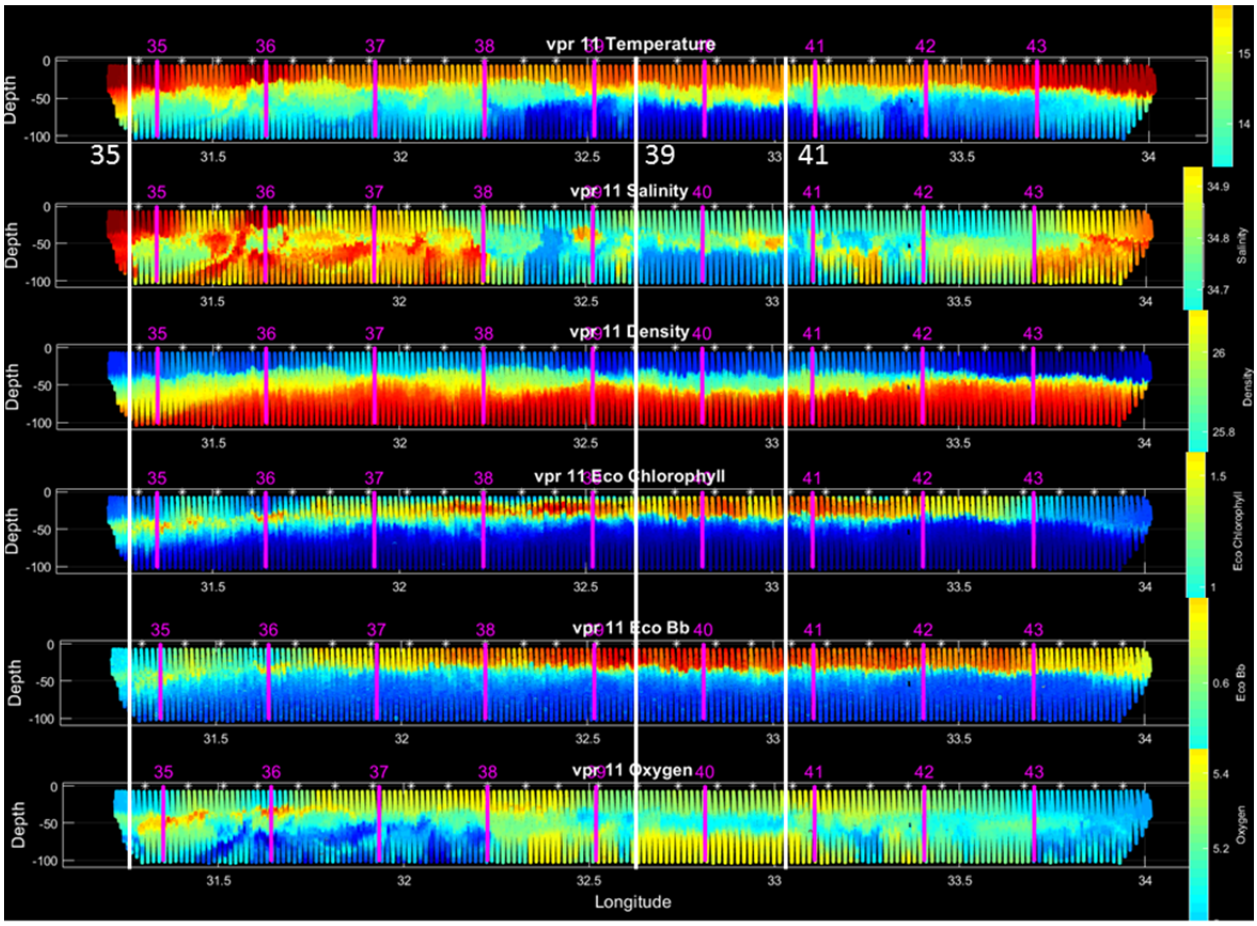

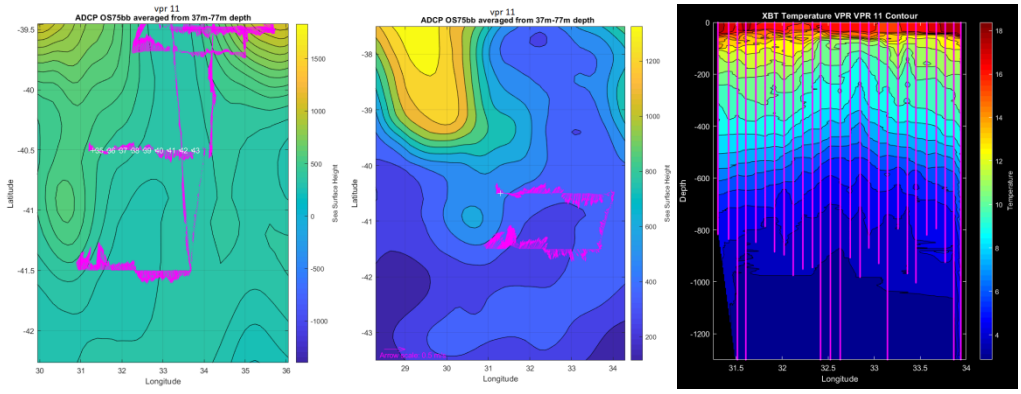

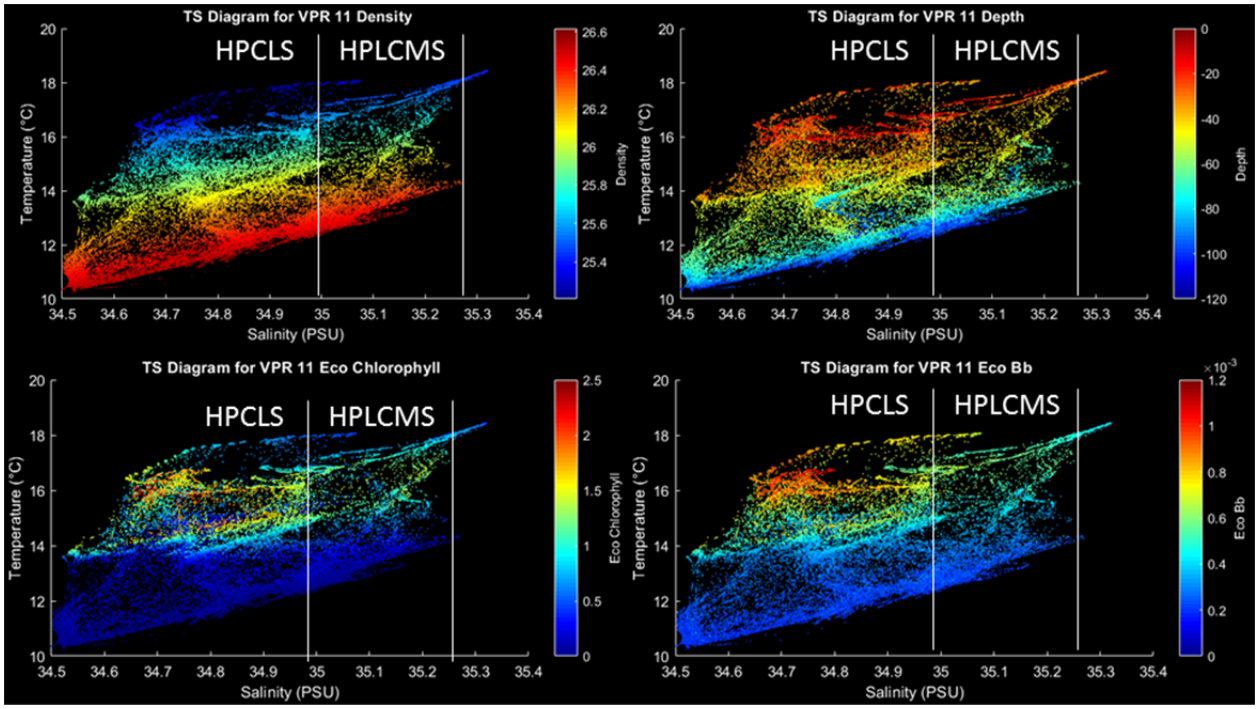

19-20 February

Completed CTD line. Deployed VPR at the the eastern end of the middle line of the high PIC region, towed north-northeast to the east end of the northern line and towed west (Figure 3.10). Positions for stations 45-51 were shifted to orient the PP/TM cast in the region of highest fluorescence and backscatter, while keeping the station spacing approximately the same.

Analysis of bio-optical characteristics in T-S space reveals consistent water mass characteristics: highest chl and Bb in HPCLS waters less than 35 psu (SAW), with lower chl and consistent Bb in HPLCMS associated with the moderate salinities of SSTW.

Transect	Station	Feature / comments
8	44	Western periphery outside feature
	45	Frontal boundary – WS over CF submesoscale feature
	46	HPLCMS
	47	HPLCMS
	48	HPCLS – PP cast, TM cast [peak chl, Bb]
	49	HPCLS – nutrients only
	50	HPCLS
	51	HPLCMS
	52	HPLCMS

Table 3.3. Station list for CTD transect 8 across northern section of the high PIC / high chlorophyll feature.

Figure 3.10. VPR survey 12, the northern section of the high PIC meander (Figure 3.8 above). White vertical bars indicate the locations of the shifted stations.

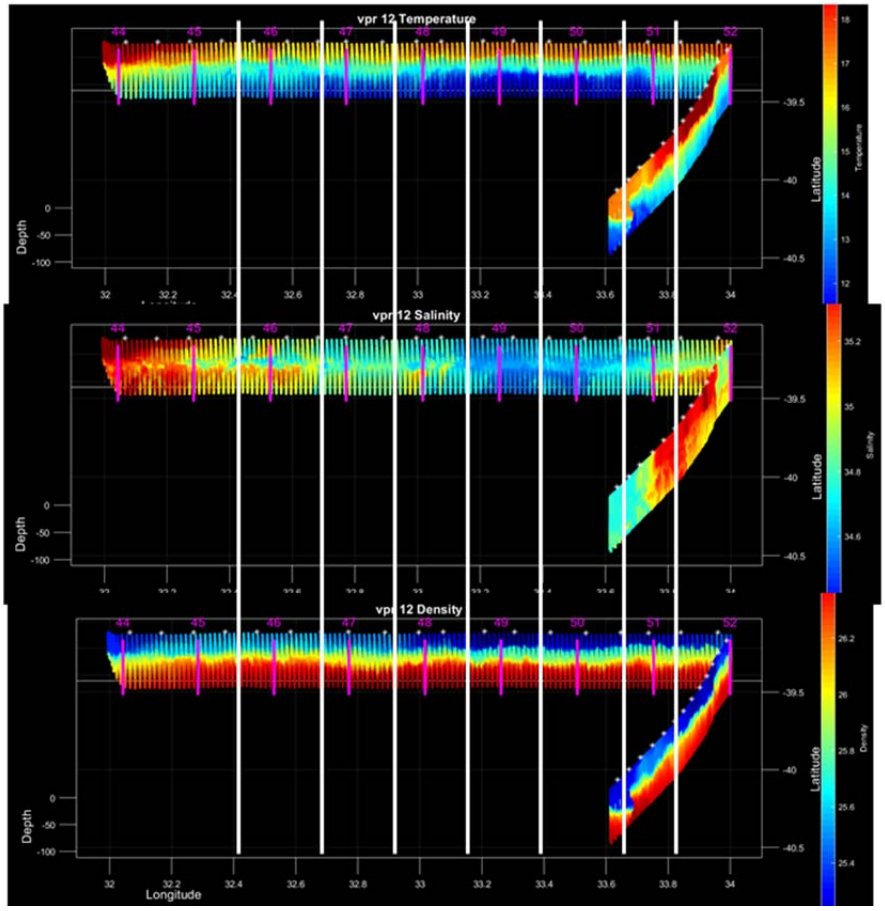

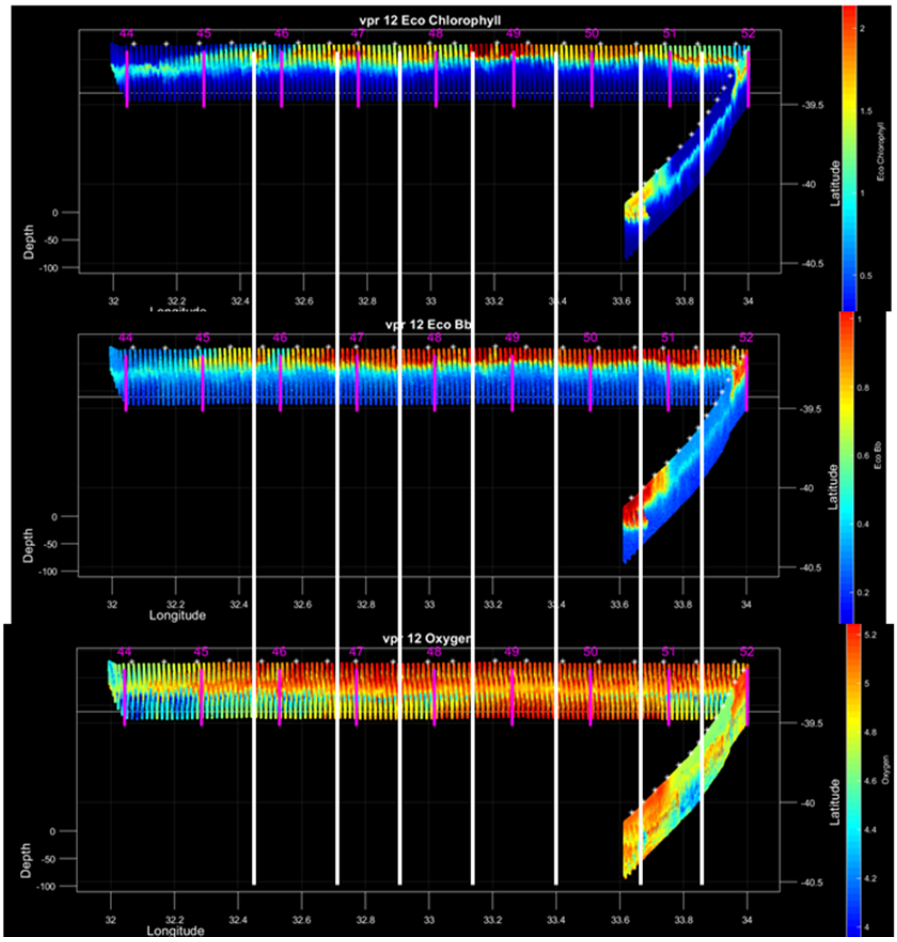
vpr 12 Eco Chlorophyll
vpr 12 Eco Bb
vpr 12 Oxygen
Depth
Latitude
Longitude
Eco Chlorophyll
Eco Bb
Oxygen

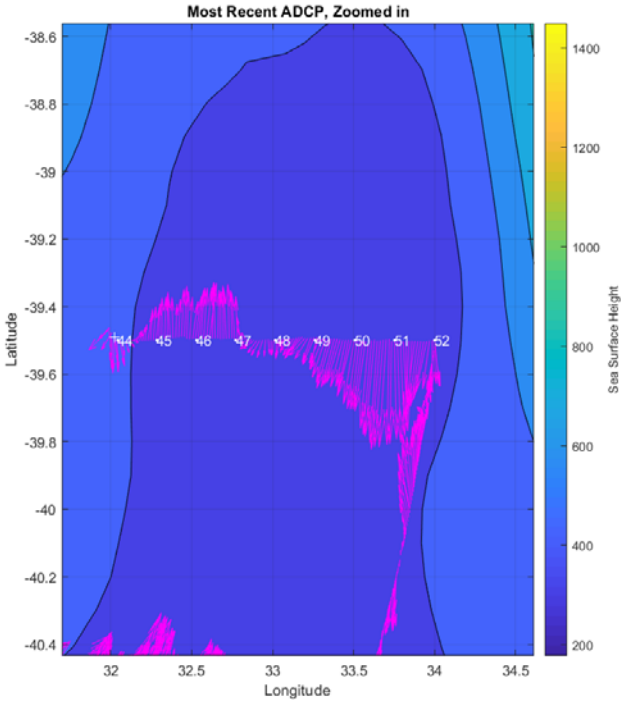
Most Recent ADCP, Zoomed in
Latitude
Longitude
Sea Surface Height

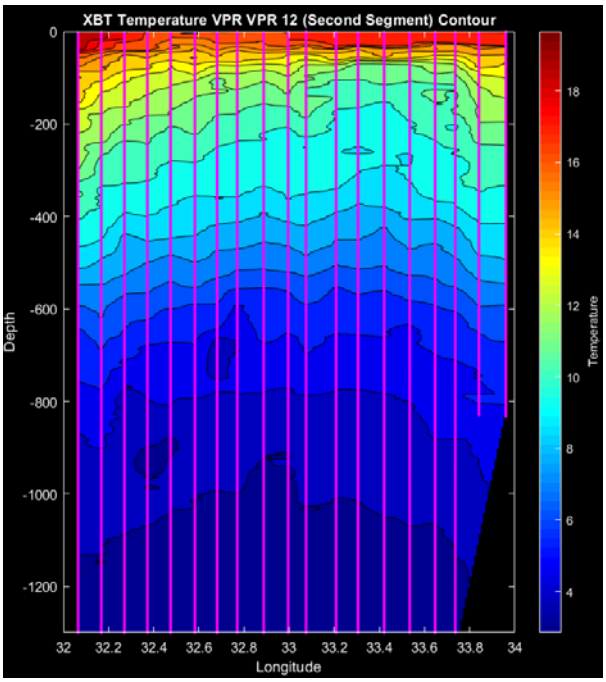
XBT Temperature VPR VPR 12 (Second Segment) Contour
Depth
Longitude
Temperature

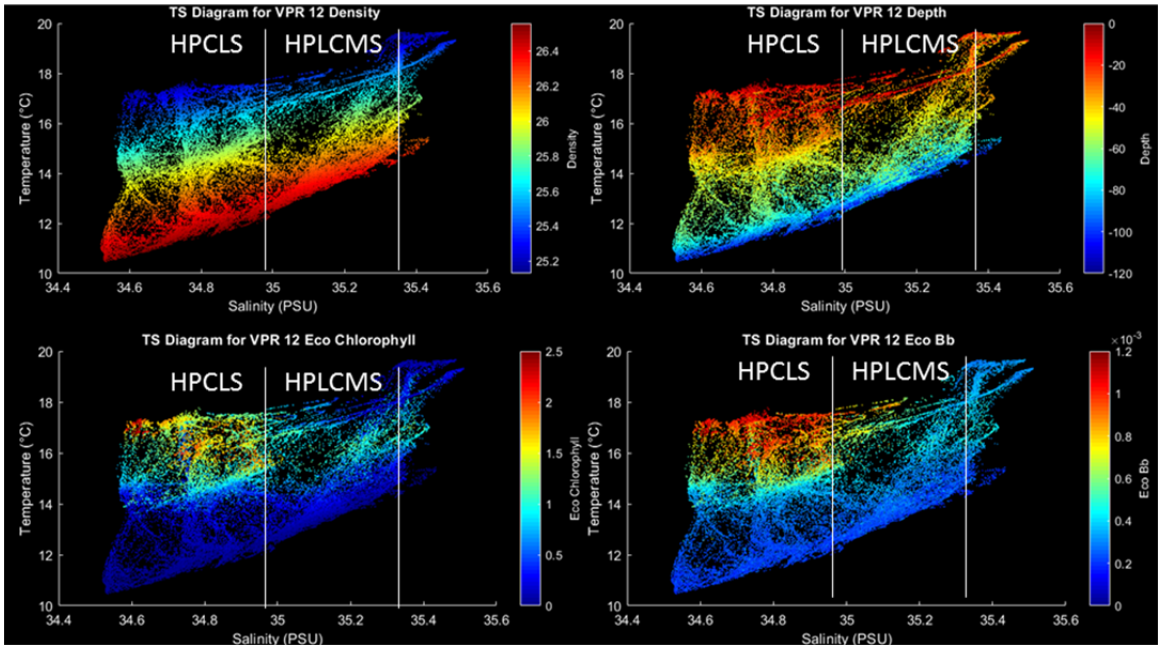

21 February
Deep CTD cast (DAVPR removed). Transit back to Eddy 3.

22 February
Satellite imagery suggest the surface signature of PIC in Eddy 3 has subsided, excepting for an area in the southwest quadrant of the eddy in the MODIS image, although this may be a cloud artefact.

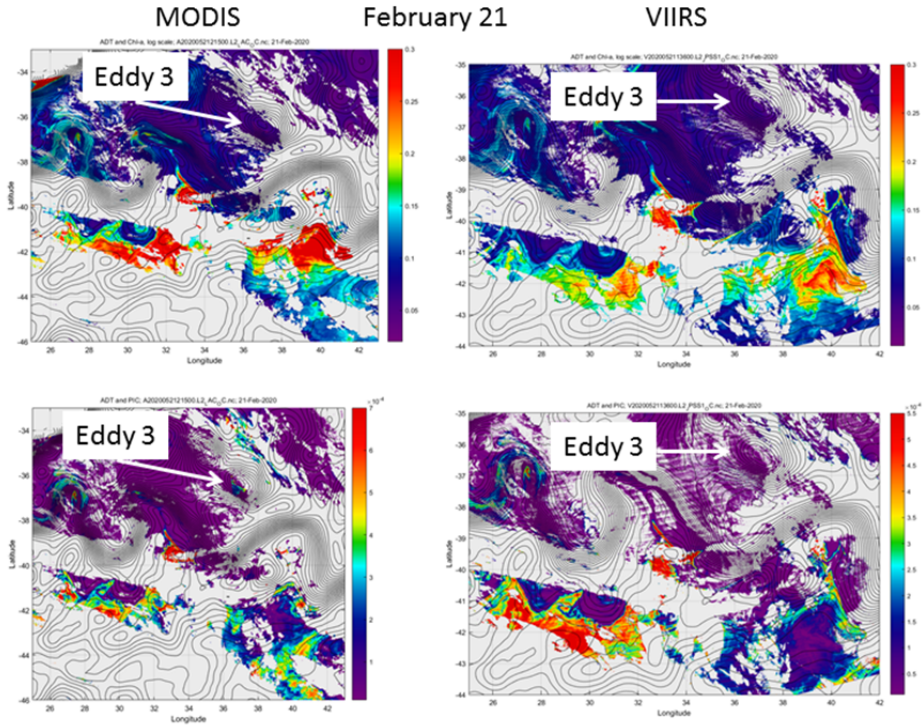

VPR survey of Eddy 3 began on the western side of the feature. As it turns out, the starting point of the VPR survey was close to eddy center, as indicated by both the ADCP and XBT data. Although the XBT observations are noisy, the peak of the main thermocline occurs at ca. 36.45 E, after which it steadily descends. Clearly, the eddy has moved further southwest than anticipated based on the altimetry. Examination of the ADT animation indicates Eddy 3 is heavily influenced by its interaction with the adjacent cyclone to the west. The pair appears to be rotating around each other in a clockwise fashion, thus displacing Eddy 4 to the southwest. Close examination of the ground tracks reveals the area to the southwest of the eddy has not been sampled recently, and thus eddy center is portrayed to the east of, rather than to the west of, the westernmost ground track. Substantial adjustment of the eddy position is expected when new altimeter data fill in the current gap.

CTD transect from east to west begun.

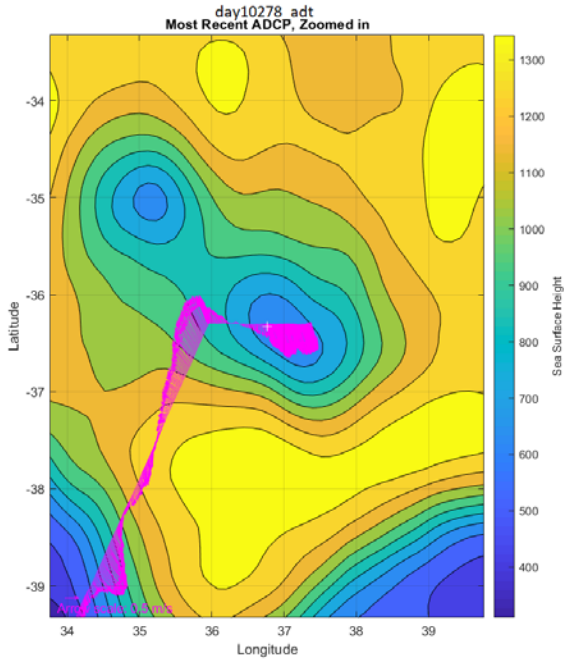

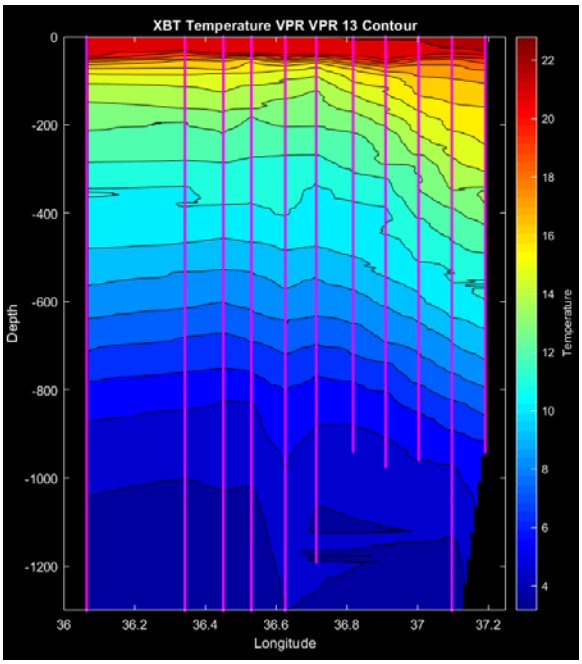

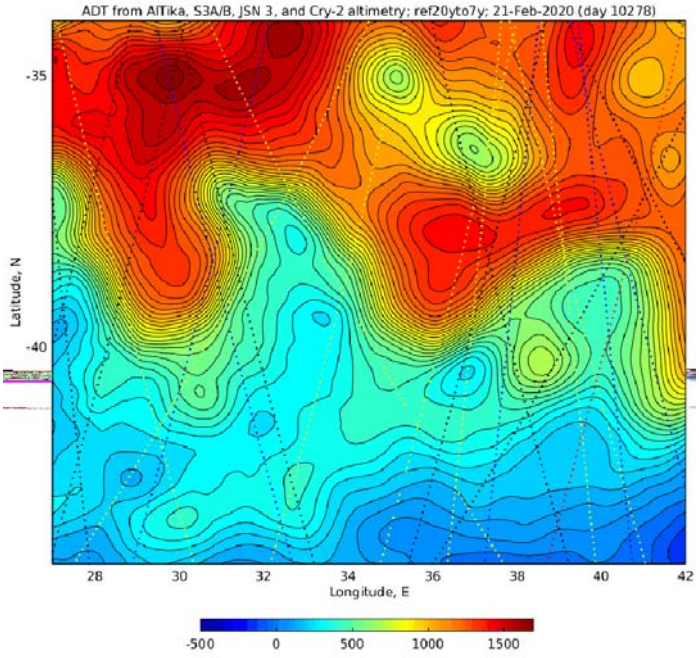
ADT from AlTika, S3A/B, JSN 3, and Cry-2 altimetry; ref20yto7y; 21-Feb-2020 (day 10278)
Latitude, N
-35
-40
28
30
32
34
36
38
40
42
Longitude, E
-500
0
500
1000
1500

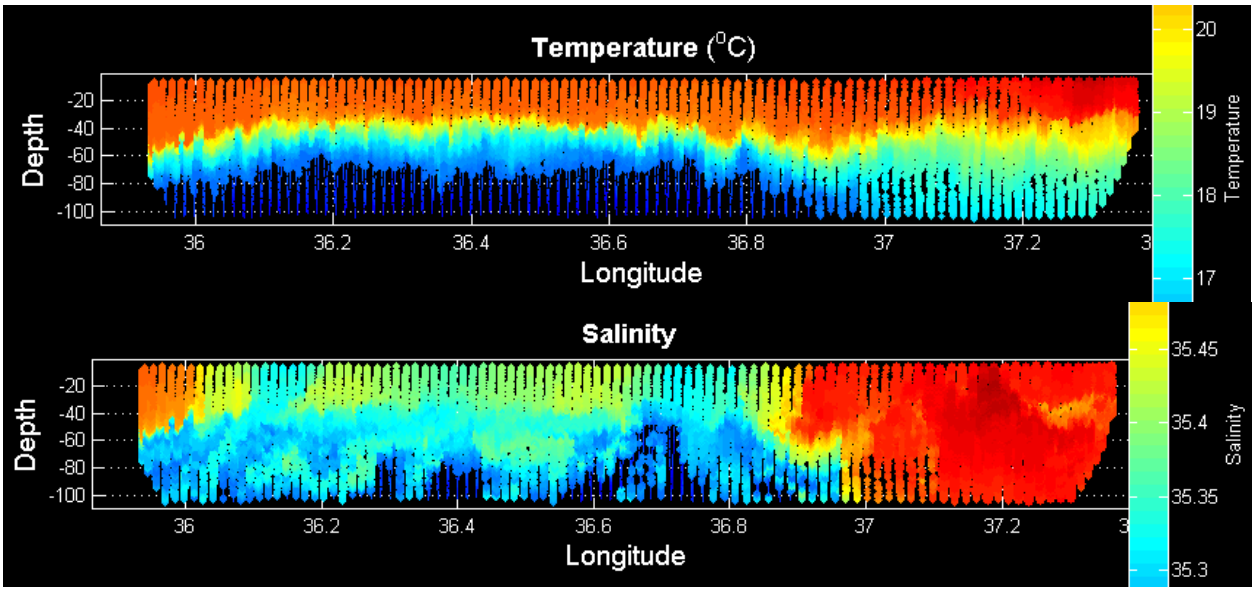
Temperature (°C)
Depth
-20
-40
-60
-80
-100
36
36.2
36.4
36.6
36.8
37
37.2
Longitude
20
19
18
17
Temperature
Salinity
35.45
35.4
35.35
35.3
Salinity

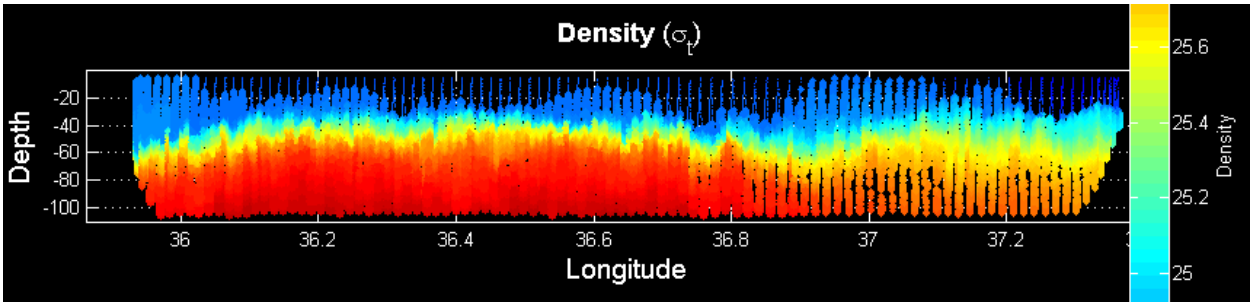
Density (σt)
Depth
-20
-40
-60
-80
-100
36
36.2
36.4
36.6
36.8
37
37.2
Longitude
25.6
25.4
25.2
25
Density

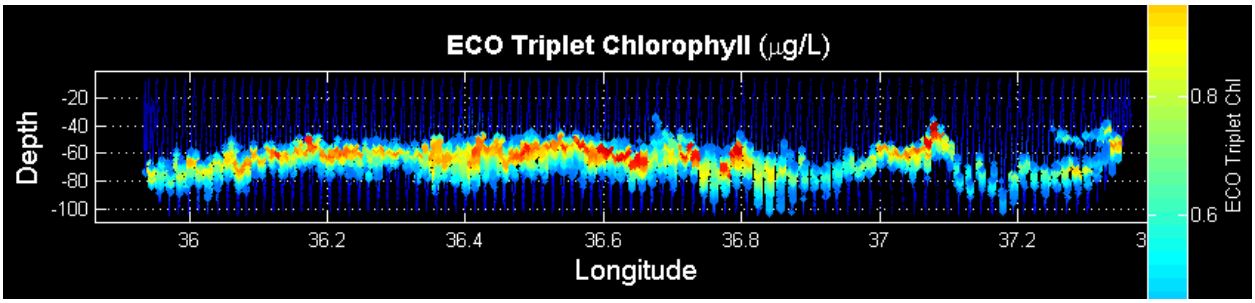
ECO Triplet Chlorophyll (µg/L)
Depth
-20
-40
-60
-80
-100
36
36.2
36.4
36.6
36.8
37
37.2
Longitude
0.8
0.6
ECO Triplet Chl

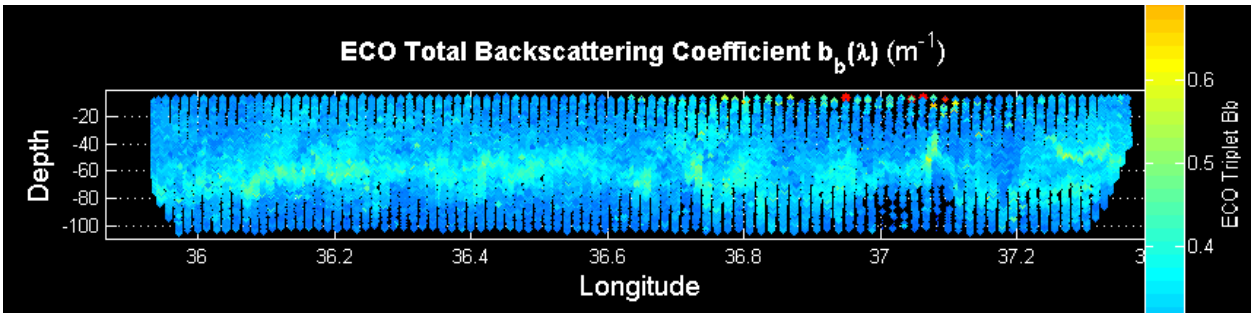
ECO Total Backscattering Coefficient b_b(λ) (m^-1)
Depth
-20
-40
-60
-80
-100
36
36.2
36.4
36.6
36.8
37
37.2
Longitude
0.6
0.5
0.4
ECO Triplet Bb

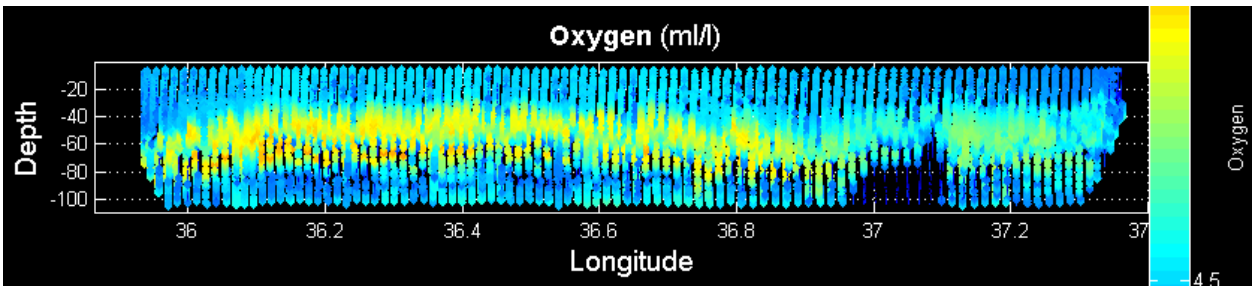
Oxygen (ml/l)
Depth
-20
-40
-60
-80
-100
36
36.2
36.4
36.6
36.8
37
37.2
Longitude
Oxygen
4.5

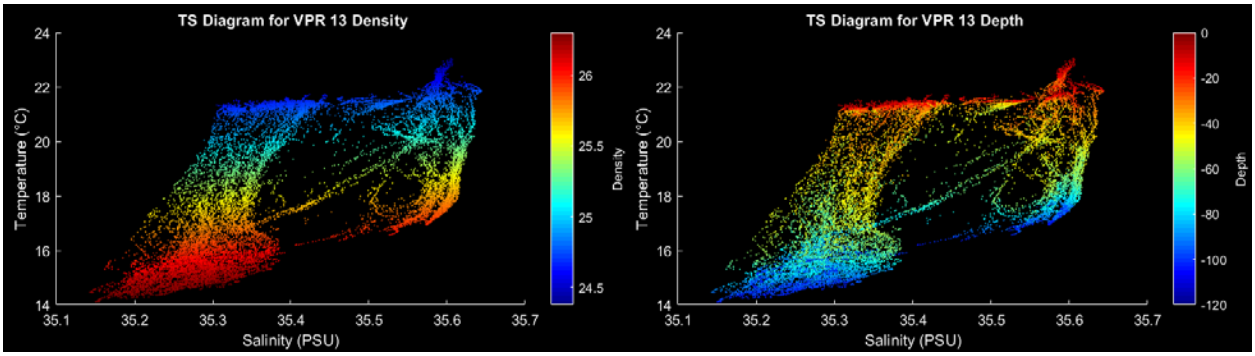
TS Diagram for VPR 13 Density
Temperature (°C)
24
22
20
18
16
14
35.1
35.2
35.3
35.4
35.5
35.6
35.7
Salinity (PSU)
26
25.5
25
24.5
Density
TS Diagram for VPR 13 Depth
Temperature (°C)
Salinity (PSU)
0
-20
-40
-60
-80
-100
-120
Depth

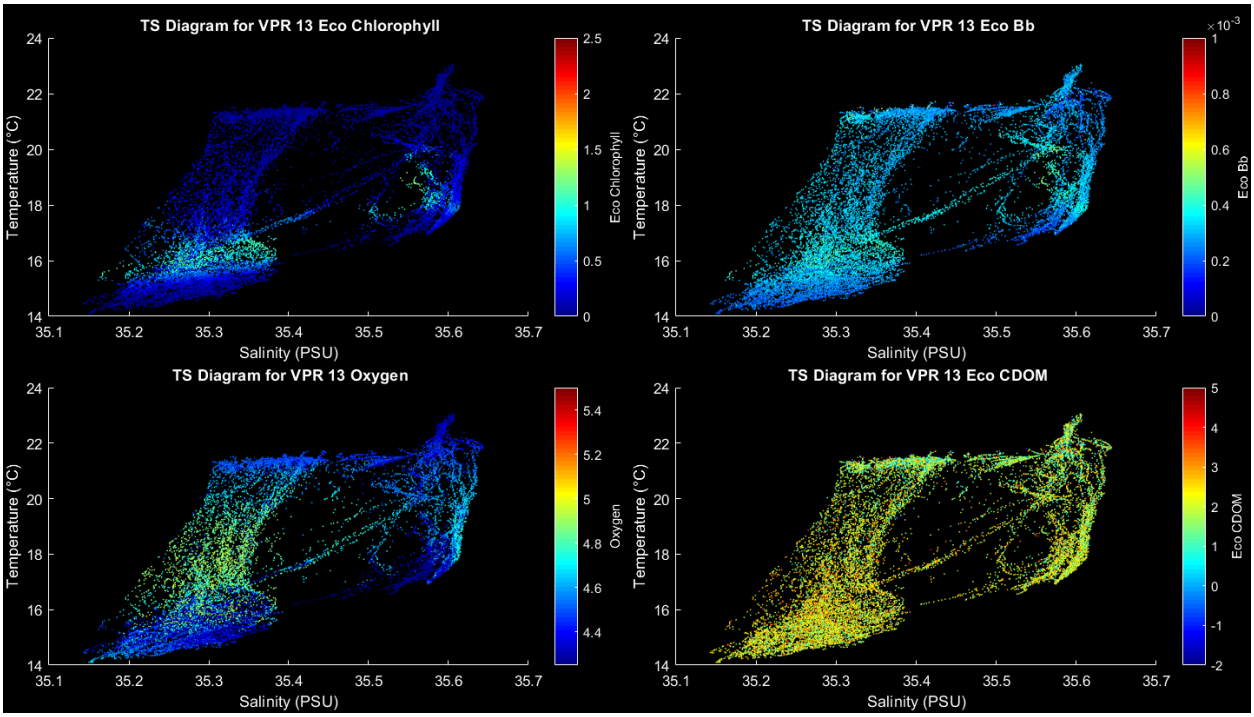

Transect	Station	Feature / comments
-	53	Deep cast
9	54	Eastern periphery – high salinity
	55	Local Smax
	56	High Bb, low S: PP cast, TM cast
	57	Smed
	58	Eddy center
	59	Smed
	60	Bb slight enhancement
	61	Local Smax
	~~62~~	~~Western periphery~~; scrubbed due to Wx

Table 3.4. Station list for CTD transect 9, from east to west across Eddy 3.

23 February

CTD transect continues. Westernomost station had to be scrubbed due to weather. Conditions were not favorble for VPR deployment either, so we transited to the northernmost station. Although VPRdeployment was possible, the forecast calls for increasing winds from the SW, which would add to the remaining swell. We therefore decided to proceed with the CTD line, starting the VPR tow after that.

24 February

N-S CTD line continues, temporarily interupted by weather conditions making CTD operations impossible.

25 February
N-S line continues; diverted to recover drifter; had to double back to Eddy Center in order to do the trace metal cast that was not possible earlier due to Wx. Finished N-S line at southernmost station.

Transect	Station	Feature / comments
10	62	Northern station
	63	
	64	
	65	
	66	Eddy center
	67	3 south of EC; diverted to get drifter
	68	2 south of EC
	69	1 south of EC
	70	Eddy center repeat / TM cast
	71	Southern station

Table 3.5. Station list for CTD transect 10, from north to south across Eddy 3.

26 February
Deployed the VPR at the southernmost station and towed north. ADCP observations indicate we passed east of eddy center, and this is consistent with the altimetry: eddy center have move west more quickly than anticipated, owing to interaction and apparent merger with another cyclone to the northwest.

Despite the transect being a bit off-center, the lower salinity of the eddy core is still visible—although in this transect it surrounds more saline waters closest to eddy center. Surface chlorophyll and backscatter are very low,with the largest signals in subsurface maxima that peak in the low-salinity band around the core and at the eddy periphery. There is a hint of enhancement of Bb in surface waters in that band, although the signal is very weak.

What is the origin of the saline water near eddy center in VPR14? The feature fills in the gap in T-S space present in VPR13 between $35.35 < S < 35.55$, suggesting continuity in water mass characteristics from the eddy core to the ambient waters outside the eddy. Perhaps this is a streamer of saline water from outside the eddy intruding into the eddy core? Zhang and McGillicuddy (submitted) document a mechanism for streamer formation that may be applicable here; detailed diagnosis of the density field will be required to make that assessment.

Upon completion of the VPR survey, we began steaming for Mauritius.

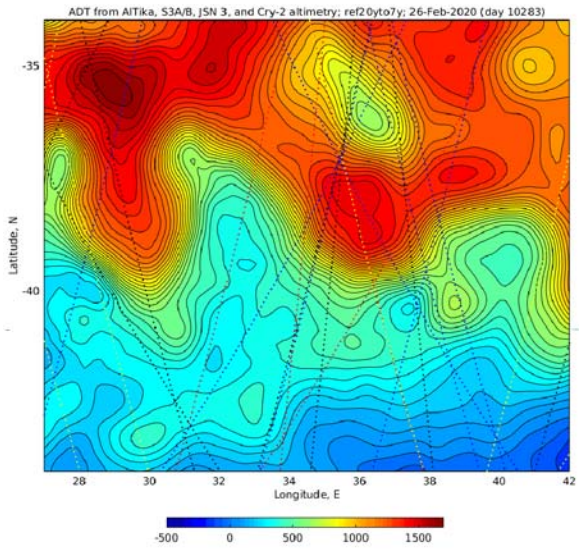
ADT from AlTika, S3A/B, JSN 3, and Cry-2 altimetry; ref20yto7y; 26-Feb-2020 (day 10283)
Latitude, N
Longitude, E

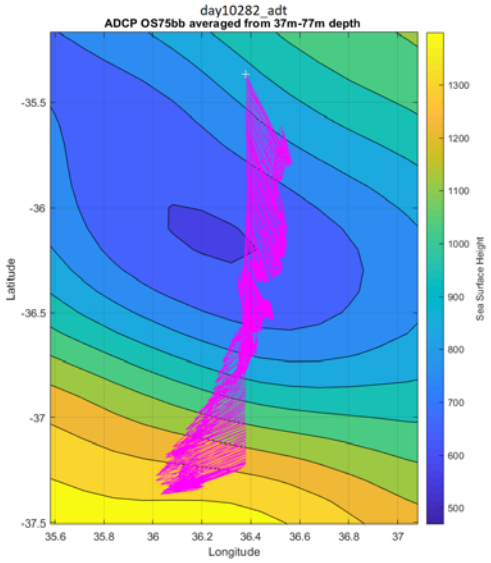
day10282_adt
ADCP OS75bb averaged from 37m-77m depth
Latitude
Longitude
Sea Surface Height

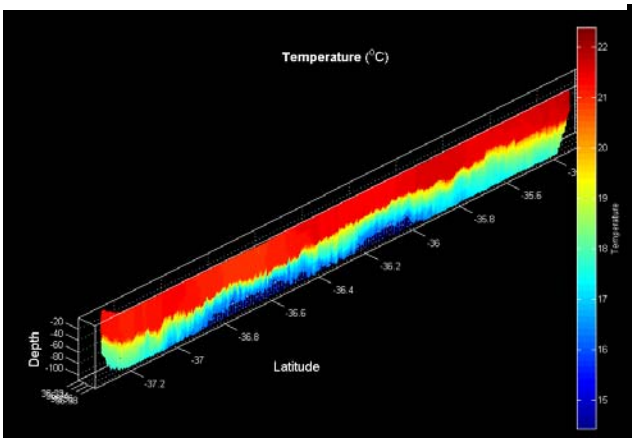
Temperature (°C)
Depth
Latitude

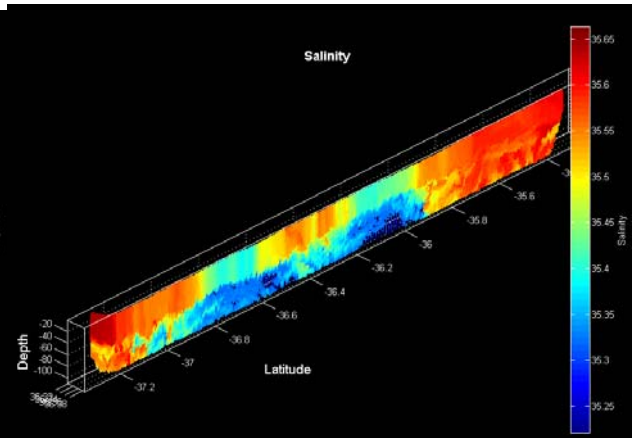
Salinity
Depth
Latitude

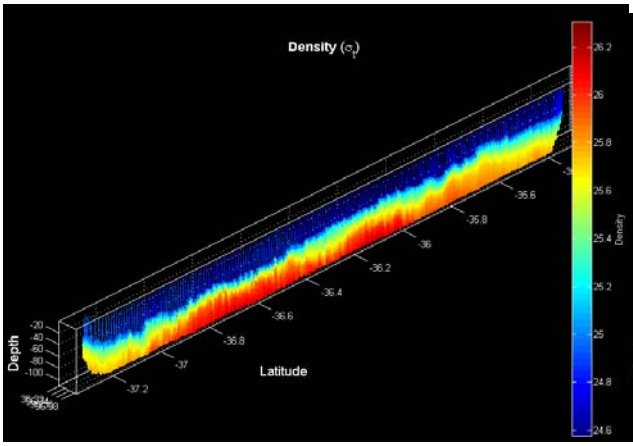
Density (σt)
Depth
Latitude

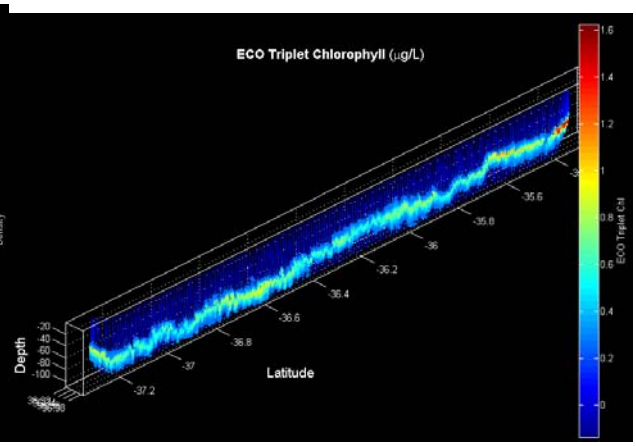
ECO Triplet Chlorophyll (µg/L)
Depth
Latitude

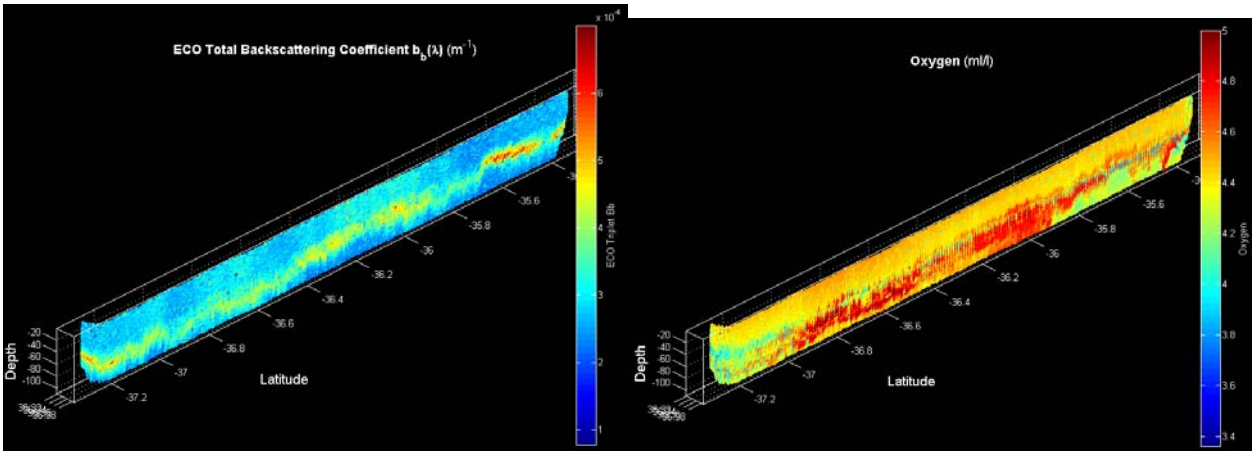

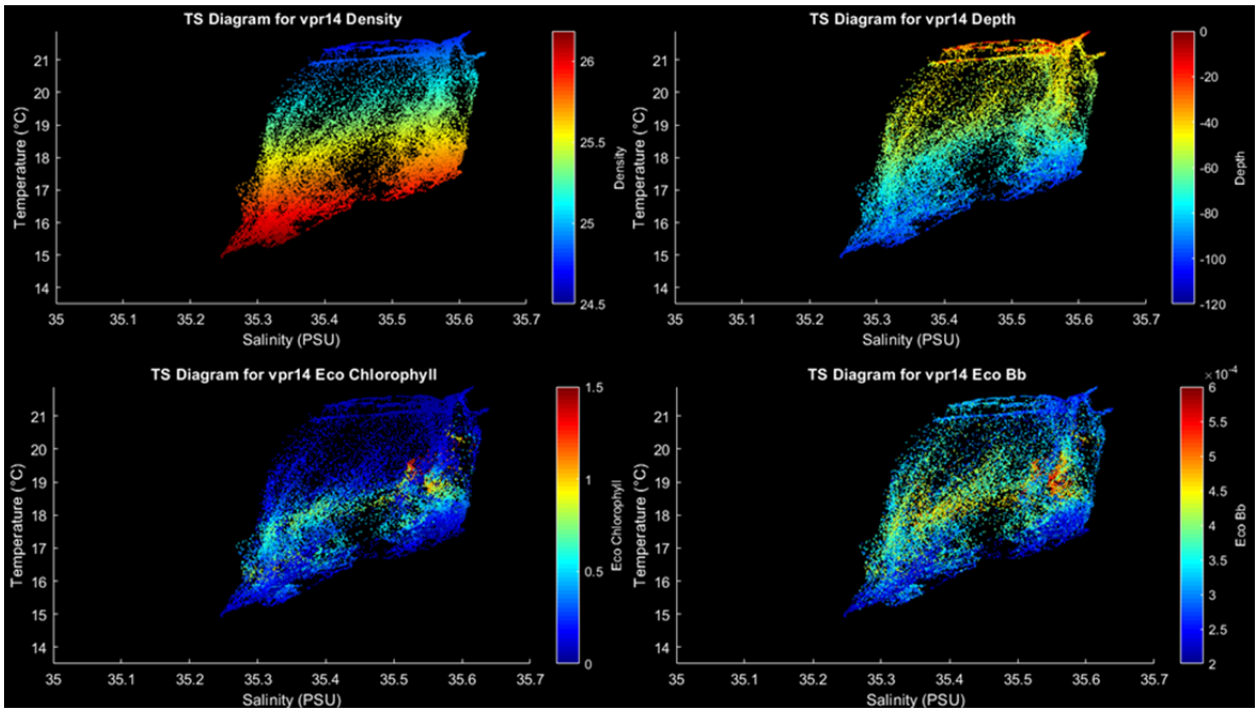

27 February – 2 March
Transit to Mauritius.

3 March
Arrival in Mauritius.

4. Summary of VPR tows

Date	Tow #	Description	Comments
1/27/20	VPR1	Eastern flank of Agulhas eddy	
1/29/20	VPR2	Transect across high PIC feature	
1/30/20	VPR3	Survey of high PIC feature	Sobel changed to acquire smaller ROIS Tow aborted when comms with flight control lost.
1/31/20	VPR4	Continued survey of high PIC feature	Flight control restored for several hours, then intermittent operation, then back to continuous operation. Intermittent dropouts of ROI detection.
2/1/20	VPR5	North-South line through high PIC feature	Strobe not working on deck; deployed anyway and strobe came to life.
2/3/20	VPR6	SE tow from northernmost CTD to easternmost	
2/4/20	VPR7	NE tow from westernmost CTD to northernmost	
2/5/20	VPR8	West to east entry into Eddy 2	
2/5/20 - 2/6/20	VPR9	Eddy 2 survey	
2/16/20	VPR10	High PIC region, southern transect	Very few rois captured; strobe out of alignment, corrected after the tow.
2/18/20	VPR11	High PIC region, middle transect	Very few rois; camera reset, normal roi rate resumes.
2/19-20/20	VPR12	High PIC region, northern transect	Started on east end of middle transect.
2/22/20	VPR13	Eddy 3 west to east survey	Lost starboard tail skid, replaced after tow.
2/26/20	VPR14	Eddy 3 south to north survey	Passed east of eddy center.

Table 4.1. VPR tows on TN376.

Bio-optical, Biological and Biogeochemical Measurements

William Balch, Dave Drapeau, Bruce Bowler, Colin Fischer
Bigelow Laboratory for Ocean Sciences
W. Boothbay Harbor, ME 04575

Marci Train
Weather Blur Program
Long Island School
Long Island, ME

Sydney Greenlee
Undergraduate Intern
Colby College
Waterville, ME

The Balch lab was involved in sampling a number of variables from the bottle casts, running an optical surface underway system, measuring discrete samples for a variety of water samples (see below). We also were involved in the carboy experiments. The Balch group sampled from 53 CTD/full water cast stations during the cruise, taking water from 8 of the 12 Niskin bottles each cast. Of those 8 bottles, 7 were usually from the euphotic zone and one from deeper in the water column (300-1000m). Water samples were taken for particulate organic carbon (POC) and particulate organic nitrogen (PON), particulate inorganic carbon ($CaCO_3$ or PIC), biogenic silica, photosynthesis/ calcification, and coccolithophore counts (to be processed ashore using polarized light microscopy). The latter technique is identical to the Canada Balsam technique for enumeration of calcite particles (Haidar and Thierstein, 2001) except we use Norland #74 brand optical adhesive instead of Canada Balsam. Chlorophyll *a* extractions ((JGOFS, 1996) were performed and for surface bottles always run in triplicate (for incorporation into NASA's SEABASS data set); deeper samples were run as single measurements). Flow-cam samples ((Sieracki *et al.*, 1998) were taken from the eight depths of each Niskin cast for enumeration of net and nanoplankton as well as deriving size distribution functions. Samples for scanning electron microscope analysis were taken and prepared for analysis ashore. At each productivity station, two samples (surface mixed layer and deep euphotic zone (fluorescence maximum)) were taken and samples concentrated for microscopy. The Filter Freeze Transfer technique (Hewes and Holm-Hansen, 1983) was used in which typically 250mL of sample were concentrated onto a 25mm, 0.4um-poresize, polycarbonate filter and the particles transferred to a glass microscope slide for examination using an American Optical polarizing microscope equipped with epifluorescence (with excitation wavelengths at about 480nm and 530nm). Samples were examined at any of four magnifications (100X, 200X, and 400X, the vast majority on this trip were photographed at 400X) under four types of illumination: bright field, polarized (to visualize calcium carbonate coccoliths) and epifluorescence (for discriminating autofluorescent, autotrophic cells versus heterotrophic, nonfluorescent cells. See figure 2 of cruise narrative for example). High resolution photos were taken with a Canon EOS Rebel digital camera mounted on the trinocular head of the microscope.

The Balch lab bio-optical underway system was run continuously over the course of the trip. This system has been described elsewhere (Balch *et al.*, 2008). Basically it measures temperature, salinity, chlorophyll *a* fluorescence and backscattering at 531nm (using a WETLabs ECOVSF sensor aimed into a specially-designed container which minimizes wall reflectance, hence maximizing the light scattering signal associated with marine particulate matter). First, the system measures backscattering of 531nm light with raw seawater (pH=8.1) running through the system for one minute. After 60 seconds of data collection (or whatever time period was set in order to achieve statistically-significant measurements), the acid controller injected 0.2um-filtered, 10% glacial acid into the seawater stream, passing through a static mixing coil to thoroughly mix it with the seawater, *upstream* of the ECOVSF. This reduced the pH to 5.5, below the dissociation point for calcium carbonate. A pH sensor *downstream* of the sample chamber measured the pH constantly. Once the pH dropped below pH 5.4, the backscattering was re-measured for 60s after which the acid additions stopped and the pH re-equilibrated and the entire cycle repeated. The difference in backscattering between raw seawater and acidified seawater represented "acid-labile backscattering" (b_b'), which can be directly related to the concentration of suspended calcium carbonate (Balch *et al.*, 1996).

The Balch lab bio-optical underway system had a separate flow loop that passed through a WETLabs ac-9, to measure spectral absorption and attenuation. In the flow path to the ac-9 was a solenoid that diverted the seawater stream through a 1um filter, then a 0.2 um filter prior to running the water through the ac-9. Every two minutes, the solenoid would alternate between filtered and unfiltered seawater, thus providing absorption and attenuation (at 9 spectral wavelengths across the visible spectrum) for raw and filtered seawater. In turn, this allows calculation of the absorption and attenuation of total suspended particles and dissolved organic matter. The difference between raw and dissolved ac-9 measurements represents particulate absorption and beam attenuation. Calibrations of the complete underway system were performed two ways: 1) daily, ultra-filtered 0.2um seawater was run through the entire system in order to estimate signals derived from ultra-clean seawater 2) approximately bi-weekly a calibration was performed by taking the instruments apart, cleaning and drying the sensors, and reassembly. This was done over the cruise as well as a final calibration at the completion of the cruise. These calibrations are used to estimate biofouling corrections during each operation period. The protocol was to run 0.2um filtered RO water from the ship's Milli-Q system, under pressure, through the entire flow path prior to cleaning ("a dirty calibration" which provides the endpoint for estimating the optical contribution of biofouling). Then the system is carefully disassembled and cleaned, reassembled and a "clean calibration" performed (which represents the beginning calibration for the next operation segment, with no bio-fouling. Post cruise, the biofouling corrections are interpolated between the initial clean calibration and the following dirty calibration.

On the bow of the *R/V Thompson* was a Satlantic SeaWiFS Aircraft Simulator (HyperSAS) system mounted to an Underway Aiming System (UAS), used to estimate water-leaving radiance from the ship, analogous to to the nLw derived by the SeaWiFS and MODIS satellite sensors, but free from atmospheric error (hence, it can provide radiometric data below clouds). The system consisted of a down-looking radiance sensor and a sky-viewing radiance sensor, both mounted on UAS. A downwelling irradiance sensor was mounted as far as possible from any potentially shading structures. These data were used to estimate normalized water-

leaving radiance as a function of wavelength. The radiance detector was set to view the water at 40^{o} from nadir as recommended by Mueller et al. (2003b). The water radiance sensor was able to view over an azimuth range of ~200^{o} across the ship's heading with no contamination from the ship's wake. The direction of the sensor was adjusted to view the water 120^{o} from the sun's azimuth, to minimize sun glint. This was continually adjusted as the time and ship's gyro heading were used to calculate the sun's position using an astronomical solar position subroutine interfaced with a stepping motor which was attached to the radiometer mount (designed and fabricated at Bigelow Laboratory for Ocean Sciences). Protocols for operation and calibration were performed according to Mueller (Mueller *et al.*, 2003a; Mueller *et al.*, 2003b; Mueller *et al.*, 2003c). Before 1000h and after 1400h, data quality was poorer as the solar zenith angle was too low. Post-cruise, the 1 Hz data are filtered to remove as much residual white cap and glint as possible (we accept the lowest 5% of the data).

At the daily pre-dawn cast, samples were taken for measuring primary production and calcification from the 30L Niskin samples. Water was sampled from 6 light depths: 38.6%, 21.1%, 11.7%, 3.5%, 1.9% and 0.3%. Estimation of those light depths was performed based on the assumption that the fluorescence maximum was located at the 1% light depth (Poulton *et al.*, 2017). Water samples for incubation were transferred from Niskin bottles to incubation bottles, typically inside the ship's enclosed hanger, under subdued light conditions. Water samples were pre-filtered through 120µm nitex mesh to remove large grazers. Incubations were performed in 70 mL polystyrene tissue culture bottles that were previously acid-cleaned, rinsed with ethanol, reverse-osmosis water, then rinsed 5x with each sea water sample prior to filling. Photosynthesis and calcification were measured using the microdiffusion technique (Paasche and Brubak, 1994) with modifications by Balch et al. (2000) (see also Fabry (2010). ^{14}C bicarbonate (30 µCi) was added for each water sample. Incubations were performed in triplicate (with an additional 2% formalin sample (final concentration) used as a killed control) in simulated *in situ* conditions on-deck, corrected for both light quantity (extinction using bags made of neutral-density shade cloth) and quality (spectral narrowing) using blue acetate bag inserts. Bottle transfers between the incubators and radioisotope van were always done in darkened bags to avoid light shock to the phytoplankton. Deck incubators consisted of blue plastic tubs open to sky light, chilled using surface seawater from the ship's flowing sea water system. Calibration of those light levels in the bag were previously made using a Biospherical OSR2100 scalar PAR sensor inserted into each bag relative to a scalar PAR sensor outside the bag. All filtrations were performed using 0.4 µm pore-size polycarbonate filters. Filters and sample "boats" were placed in scintillation vials with 7mL of Ecolume scintillation cocktail. Samples were counted using a high sensitivity Beckman Tricarb liquid scintillation counter with channel windows set for 14C counting. Counts were performed for sufficient time to reach 1% precision or 30 minutes for samples with lower counts. Blank ^{14}C counts were always run for scintillation cocktail as well as the phenethylamine CO_2 absorbent. Standard equations were used for calculating primary production and calcification from the ^{14}C counts with a 5% isotope discrimination factor assumed for the physiological fixation of ^{14}C-HCO3 as opposed to ^{12}C-HCO_3.

Carboy Experiments

Four carboy experiments were performed during the 38d cruise. The purpose of the experiments was to assess the impact of different nutrient amendments on phytoplankton-related variables measured by the Balch lab: phytoplankton biomass, POC/PON, PIC, counts of plated

coccolithophores and detached coccoliths, nutrient concentrations, biogenic silica, flowcam counts of various classes of algae, particle size distributions. As outlined earlier, the 18 cubitainors were divided as follows: three controls (no amendments), then triplicate amendments for nitrate, 10% 0.2um-filtered SAMW, silicate, iron, iron+silicate. See section from the Morton lab for all the specifics for collecting trace-metal-clean surface seawater for these experiments. All cubitainors were then placed in blue seawater incubators maintained at ambient seawater temperatures using a a chiller/heater system kept in the ship's hanger. Cubitainors were kept in neutral-density screen (which reduced the total irradiance to about 50% of incident).

Samples processed

The Balch group performed four carboy experiments over the SAMW'20 cruise, and sampled all CTD/full water casts. Underway samples were also taken every two hours while towing the VPR for a total of 95 samples. In total, 725 water samples were processed for all variables listed

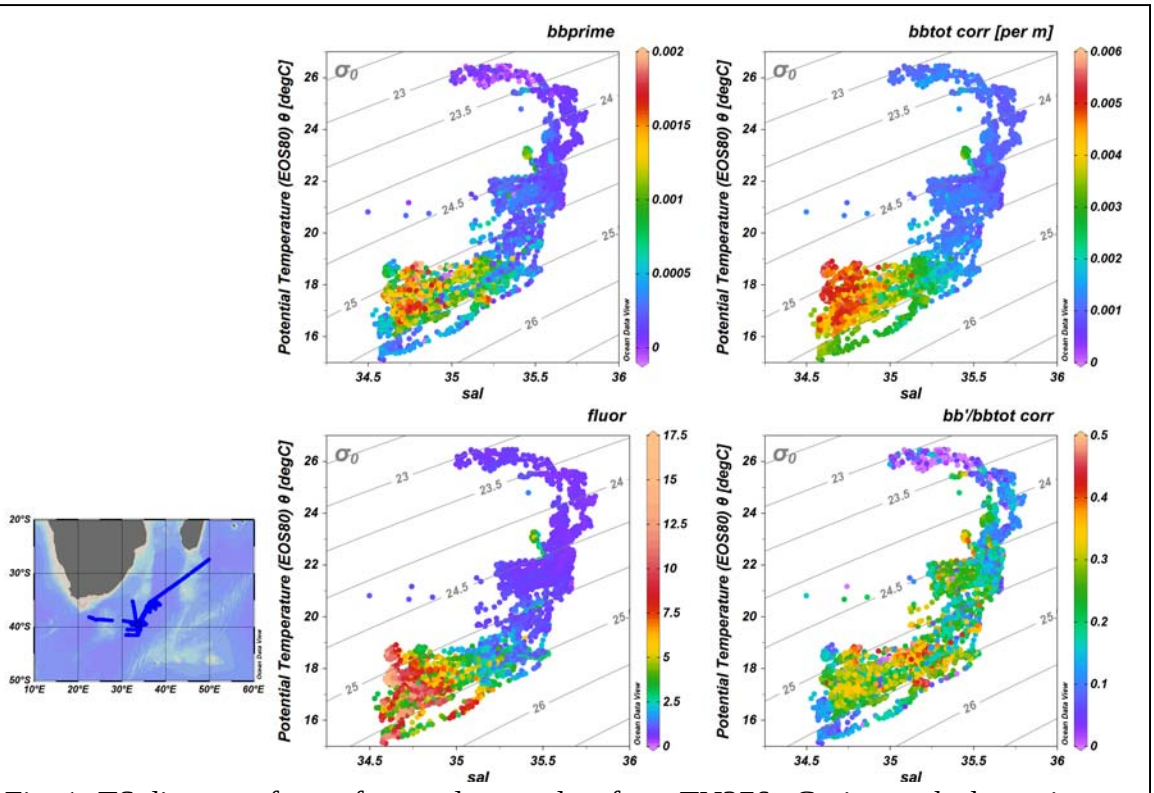

Fig. 1- TS diagrams for surface underway data from TN376. Cruise track shown in lower left corner. Top left- acid-labile backscattering is shown on the Z axis of the TS plot. Water along the 25.5 isopycnal showed peak amounts of acid-labile backscattering in the cool, fresh part of the TS diagram. Upper right panel- Total particulate backscattering at 532nm also showing peak values in the Sub-Antarctic Frontal water, decreasing as the ship moved in progressively more oligotrophic environments. Lower left panel: Fluorescence of chlorophyll a shown in TS space, showing similar pattern to total backscattering. Lower right panel: fraction of acid-labile backscattering normalized to total particle backscattering. It can be seen that in the filament, that fraction approaches 40% of the total, which decreases to 25% in the cyclonic eddy (sigma theta of 25 to 24.5), which decreases to 5-10% on leg 5 to Mauritius.

above: 72 full sets of measurements were performed for shipboard experiments on nutrient/trace metal amendments, 95 underway samples.

Data archival

The data collected from this voyage will be ultimately archived with the Biological and Chemical Oceanographic Data Management Office (BCO-DMO) at Woods Hole Oceanographic Inst. (sponsored by NSF).

Preliminary Results

Our surface underway system illustrated that the peak coccolithophore populations were found in cold, fresh water south of the Southern Subtropical Front and the Agulhas Front, representative

Table 1- Summary of all 14C incubations for measuring integrated photosynthesis and calcification. Columns are color coded to indicate relative values. Chlorophyll-normalized values are also shown but they are not included in the color coding for in station 1 where several of the samples were lost during processing so the chlorophyll integrals will be conservative, leading to the extremely high chlorophyll-normalized values.

Location	Station	Lat (dec.deg)	Lon (dec deg)	Event	year day	GMT time	Int C/P	Int Prod (mgPOC/m2-d)	Int Calc (mgPIC/m2-d)	Int Chl (mg/m2)	Int Prod/Int Chl	Int Calc/Int chl
Agulhas eddy	1.01	-38.583	24.001	20200127.0307	27	307	0.066	71.5	4.72	10.91	6.55	0.43
S of Agulhas cyclonic meander	3.01	-38.7665	27.718432	20200128.0341	28	341	0.045	100.1	4.47	28.38	3.53	0.16
N edge of Agulhas; anticyclonic meander	4.01	-38.8105	30.14899	20200128.2142	28	2142	0.004	185.5	0.81	31.43	5.90	0.03
Eddy 1; PIC max	5.01	-39.1883	33.2991	20200130.0235	30	235	0.017	344.3	5.79	49.63	6.94	0.12
Eddy 1; eddy center	7.01	-39.4751	34.1997	20200201.0052	32	52	0.048	207.9	9.92	24.88	8.35	0.40
Eddy 1; South edge	8.01	-40.49955	34.2006	20200201.2349	32	2349	0.083	167.3	13.89	28.67	5.84	0.48
Eddy 1; North edge (Agulhas)	12.01	-38.501	34.1995	20200202.2036	33	2036	0.020	35.3	0.70	16.17	2.18	0.04
Eddy 1; West edge	17.01	-39.4745	32.9172	20200204.0222	35	222	0.021	273.5	5.78	29.56	9.25	0.20
Eddy 3 (drogue); Carboy stn	18.02	-35.882	36.971	20200205.1840	36	1840	0.05001	83.9	4.20	21.77	3.86	0.19
Eddy 3; Eddy Interior South	20.01	-36.2005	37.6273	20200207.0235	38	235	0.063788	141.5	9.03	21.29	6.65	0.42
Eddy 3; Eddy Center	23.01	-35.8852	37.6282	20200208.0314	39	314	0.028654	98.0	2.81	25.24	3.88	0.11
Filament South Line; west interior	28.01	-41.4999	31.401	20200216.2208	47	2208	0.035964	159.9	5.75	30.38	5.26	0.19
Mid line filament, in middle	39.01	-40.5001	32.6202	20200219.0339	50	339	0.027993	455.1	12.74	47.29	9.62	0.27
Filament N section interior	50.01	-39.5005	33.6501	20200220.2251	51	2251	0.033521	402.4	13.49	37.63	10.70	0.36
Eddy 3 Int. East 2nd sampling	56.01	-36.3031	36.754	20200222.2300	53	2300	0.090445	93.0	8.42	21.31	4.37	0.39
Eddy 3 Center 2nd sampling	70.01	-36.3032	36.3831	20200225.1044	56	1044	0.038565	296.3	11.43	29.52	10.04	0.39

of Sub-Antarctic Front water (Fig 1) between the 25 and 25.5 sigma-theta isopycnal. It also appears that as that water moves northward along this isopycnal (verified in satellite ocean color images and altimetry), it is being conditioned such that by the northern end of the filament, the water is no longer amenable to coccolithophore growth. It is also significant that within both the filament and cyclonic eddy, the suspended calcium carbonate accounted for up to 50% of the total backscattering of the particulate material. It is no wonder that these features are visible from space. This percentage is similar to the percentages observed previously in the Patagonian Shelf part of the Great Calcite Belt. The phytoplankton fluorescence was also greatest in this cold, fresh water, consistent with the hypothesis that the total algal populations in the filament were actively growing whereas those in the eddy were waning.

A summary of the primary production and calcification results is given in Table 1. They show that the highest calcification and photosynthesis rates were observed in the filament (and values increased from the first to the second sampling, consistent with the remote sensing results). Eddy 3 calcification and photosynthesis values generally were lower than in the actively growing filament. However, the integrated calcification and photosynthesis rates at

eddy center (Eddy 3) were impressive for the amount of chlorophyll present, especially during the second sampling. We note that in the eddy 3 interior for the second sampling, 9% of the carbon was being fixed into calcite which was the highest percentage of the trip. This leads one to consider whether the community in the dying eddy assemblage was still shifting towards coccolithophores over other phytoplankton.

References

Balch, W.M., Drapeau, D., Fritz, J., 2000. Monsoonal forcing of calcification in the Arabian Sea. Deep-Sea Research II 47, 1301-1337.

Balch, W.M., Drapeau, D.T., Bowler, B.C., Booth, E.S., Windecker, L.A., Ashe, A., 2008. Space-time variability of carbon standing stocks and fixation rates in the Gulf of Maine, along the GNATS transect between Portland, ME and Yarmouth, NS. Journal of Plankton Research 30 (2), 119-139.

Balch, W.M., Kilpatrick, K., Holligan, P.M., Harbour, D., Fernandez, E., 1996. The 1991 coccolithophore bloom in the central north Atlantic. II. Relating optics to coccolith concentration. Limnology and Oceanography 41, 1684-1696.

Fabry, V.J., Balch, W.M., 2010. Direct measurements of calcification rates in planktonic organisms. In: Riebeseil, U., Fabry, V.J., Hansson, L., Gattuso, J.-P. (Eds.), Guide to Best Practices in Ocean Acidification Research and Data Reporting. European Project on Ocean Acidification (EPOCA), Bremerhaven, Germany, pp. 185-196.

Haidar, A.T., Thierstein, H.R., 2001. Coccolithophore dynamics off Bermuda (N. Atlantic). Deep Sea Research 48 (8-9), 1925-1956.

Hewes, C.D., Holm-Hansen, O., 1983. A method for recovering nanoplankton from filters for identification with the microscope: The filter-transfer-freeze (FTF) technique. Limnology and Oceanography 28, 389-394.

JGOFS, 1996. Protocols for the Joint Global Ocean Flux Study (JGOFS) core measurements. In: Knap, A. (Ed.), Report no. 19 of the Joint Global Ocean Flux Study. Scientific committee on oceanic research, international council of scientific unions. Intergovernmental Oceanographic Commission, Bergen, Norway, p. 170.

Mueller, J.L., Austin, R.W., Morel, A., Fargion, G.S., McClain, C.R., 2003a. Ocean optics protocols for satellite ocean color sensor validation, Revision 4, Volume I: Introduction, background, and conventions. Goddard Space Flight Center, Greenbelt, MD, p. 50.

Mueller, J.L., Morel, A., Frouin, R., Davis, C., Arnone, R., Carder, K., Lee, Z.P., Steward, R.G., Hooker, S.B., Mobley, C.D., McLean, S., Holben, B., Miller, M., Pietras, C., Knobelspiesse, K.D., Fargion, G.S., Porter, J., Voss, K., 2003b. Ocean optics protocols for satellite ocean color sensor validation, Revision 4, Volume III: Radiometric measurements and data analysis protocols Goddard Space Flight Center, Greenbelt, MD, p. 78.

Mueller, J.L., Pietras, C., Hooker, S.B., Austin, R.W., Miller, M., Knobelspiesse, K.D., Frouin, R., Holben, B., Voss, K., 2003c. Ocean optics protocols for satellite ocean color sensor validation, Revision 4, Volume II: Instrument specifications, characterization,and calibration. Goddard Space Flight Center, Greenbelt, MD.

Paasche, E., Brubak, S., 1994. Enhanced calcification in the coccolithophorid *Emiliania huxleyi* (Haptophyceae) under phosphorus limitation. Phycologia 33, 324-330.
Poulton, A.J., Holligan, P.M., Charalampopoulou, A., Adey, T.R., 2017. Coccolithophore ecology in the tropical and subtropical Atlantic Ocean: New perspectives from the Atlantic meridional transect (AMT) programme. Progress in Oceanography, doi: 10.1016/j.pocean.2017.1001.1003.
Sieracki, C.K., Sieracki, M.E., Yentsch, C.S., 1998. An imaging-in-flow system for automated analysis of marine microplankton. Marine Ecology Progress Series 168, 285-296.

Nutrient limitation by major and trace metals

Peter Morton, Kristie Dick, Lauren Hearn
National High Magnetic Field Laboratory/Florida State University
Tallahassee, Florida 32310

Sara Rauschenberg
Bigelow Laboratory for Ocean Sciences
W. Boothbay Harbor, ME 04575

Shannon Burns
University of South Florida-St. Petersburg
St. Petersburg, Florida 33701

In waters of the southwest Indian and Southern Oceans, limiting concentrations of major and trace nutrients can inhibit primary productivity and/or influence community composition. During the 2020 SAMW research expedition, uncontaminated seawater samples were drawn from regular deployments of nine Teflon coated 5-L Niskin-X bottles suspended from Kevlar line at varying depths between 30 m and 750 m. The addition of a deck-mounted snatch block and increased weights up to ~160 lbs. proved to be ideal for deploying the Niskin-X bottles, after the ~1600 m of Kevlar line were intentionally cut at about 850 m after the line jumped the A-frame mounted block and became stuck in the block axle (station 3). Subsequent casts using this system experienced no similar issues, even in heavier seas.

In general, unfiltered samples were drawn from each Niskin-X for salinity and major nutrient measurements (ODF). The remainder of the volume was filtered using 47 mm, 0.4 μm pore-size Isopore membrane filters installed in Advantec filter cartridges. The filtrant was stored in unused Millipore petri slides and stored frozen at -20^{o}C. The filtrate was collected into trace metal-cleaned (acid-washed) bottles for dissolved trace metal concentrations (125 mL), barium concentrations and isotopic composition (250 or 1000 mL), and organically complexed iron (500 mL).

As is customary, trace metal analysis will occur at the home institutions under strictly controlled environments to prevent contamination of precious seawater samples.

Dissolved trace metals

Dissolved trace metal samples will be extracted using solid-phase extraction (Nobias Chelate PA-1 or Toyopearl AF-Chelate 650-M) to remove metals from the high salinity matrix and concentrate the metals into a pure nitric acid matrix suitable for direct injection and analysis by high resolution inductively coupled plasma mass spectrometry (HR-ICP-MS). The analysis will produce total dissolved concentrations of Fe, Mn, Cd, Co, Cu, Ni, and Zn, which describes the standing inventories of bioactive metal nutrients. In addition, dissolved concentrations of Al and Pb can be used as tracers of mineral dust and anthropogenic aerosols, respectively. Based on previous analyses of this region, we expect dissolved Fe concentrations to be sparingly low (<0.2 nM), dissolved Mn to be <0.5 nM unless enriched in surface waters by recent dust deposition events, and

concentrations of the other bioactive elements to be low unless enriched by cross-frontal intrusions of enriched subantarctic waters where surface dissolved trace metal concentrations are much higher than in oligotrophic subtropical waters.
Dissolved barium analysis will be conducted by Julia Middleton at WHOI (see section on Ba isotopic composition).

Organically complexed Fe will be measured by two techniques. Iron-ligand concentrations and binding strengths will be measured at University of South Florida-St. Petersburg by Shannon Burns using competitive ligand equilibrium-adsorptive cathodic stripping voltammetry (CLE-AdCSV) with salicylaldoxime and BASi hanging mercury drop electrode (see section on organic complexation of metals). The analysis will produce organic ligand concentrations and binding strengths of these ligands for dissolved Fe, which provides evidence of active Fe sequestration by Fe-limited phytoplankton or bacteria.

Dissolved Pb, a tracer of atmospheric deposition of industrial pollutants, will be measured at all stations and depths as part of our usual multielement suite. In addition, 1-L samples were collected at the Agulhas Retroflection (station 12) to determine the isotopic composition of Pb, which can be used to qualitatively identify the source of Pb to the region. The Agulhas Current has previously been identified as a pathway for introducing Pb from the Indian Ocean into the south Atlantic Ocean (Paul et al. 2015), but there was insufficient data from the southern Indian Ocean to positively identify the source of Pb carried from the Indian Ocean. Station 12 is located within the Agulhas Current before leaking into the south Atlantic, and the Pb isotopic composition determined in these samples will provide valuable insights into the potential sources of Pb in the Agulhas (South Africa? Long-distance transport from industrial centers in India?).

Particulate trace elements

Particulate trace element samples will be subjected to two primary chemical treatments to determine the labile and refractory fractions of trace elements. First, the filtered samples will be thawed to room temperature, folded twice to contain the suspended particulate material (SPM) in the center of the filter, and submerged into a 25% acetic acid solution with the mild reducing agent hydroxylamine hydrochloride (Berger et al., 2008). This treatment releases biogenic (e.g., soft components of marine microorganisms) and lithogenic phases of trace metals (e.g., Fe and Mn oxides), providing an estimate of the total elemental SPM concentration that easily remineralizes and is likely bioavailable for nutrient recycling. The second treatment involves an aggressive mixture of nitric, hydrochloric, and hydrofluoric acids, that completely breaks down the more refractory mineral (e.g., aerosol dust and resuspended sediments) and biogenic phases (e.g., frustules and tests). When considered together, the concentrations of trace and major elements in each of the labile and refractory fractions, along with their relative ratios (Fe/P, Zn/Si), can be used to tease apart the biogenic, lithogenic, and authigenic composition of marine particles. Using HR-ICP-MS, a suite of elements can be simultaneously detected and their concentrations quantified, including the bioactive trace

metals (e.g., Fe and Zn), mineral tracers (e.g., Al and Ti), biominerals (e.g., Ba and Si), and other tracers like P (biology), Pb (coal combustion), and V (diesel fuel combustion).

Vertical Profiles

Dissolved and particulate trace element samples were collected from the Niskin-X bottles at 16 stations, coordinated to complement the regular productivity casts conducted with the ship's CTD rosette system. The trace metal samples drawn from these casts are summarized in the **Station Summary** table below.

Surface sampler: modified otter boat, also known as "Big Jon"

Deckboard incubations

To estimate the potential for major or trace nutrient limitation, four series of nutrient amended whole water incubations were conducted throughout the cruise. Surface whole water was collected from the starboard side of the ship using a clean sampling hose (¾" Bev-a-line and ¾" drinking water hose) kept at sea-surface depth using a modified otter boat ("Big Jon") with a snorkel that extends below and forward of the otter boat itself.

Surface samples were collected with great attention to preventing and minimizing the possibility of accidental trace or major nutrient contamination (especially iron and nitrogen species). All cubitainers, tubing, fittings, pumps, and subsample bottles were acid-washed with dilute hydrochloric acid (~10%) and thoroughly rinsed with UHPW and/or freshly collected seawater. The surface seawater was pumped into the wet lab using an air-operated double-diaphragm Teflon pump (Ingersoll-Rand PD07P-APS-PTT) at ~ 7 L/min into two 200 L acid-cleaned tanks simultaneously through a tee that improved homogeneity of the water in each tank. The cubitainers were filled with 20 L of surface seawater directly from one tank at a time (without use of the tee) using the same Teflon pump, with the hoses configured in reverse. Eighteen cubitainers were filled per experiment and amended in triplicate with one or more nutrients or filtered SAMW, except for a set of Controls which contained only surface seawater.

Nutrient amendment stocks were carefully evaluated before the cruise for unwanted concentrations of either trace metals (especially Fe) or other major nutrients.

Nitrate

The nitrate standard was prepared at sea by dissolving approximately 2.5 g of sodium nitrate salt ($NaNO_3$), carefully weighed and bottled at NHMFL/FSU before the cruise, into ~ 125 mL of UHPW from the Thompson's UHPW system. The solution was then cleaned twice by passing over a small column of Chelex-100 that had been cleaned with freshly prepared 10% HCl (v/v; reagent grade) and thoroughly flushed with UHPW to rinse away residual acid and any associated metals released from the Chelex. The stock nitrate concentration was confirmed by the SIO-ODF team to be free of contamination from other major nutrients (e.g., ammonia or silicate), and preliminary tests at home demonstrated the efficient removal of trace metals like Fe from the stock by using the

same Chelex method; nevertheless, the nitrate stock will be reevaluated at NHMFL/FSU for any potential trace metal contamination.

Silicate

Unlike nitrate, solutions of dissolved silicate salts cannot be cleaned of trace metals by Chelex resin, since dissolved silicate naturally produces a solution of pH greater than 12, which is above the effective complexation capacity of Chelex (effective at pH values 2-10). Therefore, a high-purity standard was purchased from Sigma Aldrich, certified for ion chromatography to be free of anionic contaminants such as nitrate. Two 100-mL bottles were ordered and tested for trace metal concentrations before the cruise, and all bioactive trace metal concentrations were found to be sparingly low (exact concentrations to be determined after the cruise in each relevant incubation test).

Iron

The Fe standard used to amend the +Fe and +Fe+Silicate incubations was prepared from an enriched stable isotope stock of Fe-57 (Oak Ridge National Labs) dissolved in dilute UHP HCl (0.3 M or 0.024 M). This standard has been well-calibrated in our lab at NHMFL/FSU to be free of other trace metal impurities and major nutrients, especially nitrate (e.g., from acidification by nitric acid). The use of Fe-57 enriched standard allows us to quantify the partitioning of the amendment between the dissolved fraction (apparent as dissolved Fe-57), the particulate fraction (as taken up by the ambient phytoplankton communities in the incubations), and surface adsorption on to the walls of the cubitainers (based on any differences between the sum of dissolved and particulate pools and the total moles of Fe added to each incubation). The use of an Fe-57 standard also allows us to distinguish between our intentionally added Fe and any accidental contamination of Fe.

Subantarctic Mode Water

Before each incubation experiment, a vertical Niskin-X cast was conducted to both characterize the vertical water column structure and collect subantarctic mode water (SAMW) to simulate an upwelling or mixing event into nutrient-depleted surface waters. SAMW was collected from the depth where the potential density was between 26.5 and 27.1 σ_θ. This Niskin-X bottle was subsampled differently, by using an Acropak-200 capsule filter to rapidly draw 0.2 µm filtered water into three 1-L FEP bottles. Before filling the SAMW cubitainers with surface seawater from the tanks, one of the SAMW FEP subsamples were added to each of the cubitainers, and then the tank water pumped in to thoroughly mix. If the cubitainers are assumed to contain ~20 L total volume, then the addition of 1-L of SAMW would produce a final mixture of ~5% SAMW with 95% surface seawater. While the initial nutrient and salinity concentrations from the Control experiment were assumed to be identical across all the other incubation amendments before they were amended, separate nutrient and salinity samples were drawn for each of the three SAMW amended cubitainers.

Subsampling the incubation cubitainers

Subsamples were drawn directly from the tanks for "t=0" time points, except for trace metal samples which were drawn immediately after each cubitainer was amended.

Thereafter, each cubitainer was subsampled approximately every 24-48 hours for nutrients, DIC/alkalinity, PAM fluorescence, POC/PIC, chlorophyll a, biogenic silica, dissolved and particulate trace metals, dissolved Ba concentrations and isotopes, and/or organic-metal ligand complexes. Trace metal samples were drawn into a 1-L acid-washed FEP Teflon bottle and filtered offline for dissolved trace metals, organically complexed Fe, and dissolved Ba concentrations and isotopes. Additional subsamples were drawn at the first and final time points for DNA/RNA analysis for D. Sturm, where ~200 mL from each of the three replicates was combined to produce a single "average" sample. Preliminary results showed that all features studied by incubation amendments (stations 5, 18, 28, and 56) were responsive to nitrate and the SAMW amendments, based on nitrate drawdown in both amendments and positive responses in photosynthetic efficiency parameters (see section by C. Brownlee on the topic). In contrast, very little effect was observed for amendments of Fe and/or silicate.

Issues and/or concerns

The Thompson UHP water system appeared to be compromised twice during the cruise. While in port in Cape Town, the prefilter resin cartridges and the DiamondPURE internal cartridges were all replaced. Nevertheless, the prefilter resin cartridges changed color from black to red within about one month, indicating that the cleaning capacity of the resin had rapidly been exceeded by the source water. In addition, the UHPW system resistance dropped to less than 15 MOhm-cm, which likely indicated that significant impurities had bypassed the prefilter cartridges and compromised the internal cartridges. A single 125-mL sample was collected to be analyzed at NHMFL/FSU to determine the trace metal concentrations in the compromised water. The two prefilter cartridges and internal cartridge were exchanged again, and the UHPW system resistance returned to the optimal value of 18.2 MOhm-cm.

Since this UHPW was used throughout our shipboard activities – to clean sampling components like tubing and filtration rigs; to rinse the cubitainers, subsampling bottles, and 200-L tanks; and to prepare the nitrate standard – there is the chance that the dissolved and particulate trace metal samples could be contaminated with whatever contamination was exhausting the UHPW system's resin cartridges.

References

Berger, C.J.M., Lippiatt, S.M., Lawrence, M.G., Bruland, K.W., 2008. Application of a chemical leach technique for estimating labile particulate aluminum, iron, and manganese in the Columbia River plume and coastal waters off Oregon and Washington. J. Geophys. Res. 113, C00B01. https://doi.org/10.1029/2007JC004703

Paul, M., Van De Flierdt, T., Rehkämper, M., Khondoker, R., Weiss, D., Lohan, M.C., Homoky, W.B., 2015. Tracing the Agulhas leakage with lead isotopes. Geophys. Res. Lett. 42, 8515–8521. https://doi.org/10.1002/2015GL065625

Station Summary Table

Description *(units)*	**Stn**	**Fluor max** *m*	**MLD** *m*	**dTM** *n=?*	**pTM** *n=?*	**dBa** *n=?*	**FeL** *n=?*	**PbIC** *n=?*	**SAMW** *m*
Test	1	75 (60-90)	50						
	3	45 (30-60)	35	2	2	2			
Incubation A	5	25 (0-40)	35	7	7	7	8		346
	6	50 (0-75)	37	8	8	8			
	7	60 (0-75)	60	8	8	8			
	8	60 (0-75)	60	9	9	9			
Agulhas Retroflection	12	50 (40-80)	60	9	9	9		9	
	17	18 (40-80)	50	9	9	9			
Incubation B	18	80 (60-120)	80	9	9	9	6		524
	20	56 (40-100)	40	9	9	9			
	23	57 (40-90)	40	9	9	9			
Incubation C	28	40 (0-80)	30	8	8	8			450
	39	47 (0-60)	30	8	8	8			
	50	25 (0-40)	30	9	9	9			
Incubation D	56	80 (50-120)	50	9	9	9			365
	70	75 (40-120)	46	9	9	9			

Summary of incubation nutrient amendments

		Std conc	***Final conc***	***Volume to pipette***
White	Control	*n/a*	*n/a*	*n/a*
Blue	Nitrate	222.6 mM	~12 uM	1 mL
Purple	SAMW	*n/a*	5%	1 L
Yellow	Silicate	10.52 mM	~4 uM	6.8 mL (2x 3.4 mL)
Orange	Silicate/Fe	*(+Fe+Si)*	*(+Fe+Si)*	*(+Fe+Si)*
Green	Fe	17 µM	~4 nM	4 mL
		1700 µM	~4 nM	40 µL

Summary of SAMW added to each incubation*

Station	Depth	Temperature (°C)	Salinity (psu)	Density (σ_θ)	Dissolved Oxygen (µmol/kg)	NO_3- (µM)	PO_4^{3-} (µM)	$H_3SiO_4^-$ (µM)
5	346	9.0264	34.6437	26.8410	210.46	19.33	1.34	7.7
18	524	10.3168	34.7949	26.7482	219.64	17.18	1.21	7.7
28	450	7.3291	34.4768	26.9668	206.29	23.06	1.57	12.8
56	365	10.6209	34.7544	26.6601	210.93	13.15	0.98	4.2

**added at ~5% volume to surface seawater*

TN 376 Brownlee team cruise report

1. Rationale and approaches

We have applied photophysiological and molecular genetic approaches in order to better understand the drivers and constraints on phytoplankton abundance, community composition and productivity. We have used Pulse Amplitude Modulated (PAM) fluorimetry of freshly isolated samples together with sub-samples from incubation experiments.

2. Objectives

- To determine the spatial distributions (surface, depth profiles) of parameters of photosynthetic efficiency to address the following:
- Identify correlations with environmental factors – salinity, temperature, nutrients, carbonate chemistry.
- To uncover any relationships between particular phytoplankton groups major species composition
- Use this information, broadly defined as photosynthetic efficiency parameters, together with more detailed analysis from eDNA and eRNA samples and EM preparations to gain indications of efficient growth as well as physiological stress arising from nutrient deficiency and/or potential biotic interactions (competition, chemical warfare).

3. PAM fluorimetry

PAM fluorimetry is a widely used method for rapid assessment of the physiological state of the photosynthetic machinery in plants. The approach is based on measurement of chlorophyll fluorescence of photosystem II (PSII) as an indicator of **the efficiency with which light absorbed by the photosynthetic machinery and converted into useful work in the form of electron transport in the chloroplast thylakoid membrane.** The electron transport chains are ultimately responsible for providing the chemical energy for photosynthetic carbon fixation. Figure 1 shows a simplistic scheme of the components of chlorophyll PSII system (see e.g. Murchie & Lawson (2003) for a more detailed accessible guide to PAM fluorimtery).

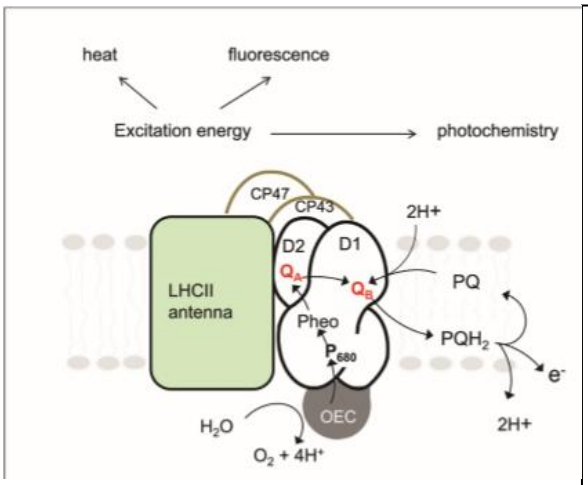

Figure 1. Energy conversion by PSII. Light absorbed by the chlorophyll light harvesting complex (LHCII) drives the hydrolysis of water into O_2, H^+ and electrons. Transfer of electrons through the components of the electron transport chain in the thylakoid membrane of the chloroplast energises the photosynthetic machinery, eventually leading to the fixation of carbon from CO_2. Excess light energy absorbed by chlorophyll/PSII is lost as fluorescence or through chemical quenching and heat (non-photochemical quenching, NPQ). From Murchie & Lawson (2013)

Figure 2 provides a simplistic cartoon to illustrate how chlorophyll fluorescence varies under the different light pulse protocols used in PAM fluorimetry. The values of chlorophyll fluorescence (Fo,Fm and F') are used to calculate the efficiency parameters.

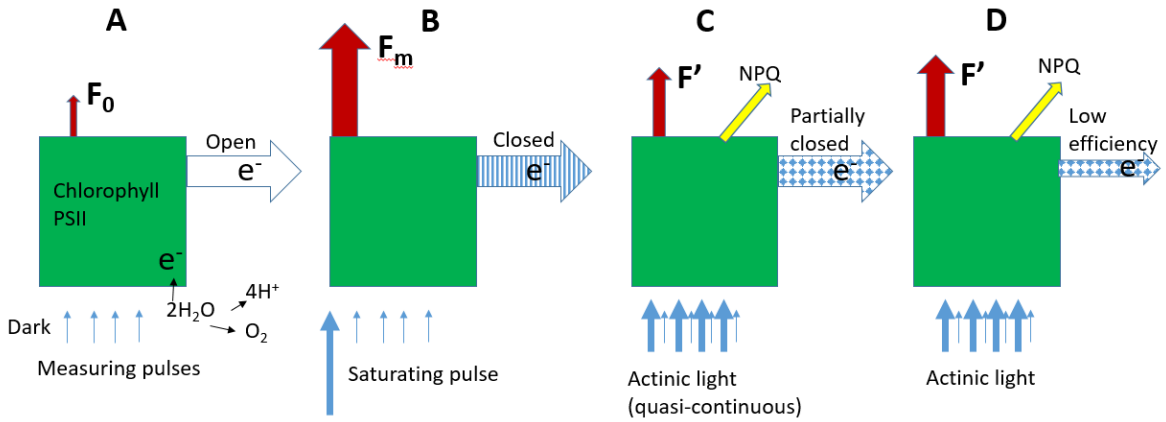

Figure 2. Illustration of how chlorophyll fluorescence measurements are made and used to assess photosynthetic efficiency in PAM fluorimetery. Light energy absorbed by chlorophyll can either be converted into electrons or lost as fluorescence or heat (NPQ). Photosyntheic efficiency is a measure of the efficiency of conversion of incident light into useful electron transport . **A:** In dark-adapted cells, the photosynthetic reaction centres, through which electrons are transferred, are open. Short, low amplitude measuring pulses of light produce low levels of resting fluorescence (Fo). **B:** A strong pulse of light saturates the electron transport chain and leads to the closure of photosynthetic reaction centres. Electrons produced by chlorophyll/PSII cannot be efficiently transferred resulting in corresponding increased fluorescence, measured immediately after the saturating light pulse (Fm). **C:** Measuring light pulses given in rapid alternation with actinic light monitor the fluorescence arising from the partial closure of reaction centres as electrons move through them in the light-activated photosynthesising state. Decreases in the fluorescence signal (quenching) may occur as non-photochemical quenching (NPQ) reactions are activated. **D:** Cells in which the electron transport chain or carbon fixation are compromised in some way (e.g. through nutrient deficiency) may show increased fluorescence due to the electron transport chain working less efficiently. By monitoring the ratio of fluorescence values after different light pulses, **by measuring values of Fo, Fm and F' during different illumination regimes,** the efficiency by which absorbed light is converted into electron transport can be calculated.

Figure 3 provides a theoretical and actual experimental quench curve used to obtain the values of chlorophyll fluorescence. Experimental measurements were made with a PAM fluorimeter (Water PAM, Walz, Germany) with 3 ml cuvette samples that were dark-adapted for >30 minutes prior to analysis.

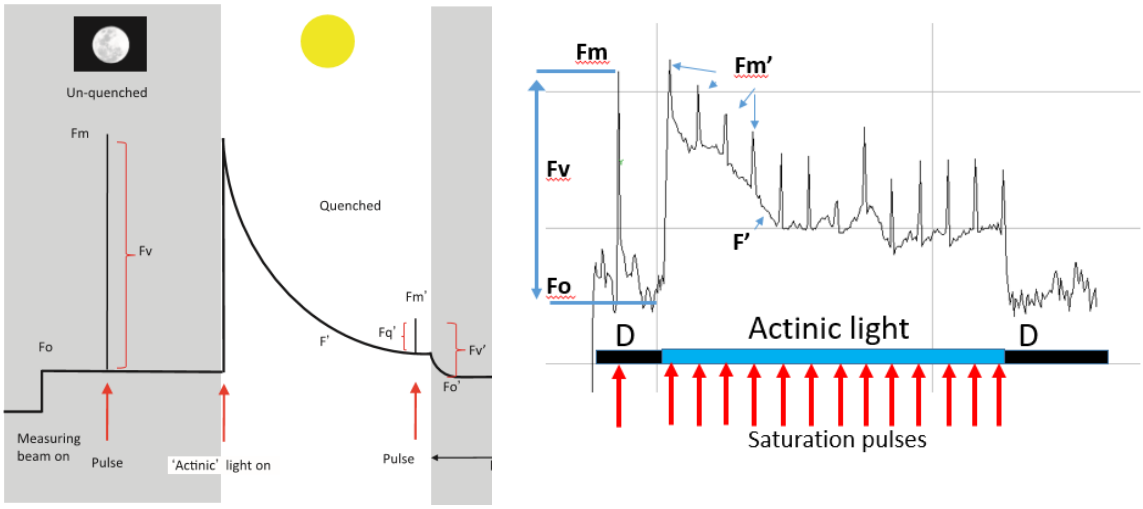

Figure 3. ***Left:*** Schematic of a PAM quench curve, showing the measurement of Fo, Fm after the initial saturating pulse and F' values during the onset of actinic light illumination. ***Right:*** Representative quench curve obtained from a cruise sample (Station 43, 5m depth). The peaks during the actinic light period are in response to additional saturating pulses that are used to measure effective photosynthetic quantum yield (YII) and NPQ. NPQ values are calculated when quenching reaches a steady state at the end of the quench period (normally around 5 minutes).

The following key photosynthetic parameters were calculated from values of Fo,Fm, F'm and F':

- Maximum photosynthetic efficiency/capacity of dark –adapted cells:

$$\mathbf{Fv/Fm} = (Fm-Fo)/Fm$$

- Effective photochemical quantum yield of PSII (photosynthetic efficiency in light conditions):

$$\mathbf{Y(II)} = (Fm'-F')/Fm'$$

- Electron transfer rate (ETR) at a given irradiance value = proportion of photons at a given light intensity that are converted into useful energy.

$$\mathbf{ETR} = Y(II) \times PAR$$

- Non-photochemical quenching

$$\mathbf{NPQ} = Fm/Fm'-1$$

- Rapid light curves were also carried out to acquire ETR values at different irradiance values, providing information on initial slope (α), ETRmax at saturating irradiance and photoinhibition.

4. Preliminary analyses

4.1. Meander surveys. Figures 4 and 5 show surface underway photosynthetic parameters (Fo, Fv/Fm, ETR) along VPR tracks during the first meander survey, together with salinity, temperature and bbprime distributions. Preliminary examination reveals generally low values of Fo in regions of high salinity and temperature. In contrast , Fv/Fm values were generally higher in low salinity regions.

High Fv/Fm values were also observed in high bbprime and higher temperature regions. ETR values showed less distinct correlations though they more closely matched Fv/Fm values in survey 1. ETR values show a good correlation with bbprime. Figures 6 and 7 show Fo,Fv/Fm and ETR values from surface CTD samples from the meander surveys 1 and 2. Fo values again showed an inverse relation with salinity and temperature. Fv/Fm values correlated positively with temperature and salinity (cf .Figs 4 and 5).

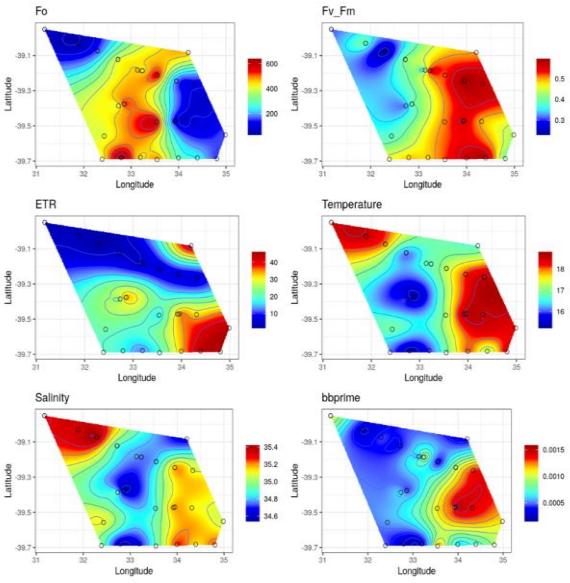

Fig 4. Meander VPR survey 1
Underway samples

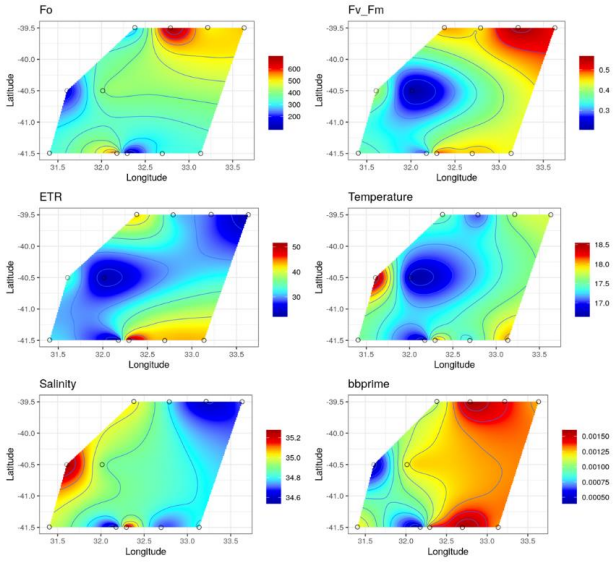

Fig 5. Meander VPR survey 2
Underway samples

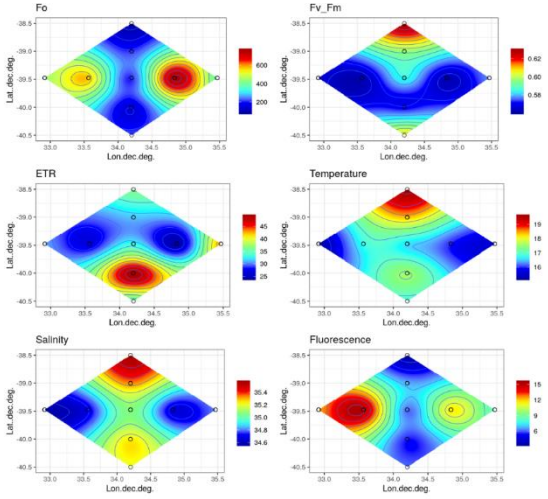

Fig. 6. CTD surface features:
Meander survey 1 (CTD 8-17)

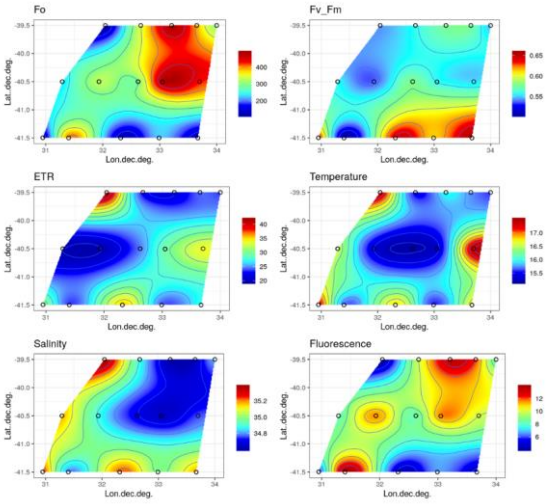

Fig. 7. CTD surface features
Meander survey 2 (CTD 18-25)

Figs 7-10 show summary depth profiles for Fo, Fv/Fm and ETR in relation to temperature,

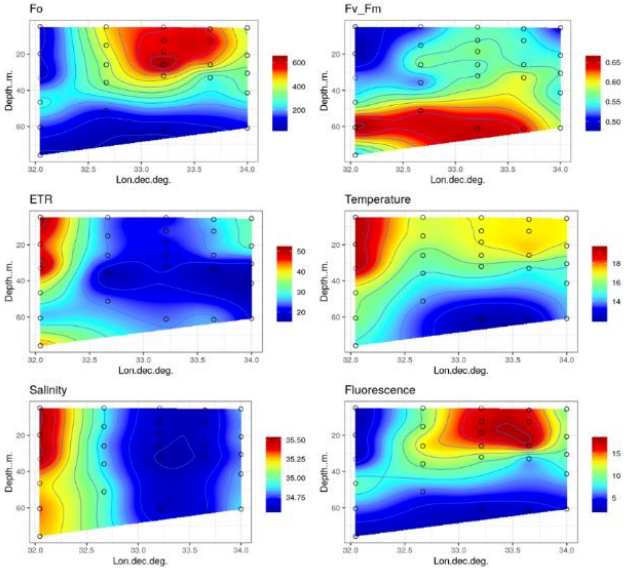

Fig. 8. CTD depth profile Meander North transect (CTDs 44-52)

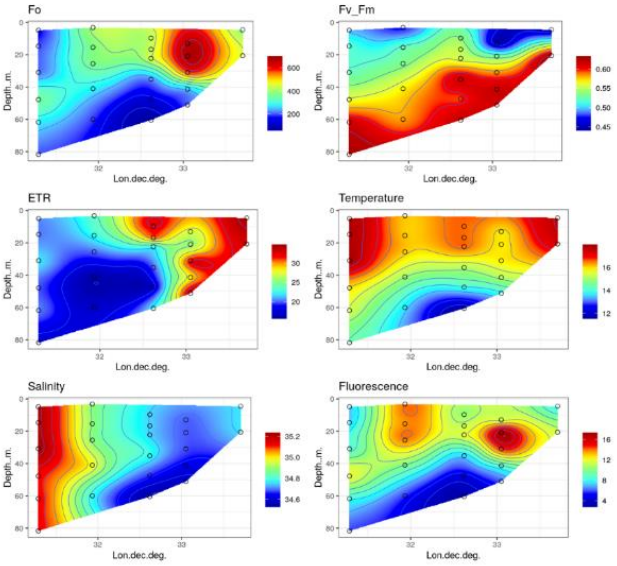

salinity and total chlorophyll fluorescence for

Fig. 9. CTD Depth profile Meander Centre transect (CTDs 35-42)

North, Central and Southern transects during the second meander survey. In all profiles there is a clear relationship between Fo values and total chlorophyll fluorescence. Fo values tended to correlate negatively with salinity and Fv/Fm. Fv/Fm values showed negative correlations with temperature and Fo/fluorescence and in the Southern transect showed an apparent positive correlation with temperature.

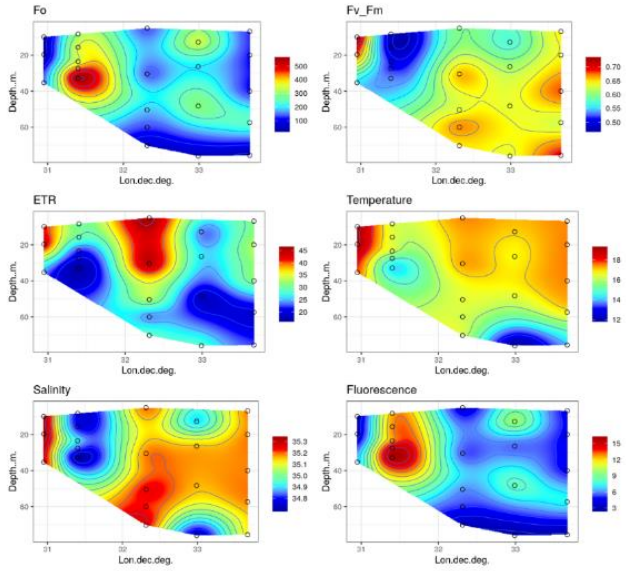

Fig.10. CTD Depth profile Meander meander

Southern transect (CTDs 26-34)

Spearman correlations derived from all Fo,Fv/Fm and ETR measurements are shown in Fig 11. Overall, Fo showed significant negative correlation with salininty and positive correlation with total chlorophyll. Fv/Fm showed an overall positive correlation with salinity and negative correlation with fluorescence. ETR was strongly correlated with temperature, salinity and fluorescence. In addition ETR showed a strong correlation with time of sample collection, showing strongest peaks in samples collected in mornings. Examples of Spearman correlations for Fo and Fv/Fv are shown in Fig. 10. Further analysis is ongoing. For example the apparent relationship between bbprime and Fo and Fv/Fm is not apparent in the Spearman correlations from all samples, suggesting location-specific relations that may reward further investigation.

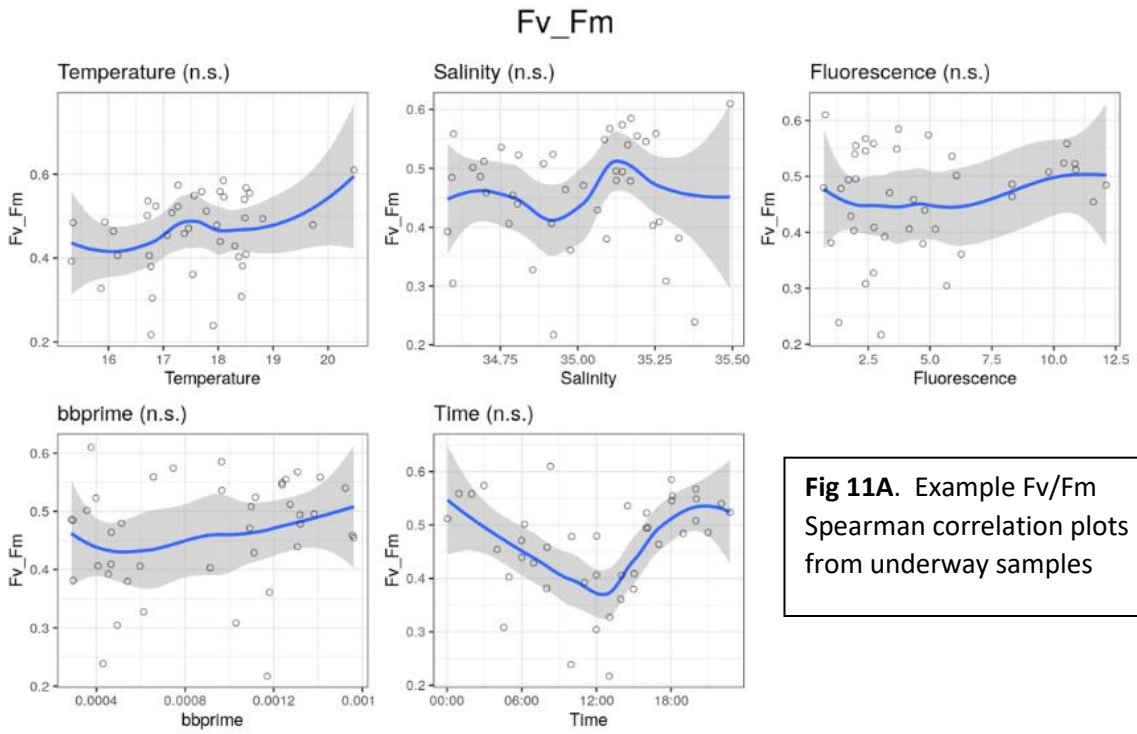

Fig 11A. Example Fv/Fm Spearman correlation plots from underway samples

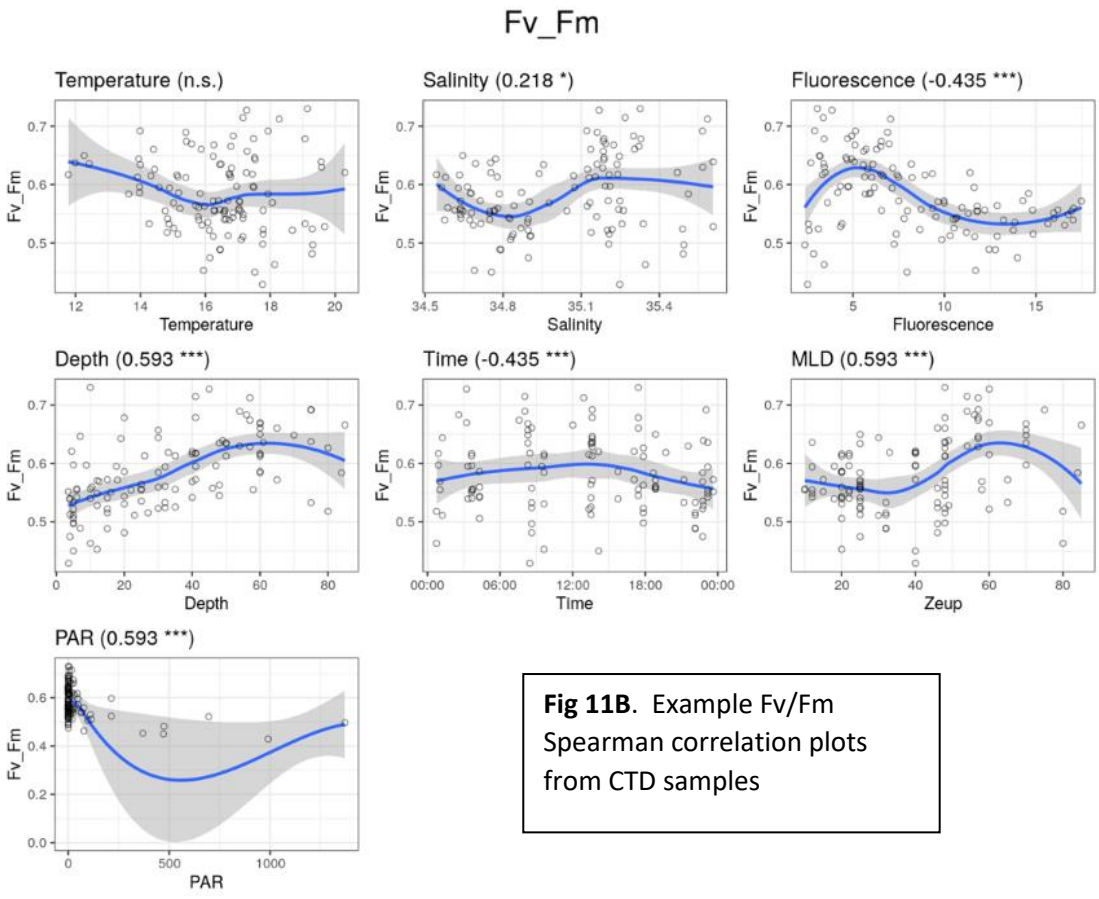

Fig 11B. Example Fv/Fm Spearman correlation plots from CTD samples

4.2. Eddy surveys. Plots of eddy surveys 1 and 2 are under construction. Fig. 12 shows surface underway values of Fo, Fv/Fm and ETR in relation to temperature, salinity and fluorescence.

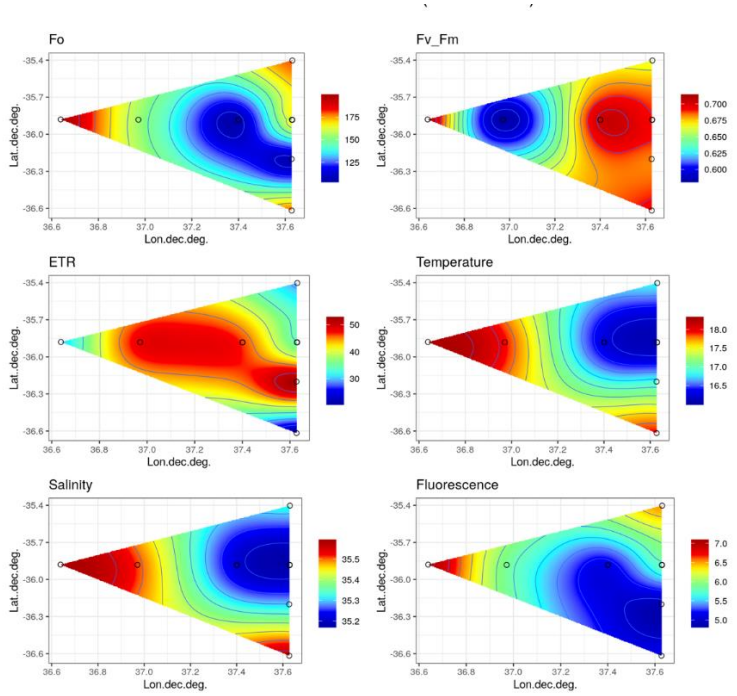

Fig. 12. Surface plots of F0, Fv/Fm and ETR for eddy survey 1.

Further analysis of this feature is ongoing.

4.3 PAM microscopy

Analysis of single cell chlorophyll fluorescence was applied using similar PAM protocols to the above PAM fluorimeter measurements. The PAM microscope (PSI, Cz) allows images of Fo, Fm, F'm and F' by using LED arrays to provide measuring pulses, saturating pulses and actinic light. Under rough weather conditions it was only possible to obtain Fv/Fm values due to focus drift associated with vertical movements of the ship. The microscope allowed acquisition of bright field and polarized light images to identify individual phytoplankton cells and calcifying coccolithophores. Cells were allowed to settle in darkness for >1 hour before gentle transfer to the microscope imaging chamber, which comprised a glass-bottomed dish and X 20 or X40 Zeiss water immersion objectives. The dish was mounted on a temperature controlled perfusion cell, which allowed cells to be maintained at the precise collection temperature. All manipulations were carried out in darkness. Bright field images were obtained using far red light, which does not activate the PSII reaction centres. Fig 13 shows a representative set of images from CTD #50 surface sample, along with Fv/Fm values of individual coccolithophore and non-coccolithophore (mainly dinoflagellates and small flagellates) cells (see TGT microscopy log.xls for all CTD and underway samples).

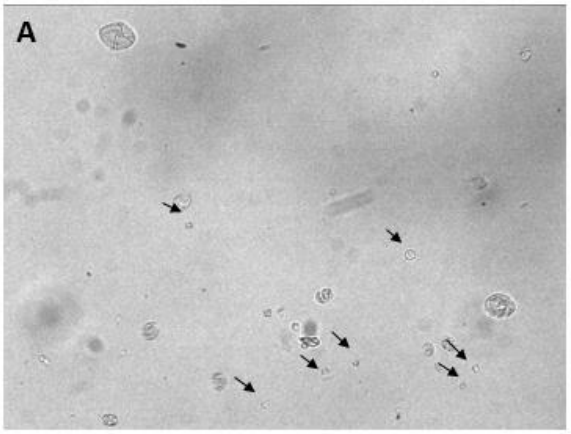

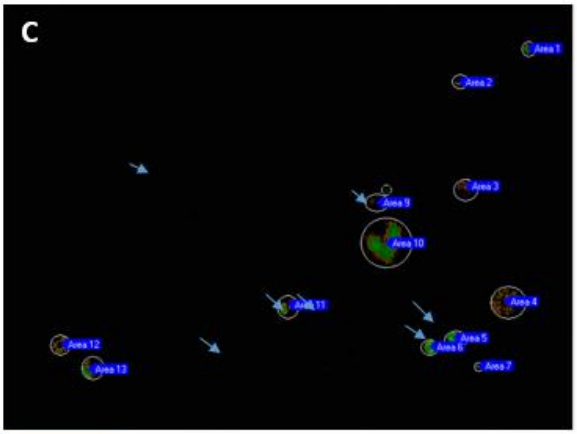

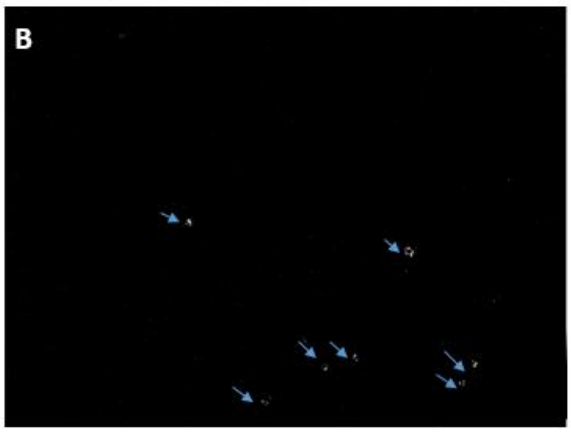

D	size [pixels]	Fo	Fm	QY_max
Area 1	78	158.43	159.03	-0.02
Area 2	25	35.14	125.31	0.71
Area 3	82	61.90	112.34	0.44
Area 4	295	67.59	111.21	0.38
Area 5	162	122.01	194.48	0.36
Area 6	174	182.33	232.85	0.20
Area 7	21	126.10	146.72	0.13
Area 9	24	37.55	104.87	0.63
Area 10	1108	30.72	143.47	0.77
Area 11	162	60.90	142.12	0.55
Area 12	171	55.65	125.68	0.54
Area 13	195	41.06	155.31	0.70

Fig. 13. **A:** Bright field image of a mixed phytoplankton sample (CTD 50). Arrows correspond to calcified cells revealed by cross polarised light **(B)**. **C:** Fv/Fv image showing ROIs of cells selected for quantification. **D:** Fv/Fm (QY) values of cells identified in **(C).**

PAM microscopy key findings:

- Approximately 175 individual underway or CDT samples, representing >250 individual cells were analysed using PAM microscopy. This pilot study demonstrates the applicability of PAM microscopy on a research vessel. Issues related to vibration were minimal, though slower vertical pitch and roll ship movements limited the application of longer term quench curves. The study focussed on obtaining a dataset of Fv/Fm values.

- The majority of samples comprised mixed populations of coccolithophores and dinoflagellates. The precise proportions of different phytoplankton classes awaits further cell count analyses. While *Emiliania huxleyi* was the most frequently occurring coccolithophore, many samples were notable for the apparent diversity of coccolithophore species.

- Preliminary analysis indicates that mean Fv/Fm values reflect the average values obtained with PAM fluorimetry. However, the single cell analyses have revealed an unexpectedly high variability in single cell Fv/Fm values (e.g. Fig 12 D, with values ranging from <0.2 to >0.7).

- So far, no clear differences have been seen in the average Fv/Fm values of different phytoplankton types, though substantial further analysis is needed to investigate this in more detail.

Questions to address:

- Can we detect differences in the average FvFm for different phytoplankton groups within a population
- Do the PAM microscopy measurements agree with the PAM fluorimetry?
- Is there greater variability within and between different phytoplankton groups and do any differences in variability in FvFm inform whether particular groups are better adapted to the current conditions?

The PAM fluorimeter measures total population fluorescence parameters, which includes the cyanobacterial signal. Cyanobacteria are excluded from the PAM microscopy measurements, being too small to resolve individual cells. However, cyanobacteria have been observed in significant numbers in fixed slide preparations. Can any differences in PAM fluorimetry and PAM microscopy reflect the contribution of cyanobacteria to the fluorescence properties, and potentially productivity of the population.

4.4 Deck incubation experiments

Fluorescence parameters were measured from 4 deck incubation experiments, carried out on surface samples from both the meander and eddy features. Incubations were sampled daily for the course of the experiment. Figs 14 and 15 show results of Incubation Experiments 1 and 3, respectively. Experiments 2 and 4 are currently undergoing analysis. From these experiments, only the addition of N (Experiment 1, Fig. 14) produced a significant increase in Fo relative to controls. It is notable that in Experiment 1, all treatments, including controls showed a sharp decrease in Fo, which was partially reversed in the +N treatment. All treatments in Experiment 1 also showed reduced ETR relative to controls. In contrast, Experiment 3 showed increases in Fo with little significant difference between controls and nutrient additions.

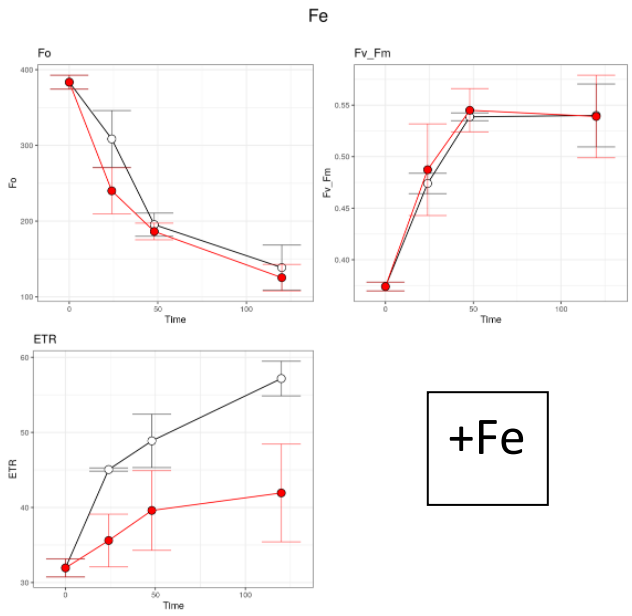

+Fe

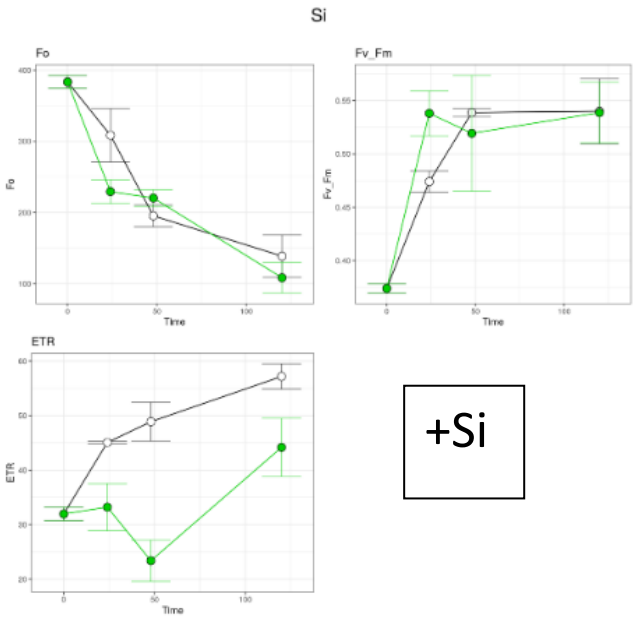

+Si

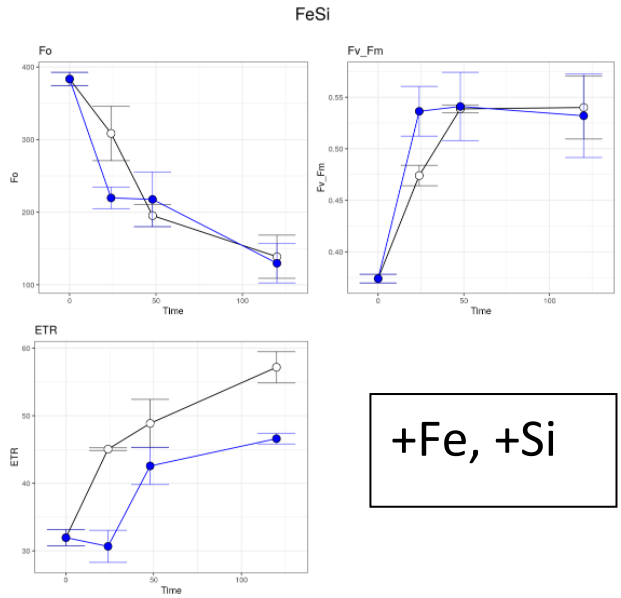

+Fe, +Si

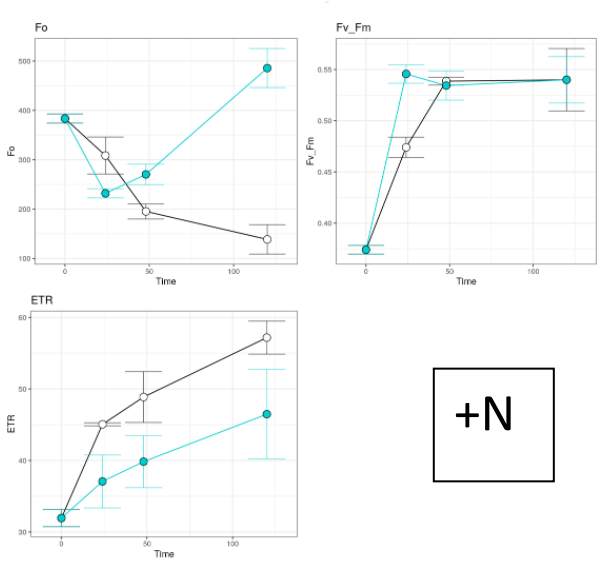

+N

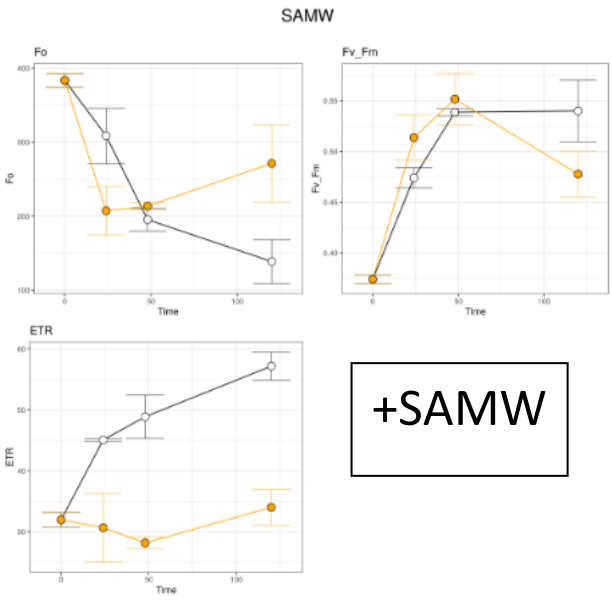

+SAMW

Fig. 14 Nutrient addition incubation 1

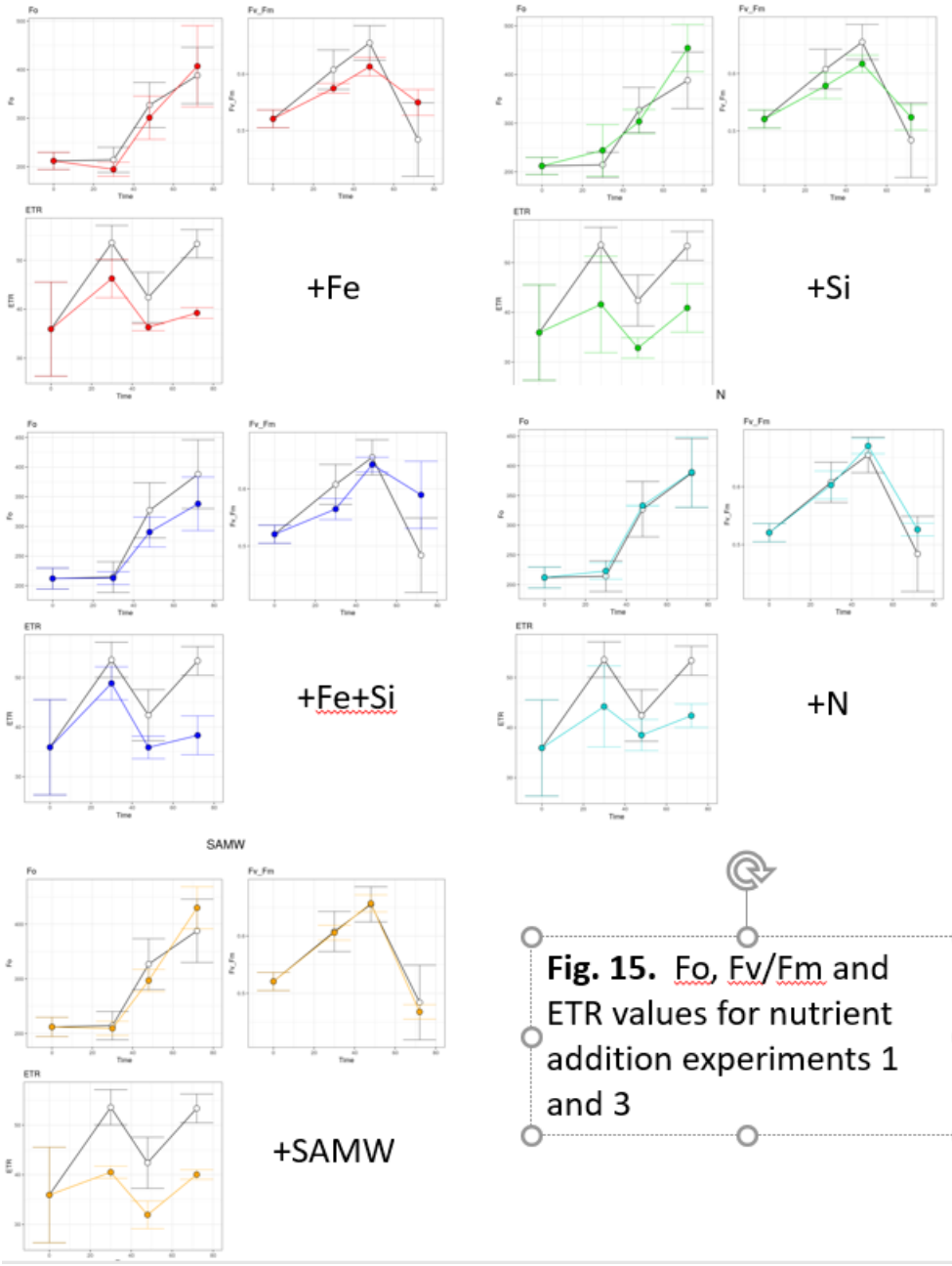

Fig. 15. Fo, Fv/Fm and ETR values for nutrient addition experiments 1 and 3

4.5 DNA and RNA

Samples for DNA and were collected from all DCM and surface CTDs (where chlorophyll fluorescence was significant) and from underway samples that showed sufficiently high chlorophyll or BB' values.

DNA samples will be analysed with high throughput sequencing. RNA samples will provide a resource for probing expression of specific genes and total population transcriptomes.

References

Murchie EH, Lawson T (2013) Chlorophyll fluorescence analysis: a guide to good practice and understanding some new applications. J. Exp Bot 64, 3983-3998.

T376

Carbon System Measurements

Nick Bates Group

Bermuda Institute of Ocean Sciences (BIOS)

Group Members:

Rebecca Garley (BIOS)

Matt Enright (BIOS)

Judith Murdoch (University of Otago)

Objectives:

To undertake high quality dissolved inorganic carbon (DIC) and total alkalinity (TA) measurements throughout the cruise from both the CTD rosette and the ships underway system. Sampling especially in features with high coccolithophore biomass in order to understand the influence of these phytoplankton blooms on biogeochemistry, carbon dynamics (including biological pump of carbon) and air-sea gas exchange. Also to support other biogeochemical measurements on the cruise as a means to understand Southern Ocean ecosystem dynamics.

We will use the carbon chemistry measurements to help understand the dynamics of preconditioning of the mode waters formed in the Southern Ocean. Inputting the DIC and TA data into CO2SYS (Lewis and Wallace, 1998; using the constants from Mehrbach et al., 1973 refit by Dickson and Millero, 1987) to compute other carbonate parameters (e.g. pH, pCO2, calcium carbonate mineral saturation states) to further understand the carbonate system of these waters.

Methods and Samples:

Samples for Dissolved Inorganic Carbon (DIC) and Total Alkalinity (TA) were collected in 250ml glass bottles according to standard JGOFS methods. Milli-Q cleaned bottles were rinsed out 3 times, bottom filled using silicone tubing, allowed to overflow at least 1 times the bottle volume, ensuring no bubbles are in the sample, and sealed with a small headspace to allow for water expansion.

Water samples were collected from all depths the CTD-rosette sampled. Two samples were collected from each Niskin bottle. The first sample set was poisoned with 100µl mercuric chloride for analysis back at the BIOS lab. The second set was not spiked and stored in the dark for no longer than 12 hours (to minimise any biological activity altering the sample) before being run on board, DIC first then TA. In addition to sampling from the rosette, samples were also collected and run on board from the underway system approximately every 2 hours whilst towing the VPR or when CTD station were further part than ~24nm. Also, samples for the 4 incubation experiments were taken; 4-6 initial starting samples, then one sample from each of the 18 cubitainers for the further 3 time points of the experiment. Both the underway and carboy samples were un-spiked, stored in the dark and run on board.

Samples were run on the VINDTA 3S (Versatile Instrument for the Determination of Titration Alkalinity) and the AIRICA (Automated Infra-Red Inorganic Carbon Analyzer) (www.marianda.de).

TA is measured on the VINDTA 3S by titration with a strong acid (HCl). The titration curve shows 2 inflection points, characterising the protonation of carbonate and bicarbonate respectively, where consumption of acid at the second point is equal to the titration alkalinity.

DIC is measured on the AIRICA by the extraction of total dissolved inorganic carbon content from the sample by phosphoric acid addition. The liberated CO_2 flows with a N_2 carrier gas into a Li-Cor non-dispersive IR gas analyser where the CO_2 levels are measured.

For both instruments within bottle replicates were run consecutively on start up to check the precision, continuing once the instrument precision was ±2µmol kg^{-1} or better. These were followed by Certified Reference Materials (CRMs) produced by the Marine Physical Laboratory at UCSD, which were run every 12 hours on the VINDTA and every ~5 samples on the AIRICA, to determine the accuracy of the measurements and to correct for any discrepancies. The TA system CRM values did not vary more than 2umol within each batch of HCl acid. The AIRICA is more susceptible to drift and can be affected by the lab temperature which is why CRMs were run much more often on the AIRICA.

The values for DIC and TA were used to calculate other parameters of the carbonate system using CO2sys (Lewis and Wallace, 1998). Parameters able to be calculated are pH, fCO_2, pCO_2, $[HCO_3^-]$, $[CO_3^{2-}]$, $[CO_2]$, alkalinity from borate; hydroxide ion; phosphate and silicate, Revelle Factor, plus the saturation states of calcite and aragonite.

Sample	# of stations	# of samples	analysis
CTD DIC/TA	73	685	Future processing at BIOS
CTD DIC/TA	73	825	Analysed on board
Underway DIC/TA	127	127	Analysed on board
Incubation DIC/TA	4	238	Analysed on board

Table 1: Summary of sample collection and analysis

Initial Findings:

Figure 1 below shows surface plots of the samples collected from the underway seawater system. With higher sample density in the 2 features that were sampled more intensively. Both DIC and TA have been normalized to a salinity of 35 to remove the effects of salinity on the data. The Agulhas mender shows a higher nDIC and nTA with lower pCO2m temperature and salinity. With the opposite in the eddy feature further to the North.

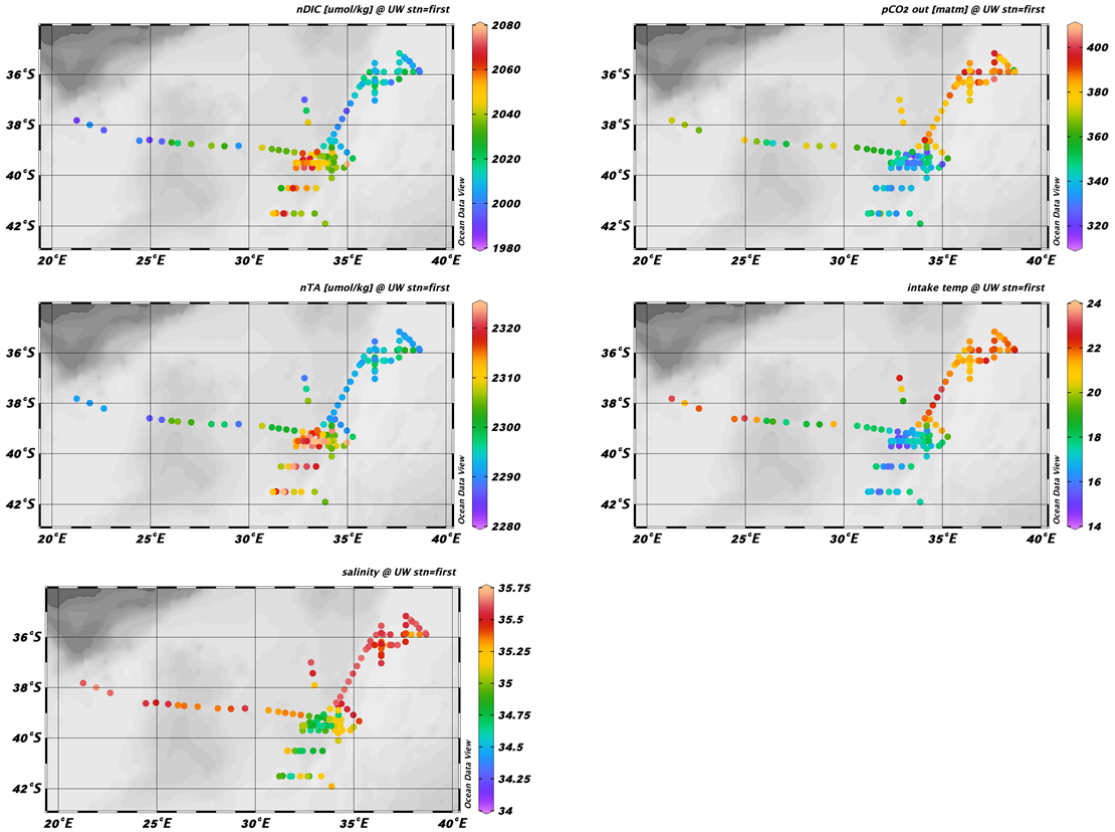

Figure 1: Underway sample data showing salinity normalized DIC (nDIC), pCO2, salinity normalized TA, sea temperature and salinity.

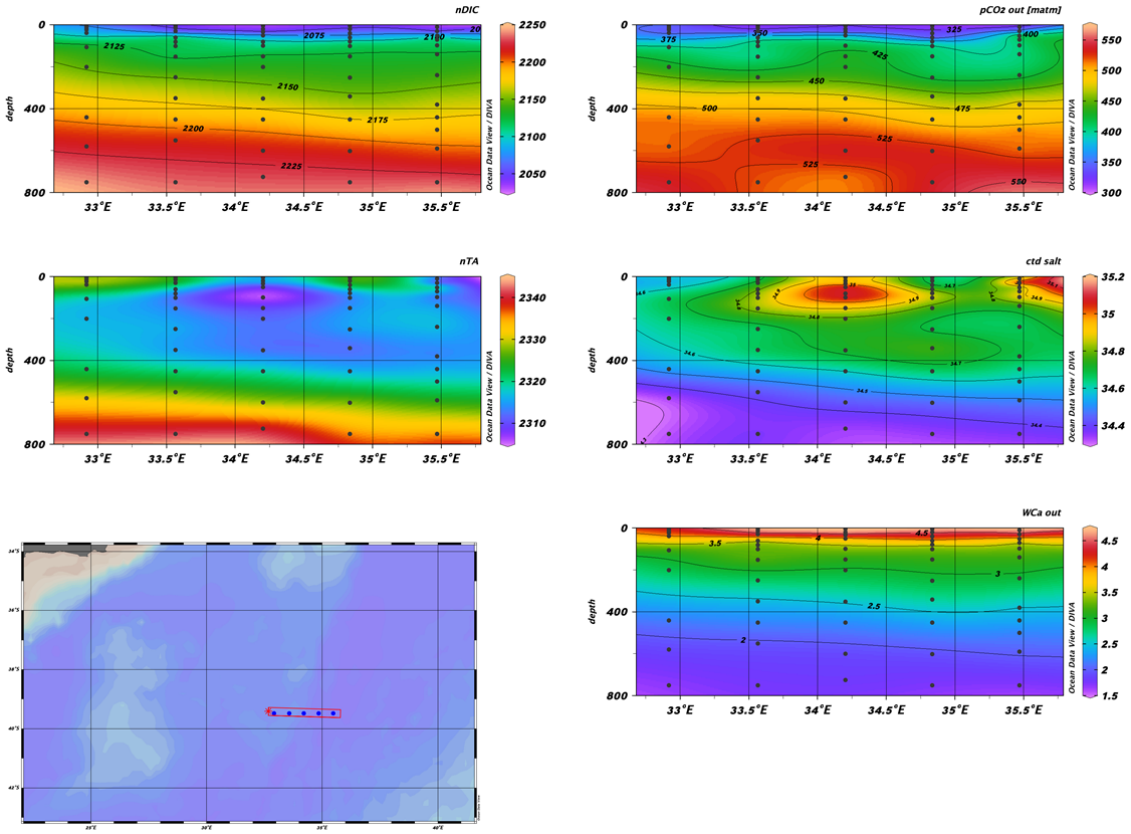

Figure 2: CTD profiles of stations 13-17 at the first sampling of the Agulhas meander. Plots of depth against longitude for nDIC, nTA, pCO2, salinity and calcite saturation state.

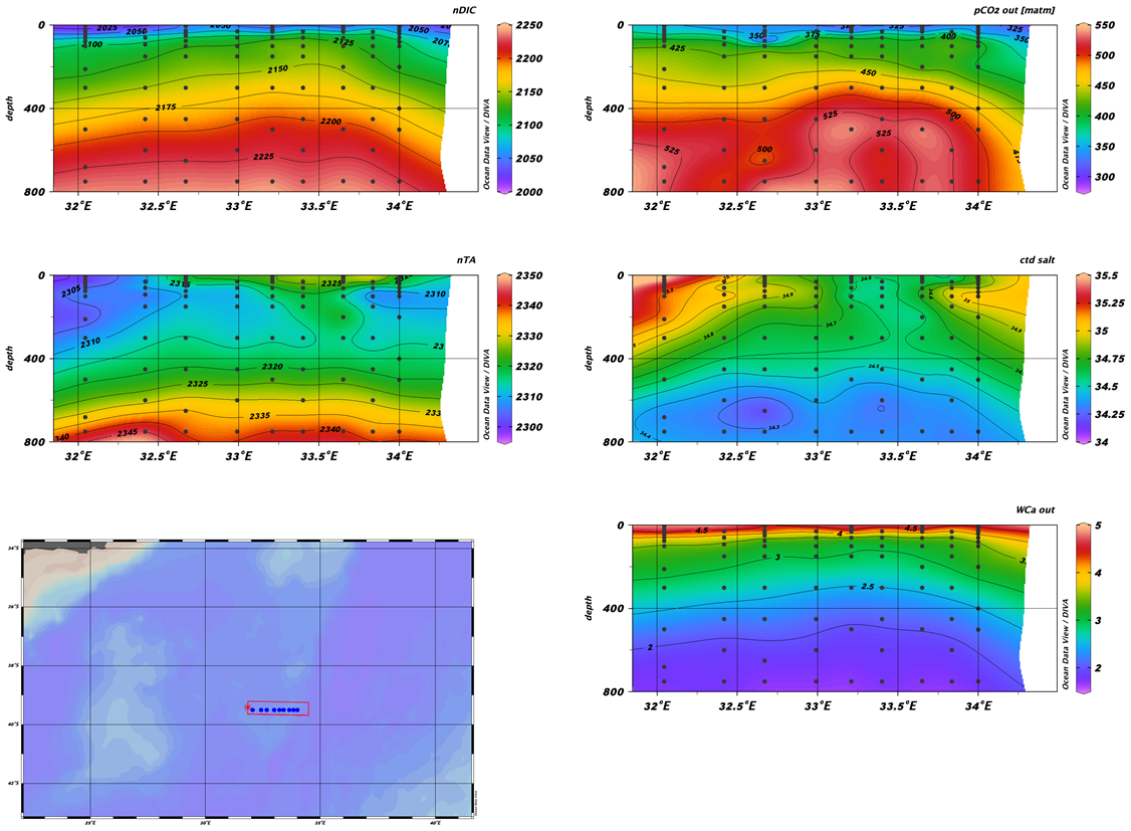

Figure 3: CTD profiles of stations 44-52 at the second sampling of the Agulhas meander. Plots of depth against longitude with nDIC, nTA, pCO2, salinity and calcite saturation state.

The CTD profiles show the temporal changes, particularly in nTA, between the 2 visits to the Agulhas meander, with CTD station 13 on 3rd February and CTD station 44 on 20th February.

Further comparisons between the surveys will be made within the carbonate chemistry data and with rest of the cruise data. Also comparisons between DIC and TA sample analysis on board and back at the lab in Bermuda.

References:

Lewis, E., and D. W. R. Wallace. 1998. Program Developed for CO2 System Calculations. ORNL/CDIAC-105. Carbon Dioxide Information Analysis Center, Oak Ridge National Laboratory, U.S. Department of Energy, Oak Ridge, Tennessee.

Robbins, L.L., Hansen, M.E., Kleypas, J.A., and Meylan, S.C., 2010, CO2calc—A user-friendly seawater carbon calculator for Windows, Max OS X, and iOS (iPhone): U.S. Geological Survey Open-File Report 2010–1280, 17 p.

Barite Formation Experiments

Julia Middleton, Woods Hole Oceanographic Inst, Woods Hole, MA 02543

The ultimate burial of particulate organic carbon (POC) represents a climatically significant sink of the CO_2 drawn down by photosynthetic organisms in the sunlit surface ocean. However, quantification of marine export production and POC burial in the sediments, and its ultimate effects on global climate, has remained a delicate problem described by a handful of proxies, each with caveats. Marine barites have emerged as one powerful proxy option based on the barite formation pathway currently invoked in the literature. Despite this potential, controls on the formation of barite in the water column are greatly understudied. Currently, consensus does not exist as to the mechanism of barite formation (Chow & Goldberg 1960, Van Beek et al 2007, Gonzalez-Muñoz et al 2012) or the depth of barite formation in the water column (Van Beek et al 2007, Horner et al 2015). Although pelagic surface waters are under saturated with respect to barite, microcrystalline barite appears throughout the water column. To overcome this apparent paradox, much of the current literature invokes the microenvironment model: Barite precipitation occurs exclusively within locally supersaturated microenvironments contained within sinking POM, of which POC is a fraction. Supersaturation occurs through the release of dissolved barium during the microbial degradation of POM. To Investigate the controls on this precipitation mechanism, incubation experiments using a stable ^{135}Ba tracer were carried out during the SAMW 2020 cruise.

Barite formation experiments were initiated at the same stations as the Balch/Morton nutrient amendment incubations (Stations 05, 18, 28, 56) and coincided with productivity and trace metal casts. From the main CTD casts, water samples from the fluorescence peak, maximum increase in beam transmission (region of decreasing particle load), and oxygen minimum were used to target areas with high phytoplankton growth, particle degradation, and microbial action, respectively. Samples were first spiked with ^{135}Ba to $\Omega_{barite} \approx 1$ to allow tracing of new barite precipitation during the course of the experiment. Notably, homogenous barite precipitation occurs where $\Omega_{barite} > 8$ (Nancollas & Purdie 1963). We explored the influence of particulate availability (microenvironments) and microbial action at each of these depths. Four conditions were carried out at each depth: 1) Unadulterated water, 2) Filtered to 0.2µm (no particulates/microenvironments), 3) poisoned with mercuric chloride (no microbial action), 4) filtered to 0.2µm and poisoned (control). Three time points were taken over the course of one week, with replicates performed for the latter two time points. The particulate fraction was saved for shore-side analysis. Pre-cruise experiments show that the uptake of ^{135}Ba into the particulate fraction can be observed over this time period. All analytical measurements for these experiments will be carried out at the Woods Hole Oceanographic Institution (WHOI) ICP Facility.

Additionally, dissolved barium samples (0.4µm Isopore polycarbonate track-etch filter) were collected from every depth of the trace metal cast. Dissolved barium samples were also

collected were collected from the A & C replicates of all nutrient amendment incubations, throughout the full time period of each experiment. Dissolved samples will be measured post cruise for barium concentration and barium isotopes at the WHOI ICP Facility.

Inventory of barite formation experiments (5 samples per line, for 3 time points)

Stn #	Niskin #	Depth (m)	Depth name	*In-situ* temp (C)	Goal [Ba]
5	2	21.7	Fluorescence max.	16.3	189
5	14	38.3	Max ▽ transmission	14.9	182
5	18	750	O2 min. (cast)	4.8	127
18	12	84	Fluorescence max.	18.2	200
18	10	93	Max ▽ transmission	17.6	196
18	2	750	O2 min. (cast)	7.4	141
28	14	32	Fluorescence max.	14.3	178
28	12	41	Max ▽ transmission	13.8	175
28	4	450	O2 min. (cast)	11.2	161
56	16	70	Fluorescence max.	14.3	178
56	14	83	Max ▽ transmission	13.8	175
56	2	751	O2 min. (cast)	11.2	161

TN376

Marci Train
Bigelow end of cruise report
March 2020

Prior to going on this cruise, I really did not know what to expect. I knew that I would be out of my comfort zone with my limited amount of knowledge about the chemistry of the ocean. Little did I know that I would be taken to a new universe of micro culture. It has been an amazing experience learning about all of the different tiny organisms that make up our oceans. It makes you realize how small one can seem in this big world of ours. It also shows how much hope a drop of water can hold.

During my time on this cruise, I have been able to gather different pieces to this elaborate puzzle. Through interviews and observations, I was able to piece together what each scientist of each discipline was contributing to this project. I also learned why it is necessary for each of them to be here in order to complete a significant study of these incredible creatures called coccolithophores. In a way, it is kind of like someone writing a symphony with all its intricate parts created separately, then waiting to put it all together to see how it plays out. It was wonderful to see how excited everyone was to explain to me what they were studying. It was like going to a grown up science fair with students excited to show how instruments work, what they found, and what they learned from it all.

I have also been excited to learn about the behind the scenes production of the crew. Each person has a job to do that is important to keep this ship running. Everyone on board works with such respect towards each other. It is also interesting to see all of the different jobs that one can have that can bring you all around the world.

It also is amazing to me that these cruises happen all around the world every day. That there are people so dedicated to their science that they are willing to leave their families and life back home to explore the oceans so intensively. I have met a lot of incredible people from all over the world with different ideas and backgrounds. I feel very fortunate to be able to be a part of this experience.

Number of Profiles: 27

Number of blog posts: 50

Number of comments or questions by others: 37

Number of clarifications and or answers from me: 35

Number of tweets: 25